AD-768 225

ADVANCED HARDENED ANTENNA WINDOW MATERIALS STUDY. III

James P. Brazel

General Electric Company

Prepared for:

Army Materials and Mechanics Research Center

July 1973

UNCLASSIFIED

Security Classification

AD-768 225

DOCUMENT CONTROL DATA - R & D

(Security classification of title, body of abstract and indexing annotation must be entered when the overall report is classified)

1 ORIGINATING ACTIVITY (Corporate author)
General Electric Company
Re-entry and Environmental Systems Division
Philadelphia, Pa. 19101

2a. REPORT SECURITY CLASSIFICATION
Unclassified

2b. GROUP

3 REPORT TITLE

ADVANCED HARDENED ANTENNA WINDOW MATERIALS STUDY

4 DESCRIPTIVE NOTES (Type of report and inclusive dates)
Final Report - May 19, 1972 to April 19, 1973

5 AUTHOR(S) (First name, middle initial, last name)

Brazel, James P. (Editor)

6 REPORT DATE	7a. TOTAL NO OF PAGES	7b. NO OF REFS
July 1973	~~25~~ 253	23

8a. CONTRACT OR GRANT NO	9a. ORIGINATOR'S REPORT NUMBER(S)
DAAG46-72-C-0173	AMMRC CTR 73-26
b. PROJECT NO 1B062113A661	
c. AMCMS Code 612113.11.070	9b. OTHER REPORT NO(S) (Any other numbers that may be assigned this report)
d.	

10 DISTRIBUTION STATEMENT

Approved for public release; distribution unlimited.

11 SUPPLEMENTARY NOTES

12. SPONSORING MILITARY ACTIVITY
Army Materials and Mechanics Research Center, Watertown, Massachusetts 02172

13 ABSTRACT

The development and characterization of the ADL-10 composite hardened antenna window (fused silica Omniweave) reinforcement/SR-350 methyl silicone resin matrix) has been completed. A nominal failure threshold of 5000 taps was demonstrated on 3/8-inch thicknesses with failure by the front face crushing mechanism. Machining the surfaces of molded specimens reduced the axial direction (minimum strength) failure stress from 10,000 psi to about 3/8 this value, indicating the benefit of using the material in the as-molded state. Additional process studies also indicated the necessity of application of the previously studied silane coupling agent to increase the shear interaction between fiber and matrix.

A variety of methods for densification of silica Omniweaves to inorganic RF transmitting composites was studied and compared. These included multiple impregnations and pyrolyses with SR-350 (the "Markite" process), pyrolysis of a silane resin, densification with "Ludox" colloidal silica sols, chemical vapor deposition of silica and boron nitride, and a series of glass-bonded boron nitride matrices. Two of these approaches yielded promising composites: "ADL-4D6", from the colloidal silica matrix in both a 4-D and 5-D reinforcement design; and "BNQ", the glass-bonded boron nitride matrix composite with 4-D Omniweave. Short beam flexures of 20,000 - 30,000 psi and a hardening threshold above 3000 taps for 3/8-inch thickness were observed for ADL-4D6. The BNQ composite in its early developmental stage had a tensile strength of 4000 psi for a fiber volume fraction of only 20 percent.

The report contains data on flexure and tensile strengths and elastic properties, flyer plate shock impact testing by both aluminum and mylar flyers, RF/dielectrics, ultrasonic and radiographic NDT, thermal conductivity and ablation testing. An analytic section compares the structural properties of 3-D, 4-D and 5-D composites of silica-silica and silica-silicone.

DD FORM 1 NOV 1473 REPLACES DD FORM 1473, 1 JAN 64, WHICH IS OBSOLETE FOR ARMY USE.

UNCLASSIFIED

Security Classification

14 KEY WORDS	LINK A		LINK B		LINK C	
	ROLE	WT	ROLE	WT	ROLE	WT
Antenna windows						
Woven fiber composites						
Quartz fibers						
Composite fabrication						
Chemcial vapor disposition						
Mechanical properties						
Shock resistance						

AMMRC CTR 73-26

ADVANCED HARDENED ANTENNA WINDOW MATERIALS STUDY III

July 1973

edited by

James P. Brazel
General Electric Co., RESD
Philadelphia, Penna.

Final Report – Contract DAAG 46-72-C-0173
D/A Project 1B062113A661
AMCMS Code 612113.11.070
Title of Project: Reduction of Vulnerability, ABM Systems
Army Accession Number DA OD4812

Prepared for

ARMY MATERIALS AND MECHANICS RESEARCH CENTER
Watertown, Massachusetts 02172

ABSTRACT

The development and characterization of the ADL-10 composite hardened antenna window (fused silica Omniweave reinforcement/SR-350 methyl silicone resin matrix) has been completed. A nominal failure threshold of 5000 taps was demonstrated on 3/8-inch thicknesses with failure by the front face crushing mechanism. Machining the surfaces of molded specimens reduced the axial direction (minimum strength) failure stress from 10,000 psi to about 3/8 this value, indicating the benefit of using the material in the as-molded state. Additional process studies also indicated the necessity of application of the previously studied silane coupling agent to increase the shear interaction between fiber and matrix.

A variety of methods for densification of silica Omniweaves to inorganic RF transmitting composites was studied and compared. These included multiple impregnations and pyrolyses with SR-350 (the "Markite" process), pyrolysis of a silane resin, densification with "Ludox" colloidal silica sols, chemical vapor deposition of silica and boron nitride, and a series of glass-bonded boron nitride matrices. Two of these approaches yielded promising composites: "ADL-4D6", from the colloidal silica matrix in both a 4-D and 5-D reinforcement design; and "BNQ", the glass-bonded boron nitride matrix composite with 4-D Omniweave. Short beam flexures of 20,000 - 30,000 psi and a hardening threshold above 3000 taps for 3/8 inch thickness were observed for ADL-4D6. The BNQ composite in its early developmental stage had a tensile strength of 4000 psi for a fiber volume fraction of only 20 percent.

The report contains data on flexure and tensile strengths and elastic properties, flyer plate shock impact testing by both aluminum and mylar flyers, RF/dielectrics, ultrasonic and radiographic NDT, thermal conductivity and ablation testing. An analytic section compares the structural properties of 3-D, 4-D and 5-D composites of silica-silica and silica-silicone.

FOREWORD

The work described in this report was carried out at General Electric Re-entry and Environmental Systems Division (GE-RESD) Materials Laboratories, Valley Forge Space Technology Center, King of Prussia, Pennsylvania. Technical supervision was provided for the U.S. Army Materials and Mechanics Research Center by Dr. Nathaniel S. Schneider. The principal technical investigator for the General Electric Company was Mr. James P. Brazel. Consultation on the program goals was provided by Messrs. John Dignam and Lewis Aronin of AMMRC and Mr. Kenneth Hall of GE-RESD.

The principal contributors to the program technical effort and preparation of this report are listed below:

Omniweave design and weaving	Melvin Wexler, Richard Fenton
Composite Formulation and Fabrication	
- ADL-10	Richard Fenton
- aqueous colloidal silica matrix	Richard Fenton
- silane-derived silica matrix	Richard Thuss
- silica-boria based matrices	Dr. Joseph Gebhardt, Thomas Ormiston
- markite hybrids	James Brazel, Richard Fenton
- chemical vapor deposition, silica and BN	Dr. Joseph Gebhardt
- BNQ glass-bonded BN matrix	James Brazel, Richard Fenton
Characterization plan, thermal characterization, program management and editing final report	James Brazel
Mechanical testing	Edward Ruzauskas
Ultrasonic characterization	John Roetling
Flyer plate testing	
- ADL-10	Marlyn Graham, Effects Technology, Inc.*
- inorganic composites	Gordon Sullivan
Electromagnetic properties	Jack Hanson
Ablation testing	Albert Saydah
Omniweave composite optimization study	Dr. B.W. Rosen, Dr. John Kibler Materials Sciences, Inc.*

*under subcontract

The report contributors also wish to acknowledge in particular the laboratory and experimental contributions of the following personnel: Francis Manning and Vincent Arcidiacono for their weaving and impregnation efforts, Jordan Konell and Charles Clampffer for mechanical testing, Arthur Oaks for radiography, Bryce Kennedy for thermal measurements, Kenneth Bleiler for thermochemical analysis and Charles Stremus for photography of ADL-10 fracture surfaces.

Support for this work was provided by U.S. Army Project 1W1 621 13A661 Reduction of Vulnerability, ABM Systems; New Materials Development.

TABLE OF CONTENTS

TABLE OF CONTENTS (Continued)

LIST OF ILLUSTRATIONS

LIST OF ILLUSTRATIONS (Continued)

LIST OF ILLUSTRATIONS (Continued)

LIST OF ILLUSTRATIONS (Continued)

LIST OF ILLUSTRATIONS (Continued)

LIST OF ILLUSTRATIONS (Continued)

LIST OF ILLUSTRATIONS (Continued)

LIST OF TABLES

LIST OF TABLES (Continued)

SECTION 1.0

TABLE OF CONTENTS

1.0 INTRODUCTION AND SUMMARY

1.1 INTRODUCTION: PROGRAM BACKGROUND

The purpose of this program is to develop hardened, radio frequency transparent, multidirectionally reinforced heat shield materials for possible ABM applications using the General Electric Re-entry and Environmental Systems Division's "Omniweave" process. The work was performed in the Materials Laboratory of GE-RESD from May 19, 1972 to April 19, 1973, mainly by personnel of the Plastics Technology and the Materials Performance and Applications Laboratories. Two subcontracts were let: Materials Sciences, Inc. performed structural analyses of these and competitive materials systems, and Effects Technologies, Inc. performed exploding foil impact testing on samples of ADL-10.

This "Advanced Hardened Antenna Window Materials Study (III)" is the third program in a continuation of the "Hardened Antenna Window Program" (July 1, 1969 to March 31, 1970) and the "Advanced Hardened Antenna Window Materials Study" (December 7, 1970 to November 7, 1971). The first effort studied four variations of a high purity silica Omniweave/SR-350* silicone resin composite designated "ADL-10". As indicated in the final report for the program (Ref. 1), ADL-10 showed excellent promise in the hardening and RF/ablation categories below 100 Btu/ft^2-sec, but the mechanical strength levels were disappointing, in the 2000-4000 psi range. "Markite", a silica version of the material produced by multiple pyrolysis and reimpregnation cycles with the same SR-350 silicone resin, was also studied.

The second effort had as its principal goal the realization of higher strength levels for the resin-based ADL-10 material via specified improvements in Omniweave fabric densities and through the thickness fiber weaving angles. Additional process improvements included variables such as fiber coating processes (using such plastics as Teflon**) and the effects of fiber etching and coupling agents. A second task was to further investigate the Markite process inorganic hardened antenna window for higher heat flux applications.

The principal goal for ADL-10 was met with the achievement of 10,000-20,000 psi ultimate axial tensile strength levels and hardening capability in excess of 4000 taps for nominal thicknesses of 1/4 to 3/8 inch as measured by magnetic flyer plate testing. This high performance and the relative low cost of the material established the ADL-10

*General Electric Co. Silicone Products Department, Waterford, New York
**E.I. duPont Trademark

series of composites as an outstanding candidate for immediate application to several antenna window and radome applications in the heat flux range below 100 Btu/ft^2-sec.

The development effort on Markite centered on the use of the much improved weaving densities and process optimization achieved for the ADL-10 material. Although systematic improvements of about 20 percent in the strength of several versions of this material were evident at successive stages of pyrolysis and reimpregnation, the desired strength and hardening levels were not achieved. The process did indicate the desirability of investigating a "hybrid" Markite in which the material would not be submitted to a final pyrolysis after a reimpregnation, with just enough SR-350 resin to increase strength but not to generate unacceptable RF attenuation at high heating levels. Tests of this concept had shown flexure strengths as high as 5,900 psi and there was evidence for extension to higher levels. The material was recommended as promising for a near term solution for high heating levels. However, it was obvious that to meet ultimate performance goals a completely inorganic hardened antenna window composite material such as pure silica/silica was required. Moreover, it was a conclusion of the structural analysis portion of the final report (Ref. 2) that a fiber-matrix interaction fundamentally different from that of the Markites studied thus far was required for achievement of the structural strength and hardening goals.

1.2 SUMMARY

The program plan and results of this third AMMRC GE-RESD study are summarized in the flow chart format of Figure 1. The program was divided into two major portions: the first completing the required characterization of ADL-10 and the second concentrating on developmen' of inorganic hardened antenna window concepts not limited by heat flux considerations.

Both portions were based on high density, nominally 1.0 gm/cc Astroquartz Omniweave reinforcement fabric. The program called for fabrication of a minimum quantity of 450 square inches with a minimum thickness of 1/2 inch in the standard 45 degree fiber pitch angle (FPA) geometry. These silica reinforcement weaving requirements were exceeded with the production of more than 600 square inches of 4-D standard 45 degree FPA Astroquartz Omniweave, 56 square inches of 5-D cubic construction and 85 square inches of a 4-D preimpregnated inorganic composite, "BNQ".

The ADL-10 material was to be fabricated by the optimum process described in References 2 and 3, with a minimum of 100 square inches in the minimum plate size of 4.00 inches x 6.00 inches submitted directly to AMMRC for large particle hypersonic impact tests. The detailed characterization was to include determination of the hardening threshold at levels above the 4000 taps available at GE-RESD and the effect of machining the molded faces on both this hardening level and the strength of axial tensile specimens. Five 4.00 inch x 6.00 inch plates were actually delivered

to AMMRC (Fig. 56) for a total of 120 square inches.* The nominal hardening threshold for as-molded material was found to be 5,000 taps for a 1-centimeter thickness, with failure by the front face crushing mode. Machining the faces reduced this threshold to 3200 to 4600 taps. The higher density variations of ADL-10 had the higher threshold and lessened effects due to machining, actually achieving an as-molded threshold of 5700 taps. In tensile tests of bar samples cut from ADL-10 panels made from four high density, excellent quality Astroquartz Omniweaves it was nevertheless found that use of the silane coupling agent studied in Reference 2 was required for full realization of the structural capability of the material. ADL-10 made with the silane coupler had a minimum (axial panel direction) tensile strength of 10,000 psi, as compared to 3000-6000 psi without silane coupler. Machining the tensile specimen faces reduced the high level material to about 3/8 its original strength, while the uncoupled material was reduced to about 2/3. Face machining thus also had the comparative effect of diminishing the strength advantage of the silane treatment.

The clear result of this study of the effects of machining the faces of the molded ADL-10 composite is that the material should by all means be designed for use in the molded-to-size state to preserve its excellent structural and elastic performance. Fortunately, this should be easily achieved since it is an easily molded material and a molded-to-size silica fiber composite antenna window has an obvious cost advantage over one which must be machined to size.

The inorganic development portion required investigation of the densification of silica Omniweave by the Ludox** aqueous colloidal silica process based on the work of Aeronutronics Division/Philco-Ford Corporation for the Air Force Materials Laboratory and SAMSO. This approach has resulted in the current state-of-the-art inorganic hardened antenna window material designated "AS3DX" (Ref. 4). The properties of this and other antenna window materials are compared with those developed in this series of programs in Table 51, Section 5, "Conclusions and Recommendations". Other composite formulations to be investigated for production of an inorganic hardened window included repeated pyrolysis and reimpregnation with a silane resin (methyl-trichlorosilane), the application of silica-boria binders then under parallel development in the NASA/Space Shuttle Program and the generation of silica and boron nitride matrices by chemical vapor deposition process (see Fig. 1). In addition, the formulation of a glass-bonded boron nitride matrix was to be investigated for densification of the Astroquartz Omniweave reinforcements already produced in the weaving tasks. The analytical models and recommendations of the program consultants, Materials Sciences, Inc., were to be applied to the composite fabrication, including the " space-frame" 5-D model for a low density, ductile ceramic advanced in Section 4 of Reference 2.

*An additional 70 square inches of ADL-10 have been subsequently delivered to AMMRC during the period of review of this report in four smaller sized plates in support of this testing when the results showed excellent resistance to particle impact.
**Trademark of E.I. du Pont

In addition, a hybrid Markite system was investigated. This consisted of a mixture of the ADL-10 and inorganic Markite processes, and used ADL-10 starting material from the previous study.

Composite densification proceeded as indicated in the flow-charted format of Figure 1. Because of the exploratory nature of the earlier work, an iterative screening characterization which resulted in revised formulation and processing cycles was followed. In contrast, the current effort was planned as a discrete, one time composite fabrication and complete characterization sequence carried out for ADL-10, whose process specification was considered fixed. It was subsequently found in tensile testing that the silane coupler stage of processing had to be added to the basic process. Consequently, several iterations, involving two molding criteria were actually performed.

The processing-screening cycle for the inorganic candidates is represented in Figure 48. Section 2 of this report, "Composite Design and Fabrication", gives the details of the processing from the Omniweave reinforcement fabric design and weaving through the various matrix formulations and composite densifications, as modified by the screening portion of the development cycle. Fundamental constituent material characterization data such as TGA, DTA, IR scans and the chemistry of the matrices are given with the individual process descriptions.

The sequence for characterization of material performance outlined in Figure 1 is described in detail in Section 3 of this report, "Characterization". The Figure 1 flow chart indicates the increasing test detail with corresponding increased definition of the processing for the more promising concepts.

These formulation concepts and the results of successive characterization cycles were incorporated throughout the time period of the program in analytic studies performed by Materials Sciences, Inc. It is important to recognize both the limitations and benefits of these analytical studies as implied in this interaction process. Analyses of the structural potential of the Omniweave multidirectional reinforcement concept had been performed prior to the first of these hardened antenna window programs and predicted levels of strength and hardening performance that were not verified by experiment at that time. Most of the reasons for these deficiencies were reviewed in Reference 2. That work also showed that higher Omniweave fabric densities achieved with improvements in weaving and fiber treatment had eliminated fiber crimping in the unit cell of the 4-D reinforcement. This basic fabric processing improvement was followed by experimental data which realized the predicted strength levels. But knowledge of certain of the constituitive properties of the matrix and the specific fiber-matrix interaction was still required for a detailed analysis of ADL-10. These data, e.g., the cured SR-350 resin matrix shear modulus, were obtained in Reference 2 and made possible a comprehensive structural analysis of the very same composites made and tested in the program. This iterative formulation-characterization test-analysis cycle has been conducted in the program described by this report and the formal analysis of Section 4, "Optimization Study of ADL-10 and Analytical Exploration of Other Omniweave Silica Materials". The analysis follows the actual material formu-

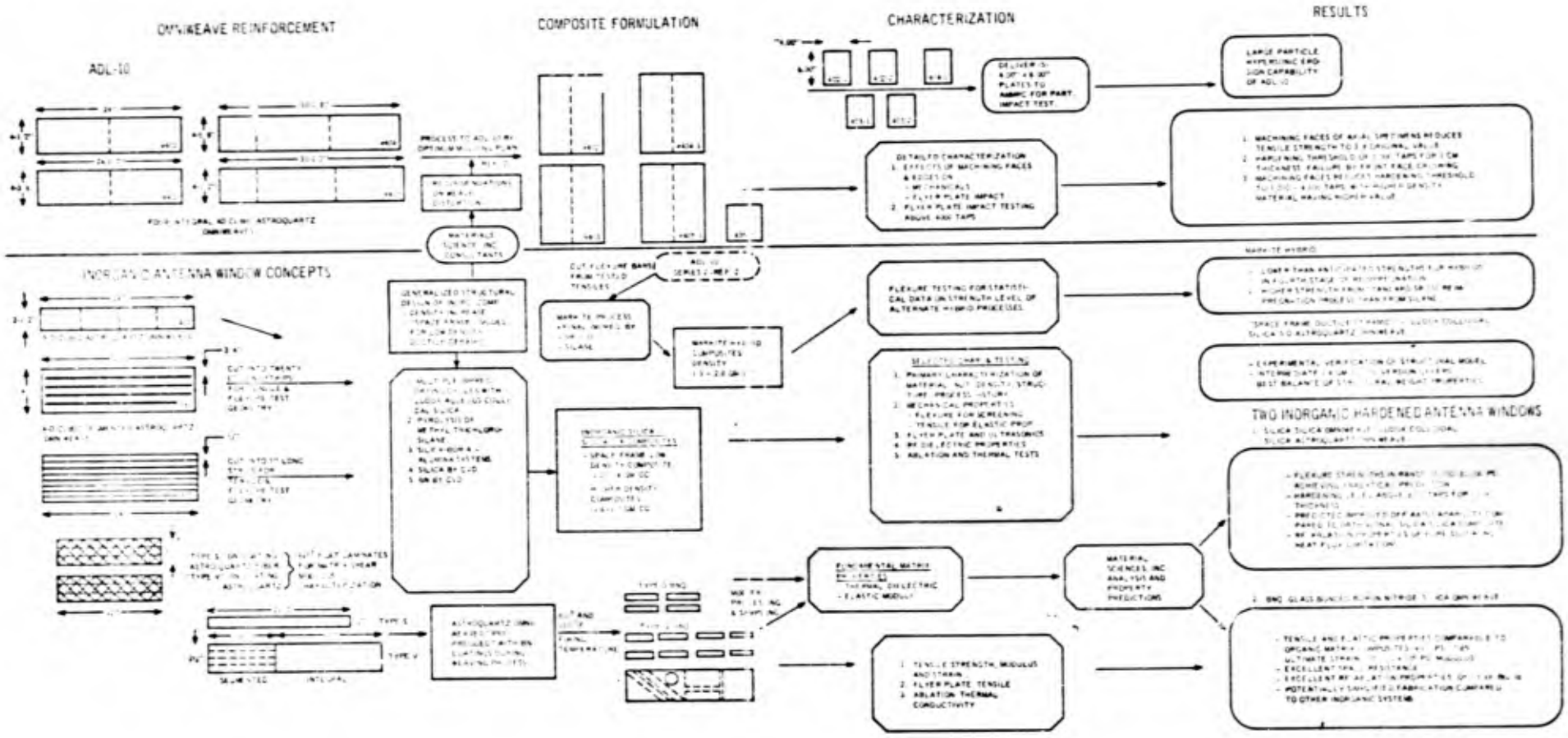

Figure 1. Program Plan: Advanced Hardened Antenna Window Material Study

lations, as developed, and to which it contributed guidance during the development cycles, the outstanding example of which is the 5-D space frame concept first recommended in the previous analysis Section 4 of Reference 2.

The results of the inorganic antenna window concept development are summarized at the end of Figure 1. The outstanding results include demonstration of the applicability of the aqueous colloidal silica densification process to silica Omniweave 4-D reinforcement. Flexural strengths in the range 10,000-30,000 psi were achieved with hardening levels in excess of 3000 taps for a 1-centimeter thickness. A second and entirely new silica Omniweave composite, designated "BNQ", using glass-bonded boron nitride as a matrix was developed. Even in a low fiber volume fraction developmental stage with a commercially available Carborundum binder, BNQ tensile strengths of 4000 psi have been measured, with excellent strain and hardening capability and an exceptionally low thermal conductivity.

The 5-D "space frame" concept for a low density "ductile ceramic" has been demonstrated. This system is probably not of immediate use for a hardened antenna window in a high shear and heat flux aerodynamic environment where ablation performance is paramount, but its excellent strain capability and the option of tailoring elastic and strength properties with density and the corresponding open internal structure should be of unique value in other less severe aerodynamic heating or sub-surface structural functions. Also, the "tailoring" promise of this 5-D system suggests improvements to be gained in study of higher order dimensional systems such as 7-D as in the case of current analogous work on carbon-carbon composites.

The alternative methods for silica Omniweave composite densification listed in Figure 1 have been treated throughout the report as competitive methods for densification despite their immediate value in producing hardened antenna window composites. Wherever possible the comparative data are presented for future reference.

The report has been prepared in the same format as its two predecessors, References 1 and 2, to facilitate ready comparison and to take advantage of the invested efforts of previous readers in these reports.

SECTION 2.0

TABLE OF CONTENTS

TABLE OF CONTENTS (Continued)

2.0 COMPOSITE DESIGN AND FABRICATION

2.1 GENERAL CONSIDERATIONS

2.1.1 PROGRAM MATERIAL DEVELOPMENT BACKGROUND

The purpose of this third AMMRC/GE-RESD study has been to develop new composite hardened materials for the ABM antenna window requirement.

To date the basic multidirectional fibrous reinforcement system has been restricted to selection of high purity fused silica as the fiber, in particular J. P. Stevens "Astroquartz", and the GE-RESD "Omniweave" system of weaving multidirectional, high density reinforcement fabric. The earliest work of this series of studies was specialized for two reasons to ADL-10(GE's SR-350 methyl silicone resin/ Astroquartz Omniweave) with some comparative studies using phenolic resin in the same reinforcement fabric (Ref. 1). The first of these reasons was that the SR-350 resin had shown potential in early screening for a "plastic antenna window" material; i.e., a composite with the excellent mechanical and insulative properties of an ablator but not forming an electromagnetically lossy carbonaceous residue or char in the ablation environment. Combined with the relatively well known weaving technology for Astroquartz fibers, samples of the ADL-10 composite did show retention of RF transmission after steady state furnace heating in air to 1800-2000°F, which temperature level TGA had shown corresponded to completed pyrolysis of the silicone matrix to a high purity inorganic silica residue. But the combined RF/ablation transient heating tests of References 1 and 2 showed that, above a well defined heat flux of 100 Btu/ft^2-sec, surface melting occurred at a nominal surface temperature of 2800°F and transpiring pyrolysis products from the resin were sealed off and cracked, forming high transmission loss free carbon products. This did not of course occur in the furnace tests and follow-up dielectric measurement because the sample was maintained almost isothermal and pyrolyzed completely without fusion of either the high purity Astroquartz fibers or the silica pyrolysis products.

The second reason for specialization to the ADL-10 composite and hardened antenna window development was that a large hardened heat shield effort was then underway at GE-RESD (and other aerospace contractors) under such programs as the U. S. Air Force HAAM and Advanced Heat Shield programs in which combinations of several silica, carbon and graphite fibers were being evaluated with the obvious matrix choice of phenolic resin. Other more basic programs were also examining the potential of the Omniweave system for carbon/carbon and carbon/graphite composites. However,

no work was underway on the antenna window application for Omniweave; therefore it was agreed with the program management officers at AMMRC to concentrate on this function, avoiding duplication of effort but utilizing the synergistic interaction between the programs.

2.1.2 DEVELOPMENT OF THE MATERIAL PROPERTY GOALS

The progress of the development of ADL-10 has been reviewed above in Paragraph 1.2, "Summary", as has the evolution of the Markite series of materials and the plan for this program to complete ADL-10 characterization and perform a comprehensive and basic study of the potential of new matrices with silica Omniweave. Because the performance of antenna windows can usually be designed to be compatible with most heat shield requirements via positioning on the shield, size and geometry adjustments and judicious mounting designs, no strict performance requirements have been placed on the complete set of materials studied on this program. The excellent mechanical, hardening, thermal and electromagnetic properties of ADL-10 below 100 Btu/ft^2-sec commended it to be fully characterized for several potential applications where the heat flux limit was not exceeded and the relative low cost and manufacturing simplicity of the material would be welcome.

There are three requirements which must be considered for an advanced hardened antenna window. The first and most obvious requirement is for transmission unlimited by heat flux requirements, or in the quantitative convention, a loss tangent less than 0.01. An immediate corollary of this, drawing on behavior of long-standing state-of-the-art materials such as the monolithic fused silicas typified by Corning 7940 and 7941 (and ADL-10), would be for a surface temperature capability of at least 3000°F (silica melting) and hopefully 5000-5100°F, corresponding to vaporization in a high heat flux environment.

The second requirement deals with the hardening level. The ADL-10 material's baseline level of 5000 taps for a 1-centimeter as-molded thickness is an obvious benchmark. Considerations of such details as the ADL-10 front face crushing failure mechanism (rather than rear face spall, see Sections 3-4), the improvement to 5,700 taps for higher density material and detailed design solutions to the intended ABM use should do little to measurably perturb this nominal minimum hardening goal of 5000 taps.

The third requirement, an allied structural requirement, is the mechanical strength and elastic properties. High values of mechanical strength are not usually required for antenna window inserts - a few thousand psi with a strain capability of a percent or so should be adequate for the mentioned design solutions to be used - as they have in some current operational systems. For a radome use where aerodynamic and maneuvering loads must be considered, both the strength and modulus must be high, while the allowable strain is again a "forgiving" feature. Again, a strength goal

based on specific vehicle design cannot be promulgated for this study. Comparison to the plastic matrix ADL-10 composite shows a minimum expected strength of 10,000 psi in the (lowest strength) face axis direction for molded plate material with the proper fiber-matrix coupling treatment. The conventional monolithic fused silicas have strengths in the range 5000 to 9000 psi, but with very low strain capability and of course they cannot be considered as shock-hardened materials.

The current state-of-the-art AS3DX silica/silica 3-D composite hardened antenna window material has a baseline flexural strength of 4300 - 4800 psi in its axial direction (highest strength for 3-D geometry), with near term potential for improvement to approximately 5000 psi. These considerations then suggest a program goal of 5000 psi. It will be seen (Para. 3.2.3.2) that flexure test results in the range 10,000-30,000 psi were obtained in this program's work as has similarly been reported in Reference 4. But the true final measure of this strength figure must be the results of uniaxial tensile testing, which will also give the strain capability of the material.

Specification of the elastic modulus is difficult, again because of the possibility for a design type solution for the application. No requirement will be made here; however a lower goal value of 10^5 psi is given in "Recommendations", Paragraph 5.2, for future work on the BNQ composite.

In summary, the primary goals of the inorganic hardened composite antenna window phase of this program have been set by reference to the baseline data of ADL-10, the monolithic (unhardened) fused silicas and state-of-the-art competitive hardened antenna windows:

Heat flux limitation:	none for RF electromagnetic transmission, i.e., loss tangent less than 0.01; equivalent to fused silica thermo-structurally and in ablation and recession rate.
Hardening:	minimum of 5000 taps (by inference from ADL-10).
Mechanical:	strength of 5,000 psi (as verified by uniaxial tensile test, with strain capability).

Secondary goals can be placed on other properties:

Thermal conductivity:	1/2 or less that of transparent fused silica (i.e., $\leq 11 \times 10^{-5}$ Btu/ft-sec-F° at 150°F)
Dielectric constant:	equal to or less than slip cast fused silica (i.e., ≤ 3.3 at 8.6×10^9 Hz).

2.2 QUARTZ OMNIWEAVE FABRIC REINFORCEMENT

Omniweave is a General Electric developed multidirectional weaving technology which is capable of producing composites having tailored fiber geometries. These omniweave fabrics are composed of interlocking fiber elements which travel in-depth so that discrete fiber layers are not formed. The absence of resin or in general, matrix - bonded layers enhances the composite shear and through-the-thickness strength.

Two types of quartz fiber Omniweave constructions were evaluated in this study:

a. Cubic Construction (4D)

This most standard Omniweave configuration involves the weaving of fibers in a three-dimensional fashion so that the reinforcing fibers follow paths which are parallel to intersecting diagonals - that is, the fibers travel from surface to surface at a constant radial angle, while forming a nominal 45-degree angle in the lengthwise (axial) and cross wise (transverse) direction. An isometric representation and block diagram of this type of body centered cubic construction are illustrated in Figures 2 and 3. Because of the projection of the fibers in four spatial directions, this construction is termed four directional (4-D).

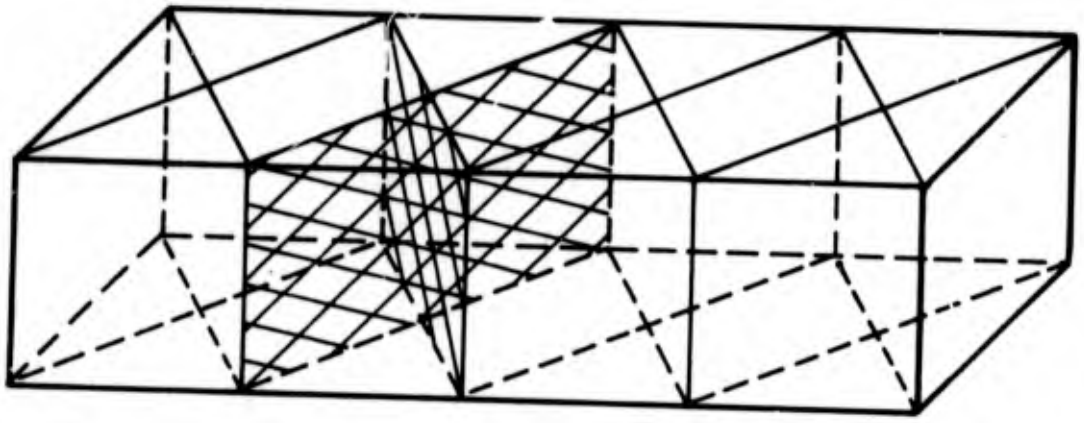

Figure 2. Multidimensional Reinforcement in which the Fibers Follow Paths Parallel to the Diagonals of Intersecting Planes

b. Cubic Construction with Transverse Reinforcement (5-D)

This Omniweave construction is a cubic configuration with horizontal (transverse) fiber elements added. During the weaving process, pre-cut fiber elements are

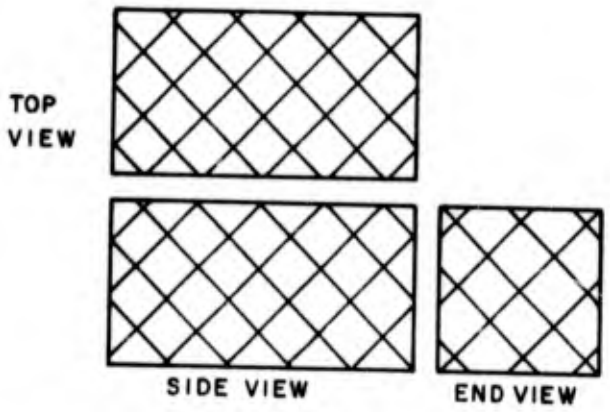

Figure 3. Plane View of Four Directional (4-D) Omniweave

laid across each set of stitch rows so that the succeeding weaving motion "sews" them into the weave. The added transverse fiber elements give the fabric five reinforcing directions (5-D): An isometric representation and block diagram of this construction are shown in Figures 4 and 5.

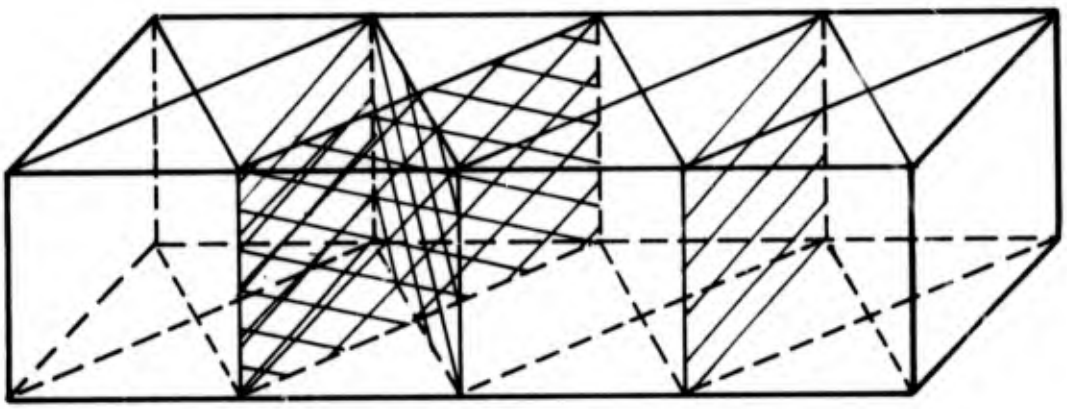

Figure 4. Isometric View of Five Directional (5-D) Omniweave

J. P. Steven's teflon coated Astroquartz 552 20 end roving was utilized in fabricating the Omniweave constructions for this program. One segmented weave (No. 381 Q3BA) utilized Astroquartz with a silane/urethane finish, due to a delay in receiving the teflon coated version.

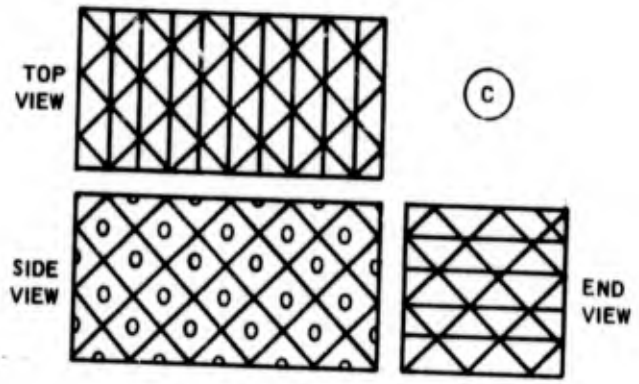

Figure 5. Plane View of Five Directional (5-D) Omniweave

Two Omniweave fabrics (Nos. 406 and 407) utilized Astroquartz with a silane finish that was prepreged in-house with boron nitride emulsions. The processing details of these particular weaves are covered in Paragraph 2.4.6.

Table 1 lists the physical characteristics of all the quartz omniweave constructions utilized in this study.

Figure 6 shows a selection of the silica Omniweaves woven for the program. Two of the integrated flats appear as the larger weaves, with four of the eight individual lengths of the 400 weave. The 5-D 401 weave is shown at bottom. In all cases the teflon coatings have been burned off for closer inspection of the weave. Figure 7a is a closeup of the face and side view of the 400 weave, showing its 4-D geometry and detail of the fiber bundles. Figure 7b is a closeup of the 5-D 401 weave face with the ends of horizontal "stuffer fibers" at top and bottom.

2.2.1 OMNIWEAVE REINFORCEMENT BASELINE STRENGTH DETERMINATION

In order to provide a baseline strength for quartz Omniweave reinforcements, two strips were tensile tested with no matrix to provide stress transfer between filaments. This data would allow an evaluation of each matrix system and rigidization process concerning quartz filament degradation due to processing and the stress transfer capability of the matrix.

Two six-inch sections from Omniweave fabric No. 400 (after Teflon burnout) were used as the tensile samples. Each end of the strip was impregnated with epoxy resin (one inch length at each end) to provide a grip surface. The strips were then saturated with a silicone lubricating oil (General Electric Versilube F-144) to allow the fibers to slip past each other with minimum damage when tensioned, while contributing no composite mode shear stress transfer. The characterization data are given in Table 2.

TABLE 1. PHYSICAL CHARACTERISTICS OF QUARTZ OMNIWEAVE FABRICS

Parameter/Weave No.	381[1]	401	400[2]	402	403	404	405	406	407
Weave pattern	4D cubic	5D cubic	←			4D cubic		→	
Thickness x width (layers)	9 x 12	4 x 32	7 x 10	←		11 x 84		→	7 x 10	7 x 44
Fiber type	←				Astroquartz 552 20E roving				→	
Fiber finish	Silane	←			Teflon			→	Silane	Silane
Fiber treatment	Urethane	←			None			→	Boron Nitride (S)	Boron Nitride (V)
Woven dimensions (inches)	26 x 3/4 x 1/2	24 x 2 1/2 x 1/4	24 x 1/2 x 3/8	24 x 4 1/2 x 1/2	24 1/2 x 4 3/8 x 1/2	30 1/8 x 4 5/8 x 9/16	31 1/2 x 4 1/2 x 9/16	21 1/2 x 3/4 x 1/2	(segmented)[3]
Finish Removal	850° F-36 hrs.	←			900° F-16 hours			→	None	None
Woven bulk density (gm/cc)	1.10	0.87	0.99	1.00	1.05	0.98	0.95	1.27	(3)
Average axial angle	45°	40°	40°	45°	43°	45°	44°	48°	(3)
Average thickness angle	45°	-	40°	40°	45°	45°	42°	-	(3)

(1) "segmented weave" 5 strips woven simultaneously

(2) "segmented weave" 8 strips woven simultaneously

(3) "segmented weave" 4 strips woven simultaneously for length of 10 1/2 inches then integrated into 1 weave which was woven 15" long.

Note: A detailed description of fabrics 406 and 407 is covered in section 2.4.6.2.

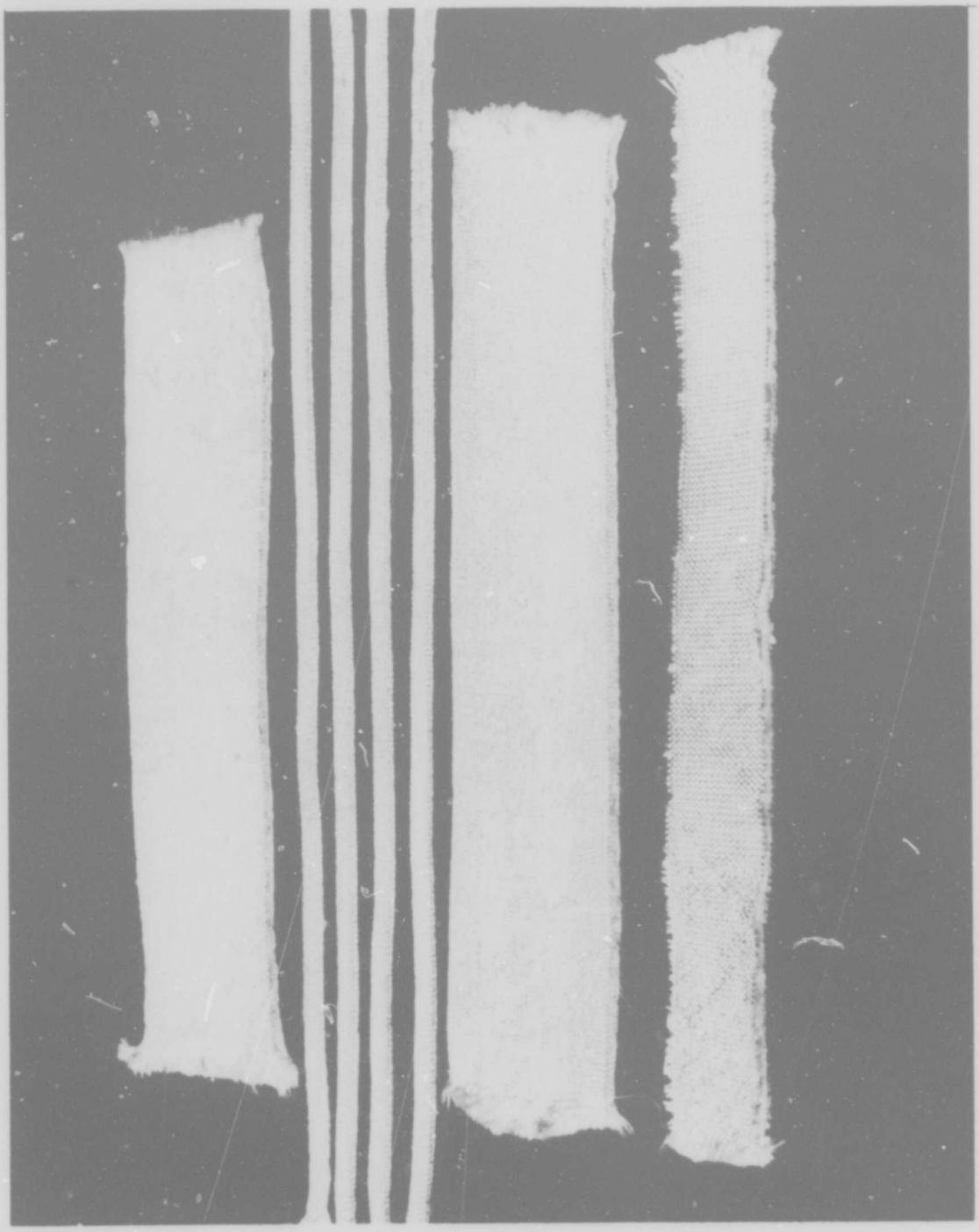

Figure 6. Four Silica Omniweaves: Standard 4-D Cubic Integrated Weave at Top and Third, Four Strips of Segregated 4-D Cubic Weave 400 and 5-D Weave at Bottom

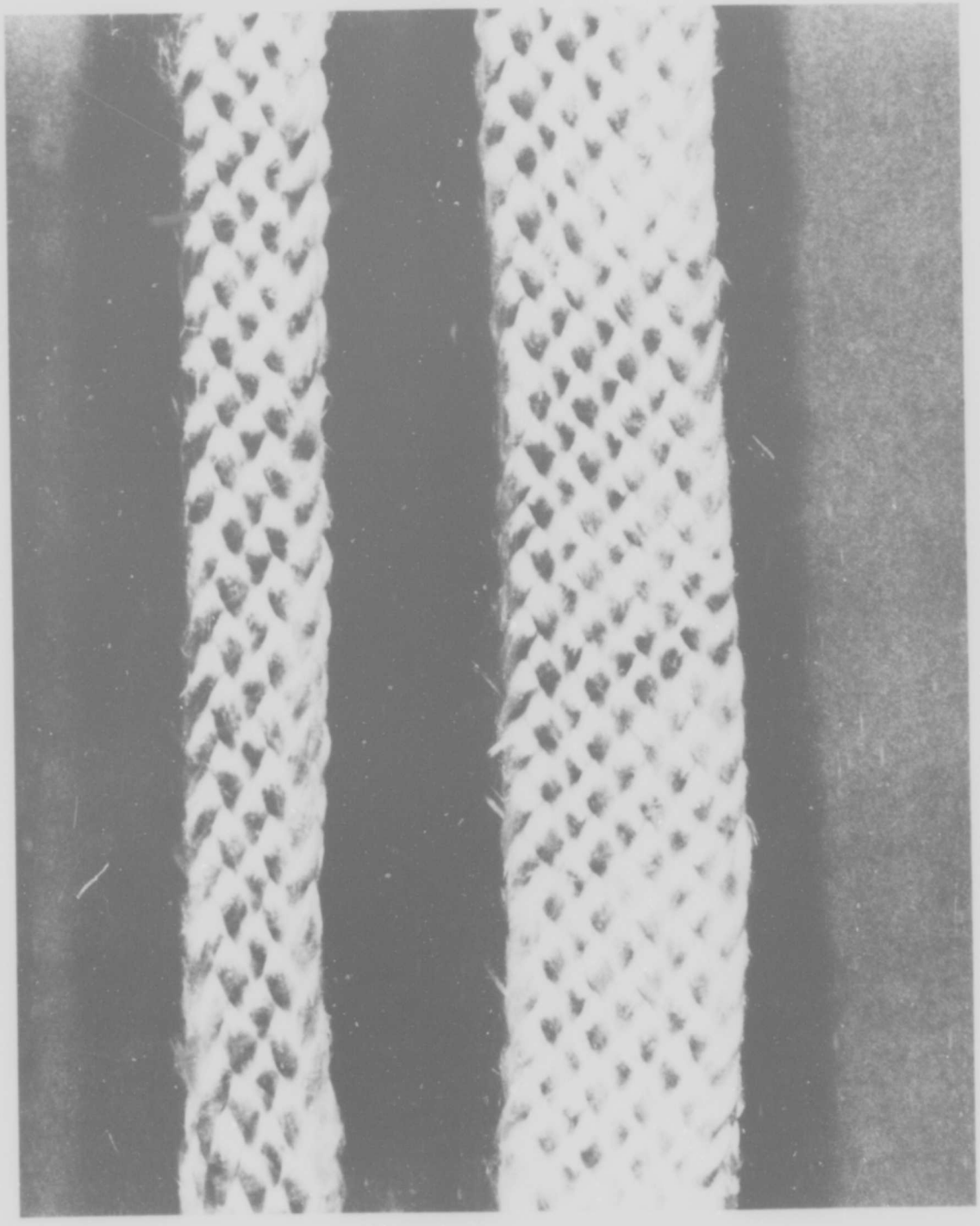

Figure 7a. Face and Side View of 4-D 400 Silica Omniweave

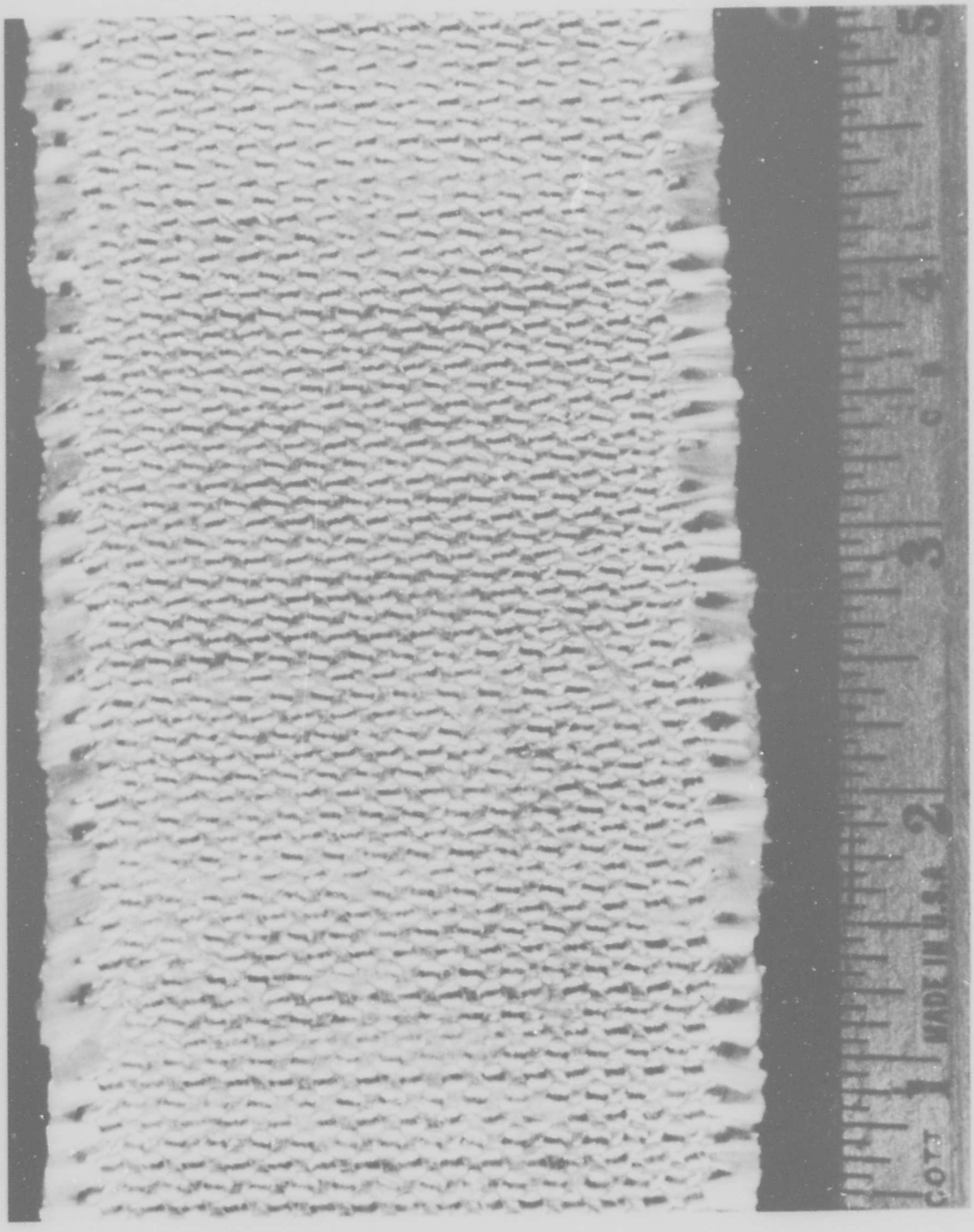

Figure 7b. Face View of 5-D 400 Silica Omniweave, with Ends of Transverse "Stuffer Fibers" Visible at Top and Bottom (Scale in inches)

TABLE 2. CHARACTERIZATION DATA OF SILICONE LUBRICATED OMNIWEAVE

Part ID	Weave Density	FPA	TTA	Fiber Vol.
400-1, 2	0.99 gm/cc	40°	40°	45%

2.3 ADL-10 PLATE FABRICATION

Processing Background*

General Electric's ADL-10 antenna window material is composed of SR-350[(1)] methyl silicone resin binder in a quartz Omniweave cubic (4-D) construction. Four ADL-10 panels were fabricated utilizing quartz Omniweave fabric numbers 402, 403, 404 and 405 and were given these identification numbers. Each Omniweave fabric was divided into two 12-inch sections (4 1/2 inches wide). These sections were processed and molded side by side to yield 9-inch by 12-inch panels.

The first step in fabricating ADL-10 is the removal of the Teflon coating on the quartz Omniweaves. This is accomplished by burnoff at 900°F in an air circulating oven. After burnoff, the Omniweave is immersed in a solution of 65 percent by weight SR-350 silicone resin in reagent grade acetone. This resin solution is filtered prior to use to remove insoluble contaminants. After submerging the Omniweave, vacuum is applied to the liquid head. The acetone level of the resin solution is reduced via vacuum and cold trapped until the solution is approximately 90 percent by weight resin solids. The omniweave fabric is kept completely submerged in the resin solution during this processing phase in order to attain a thorough penetration of the resin into the fabric with the maximum possible resin solids pickup. In order to keep a liquid head over the Omniweave, an excess volume of resin solution is used to allow for the volume decrease of the solution during solvent reduction.

When solvent reduction has proceeded to the appropriate level (90 percent solids solution), the thoroughly impregnated fabric is removed from the vacuum impregnation chamber. The thoroughness of the impregnation is evident from the transparency of the wetted quartz Omniweave. The panel is then "B" staged at 200°F for 4 hours in an air circulating oven. This treatment removes the residual acetone and advances the resin cure so that excessive resin flow will not occur during compression molding.

---

*The formulation details of ADL-10 are found in greater detail in Ref. 2 and are briefly reviewed here.

(1)General Electric Co., Silicone Products Department

The impregnated and staged fabric is loaded into an aluminum compression mold preheated to 200°F. Fluorocarbon spray type MS-122[1] is used as the release agent. No pressure is applied for 15 minutes to allow the part and mold temperature to equilibrate. Pressure is then applied to compress the weave to a predetermined thickness based on the initial Omniweave fabric density and thickness. The ADL-10 panel is then given the following cure cycle:

250°F - 1 hour

325°F - 1 hour

400°F - 16 hours

2.3.1 ADL-10 MOLDING RATIONALE

During our previous studies of the molding parameters for ADL-10 composites (Ref. 2) it was found that molding pressure should be proportional to the Omniweave fabric density and that a final molded product with a nominal 68 percent quartz fiber volume fraction was optimum for a 45°/45° cubic 4-D Omniweave. The important micro-mechanical consideration was that the individual fibers were not to be crimped in their unit cells, preventing them from uniformly taking up an applied stress.

A first molding of weave 402 at the nominal 1000 psi pressure reported in Reference 2 for panel 331-2 resulted in an unexpectedly high compression of 41 percent and a correspondingly high fiber volume fraction of 74 percent. This was a smooth-finished plate, equivalent or better in this regard than those produced in previous work (Refs. 1 and 2). Closer scrutiny of the molding history of panel 331-2, produced from a 0.79 gm/cc, comparatively lower density quartz Omniweave, showed that it had been "molded to stops", i.e., to a predetermined thickness constrained by mechanical mold thickness blocks, regardless of applied pressure. The purpose of this had been to achieve a fiber volume fraction near the (nominal) optimal 68 percent. The 331-2 panel at 1.64 gm/cc was found to be lower than desired in density and was reimpregnated and cured to a "final process density"[2] of 1.68 gm/cc, still of course at the same 68 percent fiber volume fraction.

It was therefore decided to compute the uniaxial compression of the panels which was required to give this nominal 68 percent fiber volume fraction as a function of starting quartz Omniweave density. Figure 8 shows the relationship between

---

[1] Miller Stephenson Chemical Co., Inc.

[2] Pg. 2-31, Reference 2

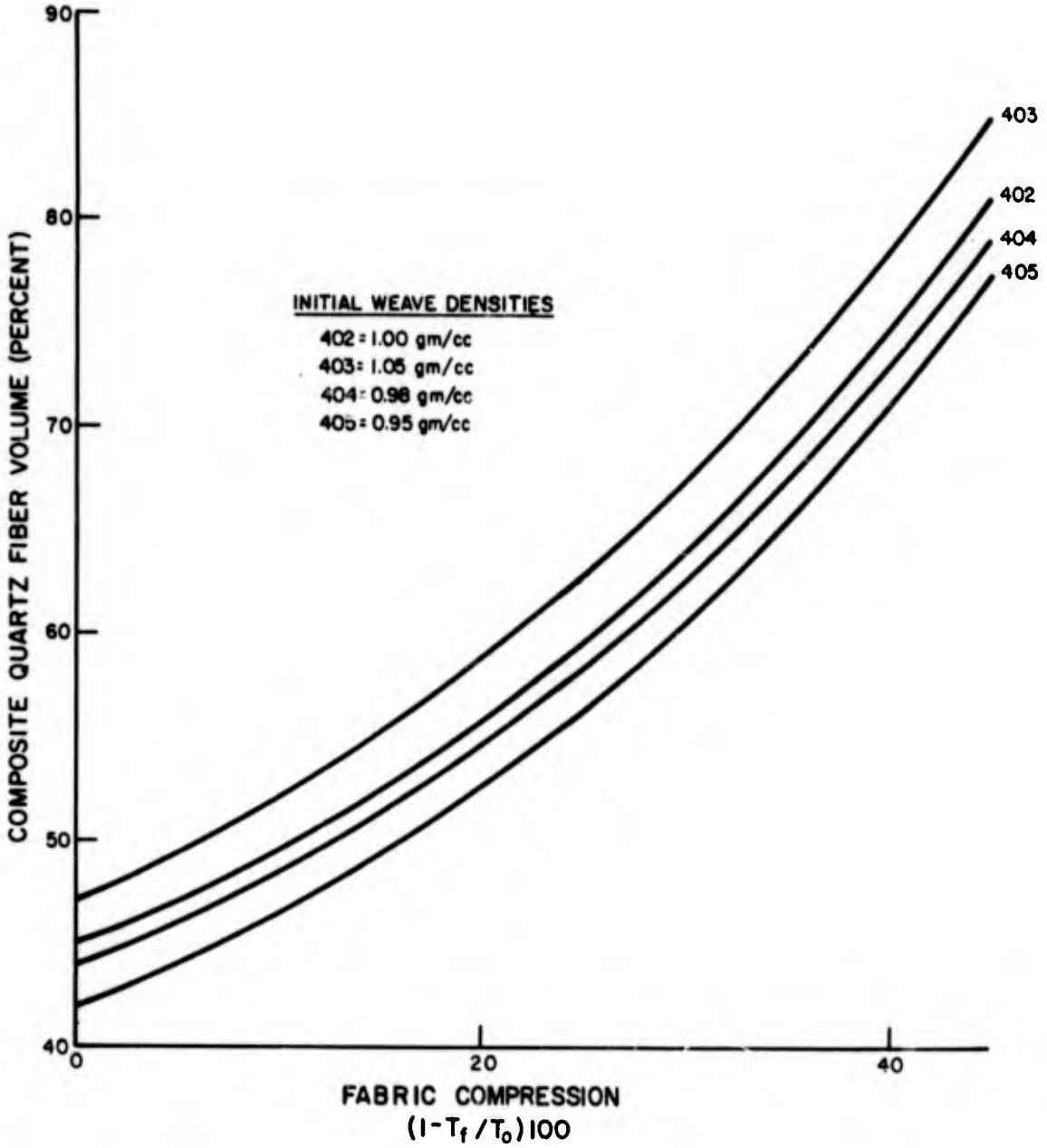

Figure 8. Composite Quartz Fiber Vol. % vs. Compression % for Omniweave Fabric used in ADL-10

quartz fiber volume fraction in the cured panel vs. the amount of compression ($1-T_f/T_o$) of the quartz Omniweave fabric during cure. This chart was used as a guideline in processing the ADL-10 panels. Note that it is based on a thickness compression and does not include consideration of lateral dimension changes.

Two Omniweave strips, no. 402 and 405, were molded under a high pressure (900 psi) to yield ADL-10 panels with a high volume percent of quartz fibers and smooth, finished surfaces as molded. Omniweave strips no. 403 and 404 were processed to yield panels containing the maximum fiber volume with minimum fiber distortion.

Analysis of the ADL-10 composite system by Materials Sciences Inc. (Section 4) indicates that all three Omniweave dimensions must be altered to obtain the maximum fiber volume with no fiber distortion in the cured panel. Note that these changes do not occur spontaneously, i.e., the panels do not automatically compensate for a compression in thickness with a corresponding decrease in width and increase in length. Since the tooling required to accomplish a simultaneous three dimensional change (compress thickness and width and extend length) during cure was beyond the scope of this program, only thickness changes were considered. Also, based on previous experience (Reference 2), a minimum of 60 vol percent quartz fiber in the finished panel was established, preferring to avoid over-compression uncertainties in the next molded panels. Considering these criteria, panels 403 and 404 were compressed only enough to yield 60 vol percent fiber in the panel. In molding, calibrated blocks were used to stop the mold travel at the desired thickness.

After tensile testing of bars cut from these three moldings showed lower strength than expected, an extra section (8 in. long) of quartz Omniweave fabric no. 405 was treated with a silane coupling agent prior to impregnation and cure. The processing history of this fabric section was the same as the previous fabrics except that after the Teflon burnoff was completed, the fabric was immersed in a 1 percent by weight solution of A1100[3] silane in distilled water. After a 15-minute immersion the fabric was dried at 220°F for 4 hours, then impregnated and molded.

Table 3 lists the processing variables and the actual resultant physical characteristics of the ADL-10 panels fabricated.

2.4.1 SILICA MATRIX FROM LUDOX COLLOIDAL SILICA

2.4.1.1 Matrix Characterization and Process Formulation

Several quartz Omniweave constructions were rigidized by impregnation with a colloidal silica sol, drying and then firing at high temperature to obtain a rigid silica matrix. Two types of Omniweave geometries were evaluated: the 4-D cubic and 5-D cubic

---

[3] Union Carbide

TABLE 3. PROCESSING AND PHYSICAL CHARACTERISTICS OF ADL-10 PANELS

	ADL-10 Panel No.				
Omniweave Fabric No.	402	403	404	405	405-2S
Omniweave Fabric Density (gm/cc) (post pyrolysis)	1.00	1.05	0.98	0.95	1.03
Cure Pressure (psi)	900	20 (to stops)	40 (to stops)	900	60 psi (to stops)
% Compression $(1-T_f/T_o)$ 100	41	22	26	44	25
Panel Density (gm/cc)	1.93	1.68	1.64	1.90	1.72
Quartz Fiber-wt. %	85	81	81	87	72
Resin - wt. %	15	19	19	13	28
Quartz Fiber-vol. %	74	62	61	75	56
Resin-vol. %	23	25	25	19	38
Porosity-%	3	13	15	6	6
Fiber Pitch Angle (deg) (surface angle)	40	43	40	40	40
Through Thickness Angle (deg) (surface angle)	25	35	30	-	37

(1) A 1100 silane coupling agent

constructions. Two types of colloidal silica sols were used in the rigidization process: Ludox HS-40[1] (sodium stabilized) and Ludox AS[1] (ammonium stabilized). Table 4 and Figure 9 show the chemical and physical properties, taken from vendor literature, for each type of silica sol used. Each silica sol was evaluated in the as-received form and in a purified form where harmful soluble impurities were removed via an ion exchange resin. The sodium content for each type of silica sol in the commercial and purified form was determined by flame emission spectrometry analysis. This data is given in Table 5.

This atomic flame emission spectroscopic technique was developed for determination of the alkali content of high purity silica fibers for the Space Shuttle Thermal Protection System application because of inadequate accuracy of emission spectroscopy analysis where the sample is sparked or arced within a matrix of carbon. The flame emission technique has been demonstrated to have extreme sensitivity and reproducibility of results in this low range of applicable ppm sodium ion concentrations.

The rigidization process was essentially the same for all parts that were densified with colloidal silica sols. The quartz Omniweave fabric was vacuum impregnated with the silica sol, then dried at 180°F for 4 hours. Parts were then fired at either 650°C or 850°C for 4 hours. This cycle was repeated until the specified density was attained. Following are the systems and process variables evaluated in this phase.

2.4.1.2 Composite Characterization

2.4.1.2.1 4-D Cubic Quartz Omniweave/Ludox HS-40

In this first series, 6 in. x 3/4 in. x 1/2 in. tensile bar size sections of Omniweave strip no. 381 were rigidized to three discrete nominal density levels of 1.2, 1.4 and 1.7 gm/cc by multiple cycles of impregnating with Ludox HS-40, drying and firing. The purpose of this gradation of densities was to test the "space-frame" silica-silica composite hypothesis for a ceramic composite advanced in Paragraph 4.7 of Reference 2, "Analysis of Markite". It will be shown below that this hypothesis was more thoroughly tested with the improved matrices obtained with the AS Ludox formulation on both 4-D and 5-D composites.

The processing variables and characteristics of each part are listed in Table 6.

---

[1] E.I. DuPont de Nemours and Co., Inc.

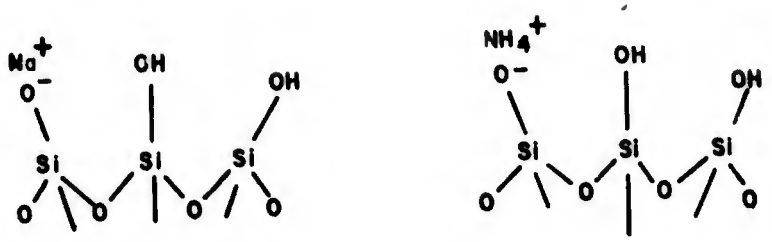

Figure 9. Surface Configuration and Ionic Stabilization of the Colloidal Particles of Silica in Water[1]

TABLE 4. PROPERTIES OF LUDOX COLLOIDAL SILICA (TECHNICAL)[1]

Property \ Type	HS-40	AS
Stabilizing Counter Ion	Sodium	Ammonium
Particle size, mμ	13 - 14	13 - 14
Specific Surface Area, sq. m/g	210-230	210-230
Silica (calculated as SiO_2), wt %	40.0	30.0
pH at 25°C (77°F)	9.7	9.6
Titratable Alkali (calculated as Na_2O), wt. %	0.43	(c)
SiO_2/Na_2O (by wt.)	93	120 (d)
Chlorides (calculated as NaCl), wt. %	0.01	0.002
Sulfates (calculated as Na_2SO4), wt. %	0.06	0.003
Viscosity at 25°C (77°F) CP (e)	17.5	20
Weight/Gallon at 60°F (16)	10.8	10.1

(c) 0.25% calculated as NH_3

(d) SiO_2/NH_3 (by wt.)

(e) Centipoise, as measured by an Ostwald (Cannon-Fenske) Pipette size depending on viscosity range

[1]Data taken from DuPont Product Bulletin #A-61777

TABLE 5. SODIUM IMPURITY LEVELS IN LUDOX SOLS, BY ATOMIC FLAME EMISSION

Silica Sol Type	Na Ion ppm
Ludox HS-40	6450
Ludox HS-40 (purified)	400
Ludox AS	950
Ludox AS (purified)	85-130

TABLE 6. CHARACTERIZATION OF HS-381 COMPOSITES: THREE DENSITIES

Part ID	Initial Weave Density (gm/cc)	FPA (deg)	TTA (deg)	No. of Densification Cycles	Firing Temp. (°C)	Final Density (gm/cc)	Fiber (vol. %)	Porosity (%)
HS-381-1	0.95	43	44	↑	↑	1.15	43	48
HS-381-2	0.97	43	44	2	850	1.19	43	48
HS-381-3	0.97	43	44	↓	↓	1.25	44	43
HS-381-4	0.96	43	44	↑	↑	1.46	44	33
HS-381-5	1.01	44	44	3	850	1.40	46	37
HS-381-6	0.97	44	44	↓	↓	1.42	44	36
HS-381-7	0.96	44	44	↑	↑	1.68	44	23
HS-381-8	0.99	43	44	7	850	1.68	45	24
HS-381-9	0.95	43	44	↓	↓	1.80	43	18
HS-381-10	1.05	43	44	↓	↓	1.65	48	25

2.4.1.2.2 4-D Cubic Quartz Omniweave/Ludox HS-40 (purified)

The Ludox HS-40 colloidal silica sol was purified by passage through a cation exchanging column[1] prior to impregnating the Omniweave reinforcement. One 6 in. x 5/8 in. x 5/16 in. section of Omniweave strip no. 400 was densified using the standard procedure. The data are given in Table 7.

TABLE 7. CHARACTERIZATION OF HSDI-400-1 COMPOSITE

Part ID	Initial Weave Density (gm/cc)	FPA (deg)	TTA (deg)	No. of Densification Cycles	Firing Temp. (°C)	Final Density (gm/cc)	Fiber (vol. %)	Porosity (%)
HSDI-400-1	0.99	40	40	10	650	1.70	45	23

2.4.1.2.3 4-D Cubic Quartz Omniweave/Ludox AS

Three flexure specimens were prepared from quartz Omniweave strip no. 400 by multiple cycles of the standard densification process using Ludox AS silica sol as the impregnant. The finished specimens were 6 in. x 5/8 in. x 5/16 in., to be tested in long bar flexure. The characterization is listed in Table 8.

TABLE 8. CHARACTERIZATION OF AS-400 COMPOSITES

Part ID	Initial Weave Density (gm/cc)	FPA (deg)	TTA (deg)	No. of Densification Cycles	Firing Temp. (°C)	Part Density (gm/cc)	Fiber (vol. %)	Porosity (%)
AS-400-1	↑	↑	↑	↑	↑	1.67	45	24
AS-400-2	0.99	40	40	6	650	1.70	45	23
AS-400-3	↓	↓	↓	↓	↓	1.72	45	22

[1] No. 9034 Demineralizer Cartridge, Barnstead Sybron Corporation.

2.4.1.2.4 5-D Cubic Quartz Omniweave/Ludox AS

Several small panels of quartz Omniweave fabric no. 401 (5-D construction) were densified using Ludox AS colloidal silica and the standard densification cycle. Panels were removed from the processing cycle at 1.2, 1.4 and 1.7 gm/cc to evaluate the density and porosity effects on mechanical strength and to compare to the above mentioned "space-frame model". The data are listed in Table 9.

TABLE 9. CHARACTERIZATION OF 5-D QUARTZ OMNIWEAVE/LUDOX AS COMPOSITES

Part ID	Initial Weave Density (gm/cc)	FPA (deg)	TTA (deg)	No. of Densification Cycles	Firing Temp. (°C)	Part Density (gm/cc)	Fiber (vol. %)	Porosity (%)
AS-401-1	↑	↑	--	2	↑	1.17	38	47
AS-401-2	0.84	41	--	3	650	1.39	38	37
AS-401-3	↓	↓	--	8	↓	1.70	38	23

2.4.1.2.5 4-D Cubic Quartz Omniweave/Ludox AS (purified)

The Ludox AS colloidal silica was purified by removing cationic contaminants via an ion exchange resin. Rexyn 101(H)[1], a strong acid cation exchange resin, was added to the silica sol in the ratio of 5 parts by weight silica sol to 1 part by weight ion exchange resin. This first exchange was allowed 24 hours for completion. The sodium content of the sol was reduced from 950 to 188 ppm. The spent ion exchange resin was filtered off and fresh resin added in the previous ratio. This second exchange was allowed 48 hours for completion. The sodium content of the sol was further reduced to 85-130 ppm after the double exchange.

Several 6 in. x 5/8 in. x 5/16 in. long bar flexure strips from Omniweave fabric no. 400 and a 4 in. x 4 in. section of Omniweave fabric no. 404 were densified using the standard process.

---

[1] Fisher Scientific Company

A photomicrograph of a polished 0.4 in. x 0.5 in. section of a flexure bar from ASDI panel 404-2 is shown in Figure 10a along with a higher magnification (25x) scanning electron micrograph (SEM) of a similar section in which the individual 8 micron diameter filaments are visible in the hexagonally distorted fiber bundles.

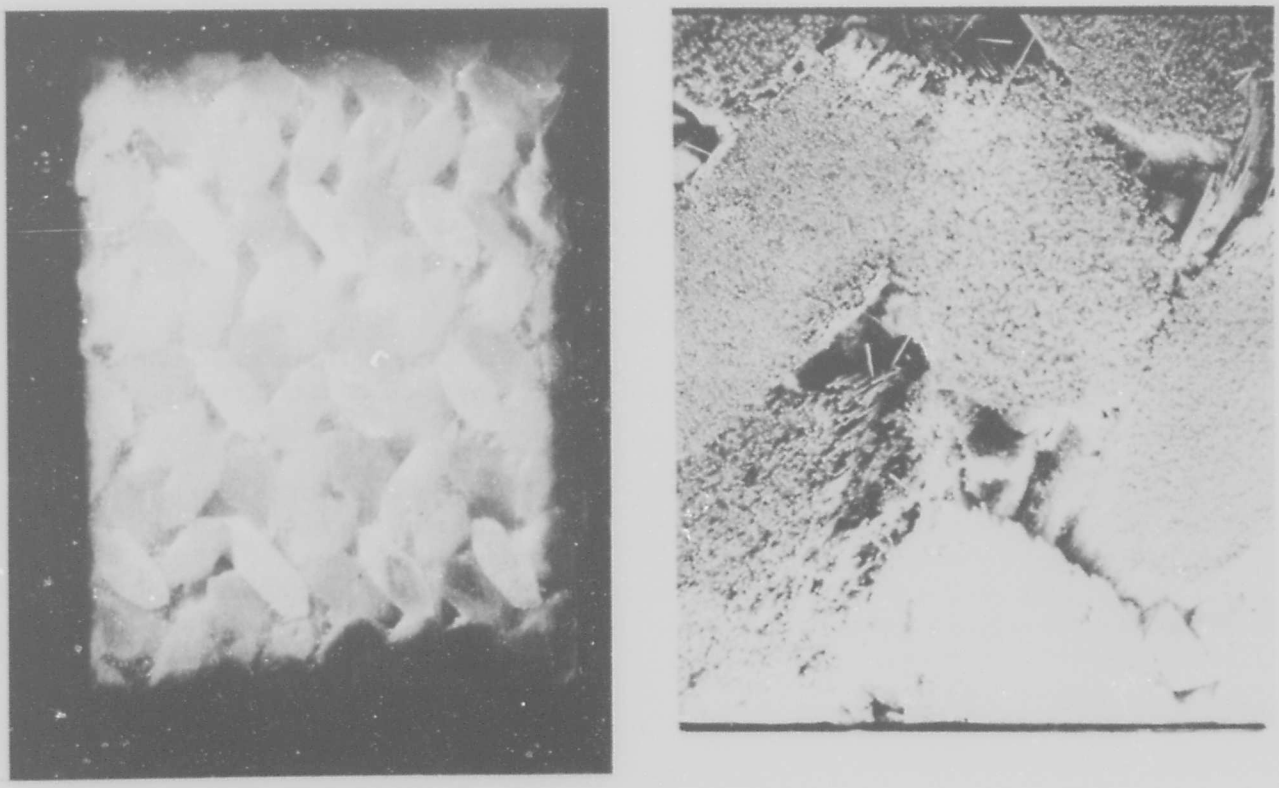

(a) (b)

Figure 10. a) Photomicrograph of polished 0.4 x 0.5 section of flexure bar from ADL-4D6 ASDI panel 404-2.

b) SEM (25X) of similar section showing individual 8 micron diameter filaments in fiber bundles

The characterization data for all the deionized AS Ludox composites is given in Table 10.

TABLE 10. CHARACTERIZATION DATA FOR DEIONIZED AS LUDOX/QUARTZ OMNIWEAVE COMPOSITES

Part ID	Initial Weave Density (gm/cc)	FPA (deg)	TTA (deg)	No. of Densification Cycles	Firing Temp. (°C)	Part Density	Fiber (vol. %)	Porosity (%)
ASDI-400-1	↑	↑	↑	↑	↑	1.70	45	23
ASDI-400-2	0.99	40	40	6	650	1.65	45	25
ASDI-400-3	↓	↓	↓	↓	↓	1.71	45	22
ASDI-404-2	0.98	45	45	↓	↓	1.58	44	29

2.4.2 SILANE-DERIVED SILICA MATRIX

2.4.2.1 Matrix Formulation

Earlier work has shown the feasibility of producing a high density silica matrix for multidimensional quartz woven structures by the controlled pyrolysis of SR-350, a highly trifunctional methyl-silicone resin (Ref. 2).

The primary benefit in the utilization of organic polymers for the generation of an SiO_2 matrix is the reactivity of the "nascent" silica formed during the decomposition of the polymer.

The silica thus formed is able to chemically react with the fiber reinforcement at much lower temperatures than is possible using particulate (not colloidal) inorganic silica fillers that require temperatures above 1200°C to react in the solid state. In this earlier work the resin was impregnated into the fiber construction in the form of a partially polymerized resin solvent solution.

Silica monofilaments, because of their highly polar surface, are covered with an adsorbed water layer up to 100 molecules thick. This hydrated type of surface, shown diagrammatically in Figure 11, however, prevents reaction of the hydrophobic methyl silicone polymer solution with the fiber surface. To increase the adhesion a silane coupling agent such as acetoxy ethyl-triacetoxy-silane was first applied to the fibers and then the fiber bundles were impregnated with the silicone resin solution (Ref. 2).

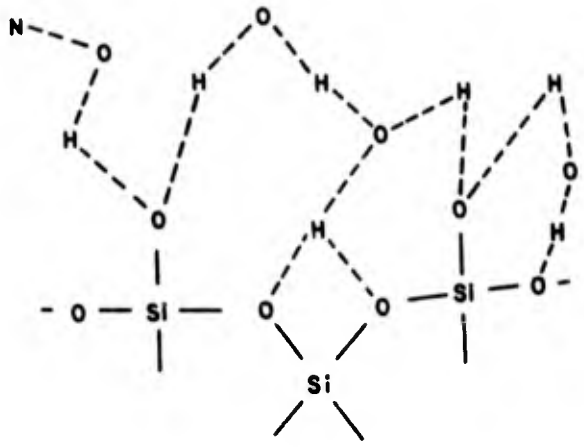

Figure 11. Hydrated Silica Surface

An alternate approach to this technique which eliminates the requirement for a coupling agent and guarantees the direct chemical linkage between the silicone matrix and the fiber reinforcement is the "in-situ" formation of a methyl silicone polymer within the fiber construction. This can be accomplished by reaction of the water layer on the fibers with a halogenated silane impregnant. Since the final objective is to produce an SiO_2 matrix by decomposition of the polymer formed, methyl-trichlorosilane (CH_3SiCl_3) which hydrolyses to a completely trifunctional polymer is the preferred reactant. This reaction takes place theoretically as shown in Figure 12.

The reaction in Figure 12 represents just one silane molecule; however, this reaction continues until all available water is reacted, forming a very large three-dimensional polymer network as shown in Figure 13.

Pyrolysis of the resin thus formed will result in the maximum reaction between the fiber reinforcement and the "nascent" silica.

Figure 14 shows a differential thermal analysis run of the silicone polymer from the hydrolysis of the methyl-trichlorosilane. The large exothermic reaction beginning at approximately 390°C (734°F) is the oxidation of the methyl group in the polymer chain.

When pyrolyzed at temperatures less than 700°C (1300°F) the silica thus formed is rigidly connected to the silica filaments but not strongly attached to itself since the silica matrix density is very low when compared to the theoretical density of fused silica. Densified composites based on relatively high density silica reinforcement produced with a silica matrix by this process can then be expected to have an effective lower modulus and increased strain capability because of the weak cohesive nature of the fine colloidal matrix. The experience cited in Reference 2 with the Markite series of silica-silica composites showed that tenacious bonding of the pyrolyzed

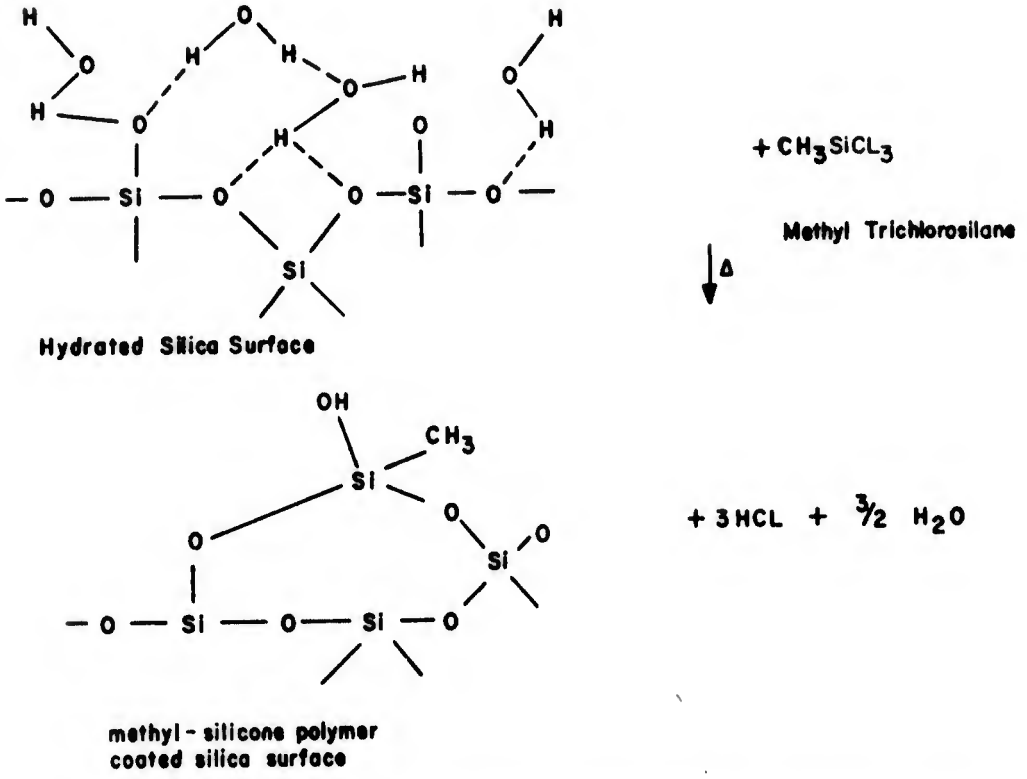

Figure 12. Reactions Between Methyl-Trichlorosilane and Hydrated Silica Surface

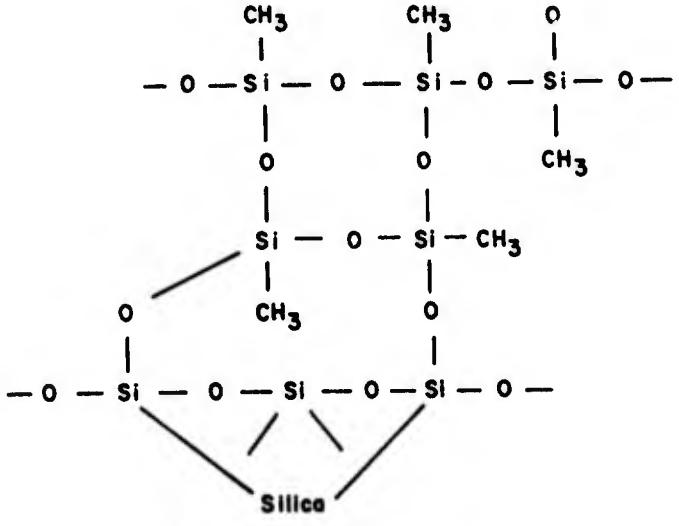

Figure 13. Silica Substrate Coated With Methyl Silicone Polymer Binder

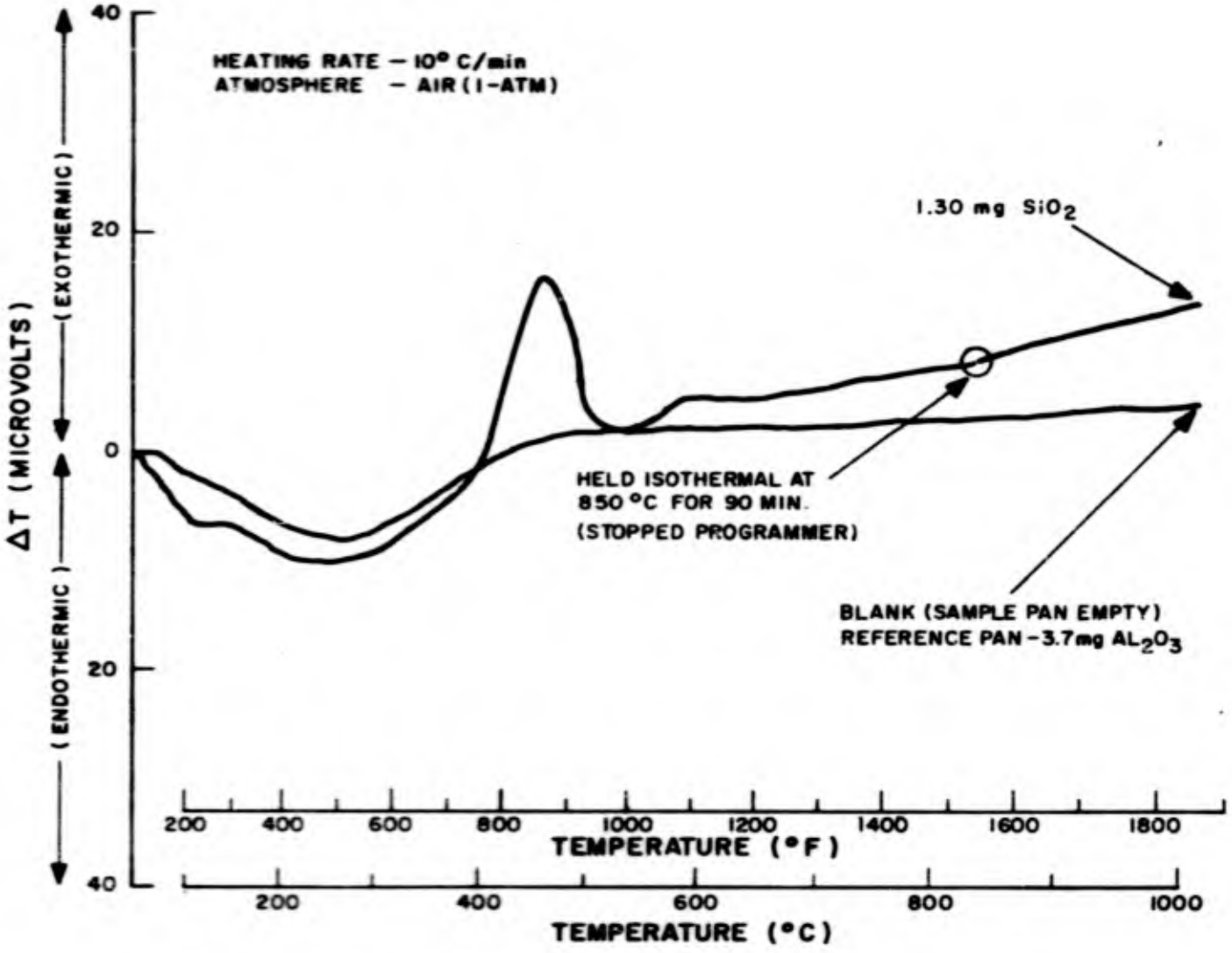

Figure 14. DTA of Silicone Polymer from Methyl-Trichlorosilane

SR-350 derived matrix to the etched silica fibers did not give satisfactory strengths and also did in fact give very low strains to failure, e.g., 0.03 to 0.28 percent (pg. 3-49, Ref. 2). The photomicrographs of these composites showed smooth, uncracked sections of matrix over spans equal to several filament diameters with smooth meniscus matrix-fiber wetting, in contrast to the more granular matrix postulated above for silane-derived matrices.

2.4.2.2 Composite Fabrication and Characterization

Several processing techniques were investigated in an attempt to densify quartz Omniweave parts via the deposition and hydrolysis of methyl-trichlorosilane[1]. Essentially each technique involved the deposition and hydrolysis of methyl-trichlorosilane to form a trifunctional methyl silicone polymer, then pyrolysis to form the silica matrix. The basic difficulty in this approach was found to be the relatively small density increase per processing cycle. These density increases become even smaller with the number of processing cycles. Three techniques, were used in densifying segments of quartz Omniweave no. 381. They are shown diagrammatically in Figure 15.

In technique number one the fiber construction was placed in a 98 percent relative humidity chamber for 48 hours. The humidity was maintained by a saturated $Pb(NO_3)_2$ solution held at 68°F.

The part was then placed in a reaction chamber where methyl-trichlorosilane saturated nitrogen gas was passed over and around it. The methyl-T reacted with the absorbed water layer on the fibers, forming the methyl silicone polymer. The reaction by-product is gaseous HCL which was then scrubbed in a triethanolamine/water mixture. The treated specimen was removed from the chamber and heated at a controlled rate up to 950°F in a closed but not sealed container. The objective was then to repeat the entire process until the density was achieved.

A length of quartz Omniweave strip 381 taken from the top of the woven section was treated for 72 hours in a 98 percent constant relative humidity. Specimen weight after treatment was 10.105 gm, density = 1.01 gm/cc. After vapor phase silanization specimen weight was 10.09 gm., density = 1.01 gm/cc. The fact that an actual weight loss was measured indicated that some of the water within the Omniweave specimen was driven off in the Methyl-T/N_2 gas stream prior to reaction.

Thus minimal methyl silicone resin was deposited on the individual monofilaments within the construction. From this data point it is apparent that a significant number of iterations would have been required to raise the specimen density to 1.2-1.3 grams/cc using this technique. A modification of this technique was therefore made for increased polysiloxane deposition.

---

[1] General Electric SC3003 methyltrichlorosilane.

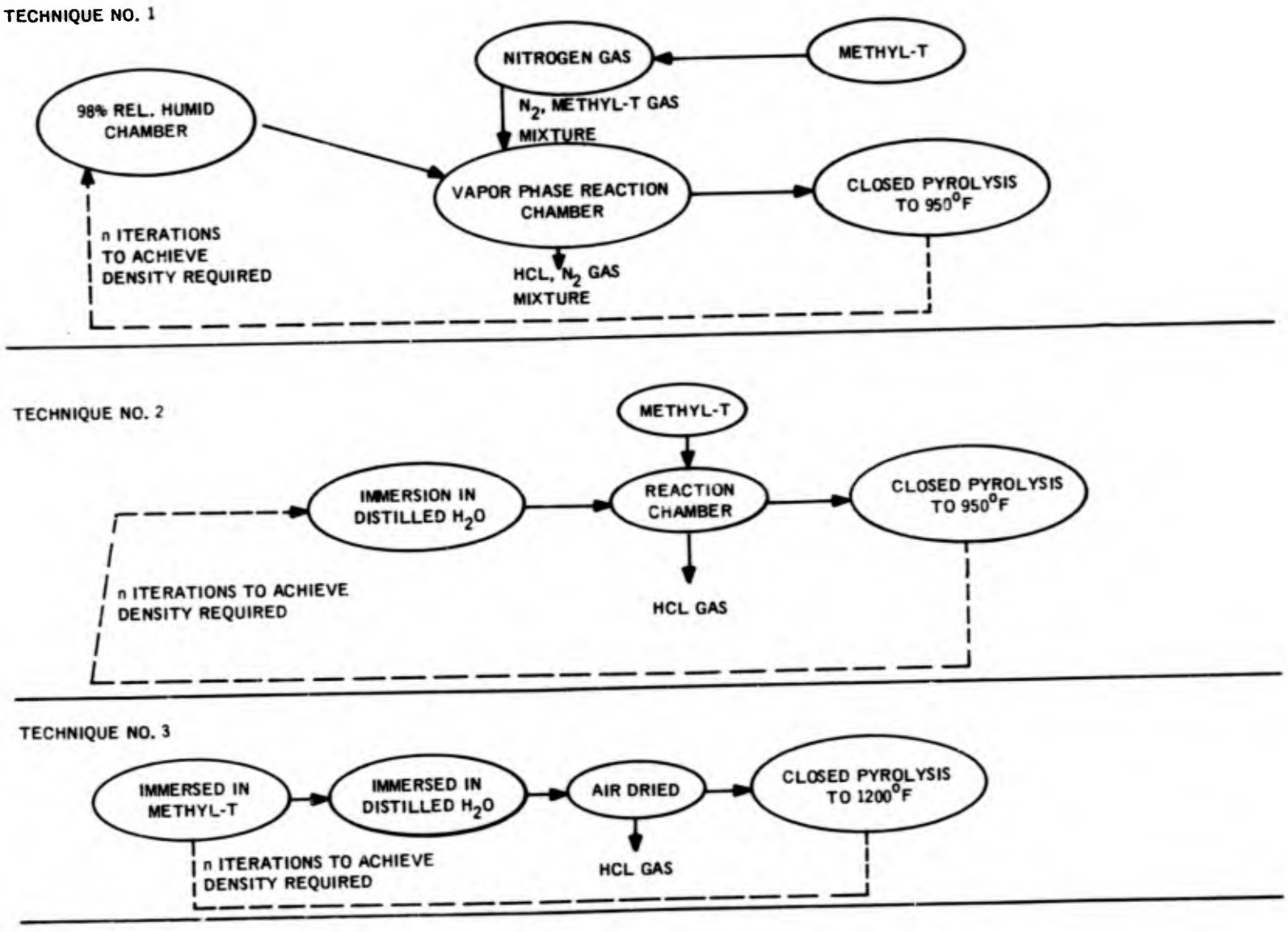

Figure 15. Three Variations of Resin Formation Technique for Silica Matrix

In the second technique, the quartz Omniweave was first immersed in distilled water, then in methyl-trichlorosilane, air dried and pryolyzed to 950°F. Parts treated by this process increased 2 to 5 percent in weight after 3 densification cycles. The parts listed in Table 11 were densified and submitted for flexure testing.

TABLE 11. CHARACTERIZATION OF FIRST SERIES OF SILANE-DERIVED SILICA/QUARTZ OMNIWEAVE COMPOSITES

Part ID	Initial Weave Density (gm/cc)	FPA (deg)	TTA (deg)	No. of Densification Cycles	Firing Temp. (°F)	Fiber (vol. %)	Porosity (%)	Final Density (gm/cc)
MTS-381-1	0.98	43	44	3	950	44	54	1.01
MTS-381-2	1.00	44	44	3	950	45	52	1.05

After flexure tests showed the low strength to be expected from the density shown in Table 11, but high strain to failure, the parts listed were subjected to a third impregnation technique in an attempt to increase the density significantly above the 1.05 gm/cc level. A flow diagram of this technique is shown in Figure 15. The specimens were first immersed in methyl-trichlorosilane, then distilled water, air dried and pyrolyzed to 650°C. Parts treated by this process increased an average of 7 percent in weight over 4 densification cycles. The parts listed in Table 12 were densified and submitted for flexure testing.

TABLE 12. CHARACTERIZATION OF SECOND SERIES OF SILANE-DERIVED SILICA/QUARTZ OMNIWEAVE COMPOSITES

Part ID	Initial Weave Density (gm/cc)	FPA (deg)	TTA (deg)	No. of Densification Cycles	Firing Temp. (°F)	Fiber (vol. %)	Porosity (%)	Density (gm/cc)
MTS-381-1A*	1.01	43	44	↑	↑	44	49	1.13
MTS-381-2**	1.05	44	44	4	650	45	50	1.10
MTS-381-1B*	1.01	43	44	↓	↓	44	50	1.11

*3-inch halves of 6-inch long flexure bar MTS-381-1.
**5-inch long portion of long flexure bar MTS-381-2 which broke at end in flexure test.

2.4.3 MARKITE HYBRIDS

2.4.3.1 The Markite "Hybrid" Process

In both References 1 and 2 studies were performed on the transformation of ADL-10 composites, with their single major limitation of an upper heat flux limit of 100 Btu/ft^2-sec for RF transmission, to an inorganic silica-silica composite designated "Markite". The studies tracked the variation of the flexure strength of the composite

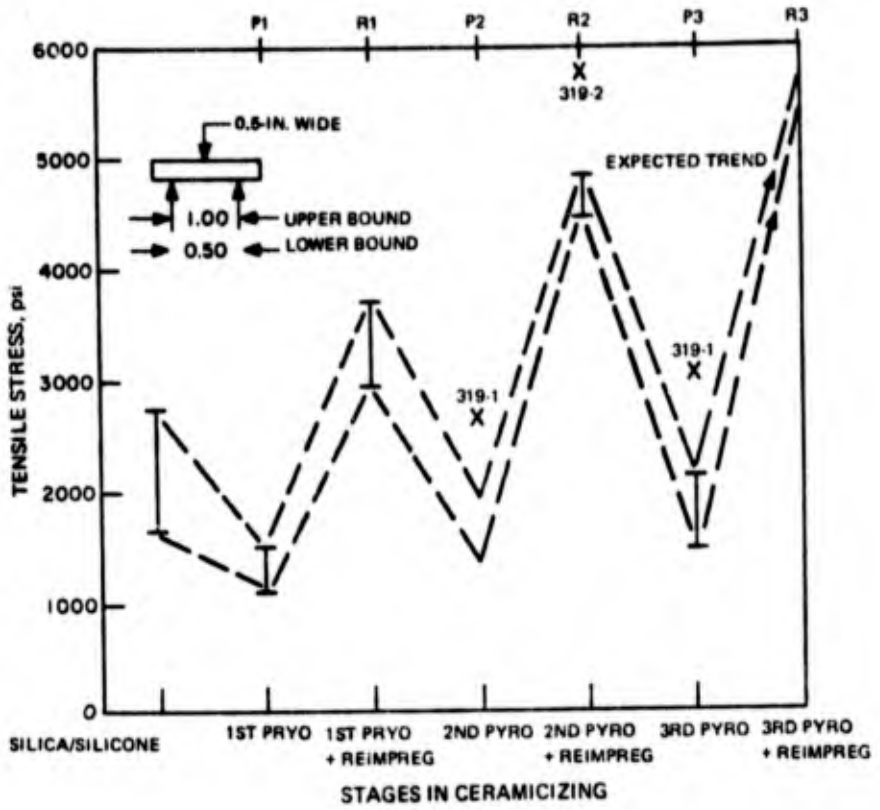

Figure 16. Silica/Silicone Transformation, Short Beam Flexure; Tensile Stress at Failure as a Function of Processing Operations, Reference 2 Values Superimposed on Data from Reference 1.

in successive pyrolysis and reimpregnation states, represented in the double sawtooth curve of Figure 16, identical to Figure 44 of Reference 2. It was found that fully pyrolyzed Markite P1, P2 or P3 (for pyrolyzed once, twice and three times following impregnations) did not increase in strength satisfactorily at all, despite achieving densities as high as 2.0 gm/cc after only 2-3 cycles. This trend is indicated by the lower bound of the sawtooth curve. But the reimpregnated version did increase appreciably with strength, achieving levels as high as 5900 psi in the R2 state (second reimpregnation after two pyrolysis cycles), as indicated by the upper bound of the sawtooth curve and the point "319-2".

In the Markite densification process successive cycles produce diminishing increases in density in both the reimpregnated and pyrolyzed state. This limiting process of densification was discussed above in Paragraph 2.4.1 and compared to the Ludox colloidal silica densification process. Because of the very slight increment of composite density in the R2 or R3 state, it was hypothesized that the very small actual resin content of a reimpregnated Markite "hybrid" should then display negligible dielectric loss properties, even at high levels of transient aerodynamic heating. This hypothesis was partially confirmed (Tables 30, 31 of Ref. 2) by post-ablation dielectric measurements; but these were in part complicated by the transient testing experimental difficulties and the low pyrolysis temperature of one of the samples. The latter of these two difficulties has been eliminated in the present study by a final pyrolysis temperature of 1600°F maintained for 1 hour; the first by performing accurate steady state cavity measurements, while placing emphasis on continued improvement of mechanical strength.

In addition to the standard hybrid process based on reimpregnation with SR-350 it was decided to also study a final reimpregnation with methyl-trichlorosilane (CH_3SiCl_3). The chemistry and basis for use of this compound as a source of matrix silica for a silica-silica composite are discussed in section 2.4.2. It is evident from that work that it is not a high silica yield process, but the ease of penetration observed for silane solutions suggests its use as the final reimpregnant in a hybrid version. The RF/ablation properties also call for investigation as an alternative to SR-350 resin.

2.4.3.2 Selection of ADL-10 Material for Markite Process

The Markite hybrid samples of Reference 2 gave improved strength over those studied in Reference 1. This is very obviously attributable to the improved strength of the parent ADL-10 material of the second study, itself due to improved Omniweave fabric densities and weaving and composite molding techniques.

To achieve the twin objectives of beginning with the highest strength ADL-10 and also taking advantage of already well characterized material, the set of tensile bar specimens identified as "Phase 1 - Series 2" in the previous study were utilized as the base ADL-10 stock for the hybrid processing study. The detailed tensile strength vs. reinforcement angle dependence of these samples is shown in Figure 17 (reproduction of Fig. 38, Ref 2). Flexure bars in the standard 1/2 inch wide by 1-1/2 inch long dimensions previously used for three-point flexure testing were machined from these 5 inch long tensile specimens, avoiding the fracture edges. It will be seen below that this sampling was further specialized to the 1 percent silane-coupled specimens that had not undergone plate-slap testing.

It should also be noted that in the previous work no directional dependence of the flexural strength of Markite composites had been observed, (Table 24, Ref. 2), despite the very steep dependence obvious in Figure 17 for the parent ADL-10.

2.4.3.3 Markite Hybrid Processing and Characterization

ADL-10 mechanical test specimens, fabricated and tested in the previous program (Ref. 2, pg. 2-22) were used as the starting materials for the Markite hybrid fabrication. Fifteen failed ADL-10 tensile bars were pyrolyzed at 900°F for 16 hours to burn off the glass epoxy bonded doublers. Forty-four flexure (Fig. 18) bars were then machined from the pyrolyzed ADL-10 material. These parts were then vacuum impregnated with a 65 percent by weight SR-350 silicone resin in acetone solution, air dried for 4 hours, then oven dried at 160°F for 16 hours. The parts were then cured and pyrolyzed as follows:

400°F	- 24 hrs
400°F - 900°F	- 100°F/hr
900°F - 1600°F	- 200°F/hr
1600°F	- 1 hr

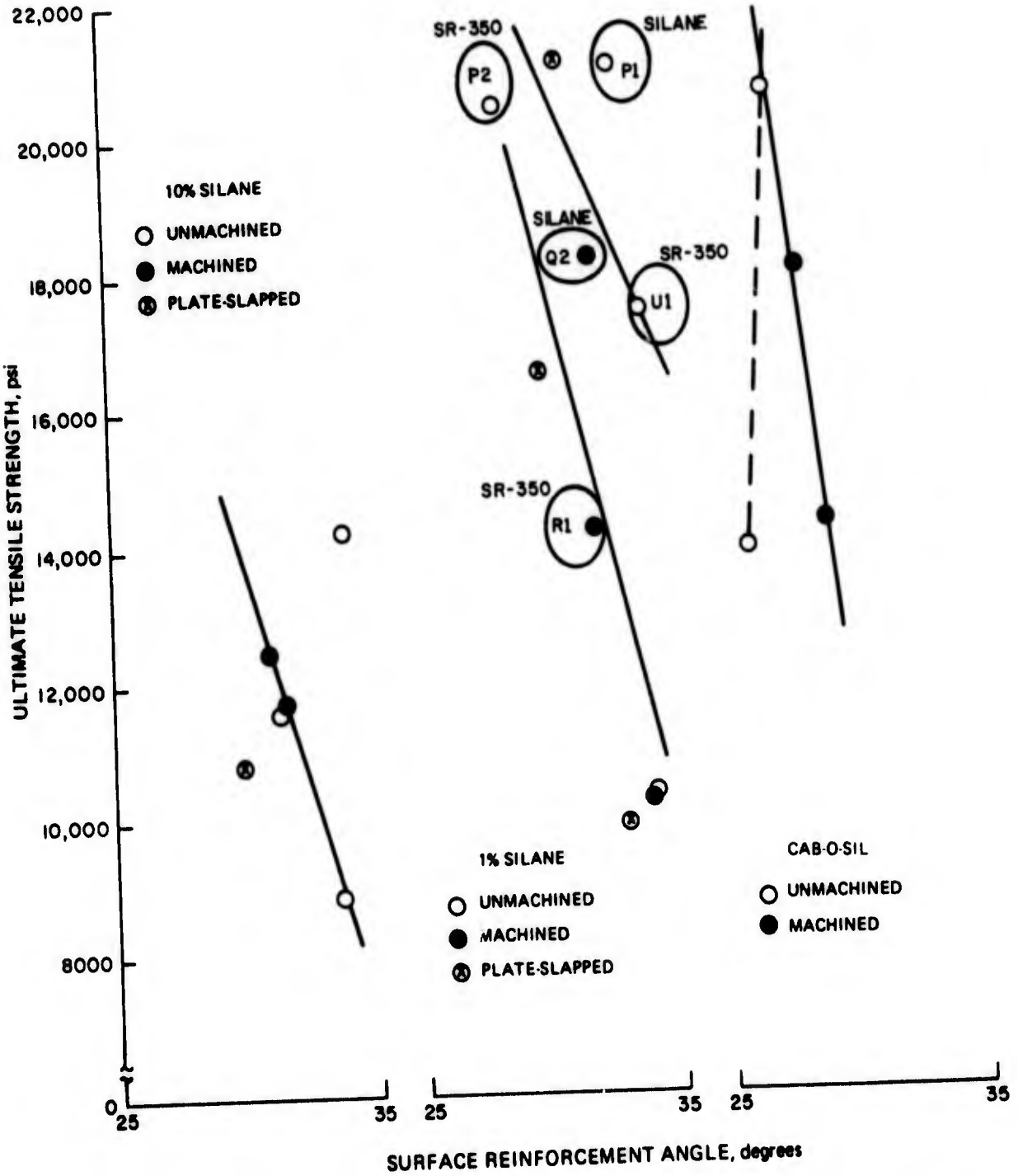

Figure 17. Ultimate Tensile Strength vs. Surface Reinforcement Angle, Series 2 Specimens from Ref. 2; Showing Selection of ADL-10 from 1% Silane Group for Markite Hybrid Study

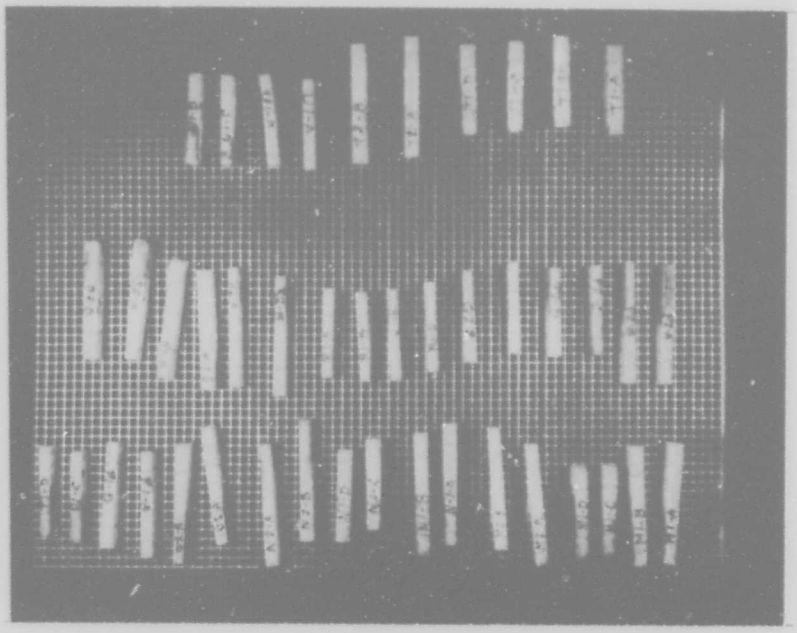

Figure 18. Flexure Bars Ready for Vacuum Impregnation

After undergoing three of the above cycles (vacuum impregnation through pyrolysis), the parts were inspected and 18 flexure bars were selected for further processing. This sampling was done on the basis of selection from only the 1% silane-coupled series 2 bars, symmetrically taken for silane and SR-350 as shown in Figure 17. The samples were divided into 2 groups; the first to be further densified through silanization and the second by silicone resin impregnation (the standard Markite hybrid process). A processing flow chart is shown in Figure 19 and a discussion of the further processing of each group follows.

Silanized Markite Hybrids

Six flexure bars were silanized according to the optimum technique discussed in Paragraph 2.4.2. After silanization, the parts were air dried for 16 hrs, then pyrolyzed to 1600°F using the previously shown cycle. After pyrolysis, the parts were subjected to another silanization treatment, air dried and cured at 400°F for 24 hours. Table 13 lists the density of the parts at each processing stage and the fiber volume of the finished flexure bar.

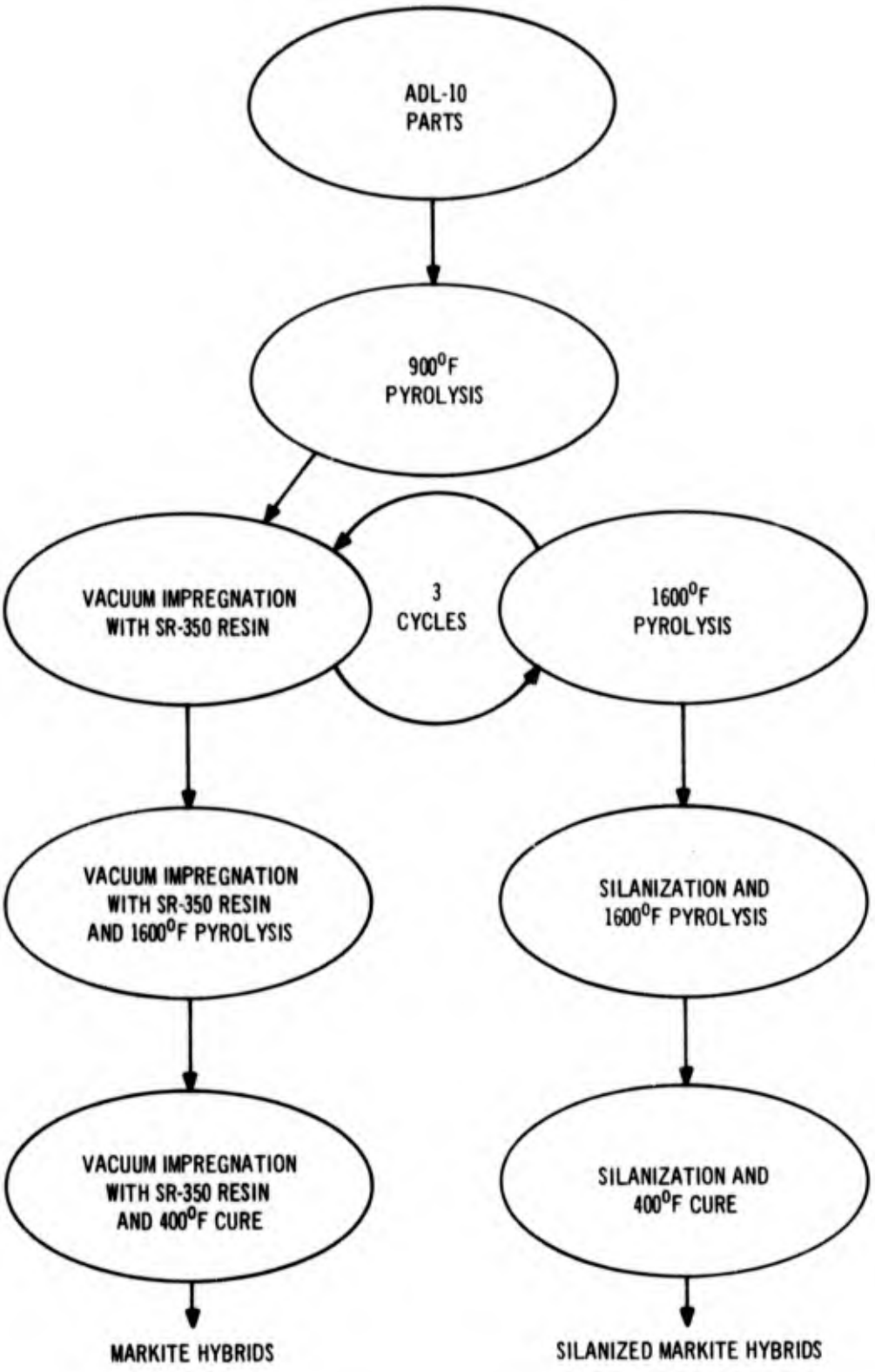

Figure 19. Processing Flow Chart for Markite Hybrid Flexure Bars

TABLE 13. FLEXURE BAR DENSITY (GM/CC), SILANE MARKITE HYBRIDS

Part ID	Original ADL-10 Sample	Third Densification Cycle (P3)	Silanization & Pyrolysis (P4)	Silanization & Cure (R4)	Quartz Fiber (vol. %)
P1A	1.72	1.90	1.92	1.93	71.4
P1B	1.72	1.90	1.91	1.92	71.4
P1C	1.72	1.93	1.94	1.95	71.4
P1D	1.72	1.95	1.96	1.96	71.4
Q2A	1.74	1.93	1.94	1.95	76.2
Q2B	1.74	1.91	1.92	1.93	76.2

Standard SR-350 Markite Hybrids

Twelve flexure bars were given a fourth cycle of vacuum impregnation with SR-350 silicone resin and subsequent pyrolysis to 1600°F. After the fourth densification cycle, the parts were vacuum impregnated with SR-350 silicone resin and cured at 400°F for 24 hours. In the terminology used in Reference 1, Figure 44, these samples would be designated "R4". Table 14 lists the part densities at each processing stage and the fiber volume of the flexure bar. The two sets of samples, silane and SR-350 reimpregnated, were then submitted for flexure testing.

2.4.3.4 Comparison of SR-350 and Ludox Processes from the Standpoint of the Yield of Inorganic Matrix Silica in Quartz Omniweave Composite Form

Figure 20 is a graphic representation of the relative density increase per processing (densification) cycle for two types of silica matrix/quartz Omniweave composites. For a silica matrix deposited via the impregnation with and subsequent pyrolysis of SR-350 silicone resin (Markite process), the process history of panel no. 319, fabricated for a previous program (Tables 11 and 24, Ref. 2), was used in obtaining the data points. Since the "Markite process" involves compression molding during the initial processing cycle, two curves were generated; one curve is based on the initial quartz Omniweave density of 1.09 gm/cc, and the other is based on a "compressed" weave density of 1.55 gm/cc (the 1.09 gm/cc weave is compressed to 1.55 gm/cc weave density during the first processing cycle). The former curve (initial weave density = 1.09 gm/cc) shows the relatively large effective density increase resulting from the first processing cycle of the "Markite" process. The latter curve uses the same processing data but treats the initial Omniweave density as 1.55 gm/cc. This treats the first process as if the 1.09 gm/cc Omniweave sequentially is compressed to 1.55 gm/cc, then impregnated and pyrolyzed. In the "Markite" densification process, density (weight) increases tend to become asymptotic after three or four cycles.

TABLE 14. FLEXURE BAR DENSITY (GM/CC), SR-350 MARKITE HYBRIDS

Part ID	Original ADL-10 Sample	Third Densification Cycle (P3)	Fourth Densification Cycle (P4)	Impregnation and Cure (R4)	Quartz Fiber (vol. %)
P2A	1.75	1.93	1.96	1.97	76.3
P2B	1.75	1.94	1.97	1.98	76.3
P2C	1.75	1.96	1.97	1.98	76.3
P2D	1.75	1.89	1.92	1.93	76.3
R1A	1.80	1.93	1.95	1.97	81.7
R1B	1.80	1.95	1.97	1.98	81.7
R1C	1.80	1.97	1.98	1.99	81.7
R1D	1.80	1.96	1.98	1.99	81.7
U1A	1.79	1.94	1.97	1.98	70.9
U1B	1.79	2.00	2.02	2.02	70.9
U1C	1.79	1.98	2.00	2.01	70.9
U1D	1.79	1.87	1.89	1.91	70.9

To generate a curve for quartz Omniweave composites with a silica matrix derived from collodial silica, the density increases for all the quartz Omniweave composites fabricated using Ludox AS were averaged at each densification cycle. This type of process generates a smoother density increase curve with increases becoming asymptotic at six to seven densification cycles.

Table 15 compares the final part characteristics for composites fabricated by the "Markite" process and the colloidal silica process.

2.4.4 SILICA-BORIA BASED MATRICES

Study of these candidate matrix systems was motivated by experience gained at GE-RESD's Materials Laboratories during the past 3 years on reusable external insulation (REI)* for use on NASA's Space Shuttle Orbiter (Ref. 5 and 6). The major portion of this study at GE has been focussed on 2 fiber systems: silica (Johns-Manville

*REI is GE's proprietary designation. NASA has designated this generic class of materials "RSI" for "reusable surface insulation". Similarly McDonnell-Douglas has developed "HCF" for "hardened compacted fibers" and Lockheed produces "LI".

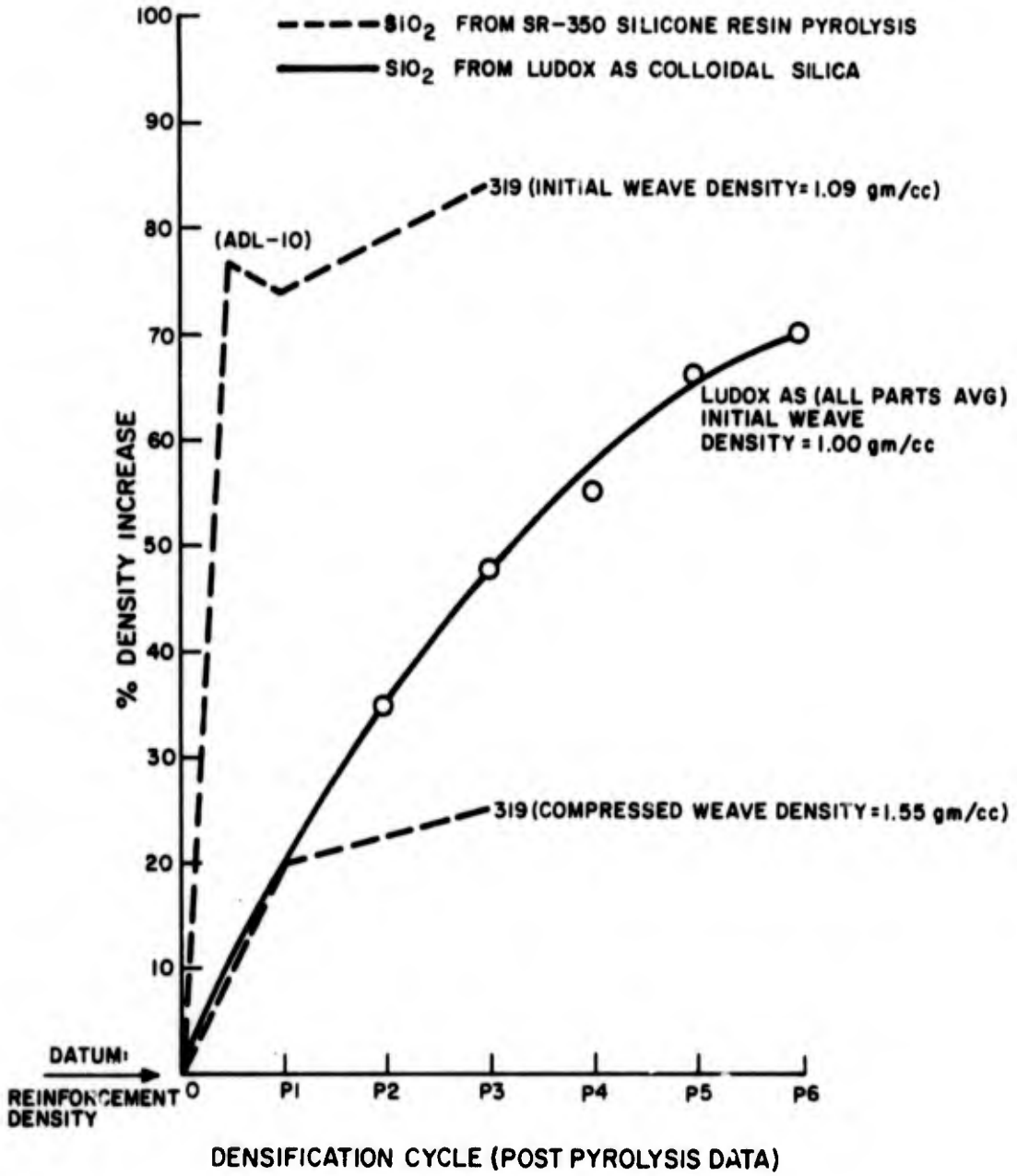

Figure 20. Incremental Density Increases for Silica Matrix/Quartz Omniweave Composites

TABLE 15. COMPARISON OF CHARACTERISTICS OF SILICA-SILICA OMNIWEAVE COMPOSITES DENSIFIED BY MARKITE AND LUDOX COLLOIDAL SILICA PROCESSES

Process:	"Markite"	Colloidal Silica
Final Part:		
(Approximate Characteristics)		
Density (gm/cc)	2.0	1.7
Fiber (vol. %)	70	45
Porosity (%)	10	25

"Microquartz") and mullite (Babcock-Wilcox), with some developmental attention to other alumina-silicate, alumina-phosphate and zirconia fiber systems. The fibers, or more accurately filaments, range in diameter from 3 microns (silica) to 6 microns (mullite) and are rigidized in a fibrous mat which is almost 2D in geometry, the fibers making shallow angles to the mat thickness or low conductivity direction. A photomicrograph of a densified REI structure is shown in Figure 21. The finished REI composites have densities in the range 8-20 lb/ft^3 (0.13 - 0.32 gm/cc), with extremely low thermal conductivities and are stable up to use temperatures of a minimum of 2300°F. The mechanical strength and strain-to-failure properties have been the most challenging to improve and to this end the "space-frame" ductile ceramic analytic models discussed in Section 4 of Reference 2 were developed. The corresponding laboratory effort has been directed toward development of refractory cements or matrices which would be both practical from a manufacturing standpoint and yield the thermally stable, minimum density framework of intersecting and connected fibers typified in Figure 21.

The following three sub-sections describe the formulation basis of three of these materials based on silica-boria and the Omniweave fabrications based on them. The experience of the processing showed that the maximum densification that could be achieved was the 1.2 gm/cc nominal density space frame composite. The first of the formulations is a simple combination of silica-boria selected to sinter at temperatures well below the devitrification temperatures of pure silica. The second is similar to the "SBA-10" binder used in Mod 1A REI-Mullite, a combination of silica, boria and alumina. The third of these combinations included a boron nitride component, providing some experience in the direct densification of Omniweaves - in contrast to the prepeg technique developed for the glass-bonded BN coatings (see Para. 2.4.6).

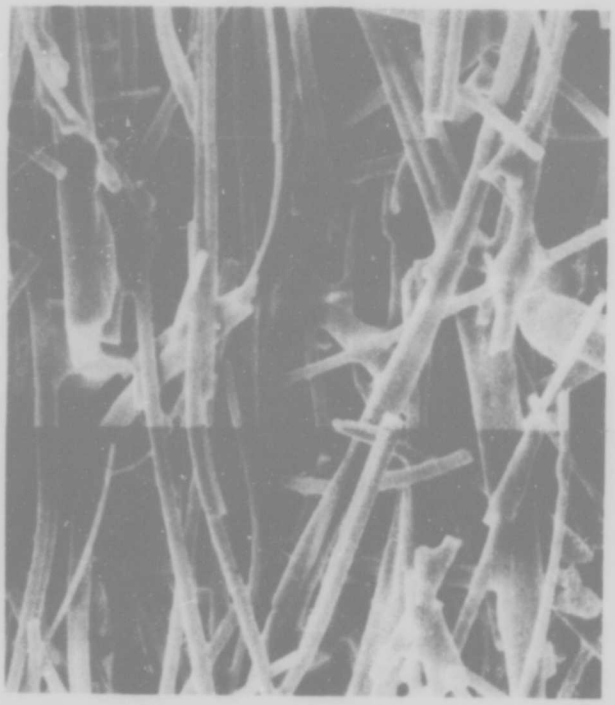

Figure 21. Typical Fiber - Binder Microstructure Associated with the Mod 1-A REI - Mullite Process

2.4.4.1 Silica-Boria

2.4.4.1.1 Matrix Formulation

The system $SiO_2 - B_2O_3$ is particularly interesting as a binder or flux with any high purity silica system because of its extreme resistance to devitrification. Combinations of B_2O_3 and SiO_2 have been held for hundreds of hours at temperatures near their glass transition point with no evidence of crystalline formation whatsoever. This glassy phase is, nevertheless, considered metastable (Ref. 7).

According to Figure 22, the phase diagram of Rockett and Foster, (Ref. 8) a composition of 64 mole % SiO_2 and 36 mole % B_2O_3 should melt at around 850°C. This liquid is so viscous at its melting point, however, that it cannot be made to flow readily until it is subjected to temperatures of 1400°C or higher. An experimental frit having this composition was prepared by mixing 118.5 gms B_2O_3 (fused Boric Acid) with 181.5 gms high purity amorphous silica (Corning 7940). The mixture was dry rolled in a porcelain ball mill for 1 hour and then melted in a high purity silica crucible. The melt was heated to 2800°F (1540°C) for 4 hours and then fritted by pouring the

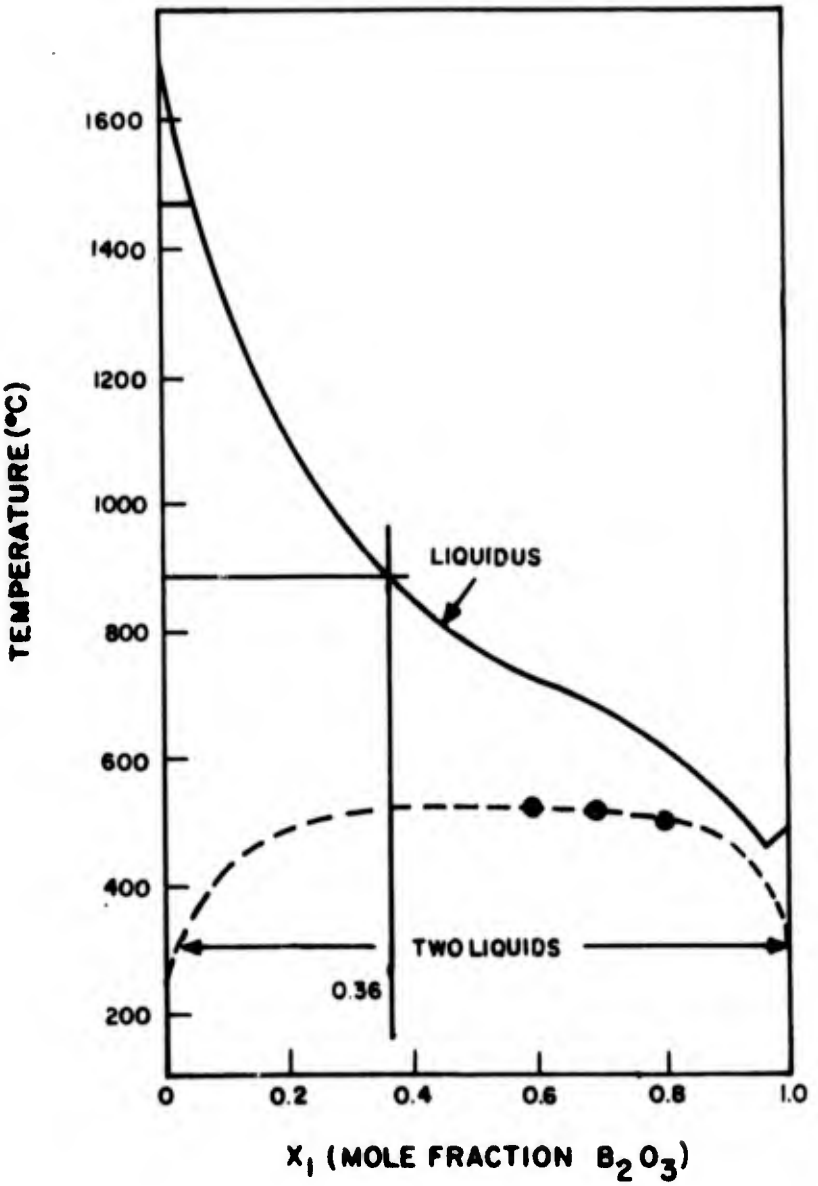

Figure 22. B_2O_3 - SiO_2 Phase Diagram (Ref. 8)

melt into a cold water bath. The frit was immediately removed from the water and dried at 250°F for 4 hours. It is important not to leave mixtures with over 10 mole % B_2O_3 in water as they are slightly soluble.

The dried frit was placed in a porcelain ball mill with high alumina grinding balls. Isopropyl alcohol was added to slurry the frit and the mixture was ball milled 16 hours. The ground slurry was then dried on an aluminum pan for 4 hours at 250°F. All material thus prepared passed through a 200 mesh sieve.

Figure 23 shows a DTA curve run on the frit. The sharp endotherm above 200°F indicates that some water was trapped by the frit and chemically bound. No melting point endotherm was observed, indicating that the material was totally amorphous, undergoing no phase change at its expected melting point.

2.4.4.1.2 Composite Densification and Firing

A suspension of 50 percent by weight silica-boria frit (36 mole % B_2O_3, 64 mole % SiO_2) in isopropyl alcohol was used to impregnate sections of Omniweave fabric no. 400. The Omniweave sections were submerged in the silica-boria suspension and subjected to vacuum (31 in. Hg) for 15 minutes, then air pressure (1000 psi) for 30 minutes. The impregnated parts were removed from the silica-boria suspension and dried at 180°F for 16 hours, then fired at 850°C (1562°F) for 4 hours.

This firing temperature was chosen for two reasons. First, it should be a suitable sintering temperature, being approximately 100F° below the previously referenced 1650°F melt temperature of the mixture. Second, 850°C was one of two nominal firing or sintering temperatures studied throughout the earlier stages of this work; see for example the Ludox colloidal silica studies. The 850°C (1562°F) temperature is also safely below the 1650°F level considered in Reference 2 for firing Astroquartz fibers without danger of their devitrifying. Table 16 lists the characteristics of the finished parts.

TABLE 16. CHARACTERISTICS OF SILICA-BORIA/ASTROQUARTZ OMNIWEAVE COMPOSITES

Part ID	Initial Weave Density (gm/cc)	FPA (deg)	TTA (deg)	Firing Temp. (°C)	Final Density (gm/cc)	Fiber (vol. %)	Porosity(1)
SB-400-1	↑	↑	↑	↑	1.24	↑	↑
SB-400-2	0.99	40	40	850	1.23	45	45
SB-400-3	↓	↓	↓	↓	1.21	↓	↓

(1) Based on a calculated matrix density of 2.30 gm/cc.

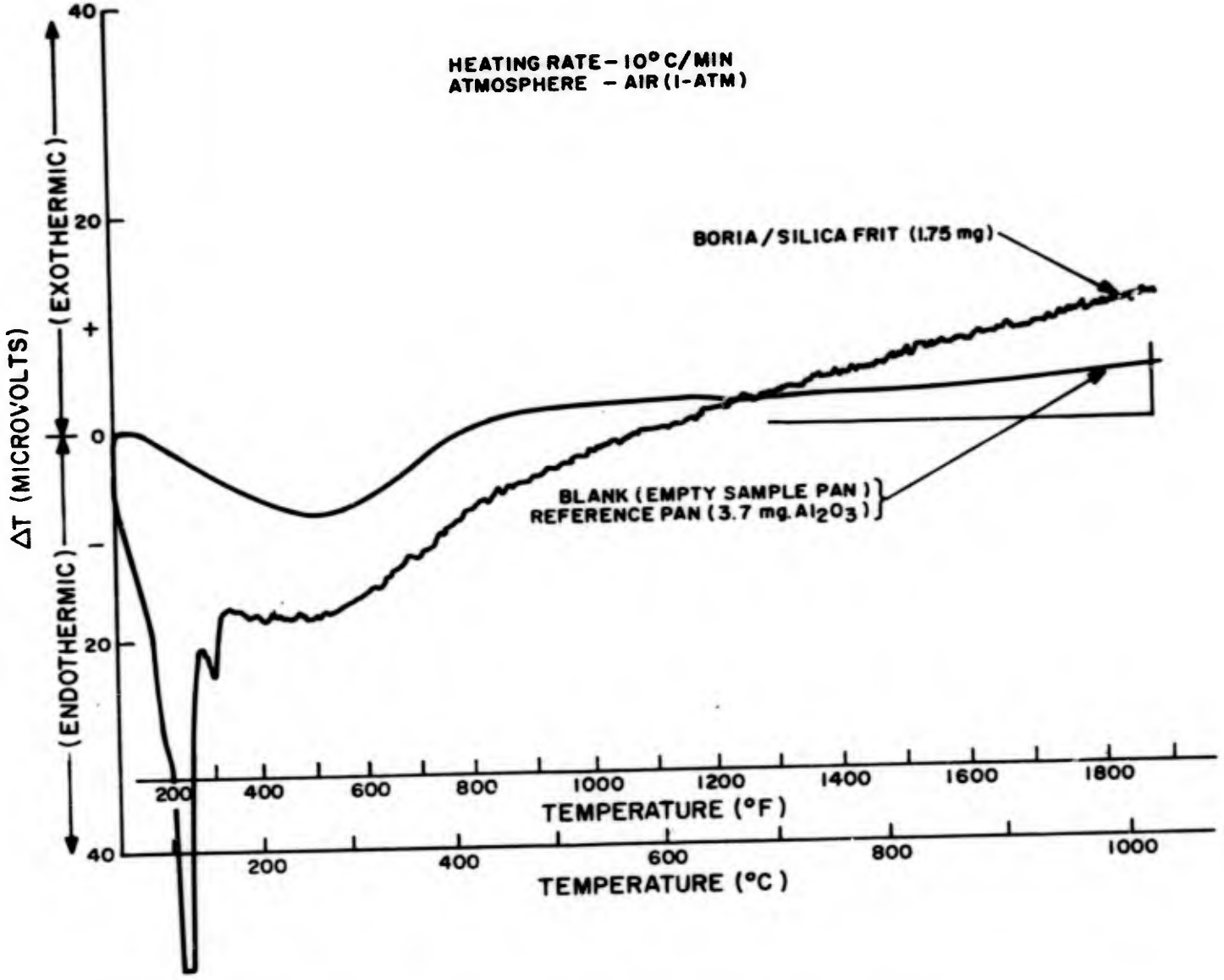

Figure 23. DTA of Boria/Silica Frit (36%/64%)

Figures 24a and 24b are SEM photos of the matrix-filament binding within an Astroquartz fiber. Note that the individual filaments have a nominal diameter of 8 microns. It is evident that the desired wetting has in fact occurred, where the matrix material is in fact deposited. In the higher magnification view (lower right hand corner) a crack has occurred in a filament, propagating through the silica-boria matrix. More extensive cracking is also evident in the lower magnification view (top left). This cracking behavior, coupled with the very low composite density, does not indicate the desired composite behavior.

2.4.4.2 Silica-Boria-Alumina

2.4.4.2.1 Matrix Formulation

The addition of a small amount of alumina to a pure borosilicate glass has the effect of lowering the viscosity of the material in its liquid state. It also reduces the surface tension, significantly allowing for greater wetting and better bonding to a pure silica surface. The GF-RESD REI-Mullite material developed for the Space Shuttle Orbiter Thermal Protection System made use of these effects to obtain a glassy bond between mullite fibers (Ref. 9).

For silica, a fairly low concentration of Alumina must be maintained to minimize devitrification. For applications below 1800°F about 3 mole % of alumina seems to be the upper limit before devitrification becomes a problem.

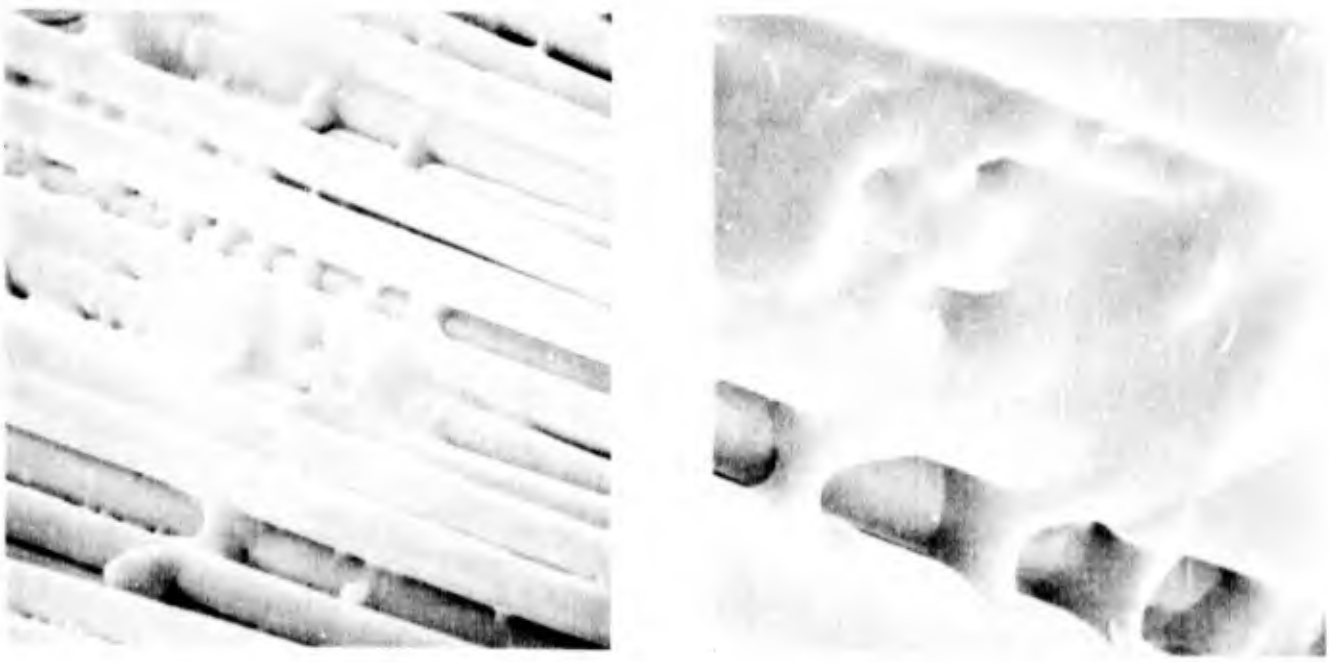

(a) (b)

Figure 24. SEM of Matrix-Filament Interaction in Silica-Boria/Astroquartz Omniweave Composite

An attempt was made to obtain the most complete fiber-to-fiber bonding possible by introducing a boron-aluminosilicate glass into the silica matrix using a polar liquid solution which completely wets silica. Alumina can be introduced in the form of aluminum chloride which is soluble in a number of polar liquids including water. Likewise B_2O_3 can be readily dissolved in any polar liquid. Silica, on the other hand, cannot be dissolved in aqueous solutions except in very dilute solutions or as a colloid dispersion. For this reason the silica was introduced as a methyl siloxone resin (GE SR-350 Resin) in isopropynol. Both the $AlCl_3$ and B_2O_3 could be readily dissolved into the isospropyl alcohol along with the silicone resin.

The solution used was composed of the equivalent of 39 mole % B_2O_3, 58 mole % SiO_2, and 3 mole % Al_2O_3. This composition has been shown to have a high resistance to devitrification and a melting point around 850°C (Ref. 10). A phase diagram of the tertiary Al_2O_3-B_2O_3-SiO_2 system is shown as Figure 22.

2.4.4.2.2 Composite Densification and Firing

A solution of 5.0 percent by weight boric acid, 1.5 percent by weight aluminum chloride, 1.5 percent by weight SR-350 silicone resin in isopropyl alcohol was used to impregnate sections of Omniweave strip no. 400. The Omniweave fingers were submerged in the solution and subjected to vacuum (31 in. Hg) for 30 minutes. The vacuum was released and the impregnated parts were removed from the solution and oven dried at 250°F for 1 hour. The parts were then pyrolyzed for 30 minutes at 1400°F, cooled to room temperature, and reimpregnated in the above manner. After the second 1400°F pyrolysis, the parts were "flash fired" at 2300°F for 15 minutes. The short term firing was intended to thoroughly melt the binder and allow it to wet the fibers without allowing sufficient time for devitrification of the fibers to occur. Table 17 lists the characteristics of the finished parts.

TABLE 17. CHARACTERIZATION OF SILICA BORIA ALUMINA/ASTROQUARTZ OMNIWEAVE COMPOSITES

Part ID	Initial Weave Density (gm/cc)	FPA (deg)	TTA (deg)	Final Firing Temp. (°F)	Final Part Density (gm/cc)	Fiber (vol %)	Porosity[1] (%)
SBA-400-1 SBA-400-2 SBA-400-3	0.99	40	40	2300	1.01	45	44

[1] based on a calculated matrix density of 2.4 g/cc.

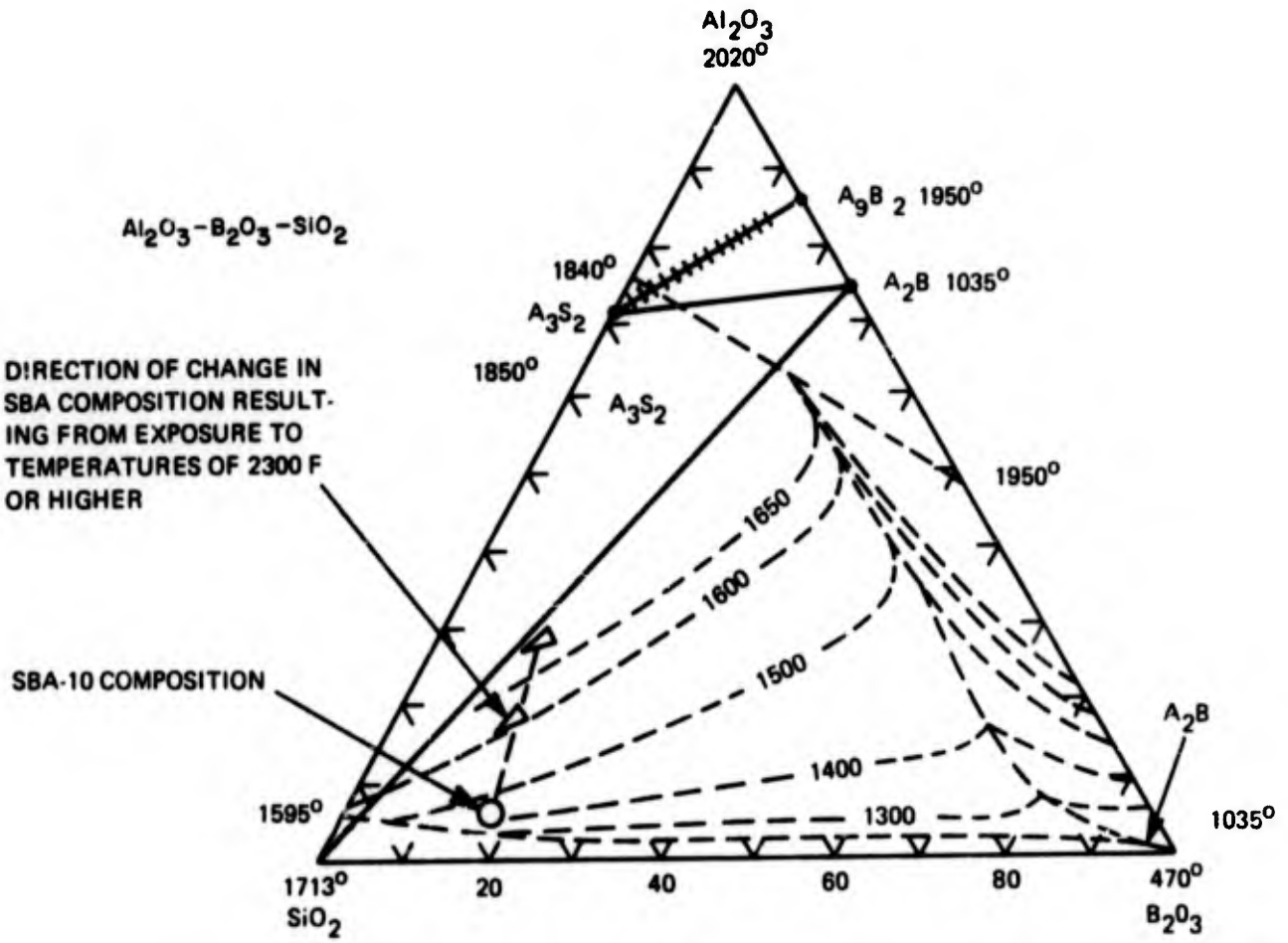

Figure 25. System Al_2O_3-B_2O_3-SiO_2; preliminary. A = Al_2O_3, B = B_2O_3, S = SiO_2

2.4.4.3 Boron Nitride/Silica-Boria-Alumina Slip System

2.4.4.3.1 Matrix Formulation

The purpose of this system was to study the possibility of developing a glass-bonded BN matrix for the dense silica Omniweave reinforcement which would have the postulated desirable internal friction and refractory properties of BN but with a glass binder system which would not require firing temperatures so high as to devitrify or otherwise damage the Astroquartz fiber Omniweave. The target characteristics of the process would be relatively easy impregnation and densification of the Omniweaves and as high a BN to glass binder phase ratio as possible, consistent with consolidation of the finished composite, i.e., strength, stiffness and surface finish.

A water-dispersed binder of boron aluminosilicate glass was first made up by adding a small amount of HCl to Ludox AS to make it acidic and adding this suspension to a solution of aluminum chloride and boric acid. This binder was roughly 67 mole % silica, 22 mole % alumina, and 11% B_2O_3. Boron nitride was then added to the solution while stirring until the composition reached a level of about 65 mole % boron nitride. This mixture was then placed in a ball mill and rolled for 4 hours. The suspension was filtered through a 200 mesh screen to make sure that all clumps of BN had been broken up.

This slip was impregnated into the Omniweave by two processes. The first was an attempt to reduce filtering effects by the Omniweave by creating a high contact angle between the slip and the fibers. It was reasoned that a non-wetting surface would not draw the liquid out of the slip and filter the particles out on the surface as is the case with a wetting surface. A silicone resin treatment was used to provide this high contact angle on the fibers. By then forcing the slip into the weave structure under low pressure, the liquid binder would be able to penetrate only the coarser pores, thereby minimizing the separation of the particles and the liquid due to filtration effects. The minimum pore size is limited by the relationship:

$$d = \frac{-4\,\gamma \cos\theta}{P}$$

where:

d = pore diameter

γ = surface tension of liquid

θ = contact angle

P = absolute pressure (Ref. 11)

A second set of samples was made up without this treatment for comparison.

2.4.4.3.2 Composite Densification and Firing

Four sections of Omniweave strip no. 400 were impregnated with the boron nitride/silica-alumina-boria glass slip. Two of the four strips were additionally given a silicone treatment prior to impregnating with boron nitride/glass slip. The pretreated strips were immersed in a solution of 1/2 percent by weight SR-350 silicone resin in freon and cured at 350°F for 4 hours. To impregnate with the boron nitride/glass, the four strips were first evacuated in a chamber, and the slip was introduced into the chamber under vacuum. When the Omniweave sections were completely submerged, the vacuum was released and the impregnated strips were immersed in an ammonia solution to gel the suspension. The parts were then oven dried at 220°F for 4 hours, then fired at 1600°F for 30 minutes. Table 18 lists the characteristics for each pair of samples.

TABLE 18. CHARACTERIZATION OF SILIA-BORIA-ALUMINA/BORON NITRIDE/ASTROQUARTZ OMNIWEAVE COMPOSITES

No Pretreatment:							
Part ID	Initial Weave Density (gm/cc)	FPA (deg)	TTA (deg)	Firing Temp. (°C)	Final Density (gm/cc)	Fiber (vol. %)	Porosity (%)
BNG-400-1	0.99	40	40	1600	1.14	45	~50
BNG-400-2	0.99	40	40	1600	1.13	45	~50

Silicone Resin Pretreatment:								
Part ID	Initial Weave Density (gm/cc)	FPA (deg)	TTA (deg)	Density After Silicone Treatment (gm/cc)	Firing Temp. (°F)	Final Density (gm/cc)	Fiber (vol. %)	Porosity (%)
SRBNG-400-1	0.99	40	40	0.99	1600	1.13	45	50
SRBNG-400-2	0.99	40	40	1.00	1600	1.11	45	50

2.4.5 CHEMICAL VAPOR DEPOSITION METHODS

Chemical vapor deposition is a method of forming a material by causing a chemical reaction to occur in the vapor phase that subsequently leads to nucleation and deposition of a solid material at a heated substrate. It has the advantage of producing unusually dense, pure and coherent free standing bodies at temperatures considerably below those customarily required in processing by conventional methods. More recently, the process has been applied to formation of matrix materials within the void structure of fibrous composites such as felts and woven structures, usually made from carbon or graphite fibers (Ref. 12). This process has come to be known as infiltration. While it has been applied chiefly to formation of so-called carbon-carbon composites, there is reason to believe that it would have advantages in formation of other matrix materials, particularly those for which there is no known liquid phase under other feasible processing conditions, such as boron nitride, for example. The material formed in the gas phase reaction deposits on all exposed heated surfaces within the fibrous structure until the supply of gas has been exhausted locally, i.e., until the flow of gas to the deposition site has been cut off by plugging of the access paths to the site in question.

Because of the need to maintain accessibility to the interior sites, control of the gas phase reactions must be precise. In the case of carbon for example, gas phase pyrolysis and condensation reactions occur until the average molecular weight of the gas-borne carbon nuclei exceeds that which can be retained in the gas phase, i.e., the gas phase becomes saturated with carbon and precipitation occurs. Another way of looking at the process would be to associate an equilibrium vapor pressure with each gas phase species, which when exceeded, leads to deposition. In all cases however, the ability to achieve significant densification of the interior portions of a woven structure depends on the ability to retain the deposition species in the gas phase until the desired deposition site has been reached by diffusion. When the diffusion rate is exceeded by the deposition rate, premature deposition occurs, clogging access paths to deposition sites farther into the structure. Since the diffusion rate is related to concentration of the species in the gas phase, it is subject to experimental variation up to the point where the kinetics of gas phase reactions increase sufficiently to cause 'sooting' or spontaneous formation of gas-borne solids, which do not form cohesive, dense deposits. Gas residence time, as modified by feed velocities to the hot zone, is one of the controlling parameters, along with concentration and temperature, used to achieve maximum depth of penetration at optimum rates.

The most common physical approach to infiltration consists of placing the porous or fibrous substrate in a furnace where it is heated by radiation. Reactive gases are fed to the furnace which is maintained at a low pressure, typically 0.1 to 10 torr; by products and unreacted feed materials are exhausted to a vent with a mechanical pump. This approach is termed 'isothermal infiltration' inasmuch as the entire substrate is at a constant temperature. Recent innovations include the use of a heated

pedestal, on which, or against which the substrate is placed in the so-called thermal gradient technique. As a result, a temperature gradient is developed in the specimen with the highest temperature farthest from the reactive gas stream. The latter is fed to the furnace at one atmosphere and at a high velocity. Because of these conditions, the reactive gas can penetrate into the substrate before reacting, and in principle, deposits only at a plane parallel to the heated substrate. As the substrate becomes denser, the deposition region advances away from the heated pedestal toward the exterior surface. More rapid and uniform infiltration results with no requirement that the specimen be removed periodically for grinding off surface deposits that prevent access of the gas to the interior. However, each specimen must be infiltrated separately in an arrangement based on its geometry, and the conversion of reactive gases is quite inefficient. It is a most useful approach to manufacturing infiltrated cylinders and plate material however, particularly when the reactive gas mixture can be recycled.

In the work performed on this program, the preliminary and experimental nature of the matrices to be formed by infiltration precluded the extensive use of the thermal gradient technique, although an effort was made to simulate it to determine if it offered a significant advantage over the isothermal method.

2.4.5.1 Chemical Vapor Infiltration of Silica

The formation of amorphous deposits of silica can be accomplished by the thermal decomposition of ethylorthosilicate, $(C_2H_5O)_4$ Si, at temperatures between 800°C and 1100°C (Ref. 13) and at atmospheric as well as reduced pressures. All of the work previously reported has been performed for the purpose of obtaining films of high purity silica on relatively open substrates such as plates or discs. In the work conducted in this program, the primary effort was directed at achieving deposition within a fibrous prewoven structure, the fiber strands of which constituted the substrates on which the decomposition reaction took place.

2.4.5.1.1 Experimental Method

The experimental arrangement for the isothermal infiltration of silica is shown schematically in Figure 26. The ethyl silicate vapor content was determined by the reservoir temperature and the equilibrium vapor pressure over the reservoir charge taken from the curve in Figure 27, assuming that equilibrium vaporization conditions prevailed in the reservoir. Unreacted silicate was trapped to protect the vacuum pump. By-products (ethane, ethanol and higher molecular weight compounds) were inconsequential because of the low conversions characteristic of most pyrolysis infiltration processes.

For isothermal infiltration, the substrate is placed in the furnace tube and the carrier gas-ethyl silicate mixture is passed over and through it at low total and partial pressure. Since the specimen was uniformly heated, the deposition rate was higher on the outer surface.

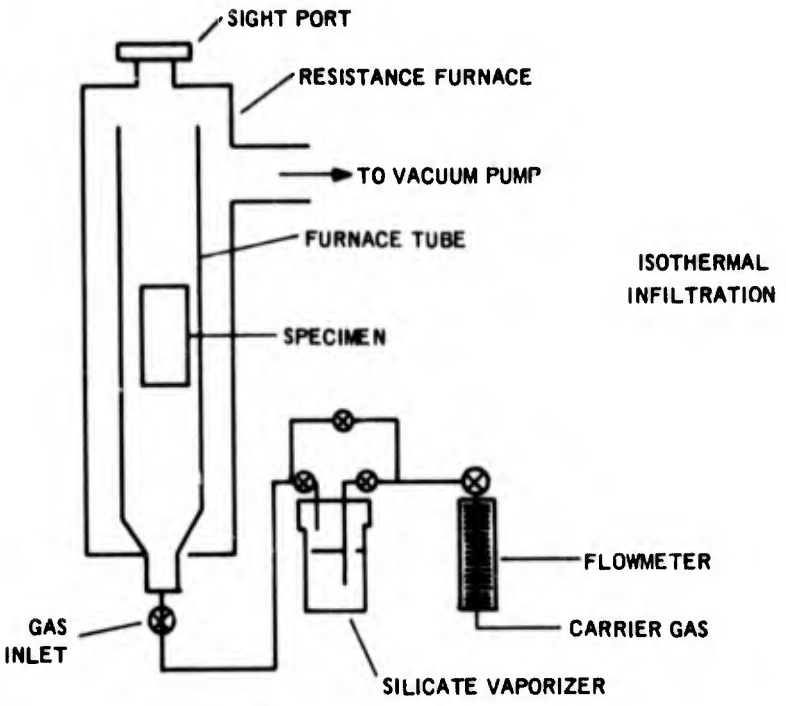

Figure 26. Schematic of CVD Silica Infiltration Apparatus

2.4.5.1.2 Experimental Results

Several experiments were performed using the isothermal approach to determine the broad limits of reaction parameters and to estimate the probability of achieving satisfactory penetration by this approach. Two fibrous specimens were infiltrated — a loosely woven carbon fiber 4-D construction (Omniweave) and a piece of National Carbon Co. carbon felt (VDP). Carbon fibrous materials were selected for initial process studies for easier detection of internally deposited films. Conditions and weight gains are shown in Table 19. Note that the silicate vapor content was higher and the total gas velocity was lower in the first run (Omniweave) than in the second (felt).

The following observations are based on preliminary visual inspection of the infiltrated specimens.

2.4.5.1.3 Structure of Silica Deposits

With a more concentrated vapor, and a somewhat lower gas velocity, three distinct deposit types were detected in the Omniweave specimen:

a. clear, glassy and relatively thick near the bottom, inlet end of the reactor (fresh, colder gas) Figure 28a.

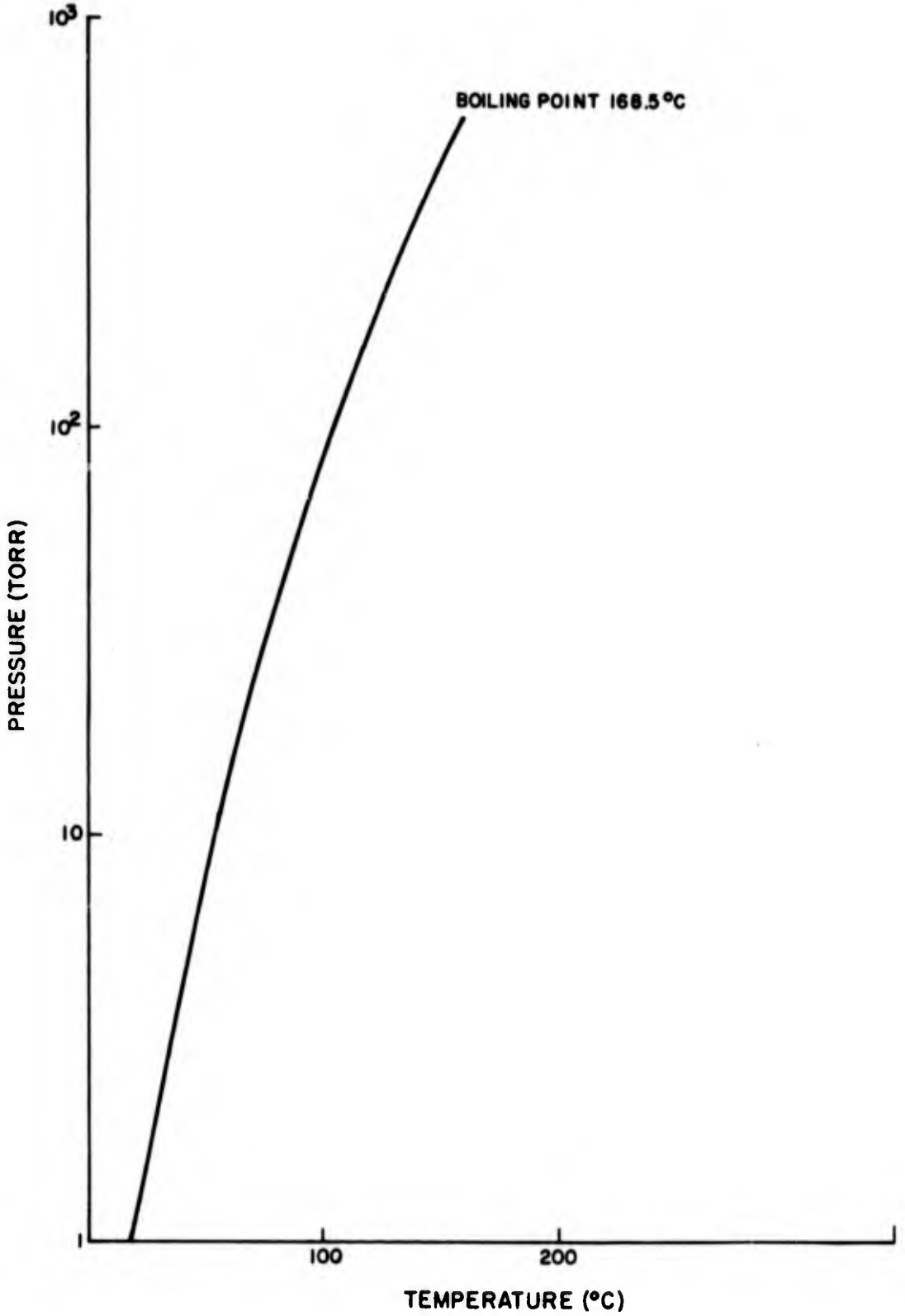

Figure 27. Vapor Pressure Curve for Ethyl Silicate (Chem. and Rubber Handbook)

TABLE 19. ISOTHERMAL SILICA INFILTRATION OF FIBROUS STRUCTURES

Specimen	1 4D Woven VYB Fibers Estimated Bulk Density 0.3 g/cm^3	2 VDF Felt.[2] Initial Density 0.05 g/cm^3
Temperature (°C)	950	950
Flow Rate (cc/min)	300	350
Pressure (Torr)	1	1
Est. Silicate Vapor Conc. (%)	0.2	0.07
Run Time (hrs)	12	24
Percent Weight Increase/hr.	1.05	1.25

b. a frosty-appearing and somewhat thinner deposit on the fibers over the upper half to two-thirds of the two-inch long specimen.

c. a white powdered material ('soot') over parts of the specimen from middle to top - easily dislodged (Figure 28b).

At a lower concentration and higher velocity, nearly all of the fibers in the felt specimen showed a clear glassy deposit. Thickness uniformity was improved and no 'soot' was apparent. Penetration was relatively uniform through the one-quarter inch thick specimen, but felted structures are generally quite easy to infiltrate, compared to woven structures in which highly bunched fiber strands provide the major portion of the available surface area. The deposits are not easily seen in photographs because of their transparency.

2.4.5.1.4 Infiltration Rate

Both specimens gave relatively low infiltration rates in terms of the weight increase per hour as shown in Table 19. Moreover, the rates are inconsistent with those obtained in carbon infiltration techniques; consequently, relatively long infiltration times (e.g., 500 hours) can be anticipated before complete densification would be achieved for felt specimens. Some in-process machining would also be necessary to remove heavy surface deposits, an undesirable step in the case of prewoven structures.

2. National Carbon Co.

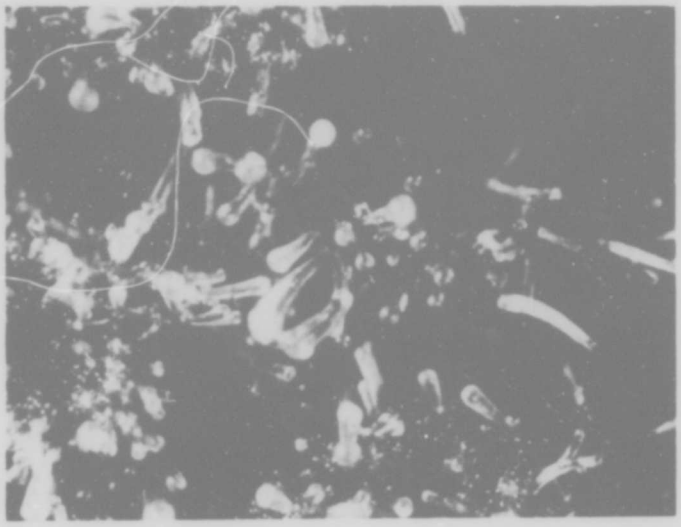

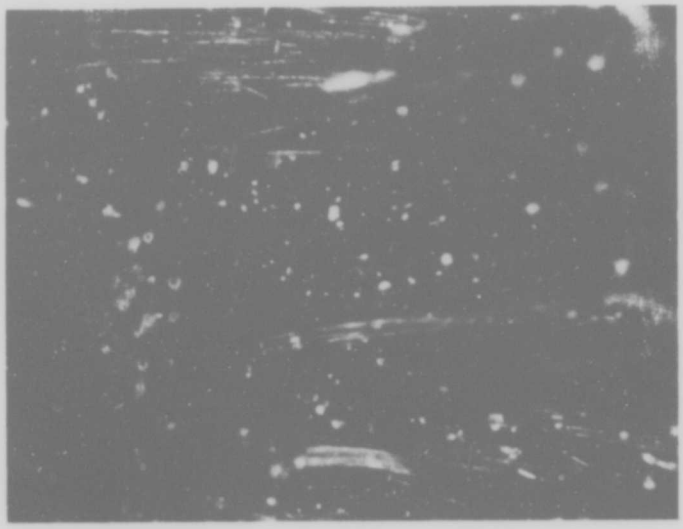

Figure 28. a) (Top) Silica deposit at lower portion of woven structure;
b) (Lower) Deposit at center portion, showing white soot specks and more granular structure. Both views 22X.

2.4.5.2 Boron Nitride Composite Materials

With the availability of boron nitride fibers which can be woven into constructions of variable geometry, methods of forming a suitable matrix for such constructions would include the use of CVD infiltration, particularly since boron nitride does not have a liquid phase to assist in bonding a particulate matrix base to the fibers and to itself. The higher temperature capability of the fibers and matrix would permit the use of a BN/BN window under more extreme conditions than would be allowable for a SiO_2/SiO_2 composite in which melting and phase changes would occur.

Alternatively, a high porosity silica fiber/BN matrix may also be expected to have improved mechanical properties over a silica-silica composite due to the lower modulus and higher strain capability to be expected of the BN component. Its recession performance should be improved or at least not reduced compared to an all silica system. This system could also be formed by CVD of BN if deposition temperatures could be maintained below the devitrification range for silica.

Boron Nitride Deposition and Infiltration

Investigation of CVD boron nitride for the purpose of forming massive free-standing shapes was carried out over a decade ago using two methods: a) reaction of boron trichloride and ammonia and thermal decomposition of the products (Eq. 1); and b) thermal decomposition of B-trichloroborazole (Eq. 2).

$$BCl_3 + NH_3 = BN + 3\,HCl \qquad (1)$$

$$B_3N_3H_3Cl_3 = 3BN + 3HCl \qquad (2)$$

To assure complete conversion an excess of ammonia is required in the first reaction, which leads to formation of ammonium chloride, a solid material which deposits on colder surfaces in the system and tends to clog gas lines and alter gas velocities. In the absence of excess ammonia, unreacted boron trichloride causes polymerization of pump fluids and premature termination of the experiment. Both approaches have yielded massive hexagonal, anisotropic deposits of boron nitride of nearly theoretical density on open and contoured substrates (p. 663-667, Ref 12).

As discussed above, it is necessary to limit the rate of formation of deposition species to permit them to penetrate into the fibrous structure; formation of solids in the gas phase leads to their precipitation on the outer surface. Since boron trichloride and ammonia form solid intermediates of indeterminate composition on mixing at the furnace inlet, deposition of boron nitride from this system can be conducted more readily on open substrates than those in which penetration is required. The use of B-trichloroborazole, which can be sublimed from the solid phase as a pure vapor, should permit a greater degree of penetration, provided its thermal decomposition can be retarded, or a very steep thermal gradient can be achieved within the substrate. Since it appeared to offer more potential infiltration, it was the method adopted, although restricted to the isothermal approach because of limited supply.

2.4.5.2.1 B-Trichloroborazole Generation

B-trichloroborazole is a moisture sensitive, sublimable solid having the structure and vapor pressure shown in Figure 29 (Ref. 14). In view of the difficulties of subliming such materials into the gas feed stream at a constant rate (particle size growth, scaling due to traces of moisture), a trichloroborazole generator developed on an earlier program was used in conjunction with an auxiliary nitrogen gas carrier for velocity control. Figure 30 is a schematic of the overall deposition system. The borazole generator consists of a externally heated steel tank containing a fixed bed of well dispersed solid ammonium chloride, through which the primary gas feed stream is led, consisting of boron trichloride and nitrogen. With the proper control of temperature and gas feed rate, the boron trichloride is completely reacted and the exit gases from the generator contain B-trichloroborazole and hydrogen chloride in addition to the carrier, as shown in Equation 3. Operation under these conditions provided a continuous supply of

$$3BCl_3 + 3NH_4Cl = B_3N_3H_3Cl_3 + 9\ HCl \qquad (3)$$

trichloroborazole at constant composition and avoided the build-up of solid by products in the reactor as well as damage to the pumping system.

2.4.5.2.2 Infiltration Studies

As stated earlier, the principal objective in a pyrolytic infiltration procedure is to bring about deposition on fiber surfaces uniformly and completely if possible throughout the entire fiber construction. A number of factors relating to weave geometry, pore size and fiber spacing influence the uniformity and completeness of the infiltration and several procedures have been developed for various circumstances (Ref. 15). In the case of boron nitride infiltration, the isothermal approach was followed, in which the entire specimen was maintained at a constant temperature in a low pressure furnace tube (1-inch i.d.) through which a stream of nitrogen was passed after having been charged with B-trichloroborazole vapor. On emerging from the furnace the gas stream passed directly into a 15 cfm Stokes vacuum pump from which it was vented.

Specimens of boron nitride felt (Carborundum Co.) and four-directional Omniweave woven silica, approximately 3 in. x 1/2 in. x 1/4 in., were suspended in the center of the graphite furnace tube for infiltration under what preliminary studies had established as a near-optimum condition — 1100° C, 3 torr. Attempts to infiltrate boron nitride at higher temperatures and pressures led to rapid sealing off of exterior void spaces and poor penetration of the internal structure.

An attempt was made to simulate the so-called isothermal infiltration conditions by using a strip of four-directional flat braided quartz fiber fitted closely to the inner heated wall of the cylindrical deposition tube from top to bottom (8 in.). A graphite rod, 1/2-inch in diameter, was suspended from the centerline of the tube to serve as both heat sink and void filler. By this means it was expected that higher gas velocities

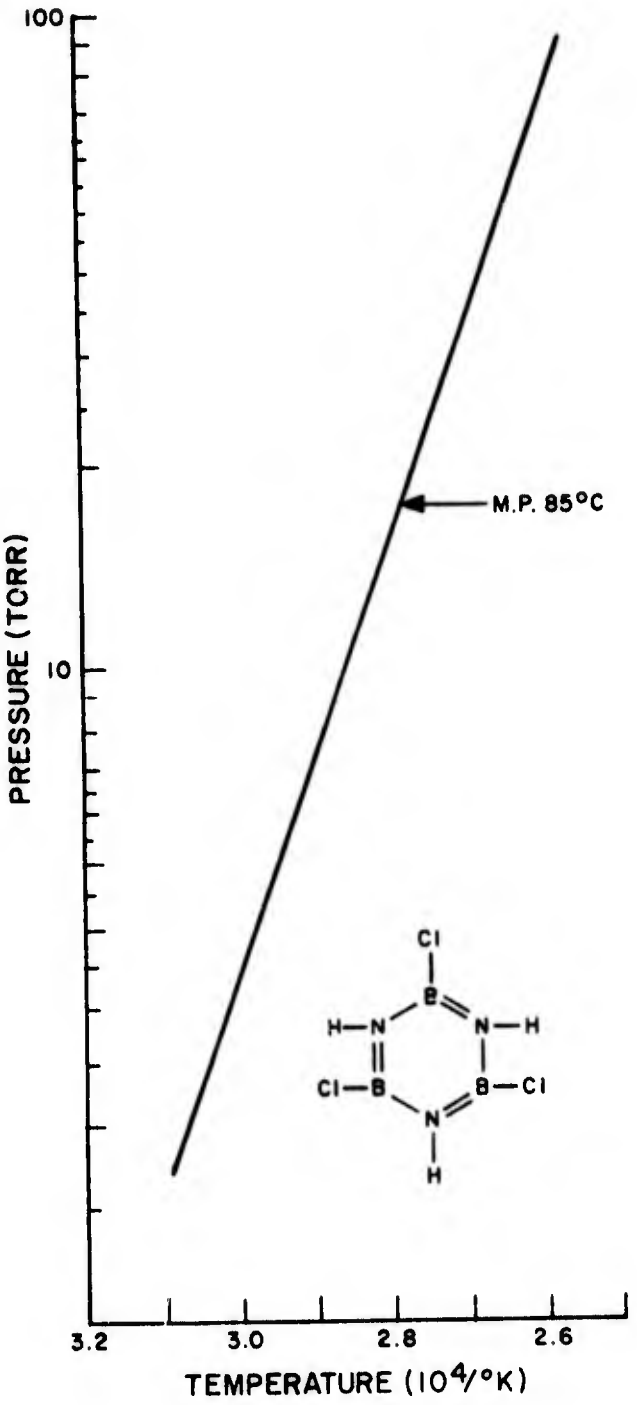

Figure 29. Vapor Pressure of B-Trichloroborazole (Ref. 14)

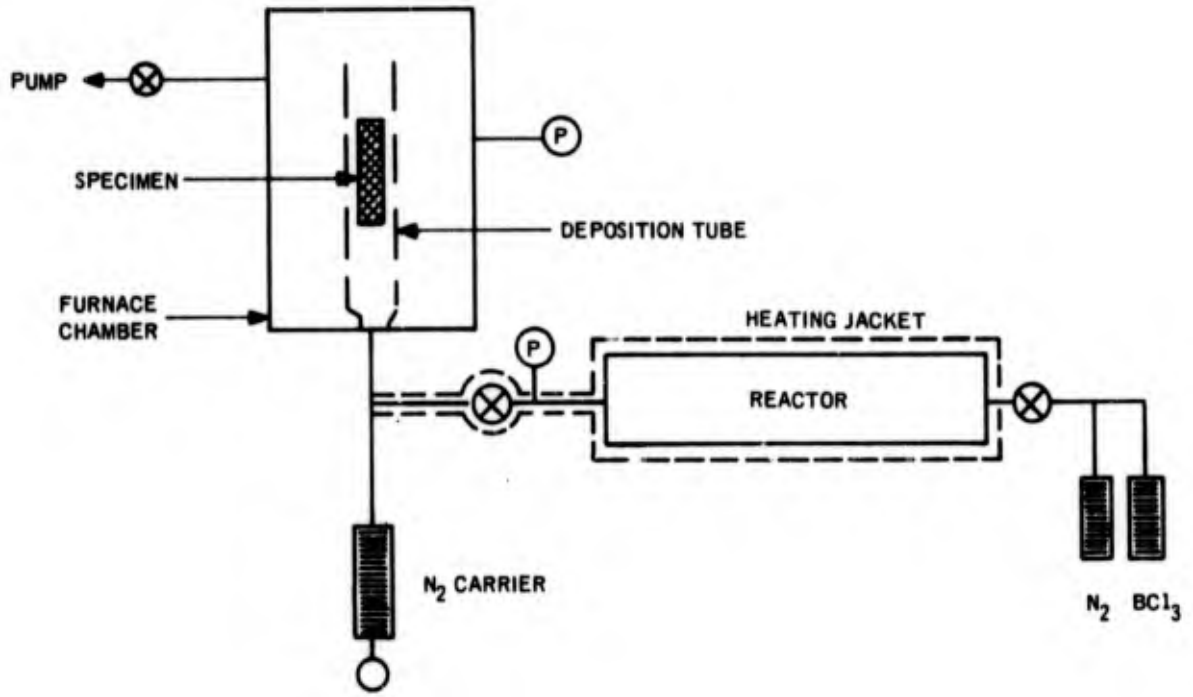

Figure 30. Schematic of Generator/Deposition System

could be achieved and that diffusion through the somewhat cooler outer portion of the braid to the hotter back face would permit deposition to occur somewhat more rapidly, and thus permit greater filling of the pores before the outer surface become clogged. The effort was only partially successful as will be discussed, principally because of the inability to keep the outer surface of the braid cooler where the deposition species were concentrated. In the usual temperature gradient procedures, the furnace pressure is maintained at one atmosphere under high flow conditions to prevent this.

2.4.5.2.3 Results

A. Infiltration

Felt Specimens

Specimens were mounted, sectioned and polished and infiltration rates at various points in the specimens determined by measuring the thickness of the deposits around individual fibers at intervals across the specimen thickness. Figure 31 illustrates the deposition gradients within one specimen at two locations along the length, about two inches apart. The rate of deposition on the outer fibers is clearly higher than that in the specimen center. This is due only partly to the fact that the specimens were heated by radiation from the wall of the furnace tube. The gradient is caused principally

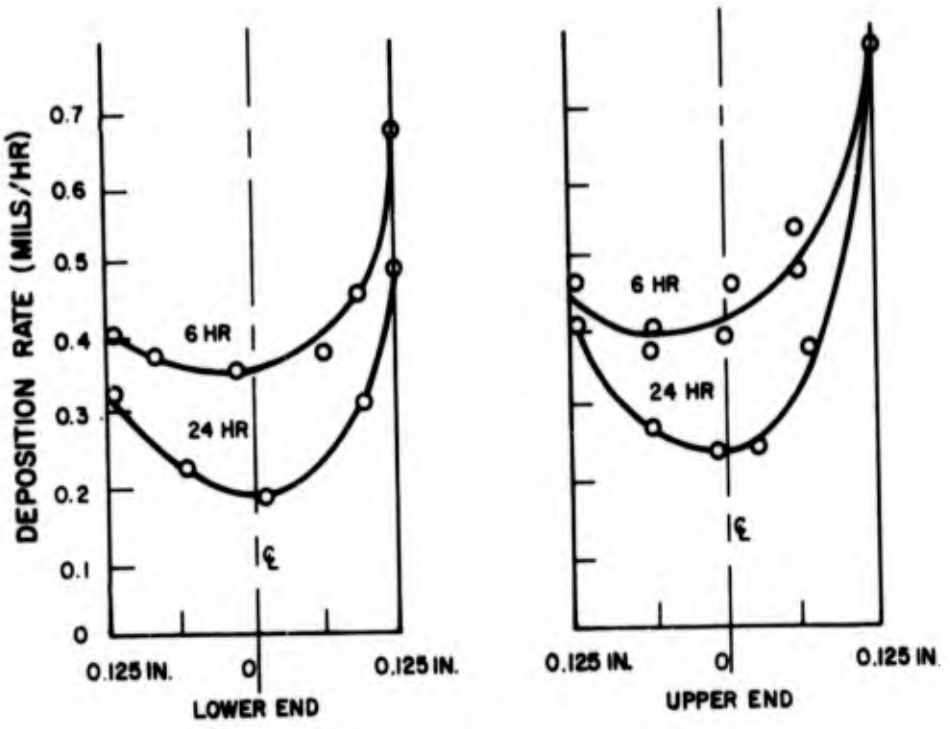

Figure 31. Deposition Gradients in BN Felt at 1100° C

by too high a deposition rate relative to the rate of penetration species. Reduction in temperature, concentration or both would tend to flatten out the deposition gradient, but would significantly increase the time required to achieve high composite density. A similar situation exists in the case of carbon infiltration where gas dilution, residence time variation and sacrifice of the outer layers of the composite can be used to increase infiltration efficiency of the inner surfaces. An additional factor in the deposition of boron nitride relates to the completeness of decomposition of the intermediate species. Deposits made at temperatures below about 1100° C in this laboratory have shown greater or lesser degrees of reactivity toward water in qualitative experiments, due perhaps to the trapping of unstable or undecomposed fragments within the deposit.

Four-directional Braid (Omniweave)

Because of its high surface area, low density and uniformly distributed void structure, felts in general are relatively easy to infiltrate pyrolytically. More complex woven and braided structures are characterized by tightly drawn fiber bundles, which are difficult to penetrate, and large geometrical voids which become sealed off before being completely filled. Figure 32 shows a section of the four-directional silica braid after fifty hours of infiltration of 1100° C in the pseudo-temperature gradient experiment described above. Penetration to the hot wall of the furnace tube through the weave was achieved; however, the deposition rate at the supposedly cooler front wall was more rapid, and access paths were sealed off. Deposition in the interior voids of

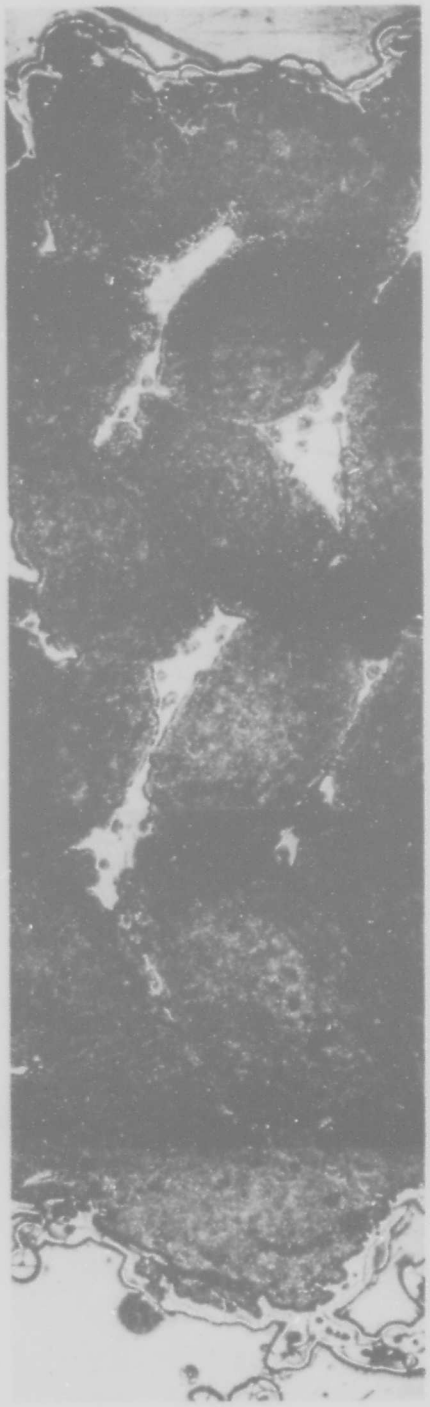

(a)

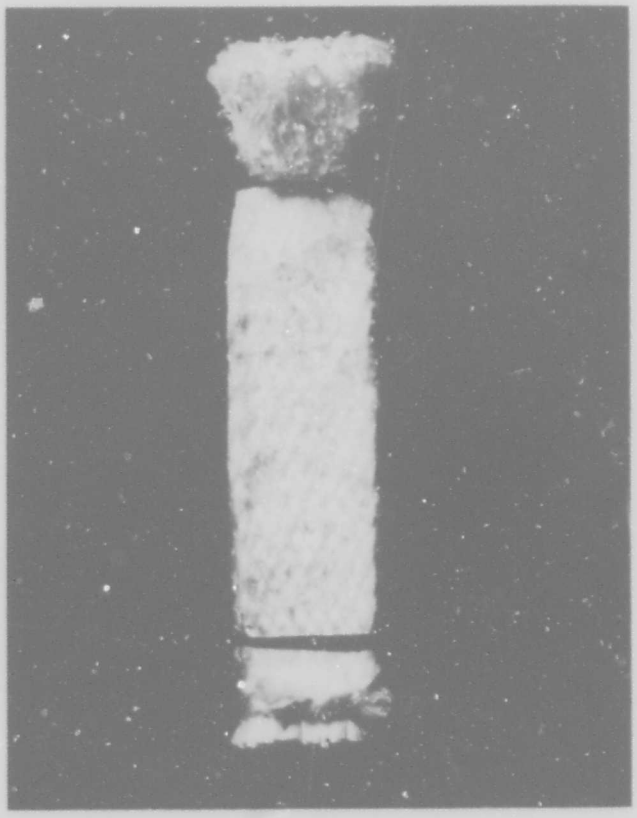

(b)

Figure 32: a) Cross-sectional Photomicrograph of 4-D Silica Braid after 50 Hours Silica CVD Infiltration by Pseudo-Temperature Gradient Experiment
b) Overall View of Specimen: Sectioned for Photomicrograph before Tensile Testing

the weave, which was only five layers thick, occurred only on the exposed surfaces of the bundles, but not within the bundles themselves. As will be discussed below, carbon infiltration of a four-directional braid which has a connected void structure has been observed to be somewhat more readily accomplished than infiltration of three-directional orthogonal weaves in which the void spaces are more or less cubic and connected only at the corners. The more rapid rate of decomposition of the trichloroborazole precursor, its lower concentration in the gas phase and the lack of volatile intermediate species in the decomposition sequence all tend to prevent penetration to constricted voids.

Infiltration Rate

Figure 33 shows the relative rates of infiltration of a boron nitride felt and a four-directional braided construction. As has been found in the case of carbon, which is also shown, the density increase obtained with felt is much greater than for the braid. In both cases however, final densities estimated by extension of the curves are less than those obtainable in carbon infiltrations. This is shown in greater detail in Figure 34 in which the influences of weave geometry, initial density and method of infiltration are shown for both carbon/carbon and boron nitride/boron nitride composites at 1100°C.

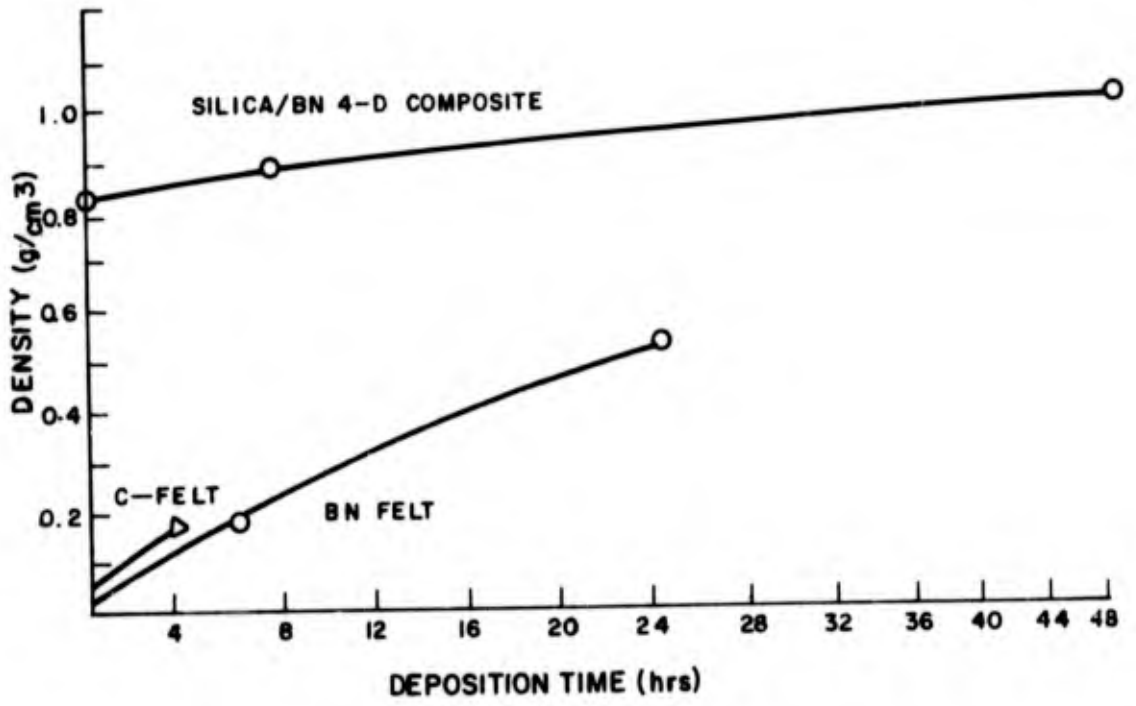

Figure 33. Densification Rates by CVD of BN, 4-D Silica versus BN Felt

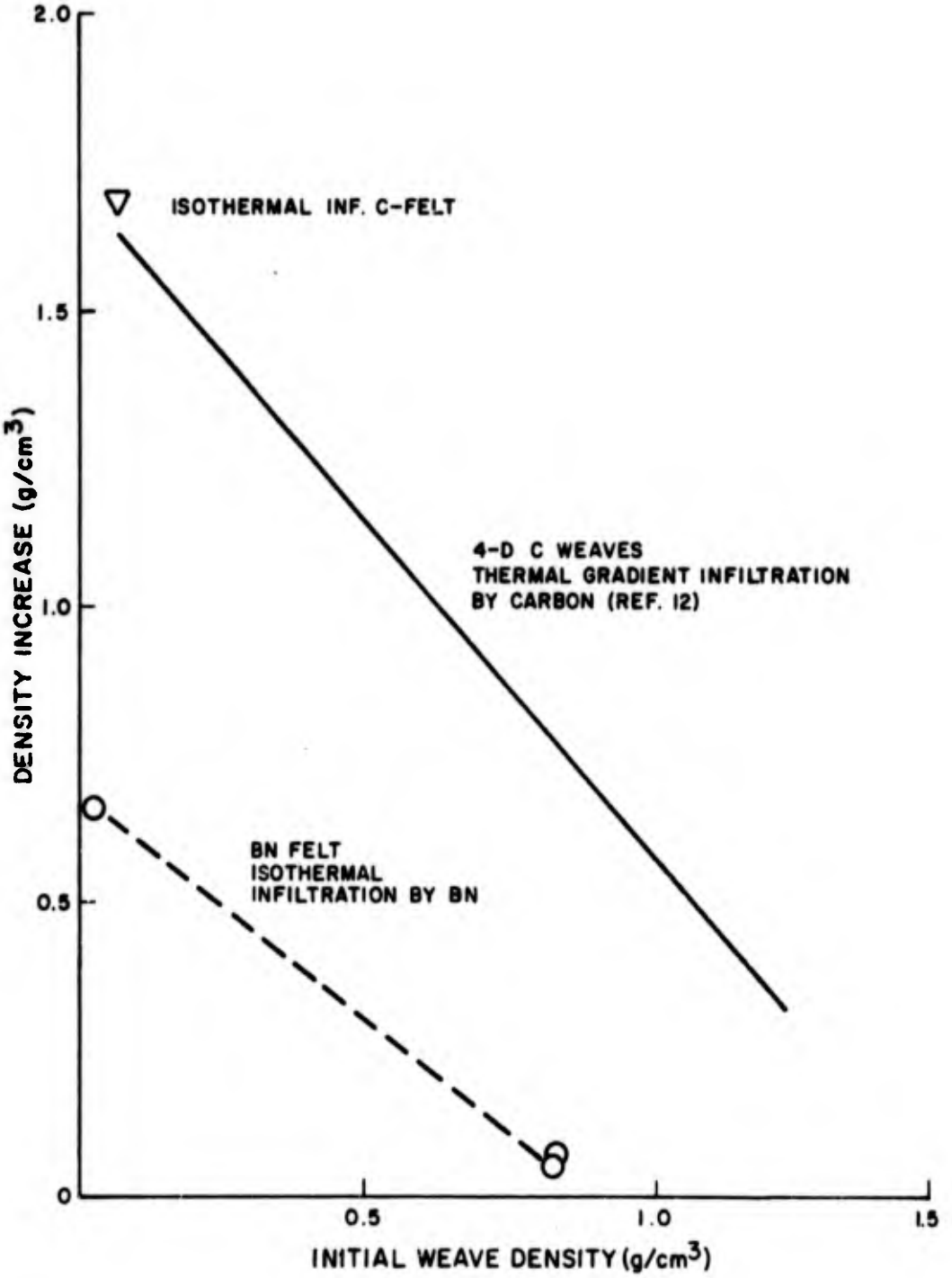

Figure 34. Correlation Between Initial Density and Density Increase by Infiltration, C/C and BN/BN Composites

B. Properties of Low Temperature Boron Nitride

Structure

The boron nitride deposits obtained at 1100° C were uniformly glassy and transparent, colorless to light yellow. Very little crystalline structure was evident in x-ray diffraction; some crystal growth occurred after heat treatment at 1800° C. The deposits formed on all fibers and in some cases the layered structure characteristic of carbon deposits can be seen. Figures 35a and b are typical views of the interior of a specimen after partial infiltration. The deposit appears to be tightly bonded to the boron nitride felt fibers.

The boron nitride deposits differed from analogous carbon deposits in that they tended to form nodular substructures more readily. The ends of projecting fibers as shown in Figure 36 for example, developed more pronounced knobs than are characteristic of low temperature carbon deposits. Fiber ends within the felt were similarly coated.

Thermal Properties

In addition to the deposits obtained on and within the fiber bodies, relatively thick layers (up to 38 mils) of transparent boron nitride were deposited on the inside wall of the deposition tube. Qualitatively, its thermal expansion coefficient appeared to be somewhat less than that of the high density (Great Lakes Grade HLM) graphite used for the tubes, since residual thermal stresses caused the specimen to develop a more or less rectangular network of cracks. Figure 37 shows this effect in deposits close to the filaments. Further evidence of instability was seen in the response of clean titanium strips, heated to 1350° C while in contact with both heat-treated and as-deposited coatings. In the former case, the strips were unaffected while in the latter, there was evidence of surface reaction in a manner which suggested volatilization or release of some component in the deposit which was reactive toward titanium.

A representative specimen deposited at 1100° C was heated to various temperatures above 1100° C in a Knudsen effusion cell; the gases evolved were subjected to mass spectrometric analysis. The principal species evolved, as shown in Figure 38 appeared to consist of hydrogen and amine fragments below about 1550° C and nitrogen gas above that temperature. Relatively small amounts of volatile boron-containing species as well as chlorine persisted to about 1650° C. Thus most of the low temperature reactivity appears to have been due to trapped -NH and $-NH_2$ fragments (Mass No. 15 and 16), while the high temperature species appear to be the result of the non-congruent volatilization of boron nitride itself which comprised the major portion of the deposit. The boron and chlorine are most likely trapped borazole fragments which were released progressively as the temperature was raised.

(a) 100X

(b) 530X

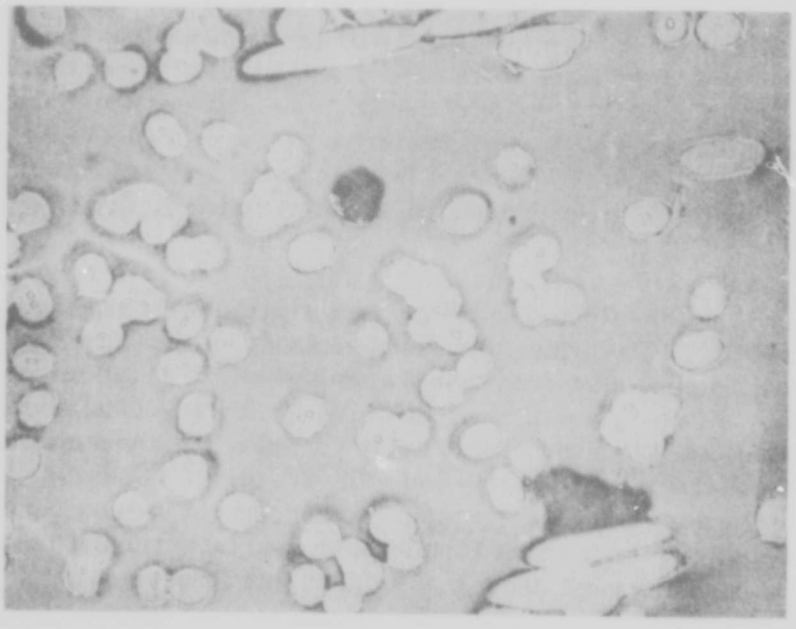

Figure 35. Structure of Partially Infiltrated Boron Nitride Felt; 1100°C Deposit for 6 Hours, No Heat Treatment

Figure 36. Structure of Heavy Nodular Deposit on Fibers on Exterior of Felt, Showing Transparent Nature of Low Temperature Material (4.5X)

Figure 37. Microstructure of Partially Infiltrated BN Felt after Heat Treatment for One Hour at 1800° C in Nitrogen. Note laminar as well as Cross Plane Cracks. (530X)

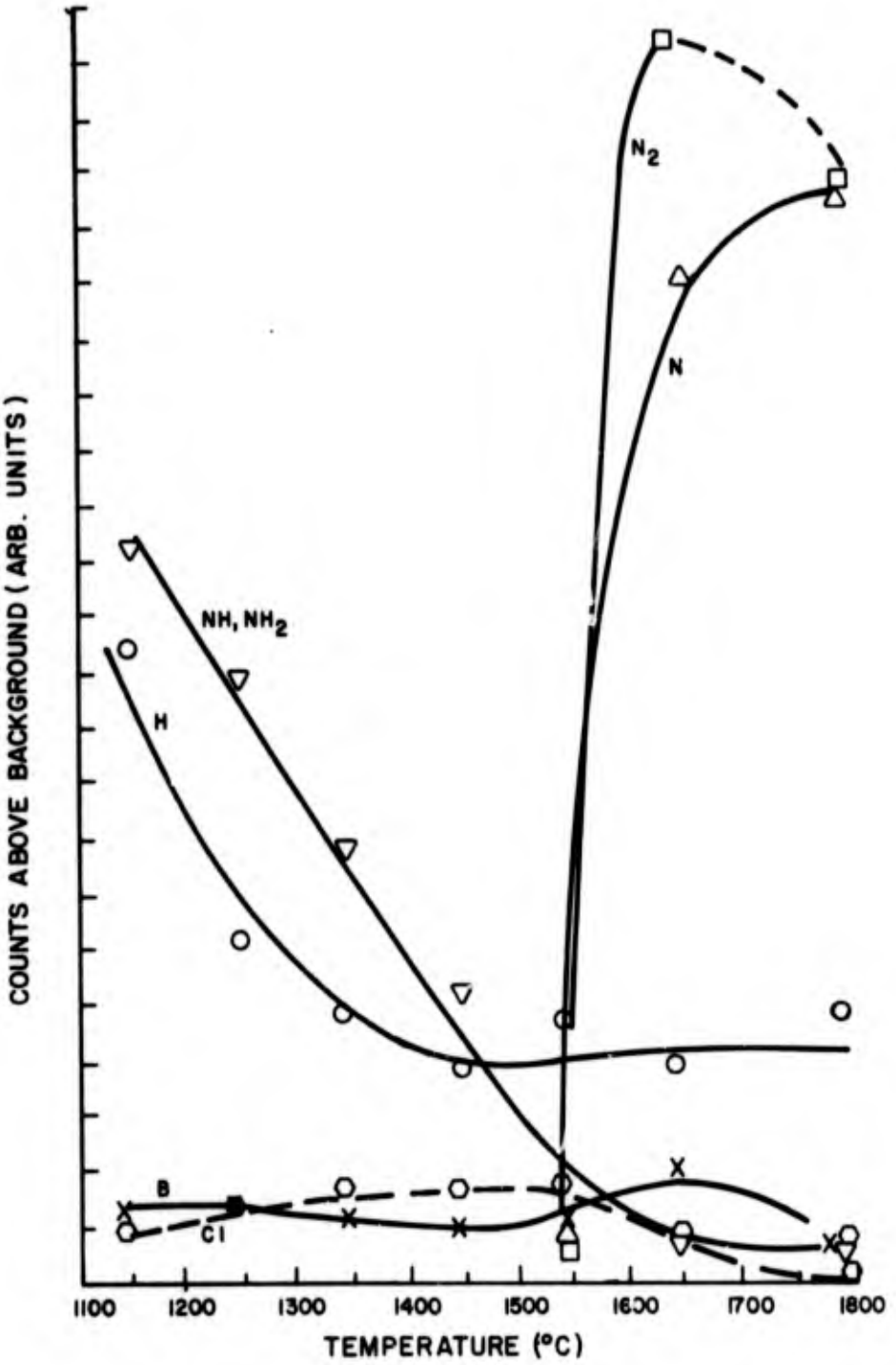

Figure 38. Gases Evolved on Vacuum Heating to 1800°C. Specimen Deposited at 1100°C.

The x-ray diffraction spectrum of as-deposited low temperature (1100° C) boron nitride showed it to be completely amorphous; heat treatment in nitrogen at 1800° C sharpened up the broad peaks, indicating crystal growth by a factor of perhaps five, and development of the characteristic hexagonal anisotropic boron nitride structure. The same result was obtained for the opaque, tan and buff colored specimens deposited from mixtures of boron trichloride and ammonia. Here the specimens also developed the characteristic white to buff color associated with high temperature boron nitride except for cases in which lemon yellow color was produced, possibly by traces of carbon in the original deposits.

Optical Properties

The transparent appearance of portions of the deposit within the felt was also characteristic of the deposit obtained on the walls of the tube at different temperatures. Initially frosty and gray in the as-deposited state, sections up to 1/4 in. x 1/2 in. were polished to colorless, glassy and visually transparent specimens. The visible to near IR spectrum shown in Figure 39 was obtained from a representative specimen. It was interesting to note that absorbance in the 2.5 - 2.6 μm region of the near-infrared was apparently high enough to heat an 18-mil thick specimen sufficiently to cause cracking, perhaps because of localized volatilization of trapped species. Therefore, various as-deposited and heat treated specimens were examined using the KBr pellet technique. These results are shown in Figures 40 and 41 for as-deposited and specimens heat-treated after deposition. Loss of spectral detail in the 2.5 - 3.0 μm region, owing possibly to loss of -NH and -NH_2 groups, and resolution of the broad bands in the B-N and lattice vibration regions were the principal changes observed.

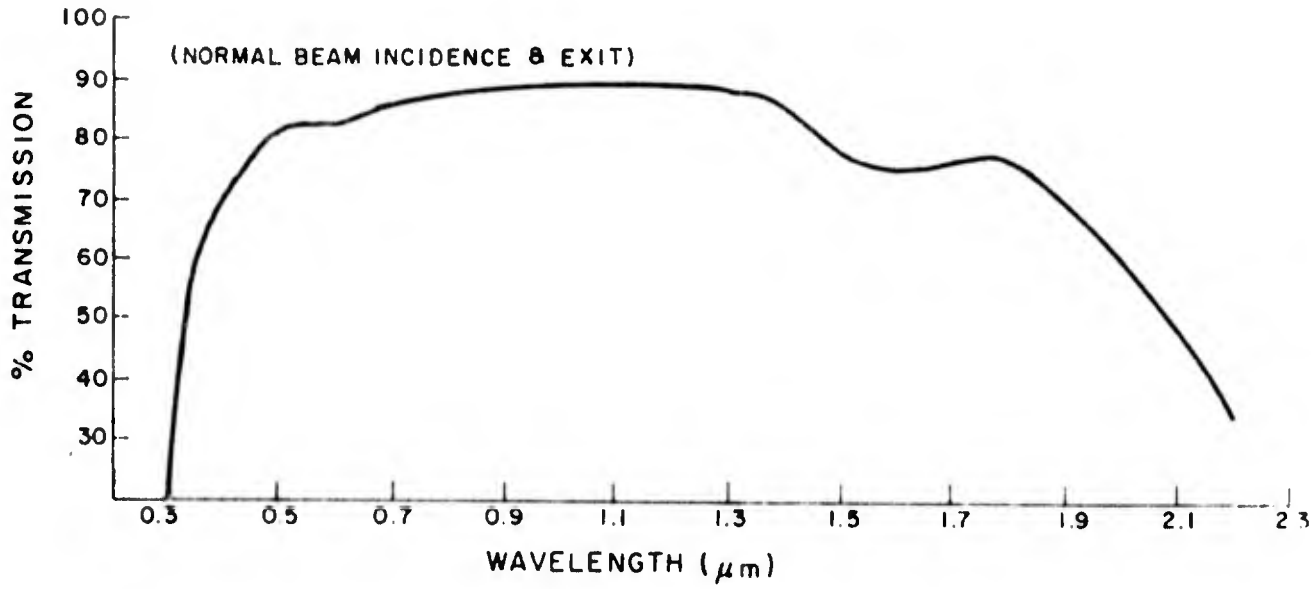

Figure 39. Visible - Near Infrared Spectrum of Transparent BN, as-deposited at 1100° C; thickness 18 mils

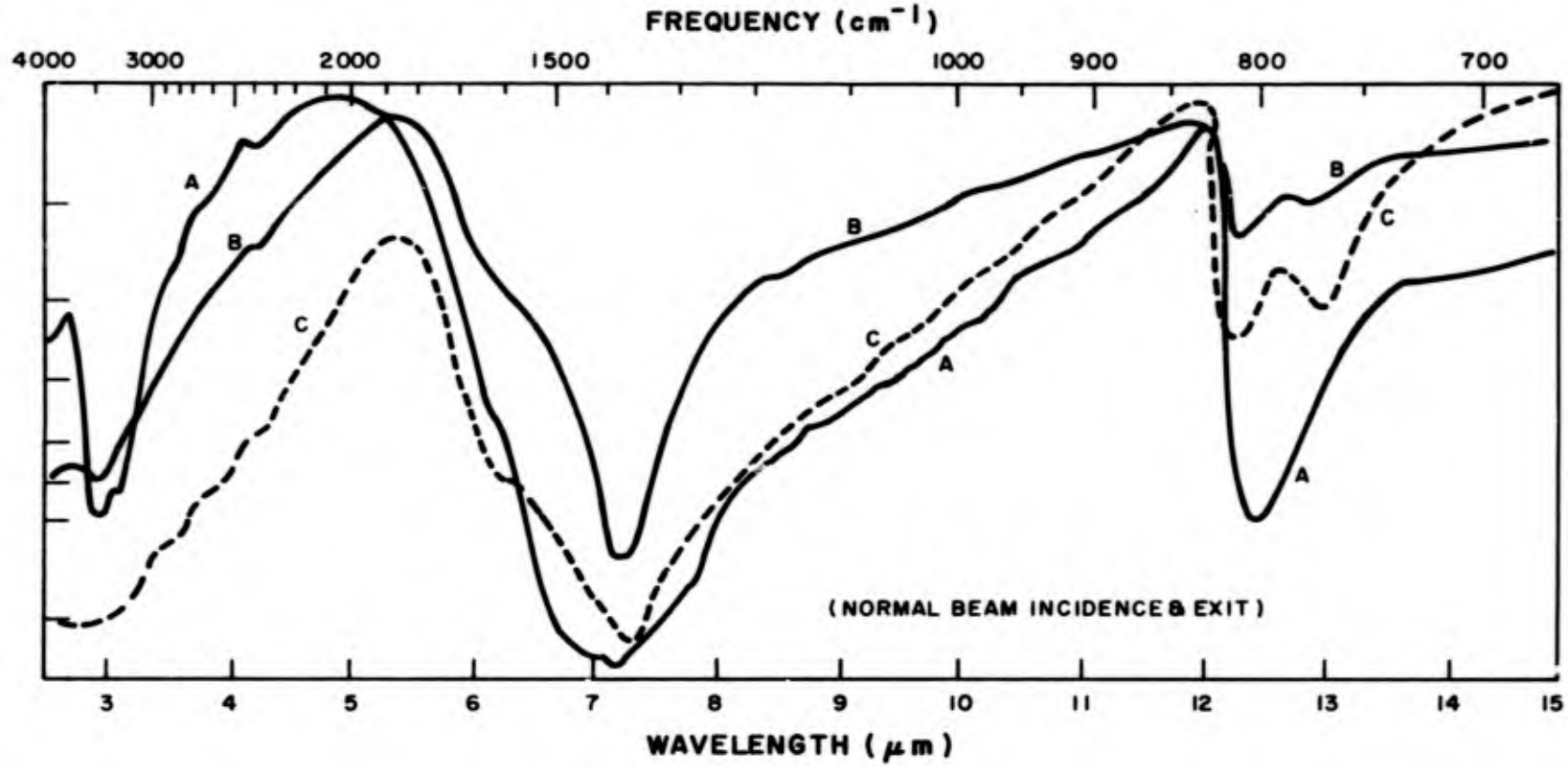

Figure 40. Infrared Spectra of As-Deposited BN; KBr Pellet
A. Deposition Temp. 1100° C; B. 1500° C; C. 1800° C

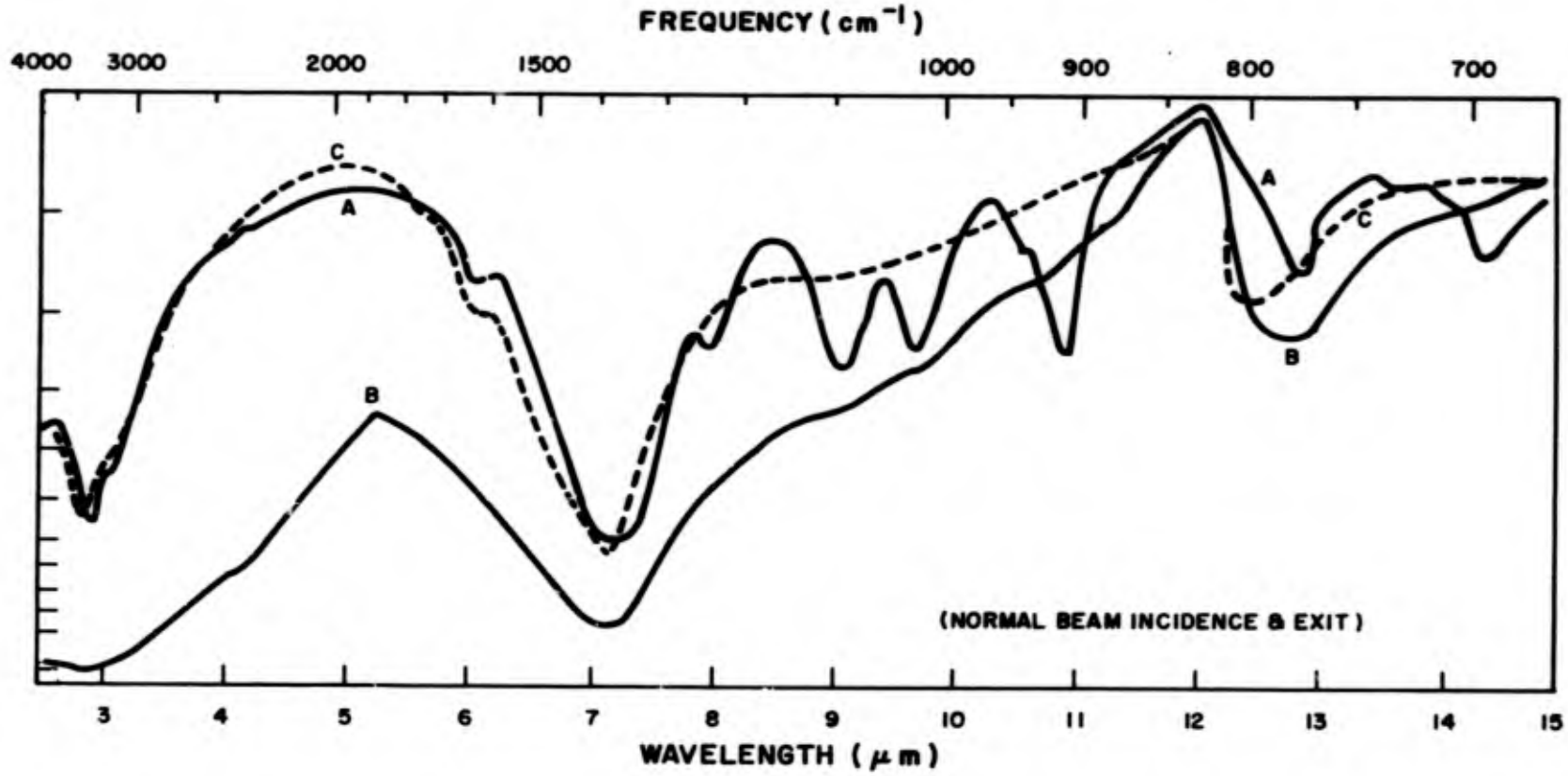

Figure 41. Infrared Spectra of Heat Treated BN Deposits; KBr Pellet
A. 1200°C (as deposited); B. H.T. 1 hr (N_2), 1800°C,
T. Dep. 1100°C; C. H.T. 1 hr (N_2), 1800°C, T. Dep. 1200°C.

Material deposited at 1800°C appears to be more crystalline than deposits made at 1100°C and subsequently heat treated at 1800°C in nitrogen for one hour. Longer exposure at higher temperature may be required to complete the transformation. The amount of trapped volatile or potentially volatile material is perhaps more dependent on the concentration of deposition species and deposition rate rather than on temperature alone. For example, the deposit made at 1200°C and subsequently heat treated shows far more complex spectra than the 1100°C deposit. This may have been due to a higher content of the same trapped fragments, or to the presence of different, more stable fragments characteristic of a gas phase pyrolysis temperature of 1200°C. Traces of these fragments appear at 9.2 and 9.8 μm in some cases even after heat treatment to 1800°C, even though the NH peaks in the 2.9-3.2 μm region have disappeared.

2.4.5.3 Discussion

Although silica, boron nitride and graphite can all be formed in dense, monolithic forms by thermal decomposition of available precursors, the necessary kinetic conditions for achieving penetration to within the structure of a fibrous preform appeared to prevail only in the case of carbon. It is essential that the first products of decomposition of the primary feed molecule (ethyl orthosilicate, B-trichloroborazole, methane) be maintained in the gas phase to prevent premature deposition. Under the circumstances existing in isothermal infiltration, only with the existence of a series of gas phase reactions, the products of which are themselves volatile, can the diffusion time for predeposition species be extended long enough for them to penetrate to internal surfaces. As far as is known, both ethyl silicate and B-trichloroborazole decompose to gaseous non-depositing products (Hydrocarbon fragments and HCl) and to a solid, i.e., a molecule whose vapor pressure at operating conditions is above the equilibrium value. By maintaining a very dilute concentration of the primary molecule, the solids formed may be sufficiently small in size to be carried to interior sites, but their deposition appears to be the consequence of physical encounter with a surface, and therefore, deposition occurs on all available surfaces at contact. Consequently, penetration to within tightly bundled fibers used to fabricate preforms cannot be achieved. Since the rate of deposition is dependent on the local concentration of deposition species, it will be higher at the outer surface of the structure and clogging of the outer pores will occur rapidly.

The situation in the case of thermal gradient infiltration is however somewhat more hopeful, although the irreversible nature of the early thermal decomposition reactions requires that extremely steep temperature gradients be achieved in the fibrous structure. In the case of carbon infiltration, this is usually accomplished by the use of a concentrated feed gas (e.g., natural gas) introduced at very high feed rates - the sequence of reactions producing higher molecular weight vapors permits generation

of the deposition nuclei to be delayed until the gas has penetrated deeply. The application of this approach to infiltration with primary source molecules which decompose very rapidly to deposition species without an intervening gas phase kinetic sequence has not yet been fully attempted under conditions which would appear to be promising. The requirements would include a sufficiently large supply of the primary source molecule to ensure maximum velocity at the highest achievable concentration below the sooting level and a temperature gradient steep enough to permit decomposition/deposition to occur only at the highest temperature in the gradient. The more forgiving nature of the hydrocarbon thermal decomposition sequence permits deposition in depth to be achieved with relative ease. More stringent control would be required to infiltrate boron nitride and silica.

The degree of outgassing encountered in the case of low temperature boron nitride suggests that some heat treatment procedure would be required to stabilize the deposit which would not disrupt the fiber preform or its properties. Thermal soak temperature-time profiles would have to be determined in future work to achieve a stable composite.

2.4.5.4 Conclusions

The partial ability to infiltrate fibrous preforms with CVD silica and boron nitride has been demonstrated. Some of the requirements for achieving greater degrees of densification and for producing thermally stable composites have been delineated. Compared to the more conventional processing techniques discussed elsewhere in this report, the CVD approach as the primary matrix formation process appears to be impractical as a manufacturing technique in its present state of development. This however does not preclude the use of CVD techniques to produce impervious coatings on composites formed by other approaches.

2.4.6 GLASS BONDED BORON NITRIDE/QUARTZ OMNIWEAVE - "BNQ"

2.4.6.1 Matrix Characterization

Emulsions of boron nitride in a high temperature glass bond phase were evaluated as matrix systems for quartz Omniweave reinforcements. Three types of boron nitride emulsions (Ref. 16), in different glass bond phases, were evaluated. The characteristics of each type of boron nitride emulsion are listed in Table 20.

Vendor (Ref. 16) data indicates that the approximate chemical compositions are 75 to 90 percent by weight of boron nitride and the remaining is the inert refractory bond phase. The vendor data also indicates that the coatings can be used for extended service up to 2500°F in a reducing atmosphere and up to 1300°F in an oxidizing atmosphere.

TABLE 20. CHARACTERISTICS OF CARBORUNDUM BN COATINGS

	Boron Nitride Emulsion Type	Glass Bond Phase	Solids (1) Content (wt. %)
increasing hardness of dried and fired coating ↓	S	Al_2O_3	34
	V	$Mg\ SiO_4$	34
	A	$AlPO_4$	54

Calculations of the boron nitride/glass phase matrix densities were approximated by taking the average of the calculated matrix densities at 75 percent by weight boron nitride/25 percent by weight inert phase and 90 percent by weight boron nitride/10 percent by weight inert phase. The densities of the inert bond phases were assumed to be 3.95 gm/cc for the Al_2O_3 phase (type S), 3.20 gm/cc for the Mg_2SiO_4 phase (type V) and 2.57 gm/cc for the $AlPO_4$ phase (type A). The approximated theoretical matrix densities are tabulated in Table 21. The actual bulk density of the Type V matrix produced by firing to 1200°F for 2 hours is also given. This density was determined by a Westphal Density Balance and would indicate an approximate Type V matrix phase porosity of 20 percent.

TABLE 21. DENSITIES OF CARBORUNDUM COATINGS IN DRY, MATRIX FORM

Matrix Type	Calculated Theoretical Approximate Density (gm/cc)	Bulk Density (gm/cc)
S (Al_2O_3)	2.53	2.00
V (Mg_2SiO_4)	2.42	
A ($AlPO_4$)	2.28	

To further investigate the basic characteristics of these candidate inorganic matrix materials, thermogravimetric (TGA) and differential thermal analyses (DTA) were performed. Figures 42 and 43 show a TGA and DTA respectively of the Type V material. The circled DTA endotherm centered around 1300°F corresponds to the larger TGA mass loss step for the 250°F dried sample, also centered around 1300°F. It will be seen below in the BNQ composite fabrication description that two firing temperatures of 850 and 1300°F were studied for their effect on composite strength and, in the description of the mechanical test results, that the 850°F firing gave better strengths for the Type V material. The TGA and DTA data do not however rule out that an intermediate temperature below the indicated endotherm may actually be closer to optimum. The choice of optimum firing temperature for these candidate

(1) Measurements done at GE; includes boron nitride and glass bond phase.

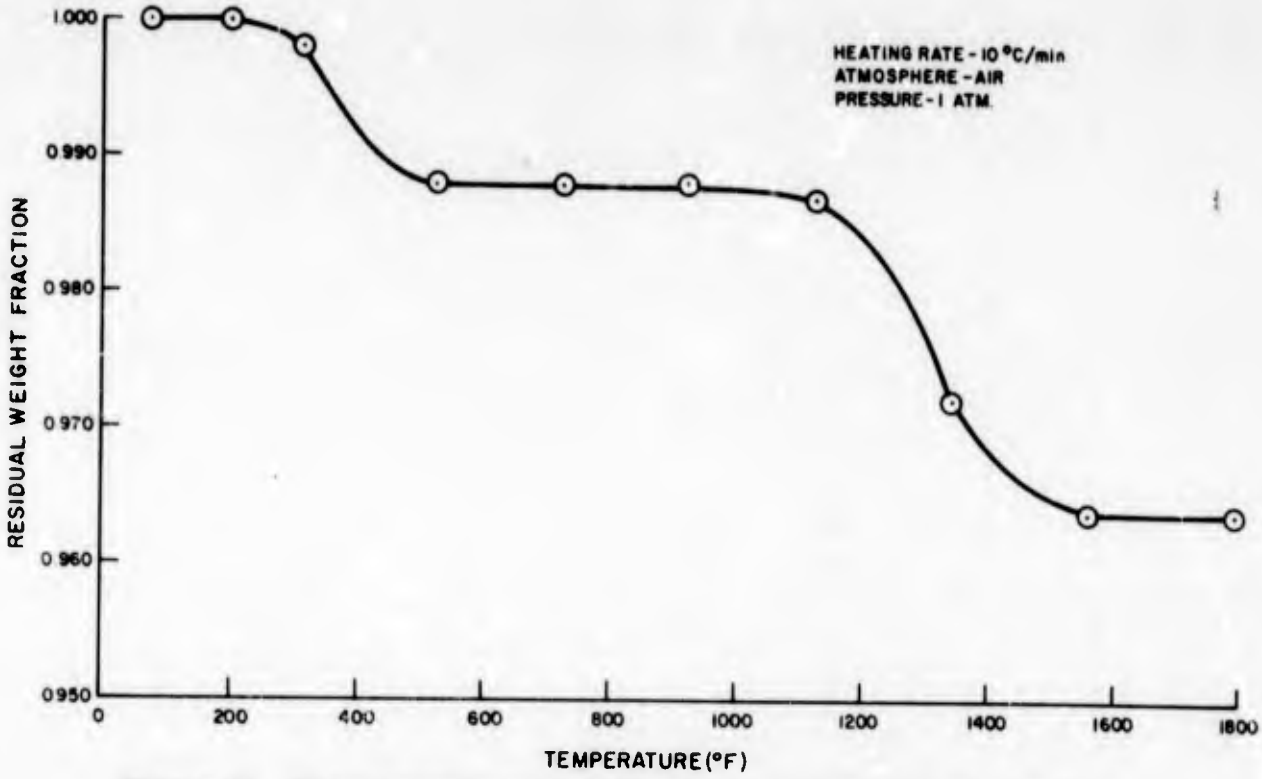

Figure 42. Thermogravimetric Analysis of Boron Nitride "Series V" ($MgSiO_4$ flux, cured at 250°F)

matrices was also influenced by preliminary screening dielectric measurements on identical samples fired to the various temperatures (see paragraph 3.5, Electromagnetic Characterization).

Similar TGA and DTA data were also obtained on the Type S and A materials, as shown in Figures 44 and 45. The DTA shows no distinctive thermal transformation effects for either material, with the possible exception of a tendency of a run more strongly exothermic than the S material above 1600°F. Concurrent fiber processing studies had shown the Type A phosphate-bonded material to have an embrittlement effect on the high purity silica Astroquartz fibers so that these studies of its thermal reaction effects were not further pursued.

The TGA of the Type S material shows a reasonable mass loss dependence on previous firing temperature. The version fired to 1200°F for 2 hours undergoes almost indistinguishable loss above 700°F, apparently 0.8 percent; the 650°F fired material loses 2.7 percent. But both lose 1.4 percent of their original laboratory environment room temperature weight upon heating in air to 700°F. The indicated increases in weight after cool-down over a few hours to room temperature in the TGA instrument open to the laboratory atmosphere also show that water is picked up. It should be noted that these are very small specimens, 10-20 milligrams, ground to a powder to increase their reactivity and therefore their surface area to volume ratio. A larger part suitable for

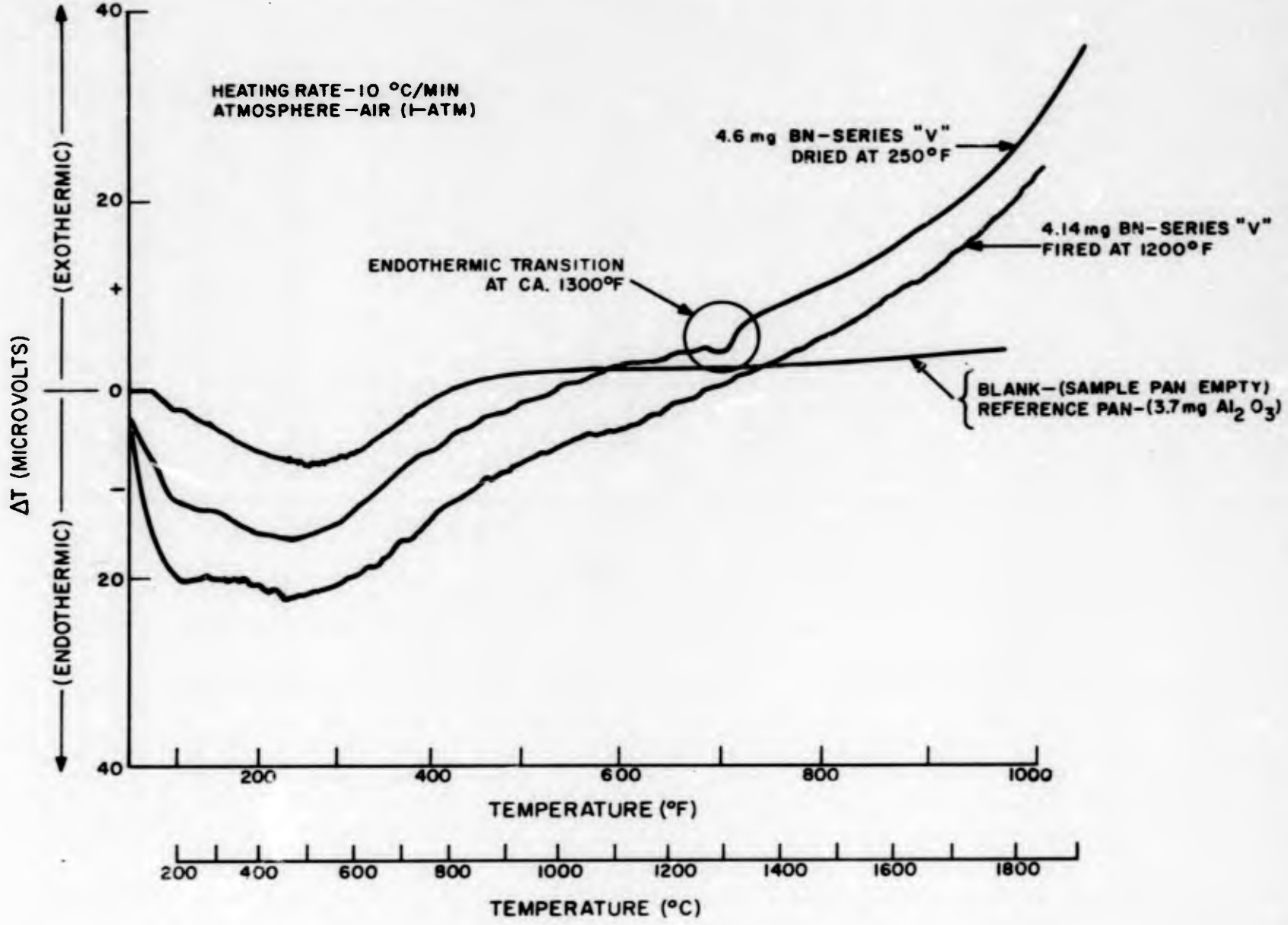

Figure 43. DTA of BN-Series "V" Specimens

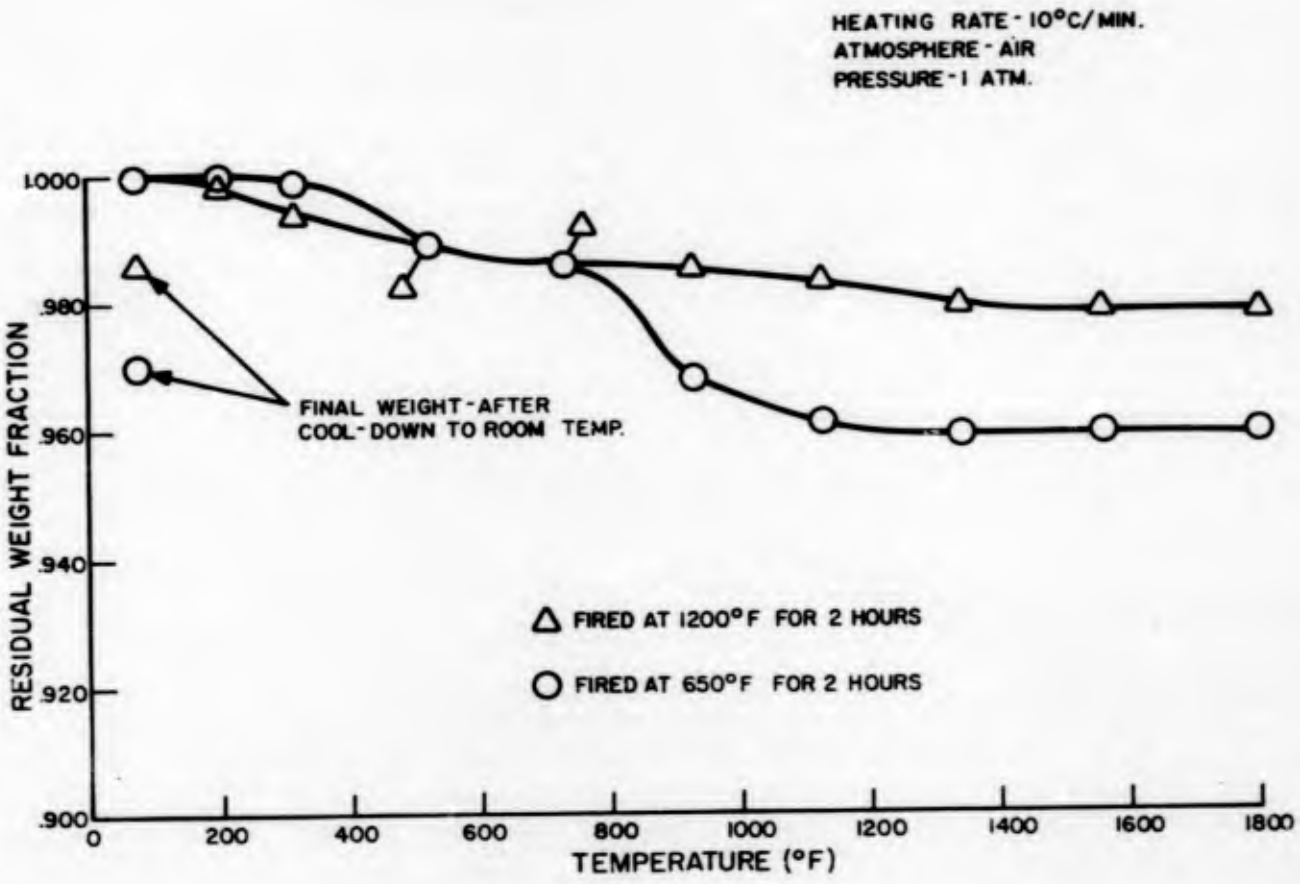

Figure 14. TGA of Boron Nitride Type S Matrix Material

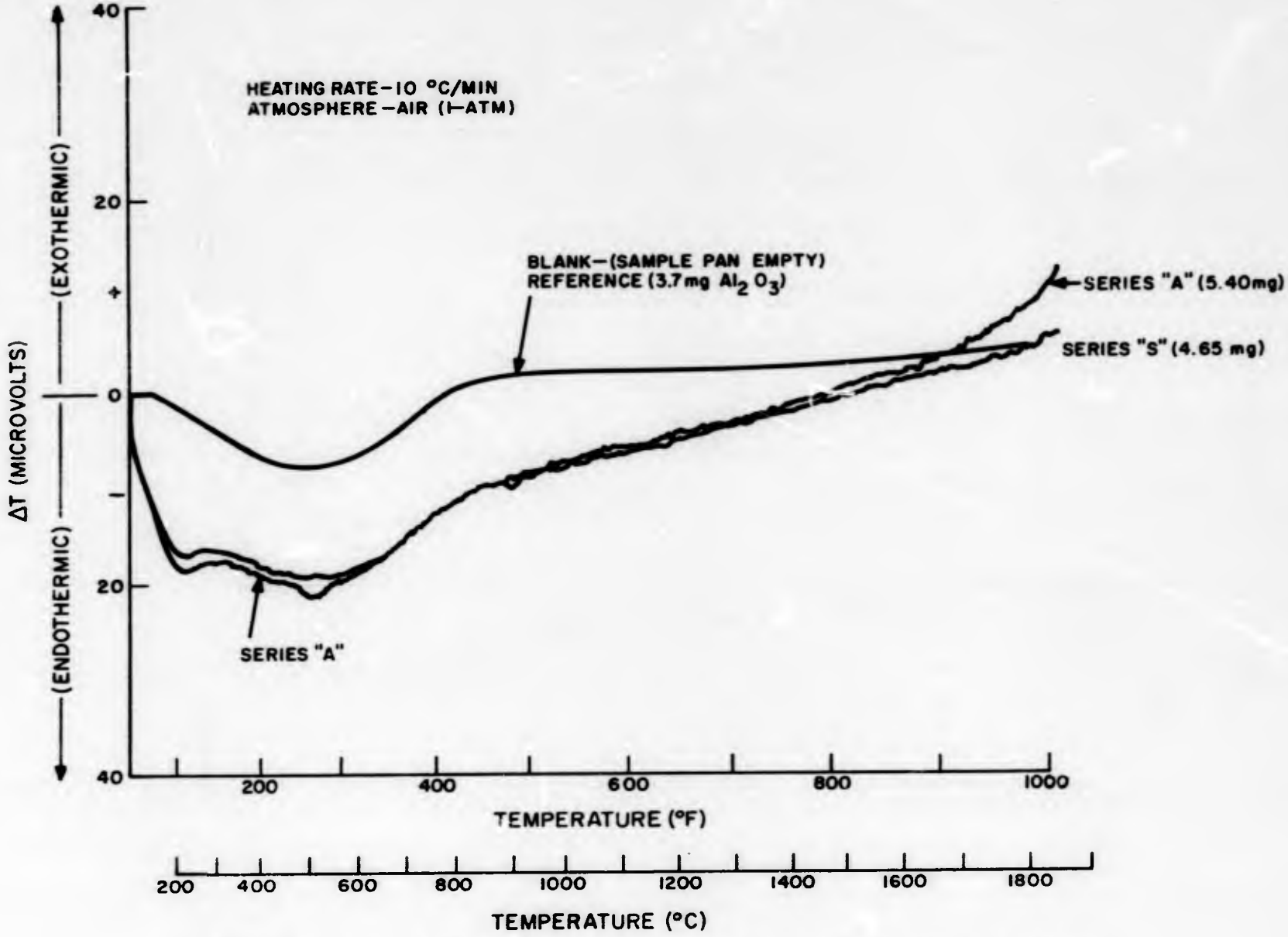

Figure 45. DTA of BN Specimens Series "A" and Series "S" (Fired at 1200°F)

antenna window use would be far less permeable. Measurements of the dependence of the dielectric properties on exposure to atmospheric moisture are given in Paragraph 3.5.

2.4.6.2 Composite Process Formulation and Characterization

Two approaches were taken in order to densify the quartz Omniweave with these emulsions: post-weaving infiltration and pre-weaving impregnation.

In post-weaving infiltration, vacuum/air pressure techniques were used to impregnate the Omniweave constructions with the boron nitride emulsions. All three types of boron nitride emulsions were first diluted to 30 percent by weight solids with distilled water, then a section of Omniweave (from strip no. 400) was immersed in each emulsion. The impregnation vessels were placed in an autoclave and vacuum (31 in. Hg) was applied for 10 minutes, then air pressure (1000 psi) was applied for 30 minutes. The parts were removed from the impregnation vessels and dried at room temperature for 16 hours, 200°F for 4 hours, then fired at 650°C for 2 hours. Table 22 lists the final densities.

TABLE 22. CHARACTERISTICS OF POST WEAVING INFILTRATED BNQ COMPOSITES

Part ID	Initial Weave Density (gm/cc)	Emulsion Type	Final Composite Density (gm/cc)
BNQ/A-400-1	↑	A	1.15
BNQ/V-400-1	0.99	V	1.10
BNQ/S-400-1	↓	S	1.15

The surfaces of the finished parts were found to be coated with the boron nitride/glass which blocked further penetration. Additional impregnations were therefore not attempted by this technique. A cross-sectional inspection of the finished parts showed that the boron nitride filled the areas between the fibers, but did not penetrate into the fiber bundles.

Due to the relatively unsuccessful attempts to densify the quartz Omniweave fabrics by vacuum/pressure techniques, an alternate approach was investigated. Preliminary studies showed that pre-impregnating the quartz roving with the boron nitride/glass emulsions prior to weaving provided better penetration of the matrix into the quartz fiber bundles. Approximately 15 feet of Astroquartz roving (silane finish) were pre-preged with each type of boron nitride/glass emulsion to determine the weaving feasibility and characteristics of the prepreg. To impregnate, the quartz roving was pulled

through a trough containing the boron nitride/glass emulsion. As the roving passed through the emulsion, it was flattened out via a roller to provide better "wetting" of the individual filaments. The emulsions were diluted with distilled water to achieve better fiber wetting. After impregnating with the boron nitride/glass emulsions, the quartz rovings were suspended vertically to air dry. The results of the prepreging investigation are shown in Table 23.

Due to the brittleness of the "A" type boron nitride/glass emulsion on air drying, it was eliminated from further processing studies. Two Omniweave fabrics were woven using boron nitride/glass prepreged Astroquartz roving. The specific emulsions used were Type S at 30 percent solids and Type V at 15 percent solids.

In fabricating the Omniweave, the required amount of Astroquartz roving was prepreged in the aforementioned manner and air dried before loading into the Omniweave loom. After loading the prepreg, weaving proceeded as in the standard fashion except that, to further densify the weave, the particular boron nitride emulsion in use was applied full strength (34% solids) across every stitch row prior to compaction. Subsequent weaving motions forced this added emulsion into the areas between fiber bundles. Upon completion of weaving, the fabric was removed from the loom and dried as follows:

24 hrs at R.T.

16 hrs at 160°F

4 hrs at 220°F

TABLE 23. RESULTS OF ASTROQUARTZ ROVING PREPREG INVESTIGATION

Boron Nitride Emulsion Type	Solids Contents	Air-Dried Wt. % Pickup on Roving	Prepreg Quality
A	30	52	Brittle, non-uniform coatings; poor fiber wetting
V	30	24	Soft, uniform coating; fair wetting
V	15	19	Soft, uniform coating; good wetting
S	30	19	Very soft, uniform coating; good wetting

Two boron nitride/glass phase quartz Omniweave fabrics were produced using this technique. The characteristics of each weave are discussed below.

2.4.6.2.1 Omniweave Fabric No. 406 (Boron Nitride/Al_2O_3 Bond Phase)

This fabric was a standard 4-D cubic construction, in the tensile test bar geometry, 7 rows thick by 10 rows wide, using Astroquartz roving/boron nitride - Al_2O_3 glass phase prepreg. During weaving, heavy combing pressure was used to compact the stitch rows, resulting in a high fiber pitch angle. The finished fabric was 21-1/2 in. x 11/16 in. x 13/32 in. and after the 220°F dry, was divided into four 5-inch sections suitable for tensile testing. The characteristics and further processing of each section are listed in Table 24.

TABLE 24. CHARACTERISTICS OF BNQ/S406 PREPREG OMNIWEAVE: TWO FIRING TEMPERATURES

Part ID	FPA (deg)	TTA (deg)	Firing Temp. (°F, 4 hrs)	Fiber (vol. %)(1)	Porosity(1) (%)	Density (gm/cc)
BNQ/S406-1	↑	-	850	↑	↑	↑
BNQ/S406-2	45 to 50	-	850	14	49	1.25
BNQ/S406-3	↓	-	1200	↓	↓	↓
BNQ/S406-4	↓	-	1200	↓	↓	↓

(1)Based on approximated matrix density of 2.53 gm/cc

2.4.6.2.2 Omniweave Fabric No. 407 (Boron Nitride/Mg_2SiO_4 Bond Phase)

This Omniweave fabric was a segmented 4-D cubic weave, whose four strips (7 rows by 11 rows) were woven simultaneously to a 10-inch length, then integrated to form one strip 7 rows by 44 rows and woven to a 15-inch length. Figure 46 is a detailed outline of weave No. 407 showing the dimensions, sections and characteristics of each section. Figure 47a is a photograph of the integrated portion of weave No. 407 while still in the Omniweave loom. The segmented strips were divided into 8 tensile bars (BNQ/V-407-1 to 8) and the integrated portion (BNQ/V-407-9) was machined into directional tensile bars, dielectric property, thermal conductivity, and ablation samples. Table 25 lists the specific characteristics and firing temperatures of each section of the weave. Figures 47b and 47c are photographs of the integrated portion (BNQ/V-407-9) after drying at 220°F.

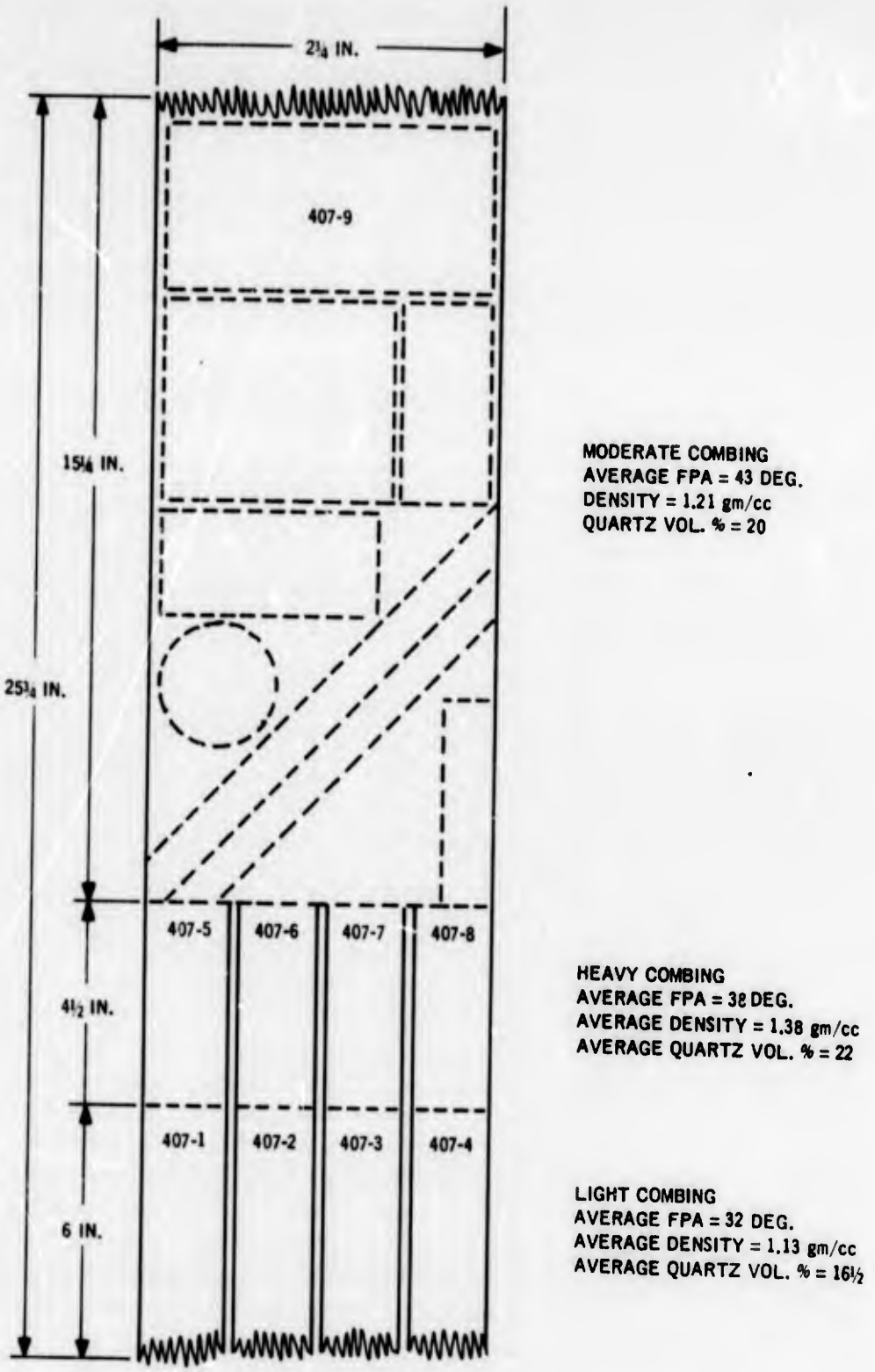

Figure 46. Composite Omniweave Fabric #BNQ/V-407: Weaving Sequence and Characteristics

(a) Composite fabric in Omniweave loom

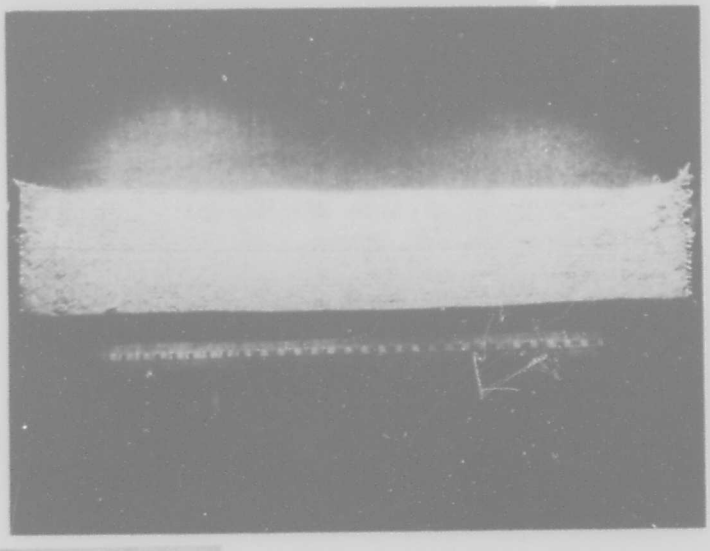

(b) Composite fabric after 220°F dry

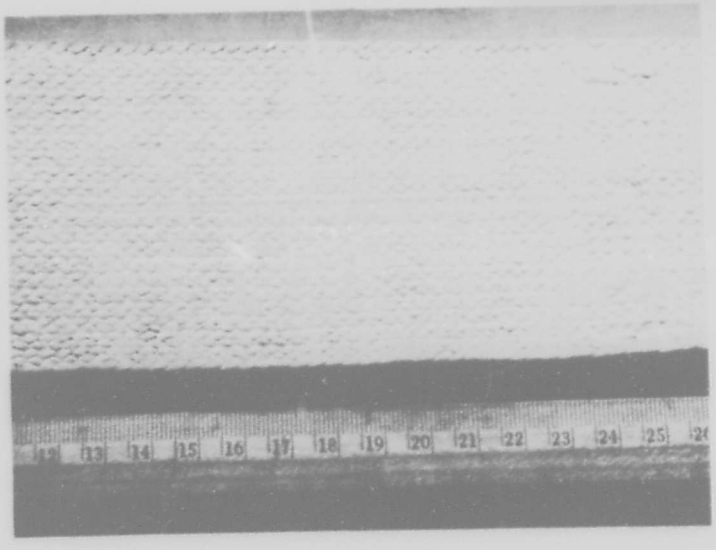

(c) Close View: Composite fabric after 220°F dry

Figure 47. Composite Omniweave Fabric: BNQ/V-407-9

TABLE 25. CHARACTERISTICS OF BNQ/V-407 PREPREG OMNIWEAVE COMPOSITES

Part ID	FPA (deg)	TTA (deg)	Firing Temp. (°F, 4 hrs)	Fiber[1] (vol. %)	Composite Bulk Porosity[1]	Density (gm/cc)
BNQ/V-407-1	35	37	↑	15	52	1.13
BNQ/V-407-2	32	35		16	51	1.15
BNQ/V-407-3	30	32		16	49	1.20
BNQ/V-407-4	30	33	850	19	45	1.30
BNQ/V-407-5	36	32		21	39	1.42
BNQ/V-407-6	39	--	↓	22	40	1.41
BNQ/V-407-7	39	35	1200	23	42	1.35
BNQ/V-407-8	40	--	1200	22	43	1.33
BNQ/V-407-9	43	37	850	20	49	1.21

[1]Calculations are based on a matrix theoretical density of 2.42 gm/cc

2.4.6.2.3 Boron Nitride-Glass Phase/Quartz Roving Bidirectional Composites

To provide further characterization data on the boron nitride-glass phase/quartz Omniweave composites, flat panels with the quartz rovings at a ±45-degree orientation to the principal axis were fabricated via the same prepreging techniques used for the boron nitride-glass phase prepreged Omniweave fabrics. The Astroquartz roving (silane finish) was prepreged with the specific boron nitride-glass emulsion and wound wet on a loom. Ten layers of quartz roving were wound at alternate orientations of +45 degrees and then -45 degrees to the principal axis. Boron nitride emulsion was brush applied to each layer prior to winding the succeeding layer. When the wet lay-up was completed, the composites were dried under low static pressure (0.5 psi) at 160°F for 48 hours then fired at 850°F for 4 hours (no pressure). Table 26 lists the characteristics of the bidirectional composites.

The 3-1/2 inch wide panels were cut, with a diamond edge saw, into tensile bar specimens 1 inch wide by 12 inches long, to which glass/epoxy end grip doublers were applied, and submitted for mechanical testing.

TABLE 26. CHARACTERISTICS OF BNQ BIDIRECTIONAL LAMINATES

Characteristic	BNQ/S ± 45 Deg	BNQ/V ± 45 Deg
Glass phase	Al_2O_3	Mg_2SiO_4
Thickness (inch)	0.249	0.177
Density (gm/cc)	1.04	1.14
Quartz (vol. %)[1]	13	19
Porosity (%)	57	51

[1]Calculations based on matrix theoretical densities of 2.53 gm/cc (Al_2O_3 glass phase) and 2.42 gm/cc (Mg_2SiO_4 glass phase).

SECTION 3.0

TABLE OF CONTENTS

TABLE OF CONTENTS (Continued)

3.0 CHARACTERIZATION

3.1 THE SAMPLING AND CHARACTERIZATION PLAN

3.1.1 INTRODUCTION

The characterization effort described in this section proceeds according to two separate outlines, corresponding to the two materials classes and their stages of development. The purpose of the ADL-10 testing effort is to complete characterization of this material at extreme environmental levels and to determine the effects of machining the finished molded composite surfaces. The explicit test matrix for this final work on ADL-10 is given in Table 27.

The detailed sampling of the ADL-10 material is given in paragraph 3.1.2.

Since the purpose of the ADL-10 testing in this program has been to virtually complete the characterization of this already developed and rather extensively characterized material, the test matrix could be laid out in the above form previous to the actual

TABLE 27. TEST MATRIX FOR ADL-10 CHARACTERIZATION

Physical Performance Test	Specimen	Purpose for Test
Tensile Strength	3/4 - 1 inch wide bar, 4 - 6 inches long with fiberglass reinforced grip doublers, with as-molded and machined faces	- Determine the effect on tensile strength of interrupting fiber continuity at the molded specimen face surface (simulating machining to size in a manufacturing operation).
Plate Impact - Magnetic Flyer (GE-RESD) - Exploding Foil (Effects Technology)	2.00 inch diameter, in as-molded thickness and with one or both faces machined.	- First: to determine the failure threshold at impact levels above that available at GE-RESD facility (4500 taps). - Second: determine effect of machining surfaces on the threshold.
Hypersonic Large Particle	4.00 inch x 6.00 inch rectangular plate	- Determine survivability on macro scale in large particle hypersonic impact environment.

material fabrication and testing. For the inorganic composite candidates however, no such clearcut matrix could be specified beforehand because of the necessarily explorative and iterative testing sequences appropriate for development of new materials, beginning in some cases, such as the BNQ glass-bonded boron nitride matrix, with the basic properties of the matrix itself. The final characterization data required by the contract for description of the inorganic candidates included tensile and flexure strength and elastic data, RF/dielectric and ablation data and the shock resistance characteristics via magnetic flyer and ultrasonic testing. The screening sequence in which this characterization was carried out and the graduation to higher levels of testing are represented in flow chart form in Figure 48. In the case of the preliminary matrix screening, and RF/dielectric loss tangent less than 0.01 was sought at the several levels of thermal transformation as indicated by DTA and TGA screening. The suitability of the matrix for composite fabrication was revealed by preliminary densification studies and is shown in the program plan flow chart of Figure 1, by elastic property studies on unidirectional laminates. In the studies on actual inorganic Omniweave composites, trial specimens were first made using the standard set of closed-edge segmented Omniweaves No. 381 and No. 400. The processing (e.g., firing temperature, degree of densification) was also varied at this stage. It will be seen that several concepts did not pass this screening phase, mainly because of difficulty in achieving sufficient levels of densification. Examples are the CVD processes and the silica - boria systems in the Omniweave impregnation processes tried. Other specific matrices failed and were replaced by variations of the same material, such as the HS Ludox which was successfully replaced by the AS Ludox. Upon passing this screening phase, entire panels of the more promising materials were made according to the partially optimized process from which specimens were cut to determine directional mechanical properties, shock and ablation properties on a sufficient number of specimens to establish statistical data for the final candidate developmental materials.

3.1.2 DETAILED SAMPLING PLAN AND RADIOGRAPHIC NDT

3.1.2.1 ADL-10 Panels

The detailed sampling layouts for the ADL-10 Plate material of this program are shown in Figures 49 through 55 along with radiographs of the 403 and 404-1 moldings. A second small portion of Omniweave No. 404 was used for colloidal silica densification as will be seen in Paragraph 3.1.2.2. Reference to Figure 1, the flow charted program plan for this study, will show the overall disposition of samples.

The required ADL-10 testing of this program called for flyer plate testing at levels high enough to establish the failure threshold and for determination of the effects of face machining (not "edge" machining of segmented weave specimens which was studied in Ref. 2) on the tensile strength and shock failure threshold of molded ADL-10. Panel 402 was the first panel fabricated, using the optimum processing conditions established in Reference 2 and taking account of the improved density of the base

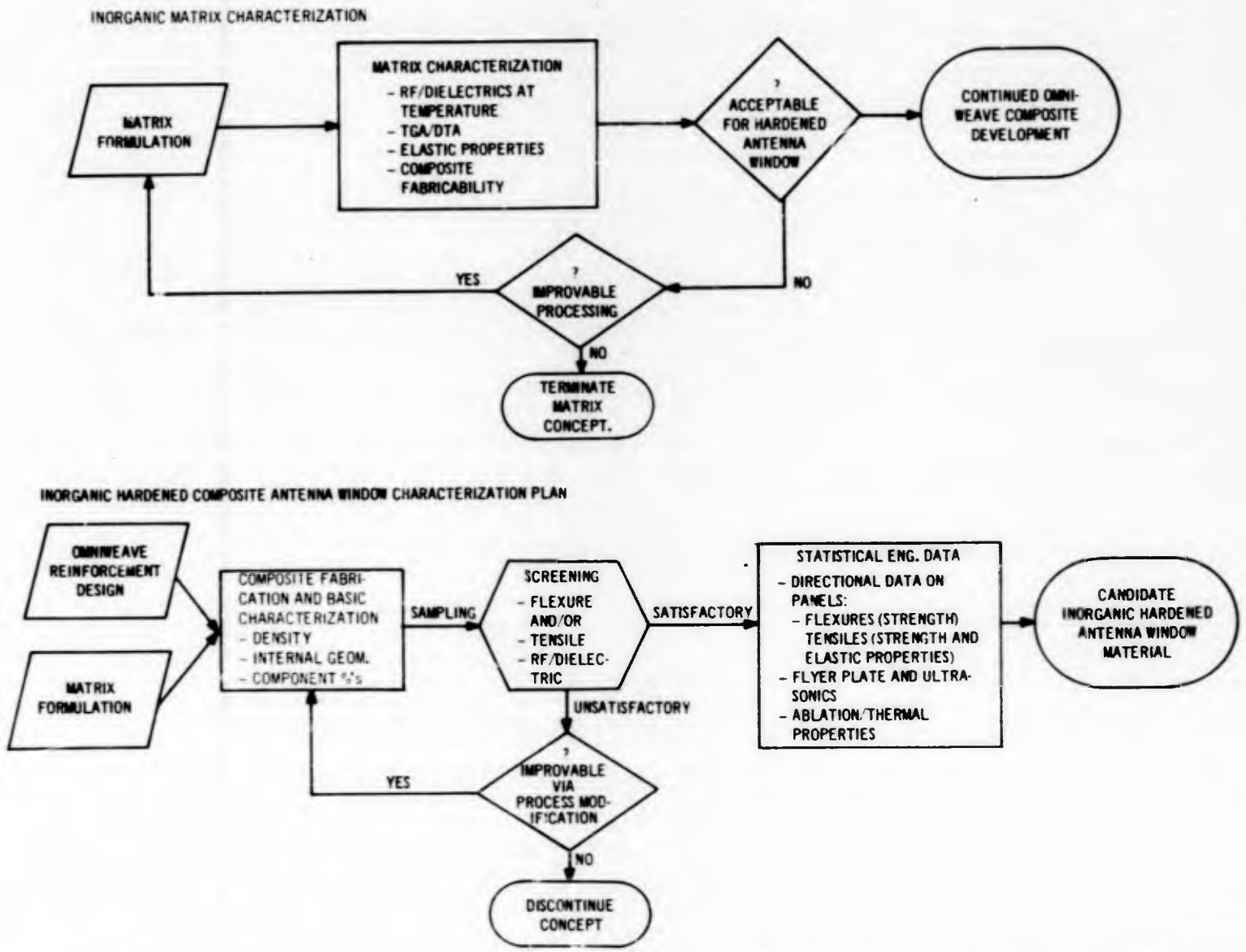

Figure 48. Development and Characterization Plan for Inorganic Hardened Antenna Window Concepts

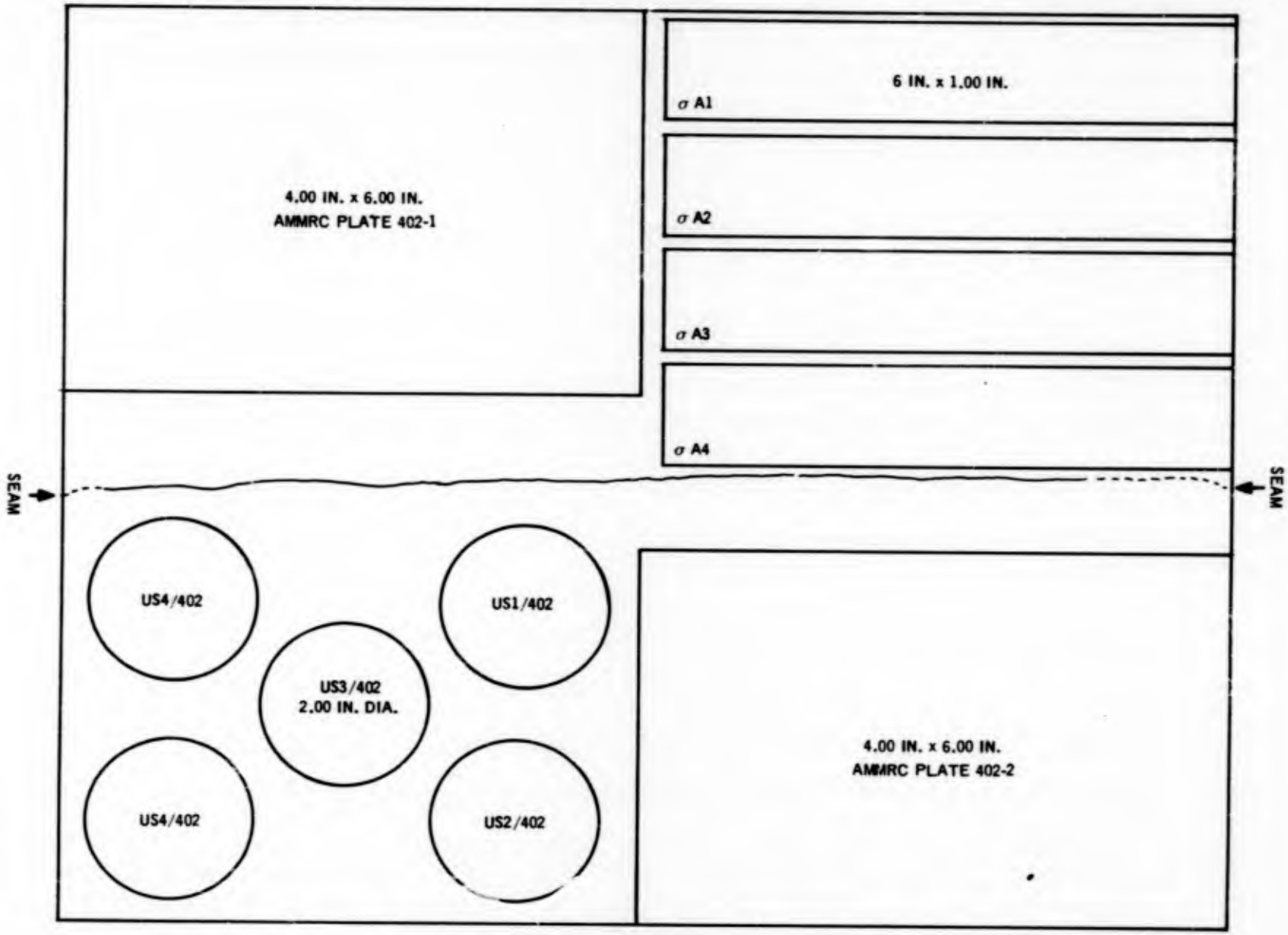

Figure 49. Sample Layout: Twin ADL-10 Plate 402

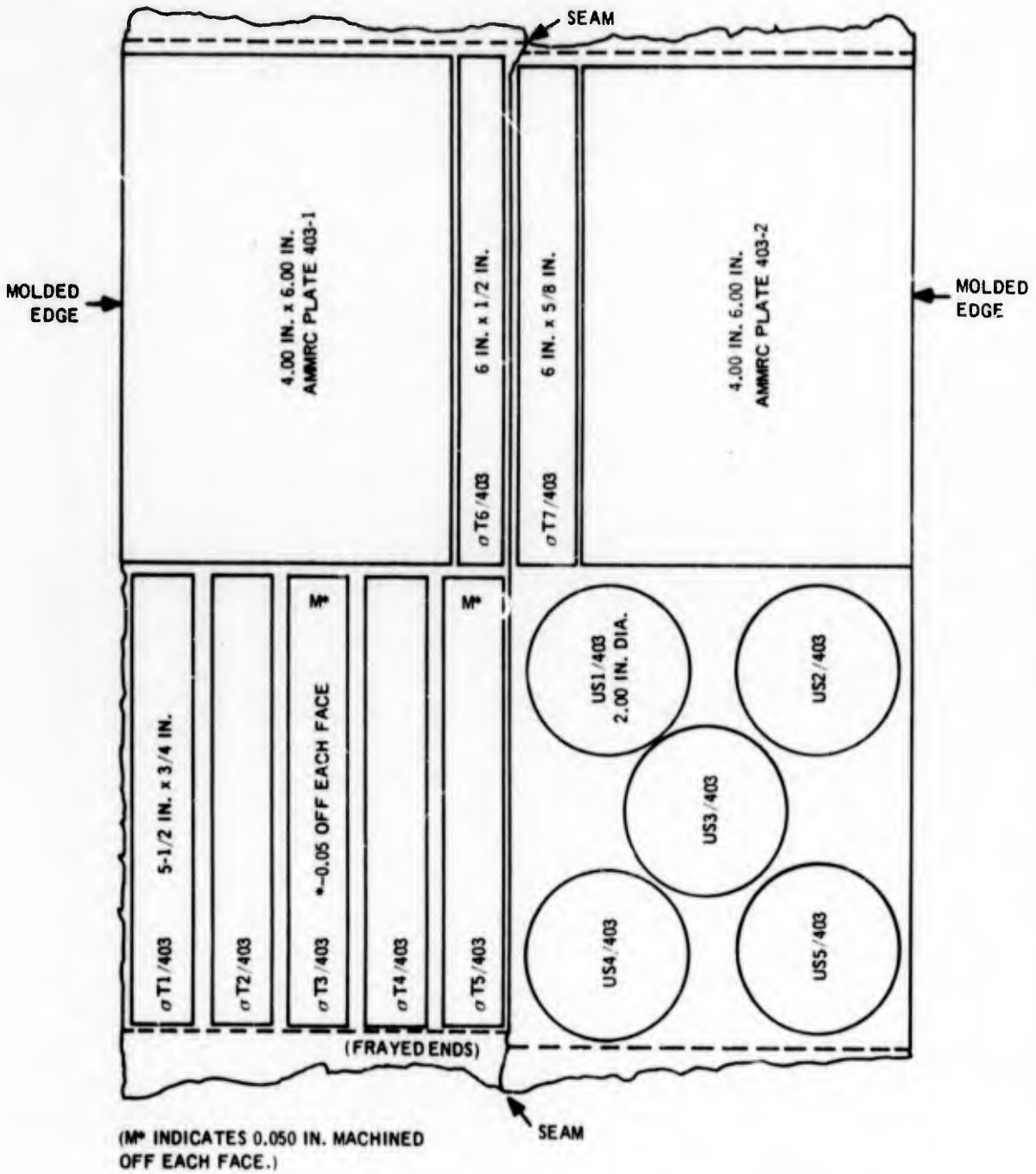

Figure 50. Sample Layout: Twin ADL-10 Plate 403

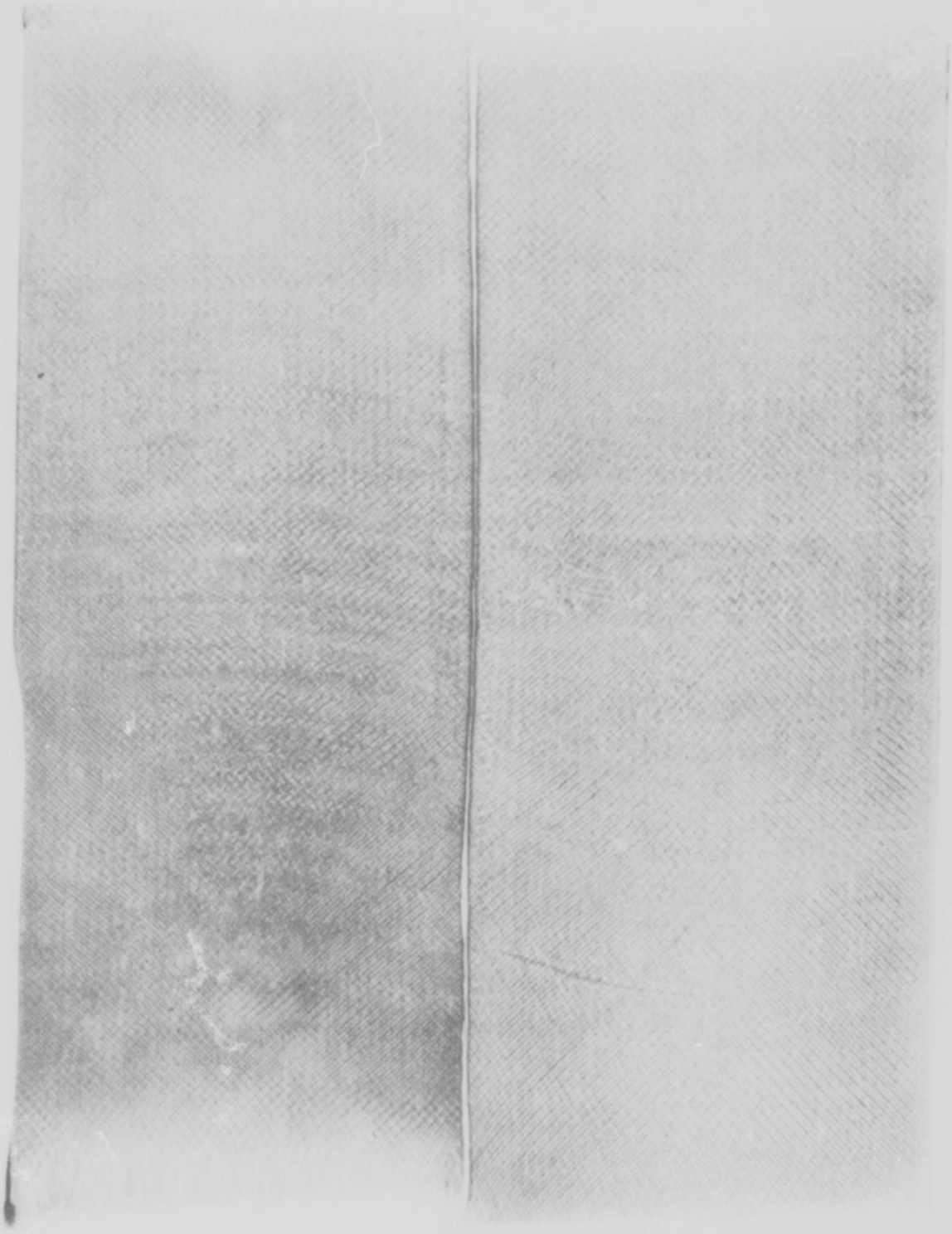

Figure 51. Radiograph of ADL-10 Panel 403

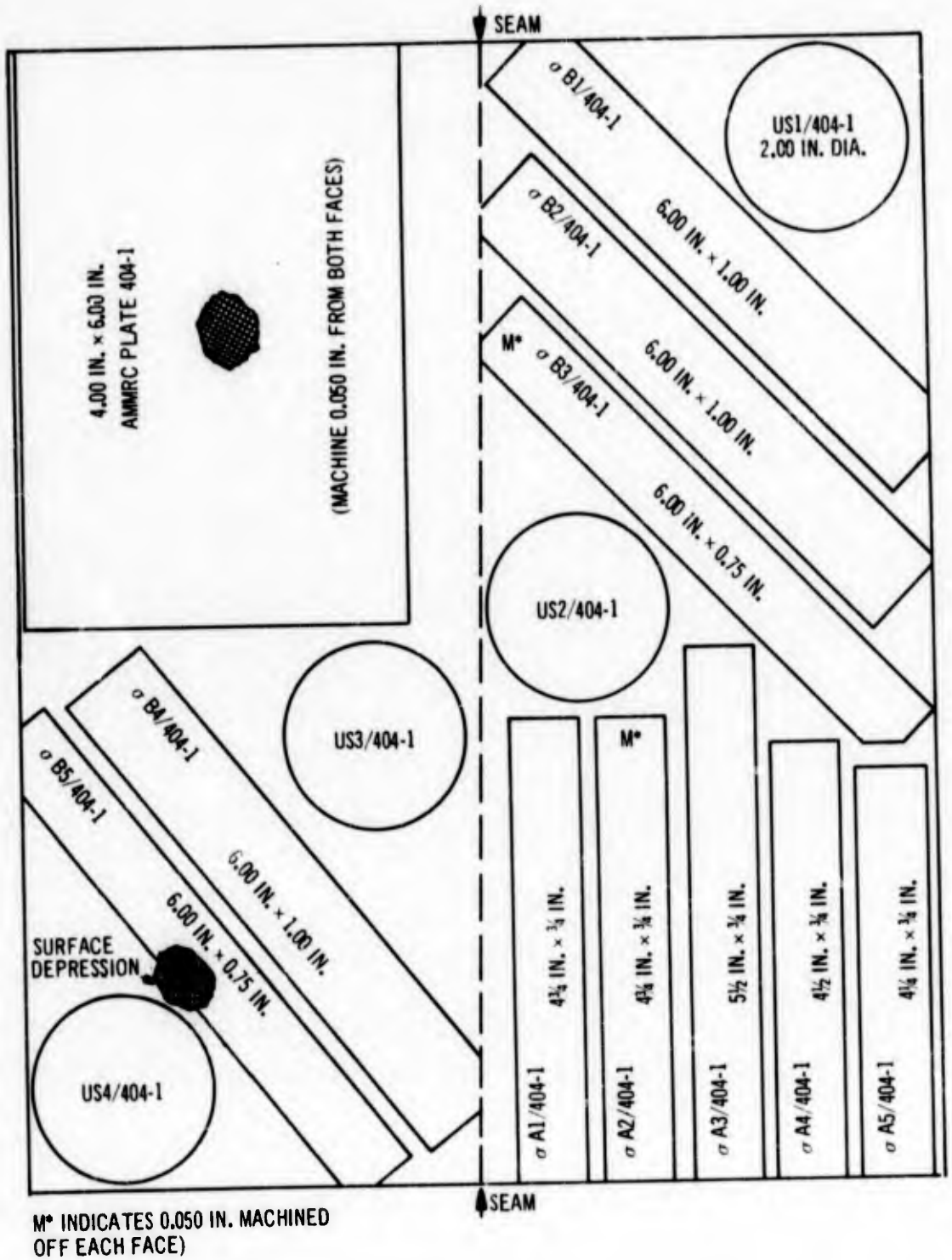

Figure 52. Sample Layout: Twin ADL-10 Plate 404-1

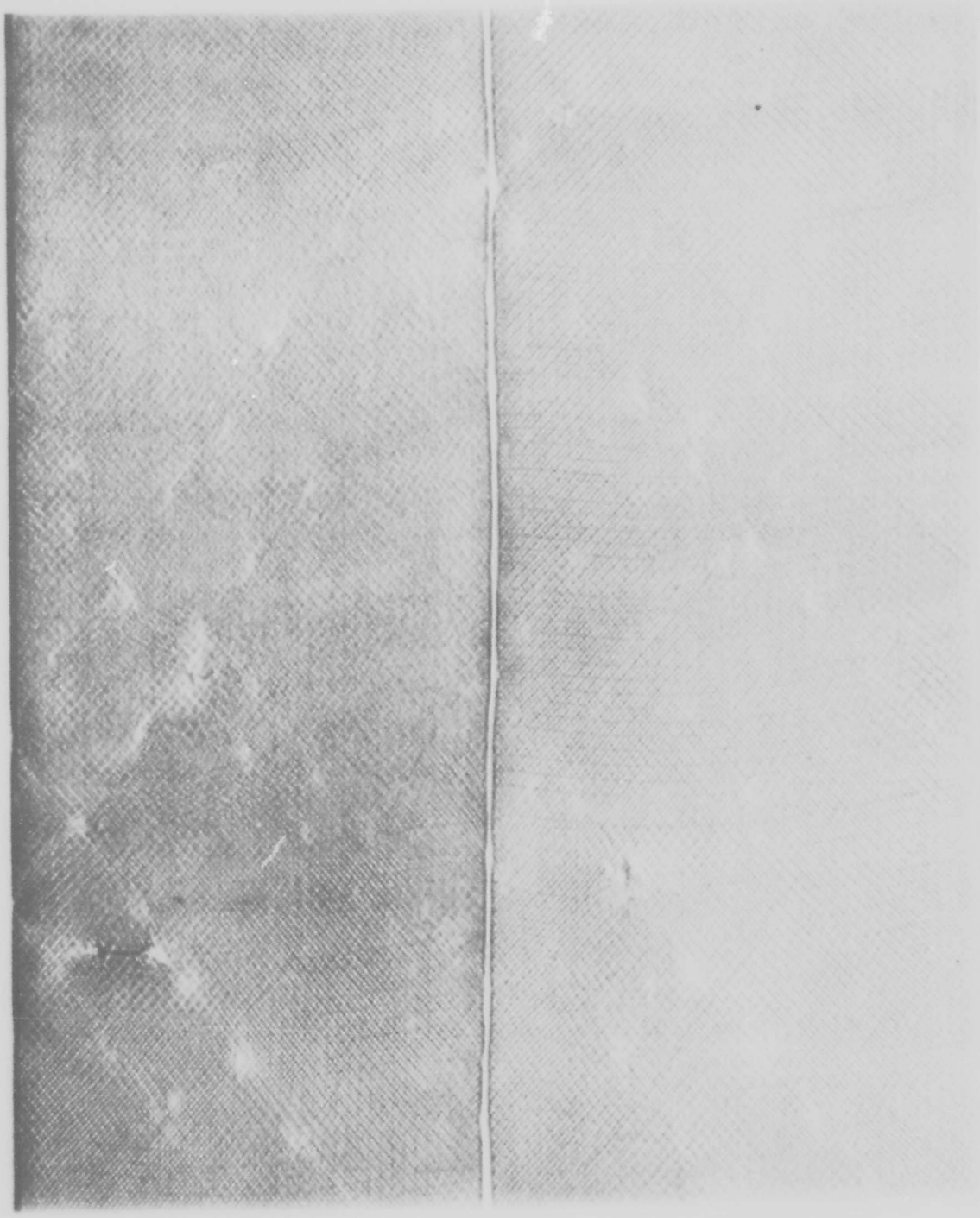

Figure 53. Radiograph of ADL-10 Panel 404-1

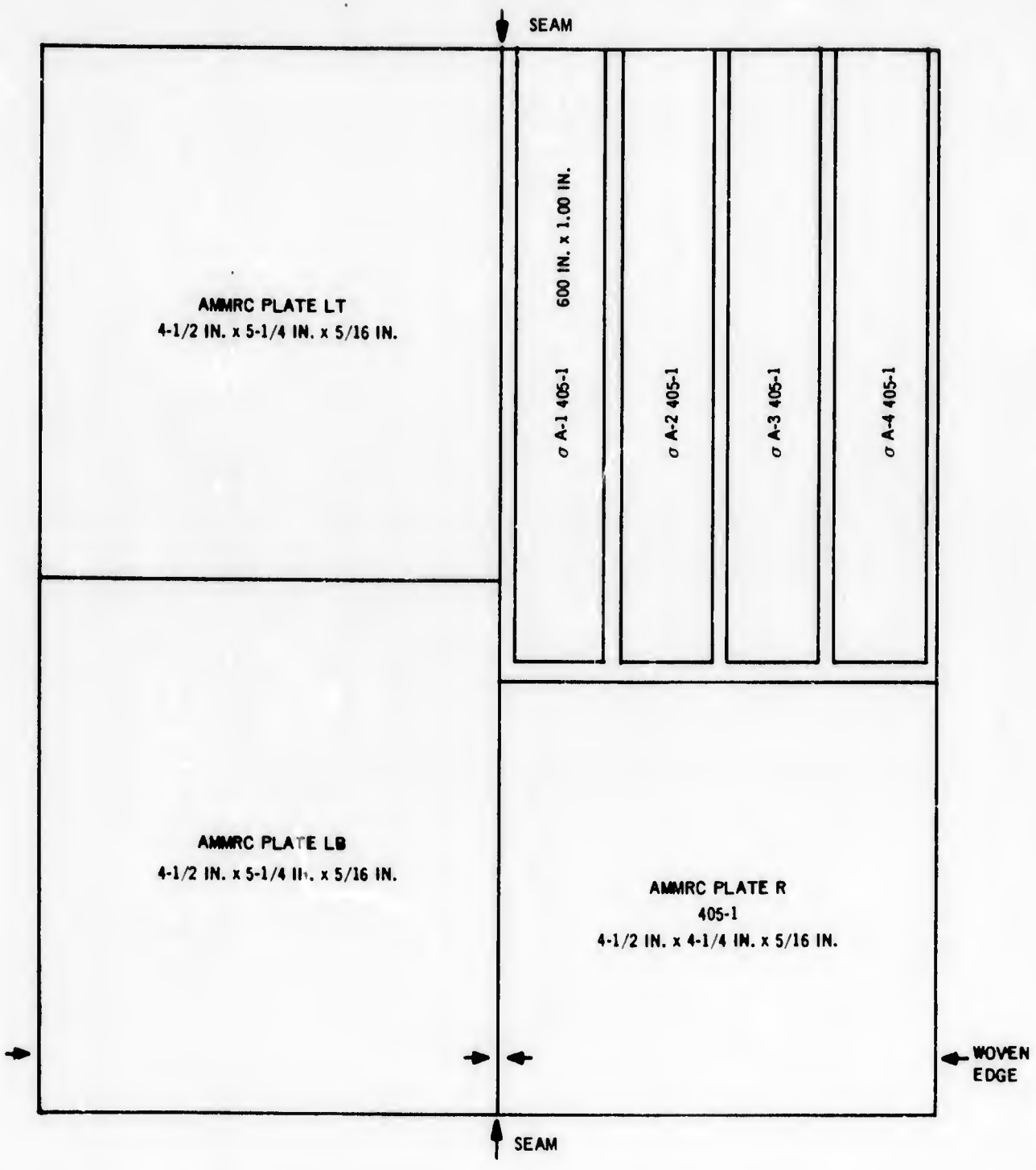

Figure 54. Sample Layout: Twin ADL-10 Plate 405-1

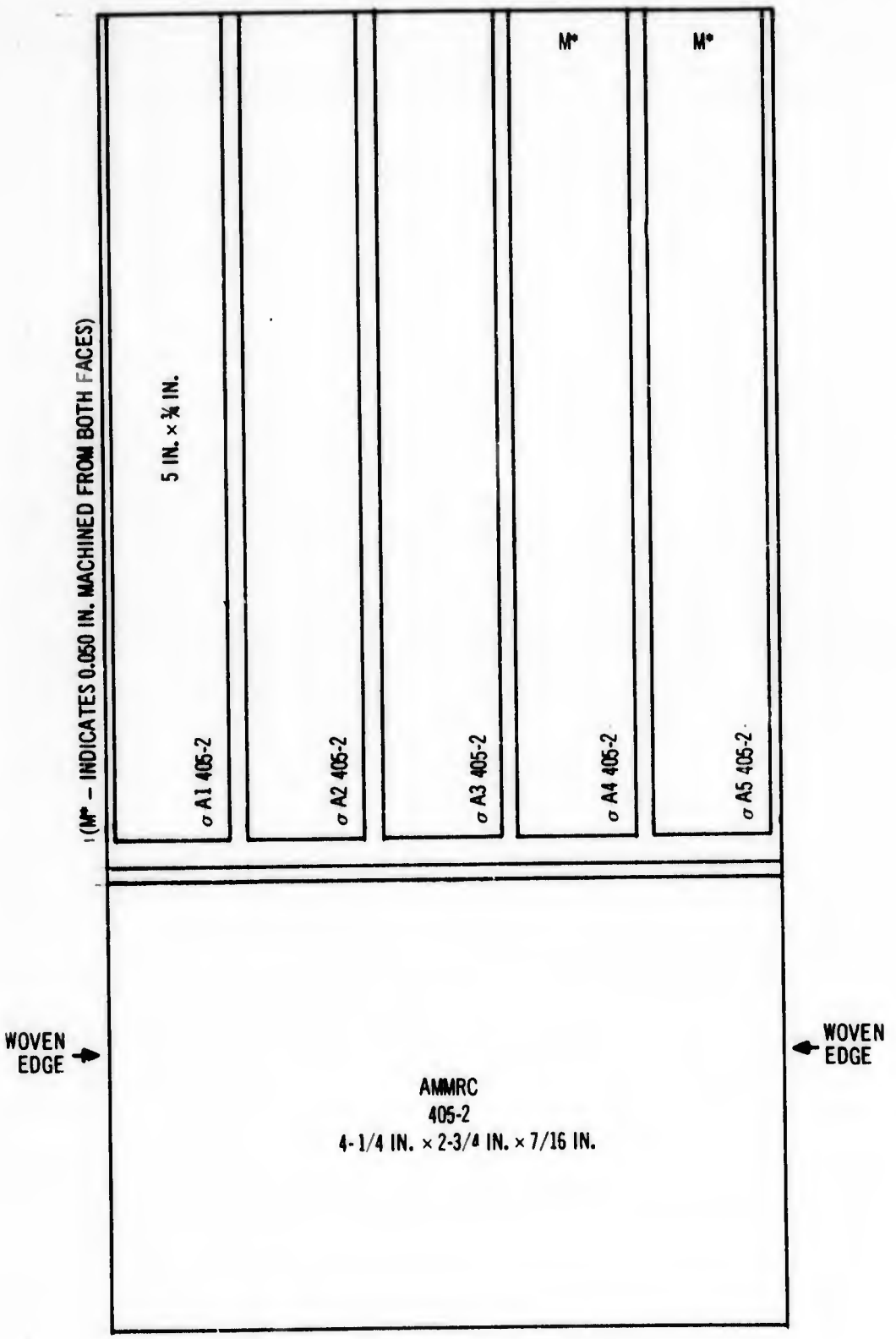

Figure 55. Sample Layout: ADL-10 Plate 405-2

Omniweave Astroquartz reinforcement. When a greater than anticipated compression and fiber volume fraction was observed for this first panel as discussed in detail in Paragraph 2.3.1, additional ADL-10 plates were fabricated beyond that required for the axial tensile, slap-plate and four 4 inch x 6 inch plate specimens for hypersonic particle impact studies. Also, when apparently anomalously low strengths were observed in the first tensile specimens, bias-direction tensiles were taken from subsequent plates to evaluate the basic composite behavior and compare to the materials of Reference 2.

The same identification symbols and test specimen geometries used in the previous work described in Reference 2 are used in this report. The symbols and labeling used in these layouts are identified below:

- σ - tensile specimen
- σF - flexure specimen
- US - ultrasonic and slap plate specimen

The sample orientations in the plate layouts are also indicated by the suffix letter designations:

- A - "axial", along the Omniweave weaving direction, along the length of the plate
- B - "bias", at an angle on the plate face, along the fiber reinforcement
- T - "transverse" to the weaving direction, across the plate width
- M - indicates machined faces

Specimens such as the US, AMMRC, ablation and thermal conductivity samples are tested in the through-the-thickness direction. In each case the panel number is labeled on the individual specimens and maintained throughout testing.

The layout of Figure 49 for panel 402 shows two 4.00-inch x 6.00-inch plates for delivery to AMMRC, one from each side of the twin molding. Four tensile bars, A1 through A4, are taken in the plate axial direction, i.e., along the weaving axis, and five of the standard geometry 2.00-inch diameter "hockey puck" ultrasonic and slap plate specimens, US1 through US5, are taken from the lower right quarter of the panel. These specimens had a very smooth surface as molded, requiring no surface machining for ultrasonic testing or reliable flyer impact testing. The first four tensile bars were tested with surfaces as molded to characterize the tensile strength and elastic properties of the panel.

Panel 403 is shown next (Fig. 50), followed by its radiograph (Fig. 51) in which separations between the two parallel Omniweaves are visible. The local weave orientation is also apparent in the radiograph. As in Reference 2, a fused silica disc 0.125 inch thick and 1 1/2 inch in diameter was inserted as a density standard reference in the lower right hand corner. Panel 403 was "molded to stops", making the optimum fiber fraction of 68 percent a specific goal. The finished panel had a rougher surface than 402. Machined face tensile specimens were taken from the rougher portions as shown by the symbol M*. The faces of these samples were machined to remove 0.050 inch of material, sufficient to remove a full fiber layer at the surface fiber crossovers. The two AMMRC samples taken from panel 403 were however sufficiently smooth as to require no finish machining.

Figures 52 and 53 show the layout and radiograph respectively of plate 404-1. This panel, like 403, was also compressed to a lesser degree than 402, resulting in some uneven surface details. The two major localized spot surface depressions are sketched into the sampling diagram, one in tensile sample σ B5/404-1, the other at about the center of AMMRC plate 404-1 where its effect on the plate's particle impact performance can be evaluated. This plate was provided to AMMRC in addition to the contractually required four 4.00-inch x 6.00-inch plates. In addition, both its faces were machined to remove 0.050 inch, assuring removal of one layer of fiber bundle surface interlocks at each face.

The layout for pl[illegible]05-1 is shown as Figure 54. As described in Paragraph 2.3.1, this panel was n[illegible] to a high degree of compression with the original intention to obtain comparabl[illegible]terial to panel 402 and to obtain additional directional data in support of the analytical studies of the larger fiber pitch angle effects resulting from use of higher starting Omniweave reinforcement densities being performed at Materials Sciences, Inc. However, upon consideration of the lower than expected tensile strength results measured on panels 402, 403 and 404, the silane coupling agent treatment omitted on these three panels and on 405-1 was applied to a remaining section of 405 Omniweave. The sample layout for this 405-2S plate is shown in Figure 55. Upon resolution of the effect of the silane coupler, the four indicated tensile specimens were then sampled from panel 405-1 for a control comparison.

The remaining material from both plate 405-1 and 405-2S was subsequently also delivered to AMMRC for particle impact testing. The dimensions of these plates, under the full size requirements for the test, are indicated in the two plate layouts. The woven edges are expressly indicated for evaluation of the shock wave effects on plate integrity.

Figure 56 is a photograph of the five 4.00-inch x 6.00 inch plates submitted to AMMRC for hypersonic large particle impact testing. Again note that the faces of plate 404-1 were machined while the other four were provided with faces as molded. The detail of the panel layouts also show that one 6.00-inch edge of each plate was also supplied as molded, with the closed woven edge intact. This provision should

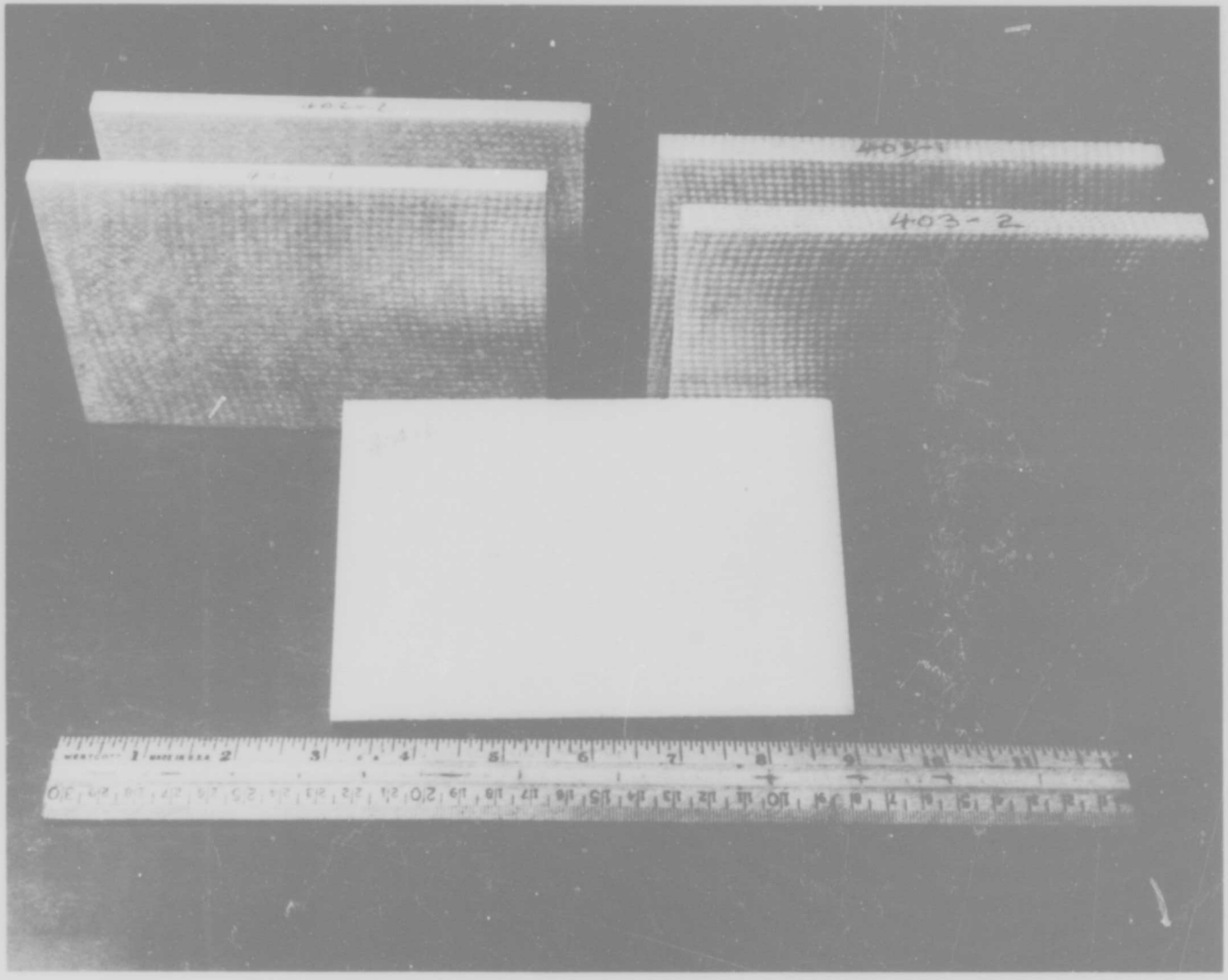

Figure 56. Five 4.00-inch x 6.00-inch ADL-10 Plates Submitted to AMMRC for Hypersonic Large Particle Impact Testing

demonstrate the dimensional accuracy with which the material can be molded to size. Testing with one edge in the woven condition should also serve to differentiate its effect on the shock resistance of the plates. Future analysis of the particle impact test results should include consideration of this basic difference in the edge constructions, in addition to the face machining and purposeful central positioning of the surface depression in plate 404-1.

3.1.2.2 Inorganic Composite Panels

Figures 57 through 60 show the plate layouts and radiographs of Astroquartz 5-D Omniweave/Ludox AS matrix plates 401-1, 2 and 3. As described in Paragraph 2.4.1 these plates were processed to 1.17, 1.39 and 1.68 gm/cc densities to test the "space-frame" model for a silica-silica composite. The testing was limited to flexure bars taken in the axial and transverse direction, the "stuffer" fibers being oriented in the transverse direction. In the diagram for plate 401-2 the absence of a stuffer fiber layer is indicated, as detected in the corresponding radiograph. The test results for this individual σ FT2 (401-2) specimen gratifyingly showed a lowered strength, although one of its nearest neighbors σ FT1 (401-2) was also lower in strength.

The layout for Astroquartz 4-D Omniweave/Ludox AS Matrix plate 404-2 is next shown as Figure 61. This plate was produced from a remaining portion of the no. 404 Omniweave scarf after flexure testing of finger specimens from segmented Omniweave no. 400 processed according to the optimized Ludox formulation showed excellent mechanical properties. The flexure bars were selected in axial, bias and transverse directions to detect directional composite properties in addition to the basic strength level. The length of the flexure bars was also varied to detect any "L/D" effects in the flexure testing, which is necessary in favor of tensile testing when sufficient quantities of material are not available. One tensile bar, σ A1, was taken in the axial direction to obtain some better measure of the uniaxial stress capability of the material, albeit only for one specimen. This specimen was prepared for tensile test by application of fiberglass-epoxy doublers to the ends (see Para. 3.2). Two flyer-plate shock and ultrasonics testing specimens were cut in the smaller 1-1/2 inch square geometry which has been used for similar testing of Philco-Ford's AS3DX material at Effects Technology, Inc. All of the specimens from this plate were machined to 1.00 centimeter thickness to remove the surface roughness of the originally 0.49-inch thick plate.

The sampling plan for BNQ-V plate no. 407-9 is shown in Figure 62 (see Figure 1 of Section 1 for the genesis and generalized sampling plan of this class of materials). A 2-1/2 inch square thermal conductivity specimen in the panel thickness was taken from the end of this densified strip, and after this testing a 2-1/2 inch x 1-1/2 inch "Tunnel Flow" ablation test specimen was cut from the same material, identical to the other similarly designated specimen. A higher shear environment and heat flux "Channel Flow" specimen (4.0 in. x 1.50 in.) was also cut in the as-molded thickness. Two tensile specimens were cut in each of the bias and axial directions. Cutting of a

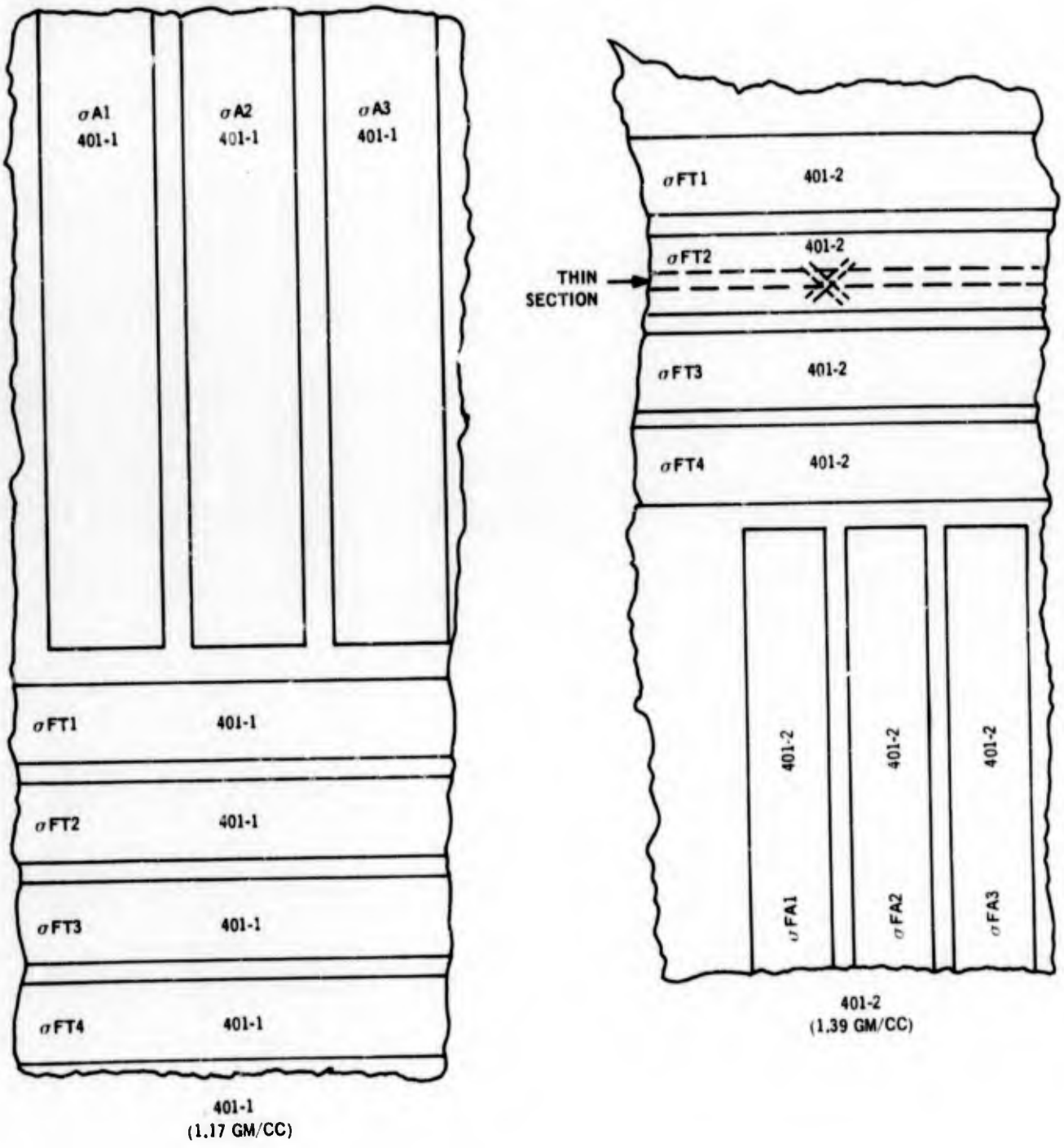

Figure 57. Sample Layouts: 5-D Plates 401-1 and 401-2

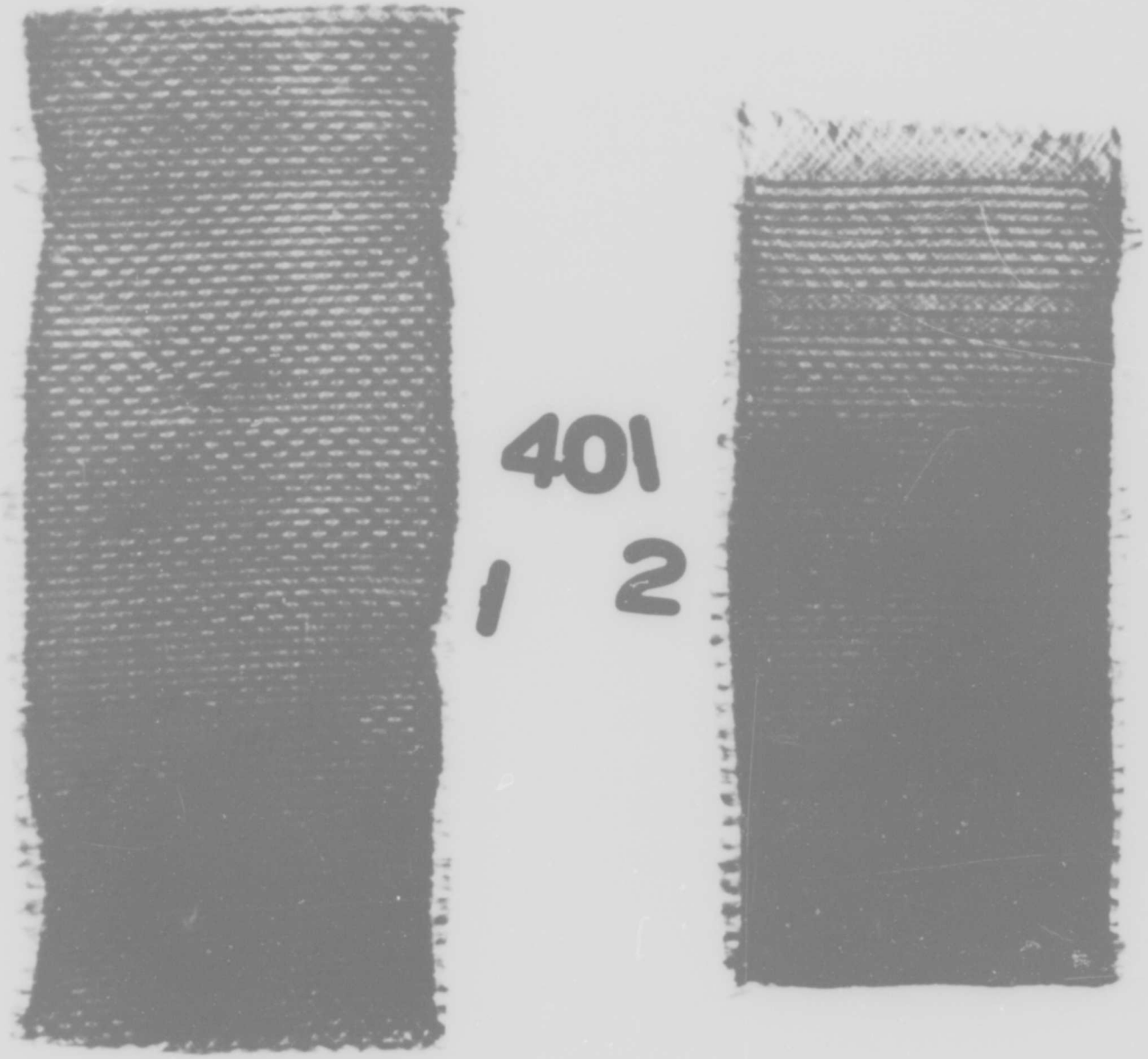

Figure 58. Radiograph of 5-D Astroquartz Omniweave/Ludox AS Plates 401-1 and 401-2

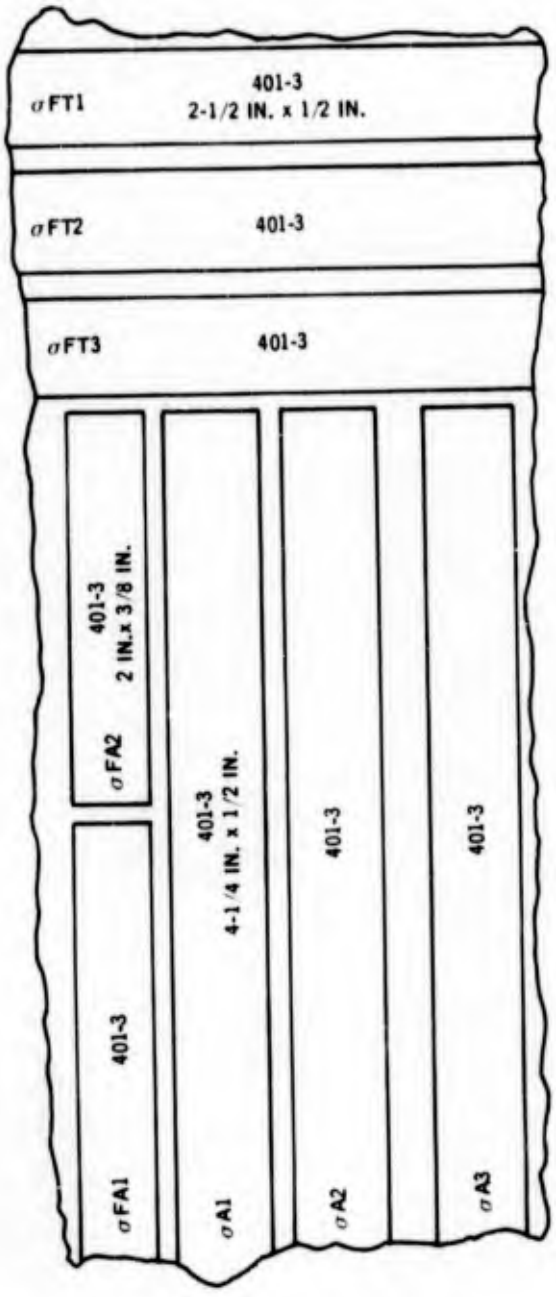

Figure 59. Sample Layout: 5-D Plate 401-3 (1.68 GM/CC)

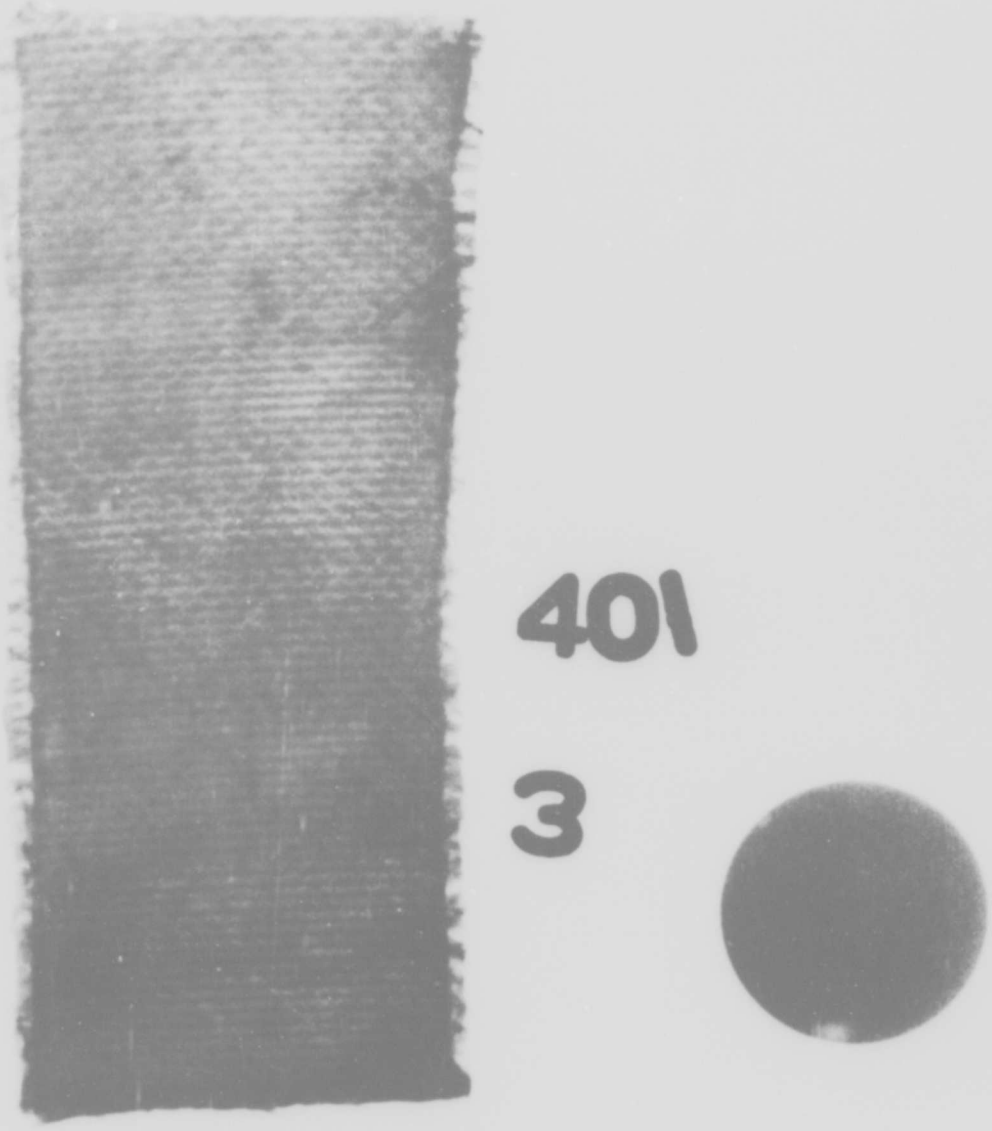

Figure 60. Radiograph of 5-D Astroquartz Omniweave/Ludox AS Plate 401-3

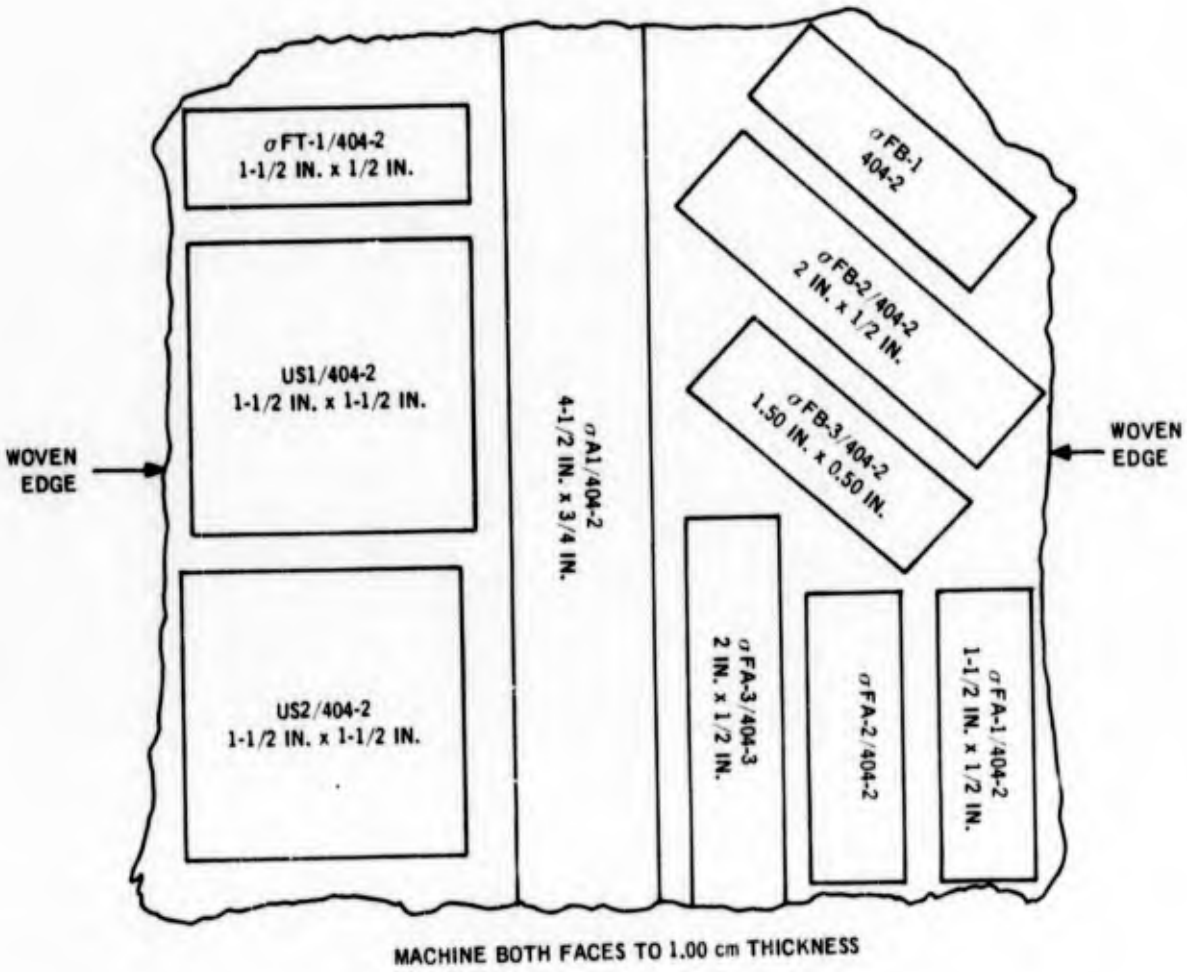

Figure 61. Sample Layout: 4-D/Ludox Plate 404-2

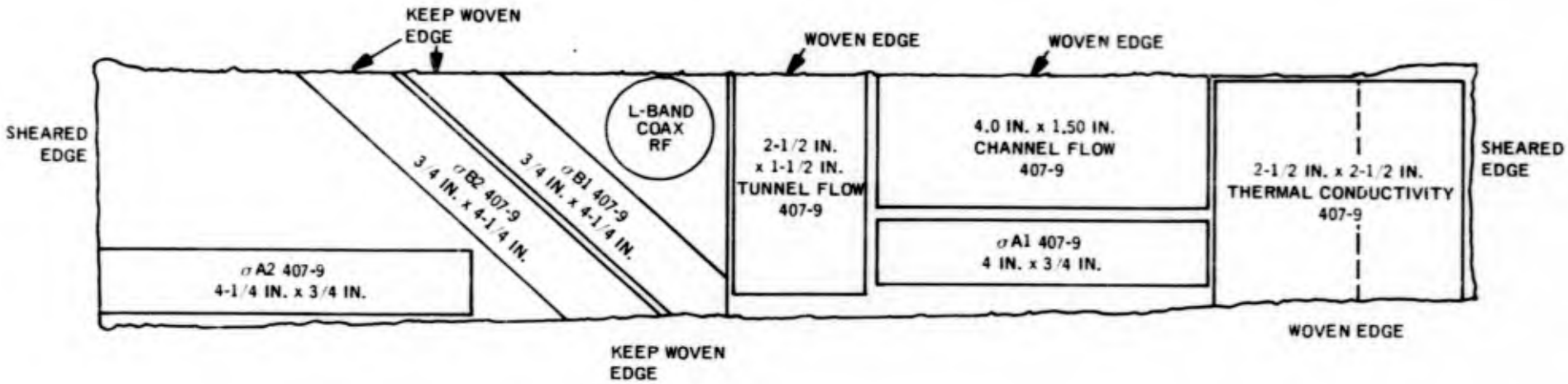

Figure 62. Sampling Plan: BNQ-V 407-9

1.00-inch diameter L-Band Coax Specimen was attempted but the material tore with the machine tools used, and resonant cavity measurements on the remainder of this material were substituted.

3.2 MECHANICAL CHARACTERIZATION

3.2.1 ADL-10

3.2.1.1 Introduction and Test Methods

The purpose of this series of mechanical tests on the ADL-10 4-D Omniweave composite material was to determine the effect on the axial strength and mechanical behavior of machining the faces from tensile bars cut from molded plate material. This objective was accomplished by performing a series of tensile tests on several panels from which both ultrasonic/flyer plate and AMMRC particle impact plates were also taken. Specimens used for tensile tests were flat rectangular bars, the configuration used in all previous ADL-10 work. Textolite fiberglass-epoxy doublers were bonded on each side at the ends in order to distribute the load evenly and prevent localized failure of the fibers.

Strain was measured by two methods:

a. Strain gages were mounted on both faces of the specimens in the axial and transverse directions. The grid area was large enough to cover several fiber bundles and thus average the surface strain.

b. A strain gage extensometer was installed on the gage length of the specimen to monitor the deformation to failure which occurs after strain gage failure.

All specimens were gripped in Instron "wedge" type serrated face grips. Several loading cycles were made in the elastic region to establish the initial load-strain curve and show reproducibility. Transverse gages were also cycled at the same time. The extensometer was then installed on the specimen and the test was continued to failure.

The resulting load vs. strain or load vs. deformation plots were used to calculate the ultimate strength, elastic modulus, Poisson's ratio and failure strain. Elastic modulus and Poisson's Ratio were calculated from the slopes of the load vs. strain curves when the specimen was cycled. Failure strain and ultimate strength were calculated from the load vs. deformation (extensometer) plot.

Three panels (402, 403 and 404) were machined into tensile specimens as shown in Figures 49, 50 and 52. Axial specimens were taken from plates 402 and 403. Both

axial and bias direction specimens were taken from panel 404. Plate thickness was approximately 0.50 inch. Specimen configuration was a rectangular bar. Sizes ranged from 5.5 inches to 6.0 inches long and 0.50 inch to 1.00 inch wide. Certain specimens in panels 403, 404, 405-1 and 405-2S had 0.050 inch machined off each face to determine the effect of the machining process on the overall mechanical behavior of the material. Others, notably in panel 404-1, were selected to evaluate the effect of weave irregularities on tensile properties.

3.2.1.2 Test Results

The test results are tabulated in Table 28 for all 5 panels. In addition, mean and standard deviation is tabulated where data allows. In certain instances, elastic data points are missing where gage failure or extensometer slippage occurred. Strength figures, however, are always present and constitute the main means of comparison.

Figures 63, 64, 65 and 66 are the plots of stress vs. strain for the five tested panels. The curves are taken from strain gage data and extend only to the point where the strain gage failure occurs because of surface fiber delamination. The range of tensile strength is given in each figure.

Table 28 shows fairly uniform results for panel 402. It was not possible to measure failure strain exactly and a lower limit is given. Fractures of specimens 2 and 3 were in the gage area while fractures of 1 and 4 were at or near the doubler. Fractures in the general vicinity of the doubler are suspect of a high stress concentration due to the gripping action. However, strengths of these specimens were uniform and it is not believed that fracture at the doubler was caused by this stress concentration.

Panel 403 shows a larger degree of variability in the properties of the unmachined specimens. The two specimens which failed at or near the doubler area (4 and 7) do have somewhat lower strengths, but are still not indicative of a catastrophic failure situation presupposed by the stress concentration. Results do appear to be quite similar.

Machined specimens in panel 403 appear to experience the same degree of property variability as the unmachined specimens. Strengths are definitely lower, however. The lowest strength is found in specimen 6 which has both faces machined and is also a smaller width than the other specimens; this is probably a specimen size effect in the material.

A two-stage stress-strain curve is found in some of the specimens. The second stage has a lower modulus than the first which is indicative of a yielding process or irreversible damage taking place in the material. Since the matrix material is generally of a brittle nature the possibility of a yielding process can be eliminated and the process of initial fiber movement to a lower overall effective modulus "E_2" is postulated.

TABLE 28. MECHANICAL PROPERTIES: ADL-10 COMPOSITES

Plate/Specimen	Ultimate Tensile Strength (psi)	Modulus of Elasticity		Poisson's Ratio		Failure Strain %	Comments **
		$E_1 \times 10^6$ psi	$E_2 \times 10^6$ psi	μ_1	μ_2		
Panel 402							
402/ A-1	4921	1.42	-	-	-	.68	A
402/ A-2	4038	1.44	-	-	-	.39	
402/ A-3	3903	1.66	-	-	-	.39	
402/ A-4	4410	-	-	-	-	-	B
$\bar{X}$	4318	1.51	-	-	-	.49	-
S.D.	456	-	-	-	-	-	-
Panel 403							
403/ A-1	4053	0.325	0.117	-	-	4.11	
403/ A-2	3758	0.284	0.193	-	-	2.68	
403/ A-3*	2400	0.476	-	-	-	2.13	
403/ A-4	3015	0.540	0.460	-	-	1.66	B
403/ A-5*	2145	0.229	-	-	-	4.52	A
403/ A-6*	1761	0.236	0.110	-	-	1.49	A taken from edge of weave, smaller cross section than others in set.
403/ A-7	3378	0.609	0.337	-	-	2.68	A
$\bar{X}$	331	0.424	0.216	-	-	2.75	Non Machined Specimens only
S.D.	72	0.149	-	-	-	0.94	
$\bar{X}$ *	2102	0.313	-	-	-	2.71	Machined Specimens only
S.D. *	-	-	-	-	-	-	
Panel 404 (axial)							
404/ A-1	2760	0.287	-	0.42	-	2.14	B
404/ A-2 *	2900	0.431	-	0.63	-	1.90	A
404/ A-3	4408	0.384	-	0.70	-	2.62	
404/ A-4	5450	0.368	-	0.61	-	1.66	B
404/ A-5	4761	0.545	-	0.87	-	1.54	A
$\bar{X}$	4345	0.396	-	0.65	-	1.99	Non machined specimens only
S.D.	1141	0.108	-	0.19	-	0.49	
Panel 404 (bias)							
404/ B-1	5265	0.553	0.820	0.49	0.61	0.491	
404/ B-2	4900	0.512	0.545	0.45	0.47	0.836	
404/ B-3 *	1696	-	-	-	-	0.410	Sample width = 3/4"
404/ B-4	4933	0.665	0.848	0.63	0.63	-	B
404/ B-5	5262	0.453	0.894	0.15	0.27	-	Weave defect located in center of specimen no effect on strength
$\bar{X}$	5090	0.546	0.776	0.43	0.46	0.664	Non-machined Specimens only
S.D.	201	0.089	0.157	0.20	0.17	-	
Panel 405-1							
405/ A-2 *	6120	2.55				~ 1.49(c)	
405/ A-4 *	6200	2.29				> 1.4 (c)	
$\bar{X}$	6160	2.42					Non-machined Specimens only
S.D.	57	0.25					
Panel 405-2S							
405-2S/A-1	10,401	0.795			1.00		
405-2S/A-3	10,772	0.757			0.847		
404-2S/A-4*	3,493	0.304			0.780		
405-2S/A-5*	3,924	0.354			0.850		
$\bar{X}$	10,587	0.776			0.924		Non-machined Specimens only
S.D.	525	0.28			0.17		
$\bar{X}$	3,709	0.329			0.815		Machined Specimens only
S.D.	304	0.35			0.05		

* Both Specimen Faces machined

** A - Failure Near Doubler
B - Failure Under Doubler
C - Strain indication at failure of foil type strain gage, strain at failure of sample is larger

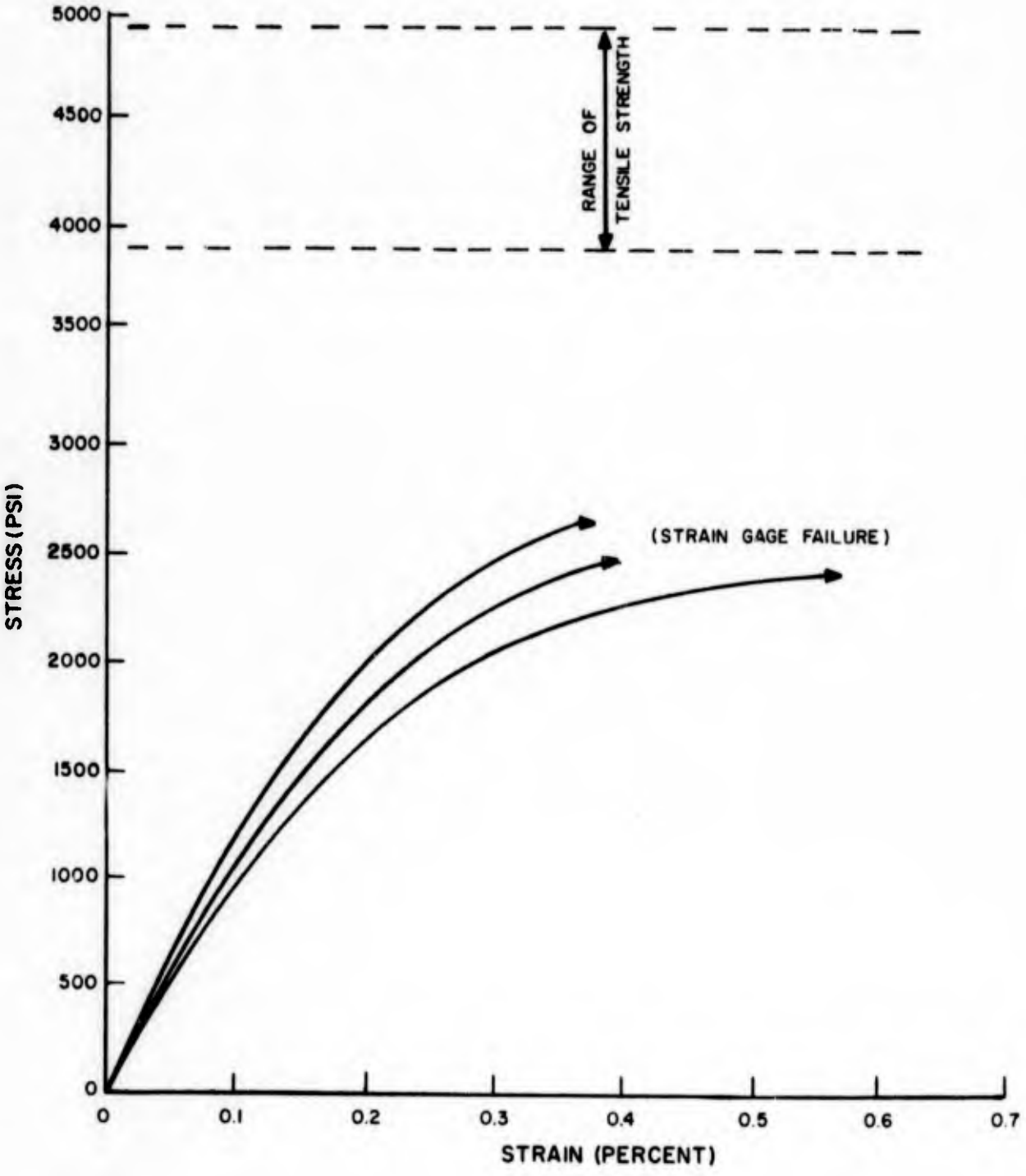

Figure 63. Stress-Strain for Panel 402 ADL-10 Composite

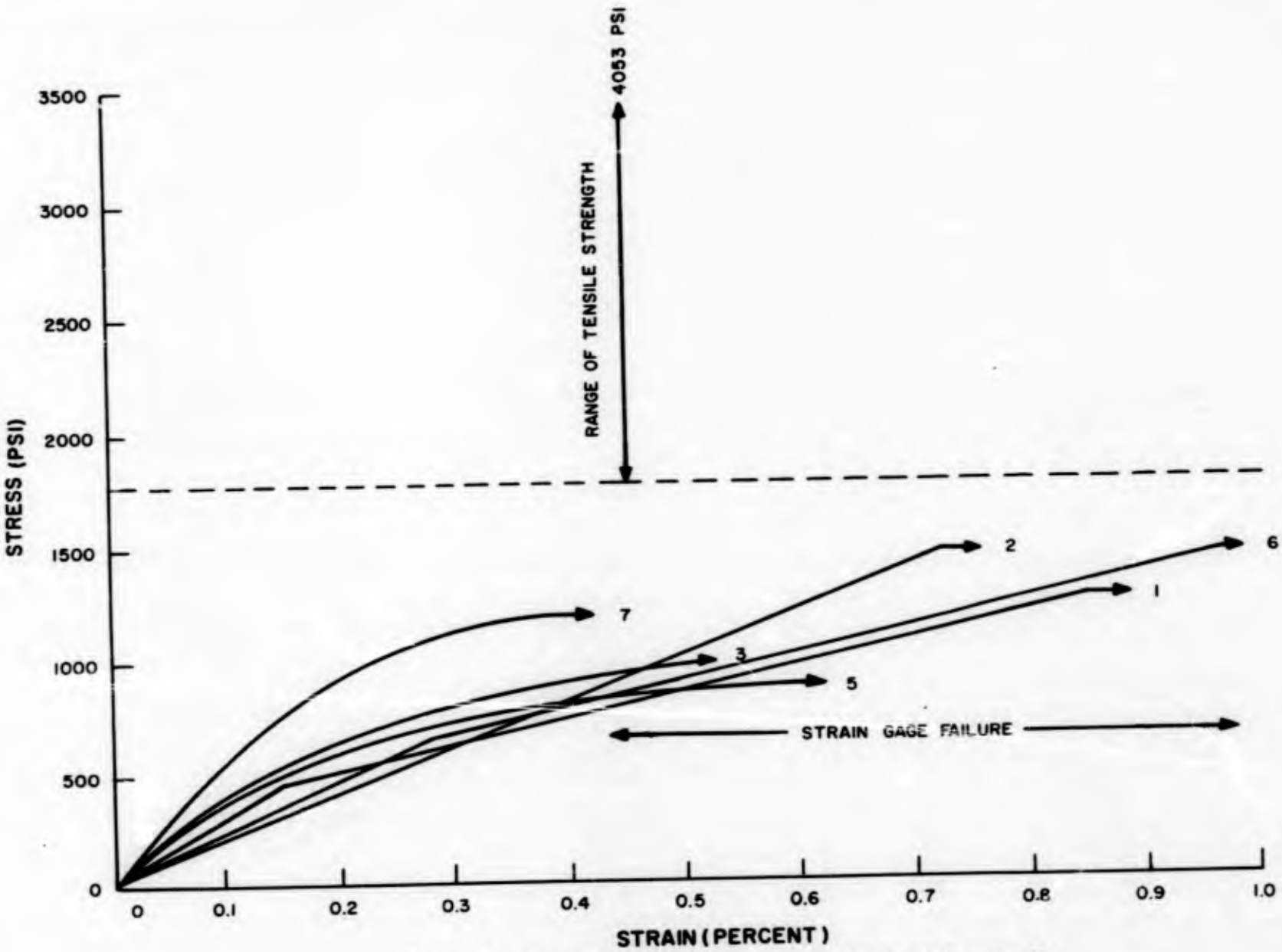

Figure 64. Stress-Strain for Panel 403 ADL-10 Composite

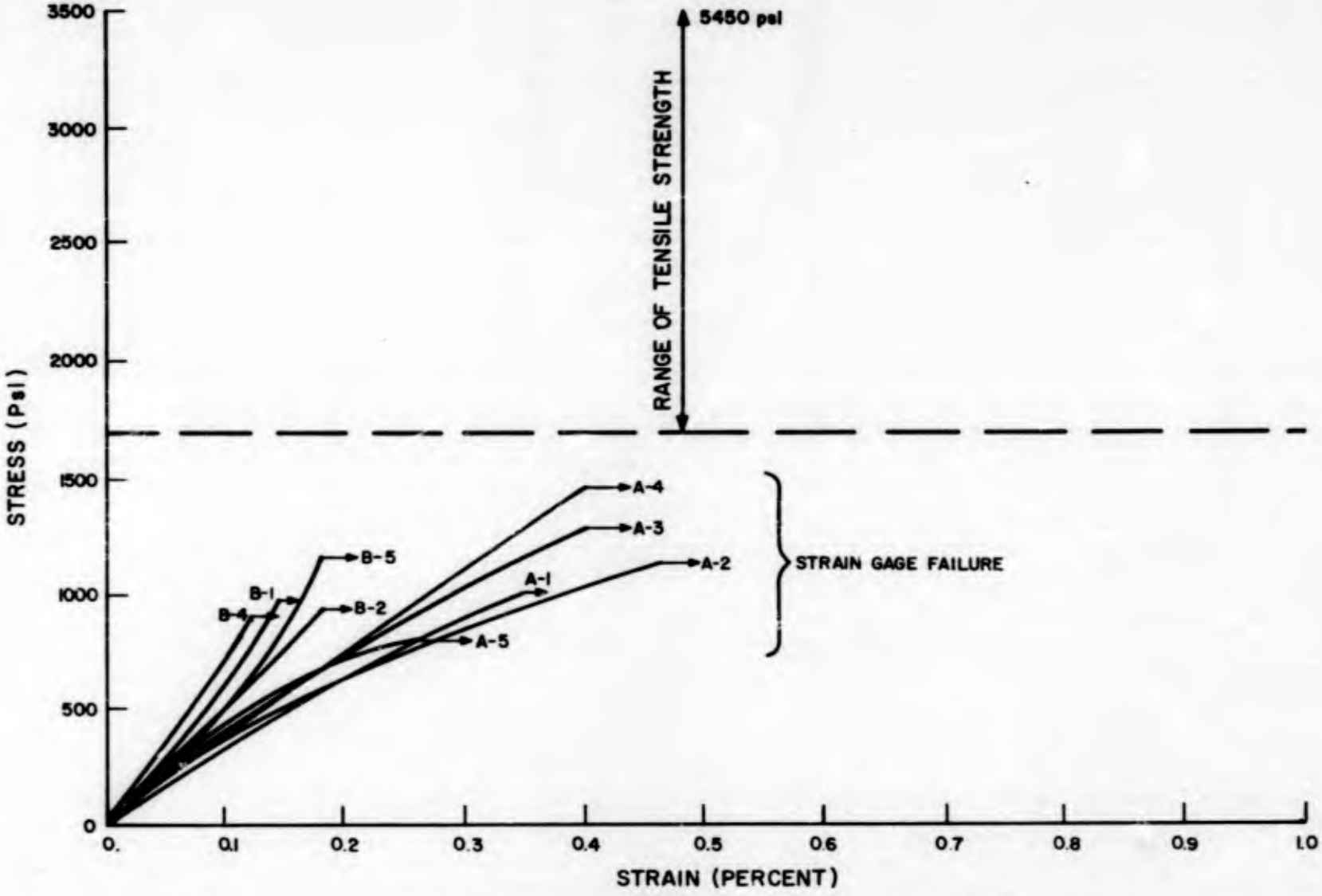

Figure 65. Stress-Strain for Panel 404 ADL-10 Composite

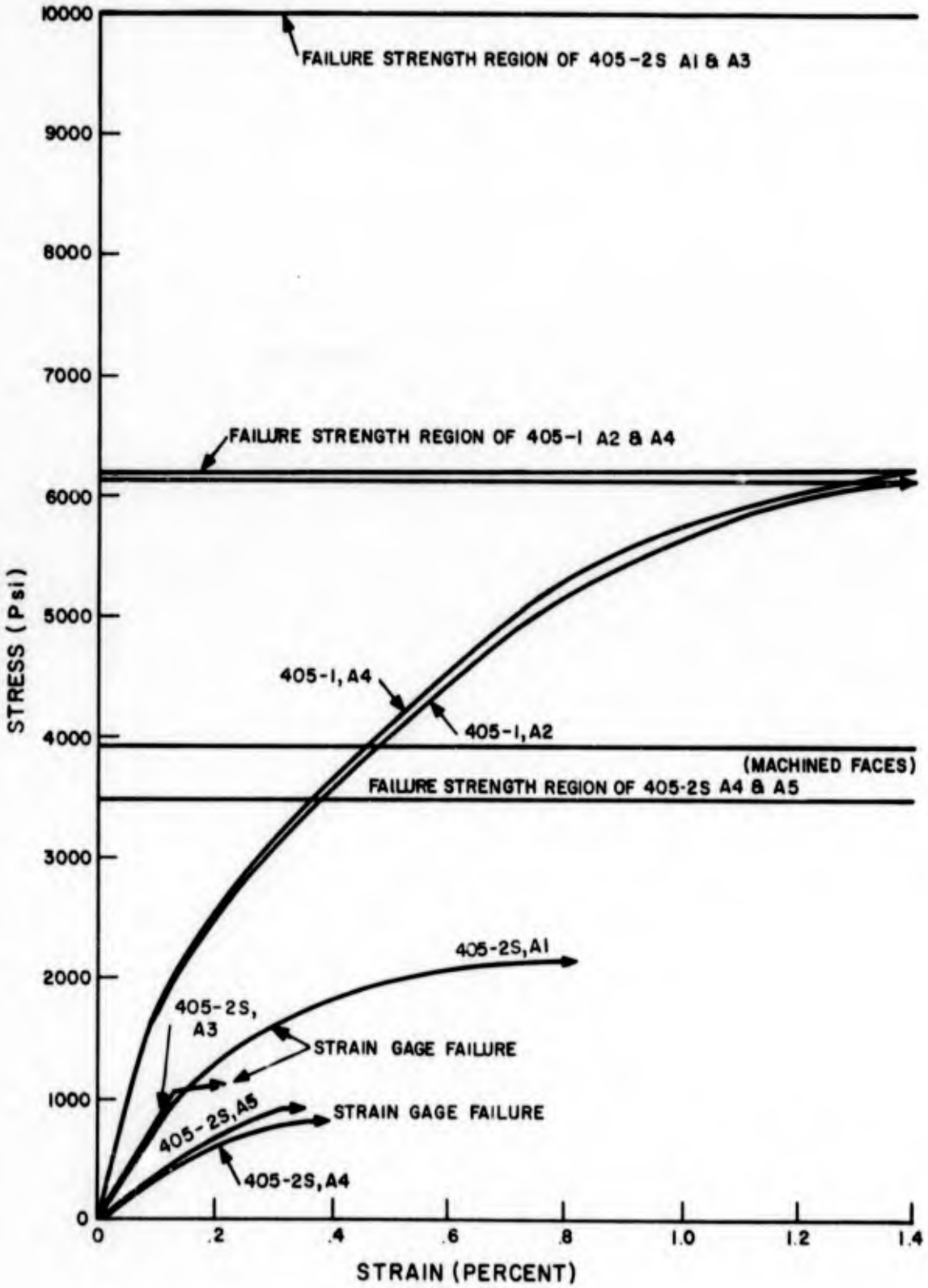

Figure 66. Stress-Strain for Panels 405-1 and 405-2S ADL-10 Composite

Axial specimens in panel 404 with unmachined faces appear to have fairly uniform strength except for specimen 1 which has a lower strength but also has a lower modulus. This specimen was taken from an area adjacent to the seam. Two possibilities for the lower strength are present:

a. Failure in the doubler region caused by a reduction in strength by stress concentration.

b. Possible material variations near the edge of the woven material. Location near Omniweave edge seams has not been observed in past work to have any particularly deleterious effects on strength.

It is not possible to resolve factors here, but only to postulate probable causes.

Specimens machined in the bias direction appear to be stronger than axial specimens as would obviously be expected for a directional composite material. However, the standard deviation of axial strengths is higher than that of bias direction strengths. The error bands overlap in these cases and a conclusion to determine the stronger direction is difficult to make for this lower density non-selane coupled ADL-10.

A difference is evident when examining the stress-strain curves of specimens from panel 404-1 tested in these two directions (Fig. 65). The axial specimens experience a one-stage stress-strain curve in the linear region. The bias specimens experience a two-stage stress-strain curve. The unusual feature of this two-stage curve is that the second modulus is reproducibly higher than the first. The mechanism believed to be causing this is the following:

a. Upon initial loading, fibers experience a "scissor" effect whereby fibers move to increase density and lock against other fibers.

b. The resultant structure is a higher modulus structure which more efficiently utilizes the individual fibers.

Note that specimen σ B5 from this 404 panel was selected to purposely locate a weave irregularity or "pock-mark" over the central section of the tensile specimen. The results show a tensile strength virtually identical to the strongest bias bar, 5262 psi vs 5265 for σ B1. This has an encouraging "defect tolerance" implication for gross samples of manufactured material in the as-molded condition.

When it was observed that the strength levels for these three panels fell below those measured for both the closed weave and the panel ADL-10 material described in Reference 2, a silane-coupled panel designated 405-2S was fabricated. At this point in the program the tests planned for panel 405-1 were also suspended until the results of measurements on the silane treated material were available.

Tensile specimens were machined from omniweave panel 405-2S which had been treated with silane coupler. The sampling plan is as shown in Figure 55. The specimens measured roughly 0.50 inch x 0.75 inch x 5.0 inch, and were rectangular in shape. Textolite doublers were bonded to both gripping ends in order to distribute the load evenly. Strain gages were mounted on both sides in the longitudinal and transverse positions so that modulus and Poisson's Ratio could be determined. Due to the unusually large size of the specimen, and the need to use larger "elephant grips" with less access room for instrumentation, no extensometers could be attached and therefore failure strain could not be determined since strain gages fail before the specimen does.

The results of tensile testing on two tensile specimens from this panel in the as-molded and face-machined state are recorded in Table 28. It is immediately apparent that the tensile strength of this material recovered to the desired level, averaging above 10,000 psi for the as-molded material in the axial orientation. Machining faces thus has the effect of drastically reducing the strength of 1/2-inch thick silane treated plate material to about 3/8 its original value, a more dramatic reduction in both strength and modulus upon machining than that observed for the ADL-10 produced without silane coupling.

To obtain a more accurate measure of the effect of coupling agent, tensile samples were also machined from (the already molded) panel 405-1, as depicted in Figure 54. The test conditions were identical to those for panel 405-2S specimens except that no Poisson's modulus gages were mounted. The results in Table 28 show a lower mean strength level of 6160 psi for as-molded material but a comparable modulus. The strains indicated by the foil type strain gages at their failure points are indicated - note that the actual failure strain of the material would definitely be larger than these values.

In order to make a quantitative evaluation of the effect of machining faces on the overall strength of the material, a ratio quantity is hereby defined:

$$R = \frac{\text{Tensile Strength w/faces machined}}{\text{Tensile Strength w/faces not machined}}$$

Table 29 gives the calculated R values for the individual panels. For the material prepared without silane couplers the axial direction appears to undergo approximately a 1/3 strength reduction by machining faces. The single machined bias direction specimen tested shows a drastic 2/3 strength reduction. Although one specimen, and a 3/4-inch width one at that, is no basis for a valid comparison, the larger reduction in the bias direction does appear however to agree very well with the nature of the two-stage stress-strain curve. If the faces are machined, and there is no continuity between fiber rows, densification of the fibers in the second stage of stress-strain is impossible and the composite tends to fail easier. The general conclusion from these tests is to avoid machining ADL-10 faces to conserve the high original strength and strain to failure.

TABLE 29. EFFECT OF MACHINING OF FACES ON OVERALL STRENGTH OF ADL-10 COMPOSITE MATERIAL

Panel	R (reduction to fraction of:)
402	No machined faces
403	0.619
404 (Axial)	0.667
405-1	No machined faces
405-2S	0.35
$R = \frac{\text{Strength w/faces machined}}{\text{Strength w/faces not machined}}$	

3.2.1.3 Description of Fracture Surfaces

The fracture surfaces of typical specimens from each panel are shown in Figures 67, 68, 69 and 70. In panel 402 (Figure 67), the fracture appears to be of a brittle nature with very little apparent fiber movement prior to failure. The macroscopic features of this failure surface resemble the classic ductile cup and cone type failure in that one piece of the specimen always contains a depression and the other contains an extension. The mechanism of this composite fracture can not indeed be similar, but a small degree of shear failure must be concluded to have occurred. Fiber ends are slightly frayed and not uniformly fractured but have ragged edges.

Failure surfaces of specimens from panel 403 (Figure 68) which was molded to a lower fiber volume fraction than 402 all appear similar. Machining faces has no effect on the fracture surface. The fracture however, appears to be of a different nature than the specimens taken from panel 402. The fracture surface in these (403) specimens approaches a planar configuration. The fibers appear to be more brittle showing cleaner breaks and no frayed ends. The cured SR-350 matrix material appears to be very rigid and brittle, thus allowing no movement of the fibers. Upon picking out one of the fibers, it too appears to be very rigid and brittle.

Axial specimens from panel 404 (Figure 69L) resemble certain features of fracture surfaces of specimens from panels 402 and 403. The failure in these specimens (404 axial) have the same brittle characteristics of fiber and matrix of panel 403; however, the shape of the fracture surface tends toward the depression - extension type similar to that of specimens from panel 402.

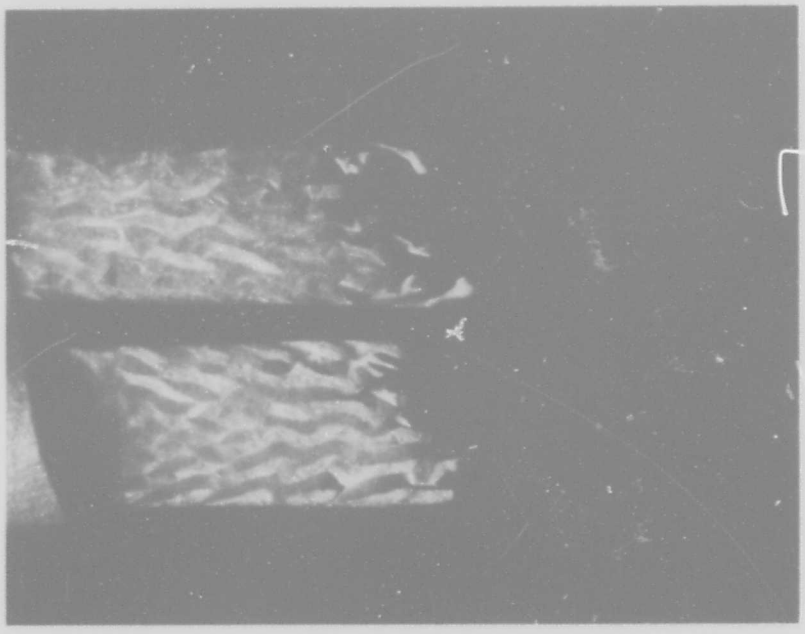

(a) Side View

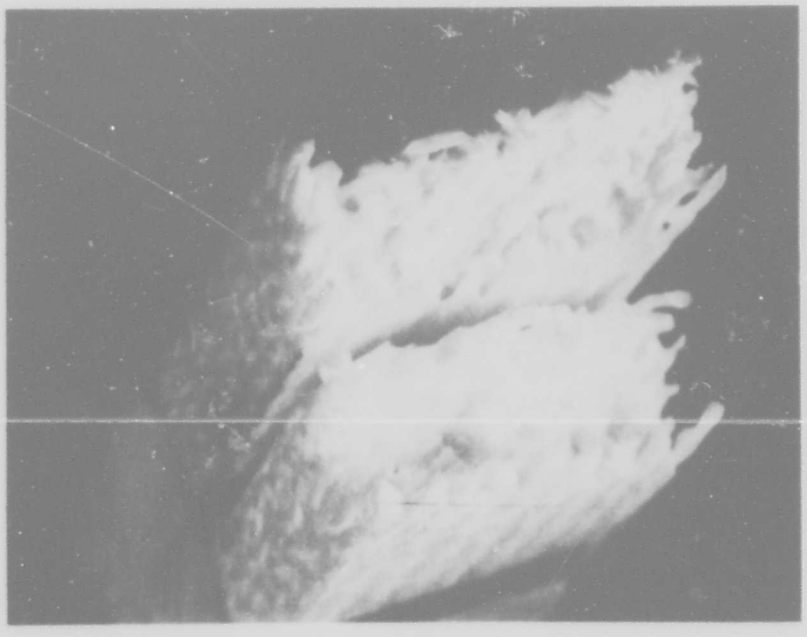

(b) Three-quarter View

Figure 67. Fracture Surface of Axial Tensile Specimen from ADL-10 Panel 402

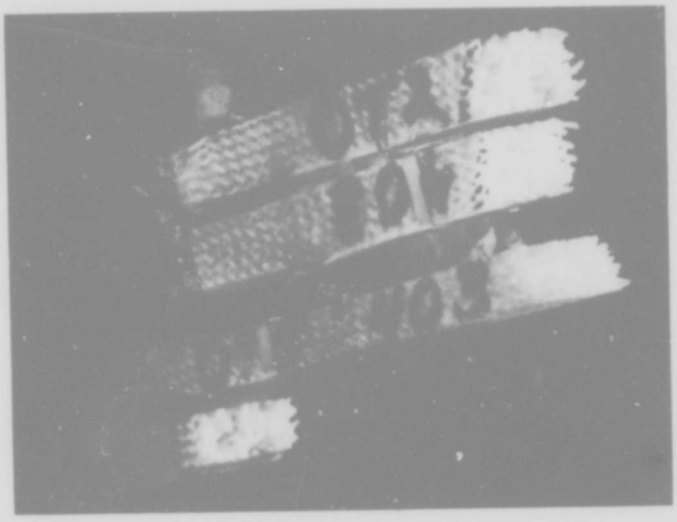

Top: 403/A-2
Below: 403/A-5* (Machined Faces)

Figure 68. Fracture Surfaces of Two Tensile Specimens from ADL-10 Panel 403

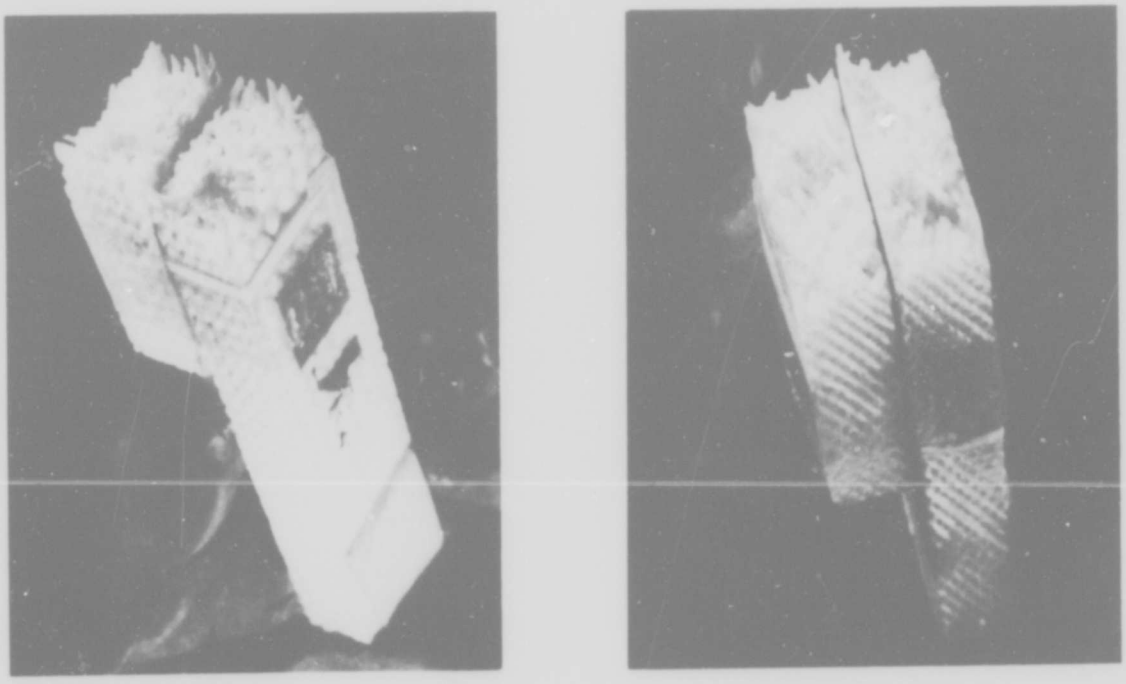

L: Axial Direction Specimen R: Bias Direction Specimen

Figure 69. Fracture Surfaces of Two Tensile Specimens from ADL-10 Panel 404-1

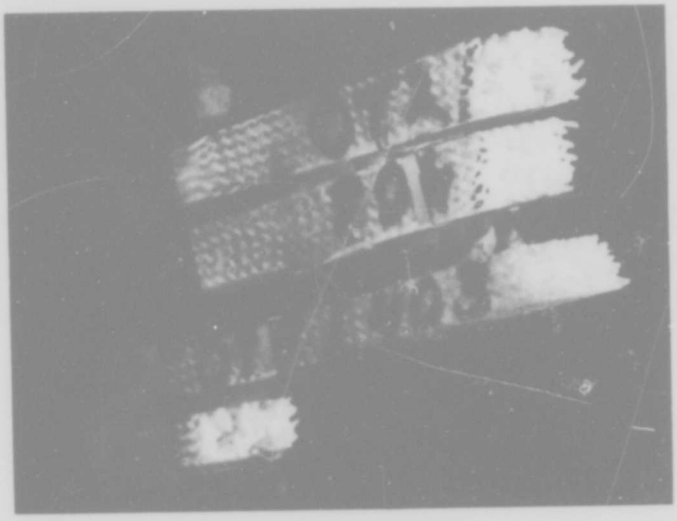

Top: 403/A-2
Below: 403/A-5* (Machined Faces)

Figure 68. Fracture Surfaces of Two Tensile Specimens from ADL-10 Panel 403

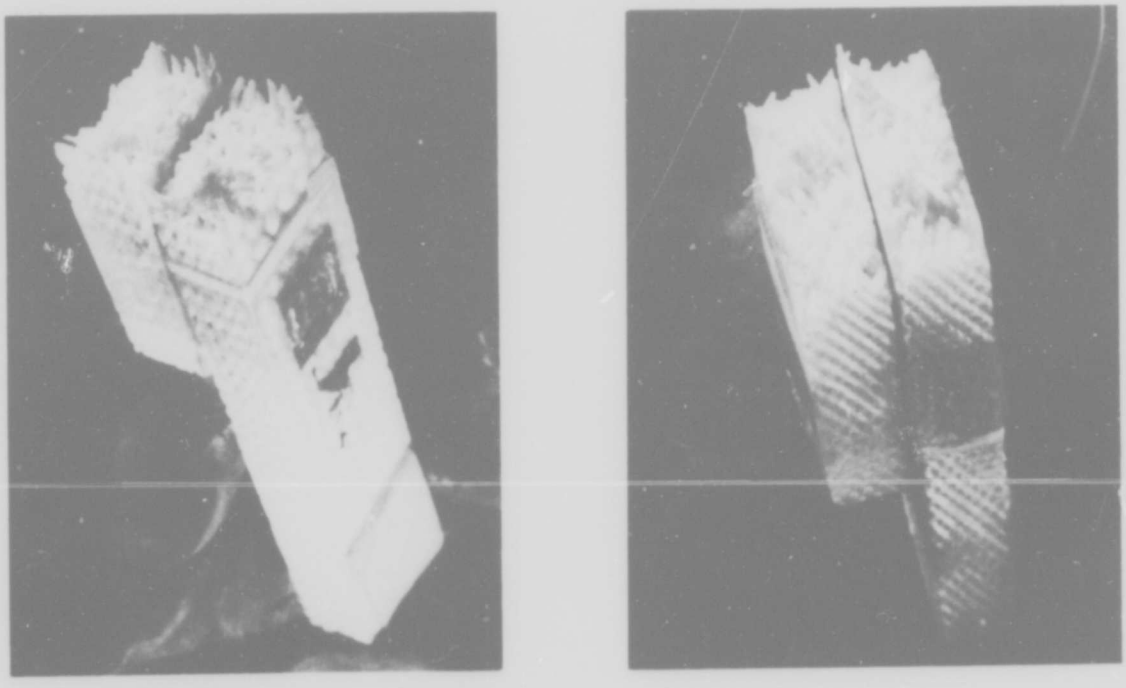

L: Axial Direction Specimen R: Bias Direction Specimen

Figure 69. Fracture Surfaces of Two Tensile Specimens from ADL-10 Panel 404-1

The fracture surface of a bias direction specimen from panel 404 (Figure 69R) appears to have less visible matrix material. The fibers running directly along the length of these specimens have clean breaks, while fibers running at almost right angles to these fibers appear to have experienced some movement adjacent to the fracture. The major portion of the load appears to have been carried by the fibers running in the sample axis direction, while the angle fibers appear to have acted as interlocks to strengthen the composite, somewhat similar to the "trussing" mode of composite action proposed for the space frame model of Section 4, Reference 2. These observations can be directly linked to the two-stage stress strain curve found in testing.

In general, the results of this effort show that strength levels attained previously in Reference 2 were not reproduced with this material despite use of the apparent optimized processing for ADL-10. A lower strength and elastic capability composite material was found. Comparison of the present fracture surfaces to one from ADL-10 plate 331-2 (Reference 2) which had a strength of 18,000 psi (Figure 71) indicates a difference in the basic nature of the failure of the material. In the previously made material, the fiber ends frayed extensively and fibers were more free to move. This overall micromechanical behavior of the specimen would be such as to result in higher strength. Note that this material was not silane-treated.

The fracture surfaces of a silane-coupled ADL-10 tensile specimen from panel 405-2S are shown in Figure 70R compared to fracture surfaces for an untreated sample from panel 405-1. The untreated fracture surface shows a greater degree of inter-bundle infiltration while the treated fracture surface shows infiltration and hardening within the bundles. In the treated specimen fiber movement is more prominent.

The analysis of Section 4 discusses the effects of varying fiber-matrix shear strength on ADL-10 composite strength.

3.2.2 UNIMPREGNATED OMNIWEAVE FABRIC MECHANICAL CHARACTERIZATION

In order to determine the maximum strength of as-woven Omniweave fingers, two pieces were tested in tension. The ends of the matrices were impregnated with epoxy resin to give them strength for gripping purposes. The gage length was soaked in silicone oil to allow all the fibers to slip freely with reduced frictional restrictions from other fibers. No means of deformation measurement was used. Results are as follows:

Specimen 1	3071 psi
Specimen 2	3150 psi
Average	3111 psi

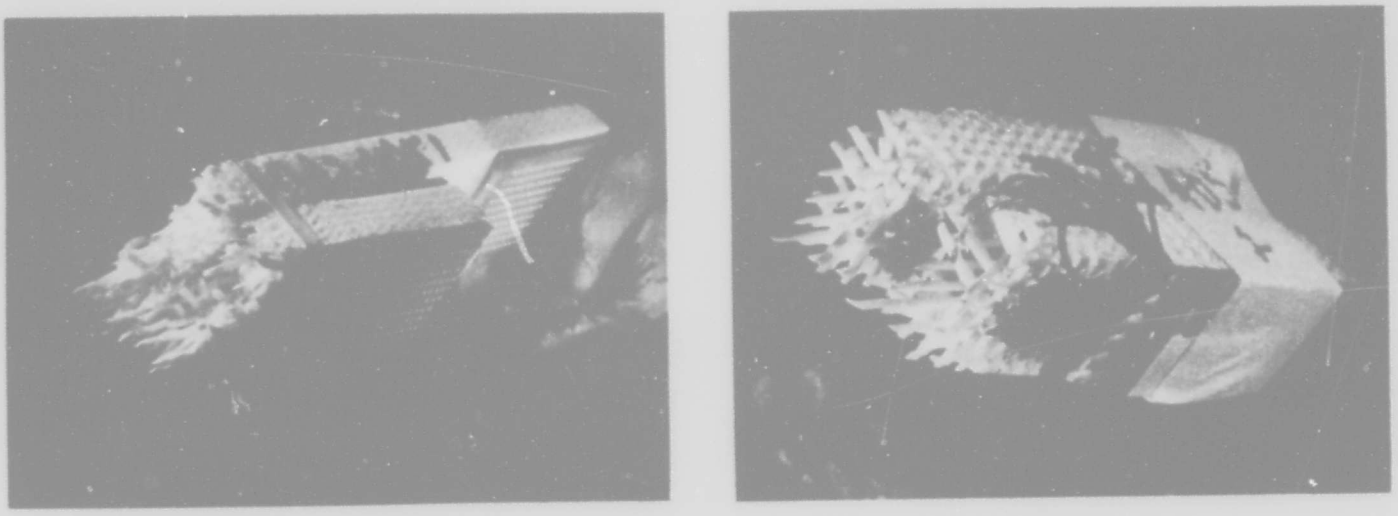

(L) (R)

Figure 70. Fracture Surface of Tensile Specimens from Panels 405-1 (L), and 405-2S(R)

Figure 71. Fracture Surface of Tensile Specimen B2 from ADL-10 Panel 331-2

This is the baseline capability of the unimpregnated Omniweave.* Previous results have shown how the strength can be reduced or increased by impregnating the weave with various materials. Sometimes, increase in rigidity is favored and strength is sacrificed. The ideal situation would be to increase both the strength and the rigidity but not enough to cause a brittle condition.

3.2.3 QUARTZ OMNIWEAVE-LUDOX COLLOIDAL SILICA COMPOSITES: ADL-4D6

3.2.3.1 4-D Cubic Quartz Omniweave/Ludox HS-40

Either flexure, tension or both were run on the Omniweave specimens which were impregnated with sodium-stabilized Ludox HS-40. Specimens with a high degree of flatness were used in the tensile tests and the large remnants were tested again in flexure. Specimens with any warp or curvature were only tested in 4 point flexure with a span length of 5.5 inches and a load length of 2 inches.

Ultimate tensile strength is tabulated in Table 30 for all three densities tested. These measurements were made early in the program in an effort to evaluate the space-frame model for a low density ductile ceramic and for comparison to the 5-D material.* In addition, one specimen impregnated with deionized Ludox HS was tested in flexure. The results indicate an optimum strength level for the 1.43 density specimens and a large reduction in strength when density is increased to 1.70. The effect of using deionized HS Ludox is obvious. A large increase in strength is evident in the one specimen having a density of 1.70. Strain level appears to be similar to the standard HS Ludox.

Specimen fracture appears to occur in a brittle fashion. Fibers have clean breaks with no fraying at the ends. Also, individual fibers show no movement prior to failure. Even though these specimens were closed weave fingers, failure apparently initiated by fracture of individual surface fibers. On pulling an individual fiber from the surface, it is noticed that the fiber is very rigid, but lacking in toughness thus contributing to an overall high modulus - low strength composite.

In the failure surface of the standard HS Ludox specimen, the individual fibers remain intact, however in the deionized HS Ludox specimen, fibers do not remain intact, but split longitudinally to form a nearly flat fracture surface with transparent light pipe fiber ends. A comparison of the fracture surfaces of the 1.70 gm/cc Ludox HS specimens in the standard and deionized form is given in Figure 72.

*In the "lock-up" angle configuration to which it was distorted in the tension test.
*A valid comparison to the 5-D material data would of course require use of the same AS type Ludox matrix, rather than the HS-40 type.

TABLE 30. MECHANICAL TEST RESULTS FOR LUDOX HS/ASTROQUARTZ 4-D OMNIWEAVE COMPOSITES

HS-381				
Specimen	Density (gm/cc)	Ultimate Tensile Strength (psi)	Modulus of Rupture (psi)	Comments
HS-381-1	1.15	122	-	-
HS-381-2	1.19	167	-	-
HS-381-3	1.25	141	460	Flexure run on tensile remnants
$\bar{X}$	1.20	150	460	-
HS-381-4	1.46	212	632	Flexure run on tensile specimens
HS-381-5	1.40	122	611	
HS-381-6	1.42	164	730	
$\bar{X}$	1.43	160	650	-
HS-381-7	1.68	-	32	(outer fiber strain at failure) = 0.11%
HS-381-8	1.68	-	42	= 0.15%
HS-381-9	1.80	-	95	= 0.67%
HS-381-10	1.65	-	38	= 0.17%
$\bar{X}$	1.70	-	52	" = 0.28%
HSDI-400-1				
HSDI-400-1	1.70	-	1633	" = 0.157%

3.2.3.2 4-D Cubic Quartz Omniweave/Ludox AS

Flexure tests were run on quartz Omniweave impregnated with standard and deionized ammonia-stabilized Ludox AS. The standard Ludox AS specimens were tested in 4 point flexure with a span length of 5.5 inches and a load length of 2.0 inches. Long finger closed weave deionized specimens from panel 400 were tested with a span length of 5.0 inches and a load length of 1.5 inches. Panel 404-2 cut and face-machined specimens were shorter, thus necessitating tests in 3 point flexure with a span length of 1.44 inches or 1.75 inches (noted in Table 31). One tensile test was run on an axial direction specimen from panel 404-2. The size of this tensile specimen was approximately (4.5 inches x 0.75 inch x 0.40 inch) in a rectangular

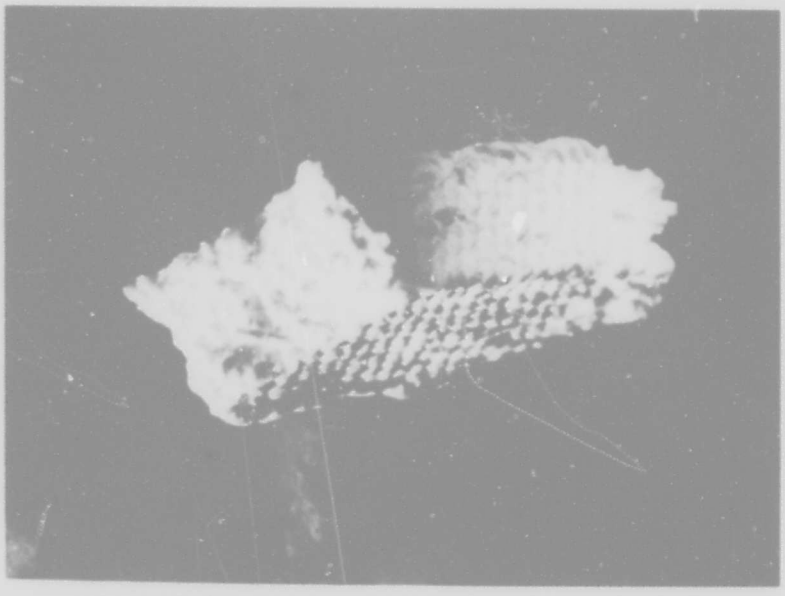

(a) Standard

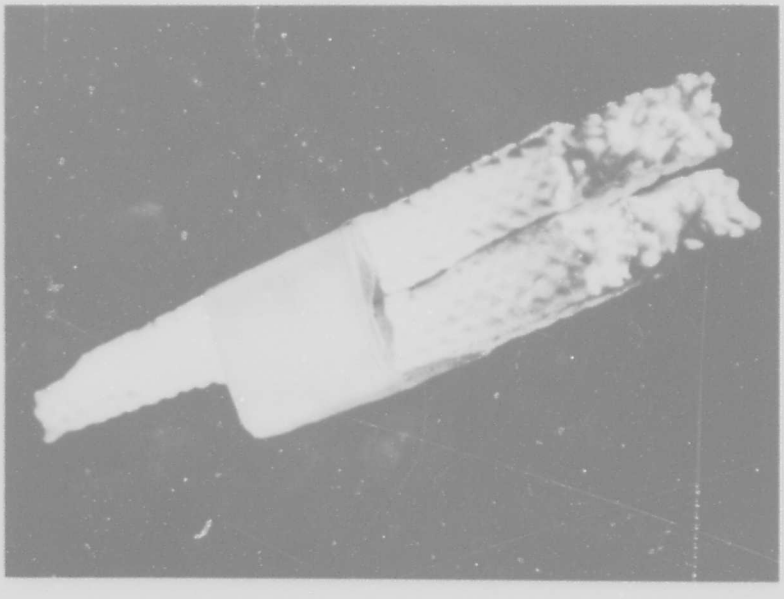

(b) Deionized

Figure 72. Fracture Surfaces of Standard and Deionized Ludox HS Tensile Specimens

TABLE 31. MECHANICAL TEST RESULTS FOR LUDOX AS/ASTROQUARTZ 4-D OMNIWEAVE COMPOSITES

Specimen	Density (gm/cc)	Ultimate Tensile Strength (psi)	Modulus of Rupture (psi)	Failure Strain, Comments
AS-400-1	1.67	-	2047	E_μ = .079% (failure strain)
AS-400-2	1.70	-	2152	.082%
AS-400-3	1.72		2161	.073%
$\bar{X}$	1.70	-	2120	0.078%
ASD1-400 (Deionized as Composites)				
ASDI-400-1	1.70	-	3220	
ASDI-400-2	1.65	-	2614	
ASDI-400-3	1.71	-	2247	
$\bar{X}$	1.69	-	2694	
ASDI-404-2* (Deionized as Composites, Cut Machined Surfaces)				
ASDI-404-2-FT-1	1.58	-	26,765	E = 2.32 x 10^6 psi Span = 1.44"
ASDI-404-2-FA-1	1.58	-	28,573	E = 1.31 x 10^6 Span = 1.44"
ASDI-404-2-FA-2	1.58	-	32,776	E = 2.48 x 10^6 Span = 1.44"
ASDI-404-2-FA-3	1.58	-	31,443	E = 3.41 x 10^6 Span = 1.75"
$\bar{X}$	1.58	-	30,931	E = 2.40 x 10^6
ASDI-404-2-FB-1	1.58	-	47,321	E = 3.43 x 10^6 Span = 1.44"
ASDI-404-2-FB-2	1.58	-	39,476	E = 2.88 x 10^6 Span = 1.75"
ASDI-404-2-FB-3	1.58	-	50,542	E = 3.47 x 10^6 Span = 1.44"
$\bar{X}$	-	-	45,780	E = 3.26 x 10^6
Tensile Test				
ASDI-404-2-TA-1	1.58	2197	-	Specimen Broke at Doubler E = 0.68 x 10^6 psi
ASDI-404-2-TA-1-R	1.58	2587	-	Remnant of previous specimen tested in tension. Failure at Doubler E = 0.67 x 10^6 psi

*Note: FT, FA, FB indicate transverse, axial, bias specimens

configuration. Textotile doublers were bonded to the grip area to distribute the load and attempt to avoid localized failure of the material due to the tearing action of the grip faces.

Modulus of rupture* for all specimens is tabulated in Table 31. The results indicate a higher strength of Omniweave when impregnated with Ludox AS compared to impregnation with Ludox HS. Once again, the deionized Ludox results in a stronger composite than the standard Ludox for the same density (1.70) material. Specimens machined from the 404-2 plate with its lower density of 1.58 gm/cc show even greater strength over densified closed-weave specimens. In this density (1.58), anisotropy is investigated and the bias direction is found to be the strongest, with the transverse and axial directions having somewhat similar strengths.

The tensile specimen has a much lower strength and modulus than the flexure specimens. This low strength behavior is quite possibly due to the stress concentration effect of the doubler on the specimen. In each of 2 runs the specimen failed at either the edge of the doubler or under the doubler. Evidence of a depression at the edge of the doubler was found leading to the conclusion that the strength given in Table 31 is not the true tensile strength, but a reduced value because of concentration induced failure. A re-evaluation of the gripping process must be made to correct this type of failure or specimen configuration should assume the dogbone shape in order to force failure to occur in the desired region.

The failure surface of the standard Ludox AS specimens shows a very dense, homogeneous material in which it is very difficult to discern the difference between fiber and matrix by visual means. There is no fiber movement and no fiber pullout. Ends of the fibers fractured in a clean manner with no fraying. Figure 73 is a photograph of a flexure bar and the fracture surface.

Failure surfaces of the dionized Ludox AS specimen (1.70 density) are not available since the specimen did not separate but continued to deform until the ends bowed up to touch the loading device. No evidence of any crack initiation is present on the tension face; however a slight amount of fiber fraying is evident on the corners of the specimen. This behavior is unusual for a ceramic material and should be investigated in specimens which are not woven fingers but are sections of a woven plate. The effect of fiber continuity could then be determined for this composite.

In general, specimens impregnated with Ludox AS (deionized) and machined from plate 404-2 also had no actual experimental fracture surface to examine. The

*Modulus of Rupture (MOR) - Strength calculated at maximum flexure load. Calculation based on linear elastic formula. Material with any degree of plastic or pseudoplastic deformation has a failure strength in flexure actually lower than MOR.

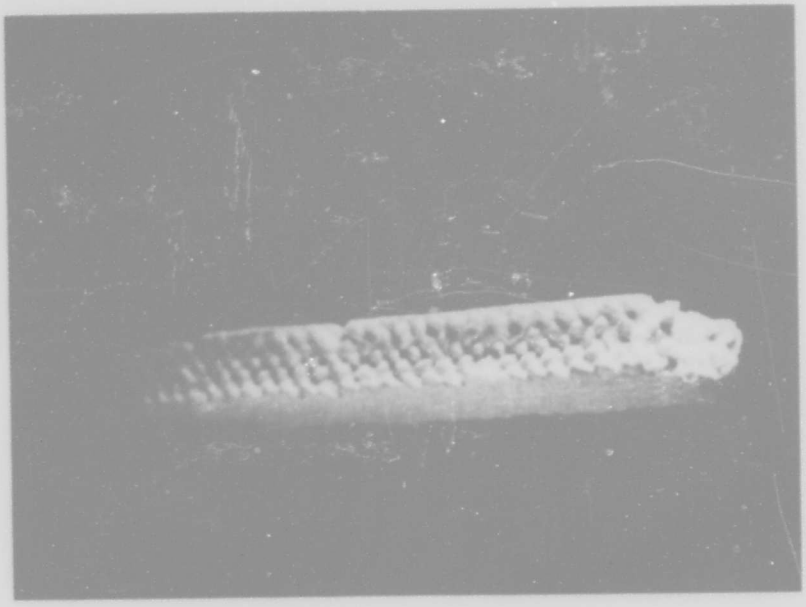

Figure 73. Fracture Surface of Standard Ludox AS Tensile Specimen

specimens yielded and the load dropped off; however there was no separation and no crack initiation on the tensile surface. These specimens were machined from a plate and thus had no fiber continuity. The resulting strengths are unusually high compared to the other materials tested. The possibility of a size effect should be examined, but judging from the behavior of the material, the strengths are higher than the other materials tested. Figure 74 is an SEM composite photo of the fracture surface of the one flexure bar (A3) from panel 404-2 that did break in test. In most areas, fibers are not infiltrated uniformly. Infiltration between bundles appears uniform.

The fracture surface of the tensile specimen (Figure 75) shows a uniform impregnation around the fibers, but the fibers appear not to be penetrated. Fiber ends are frayed and ragged. In this way the individual fibers are free to move and thus deform without fracturing as is evident in the flexure tests and Figure 74.

The results of tests on panel 404-2 show a material which stands out among the others tested. The combination of higher strength and ability to deform without fracture are recognized as being important mechanical qualities.

Figure 74. Composite SEM Photo of Fracture Surface of ASDI Ludox Sample A3 from ADL-4D6 Plate 404-2 (0.5 x 0.4 Inch Section)

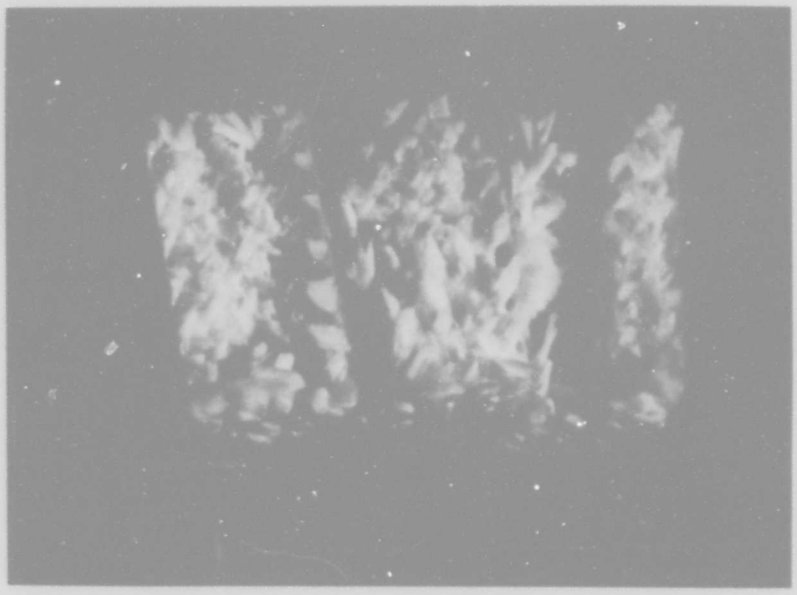

Figure 75. Fracture Surfaces of ASDI Tensile Specimen A-1, from ADL-4D6 Plate 404-2 (Broken Twice)

3.2.3.3 5-D Cubic Quartz Omniweave/Ludox AS Characterization

The Astroquartz 5-D Omniweave panels processed to three densities were machined into flexure bars as shown in Figure 57 and 59. Two orientations were selected for tests; both the transverse direction which was parallel to the stuffer and the axial direction which was perpendicular to the stuffer. Specimen sizes were dependent upon panel size but were generally in the range 0.20 inch thick x 0.35 inch - 0.75 inch wide x 2.0 inches - 3.7 inches long. The intent was to test all specimens in 4 point flexure but this unfortunately was not possible on the smaller specimens; 3-point flexure was therefore used here. The tips of the flexure fixture were covered with rubber to prevent indentation on the specimen surface.

Results are tabulated in Table 32 together with mean values and standard deviation where enough data exists for these values to be meaningful. For each specimen, the type of flexure test and dimensions are also included.

The values are also plotted (Figure 76) vs. density for both directions. A small density effect is obvious for transverse specimens while a much larger density effect exists for axial specimens. An optimum strength appears to occur in the vicinity of 1.4 gm/cc.

TABLE 32. CHARACTERIZATION OF 5-D ASTROQUARTZ OMNIWEAVE/LUDOX AS COMPOSITES

Mechanical Properties			
Specimen	Density (gm/cc)	Modulus of Rupture (psi)	Comments
AS-401-1FT1	1.17	5091	3 point flex, 2 in. span
AS-401-1FT2		3833	
AS-401-1FT3		5954	
AS-401-1FT4		6007	
$\overline{X}$	-	5221	-
S.D.	-	1016	-
AS-401-1-SA1	1.17	2857	4 point flex, 3.5 in. span, 1.0 in. load
AS-401-1-SA2		2778	
AS-401-1-SA3		2997	
$\overline{X}$		2877	
AS-401-2-FT-1	1.39	4224	3 point flex, 2 in. span
AS-401-2-FT-2		5179	
AS-401-2-FT-3		5511	
AS-401-2-FT-4		5384	
$\overline{X}$	-	5075	
S.D.	-	583	
AS-401-2-FA1	1.39	4767	3 point flex, 2 in. span
AS-401-2-FA2		3979	
AS-401-2-FA3		4150	
$\overline{X}$	-	4299	
AS-401-3-FA1	1.68	1557	3 point flex, 1.75 in. span
AS-401-3-FA2		4323	
AS-401-3-SA1		3226	3 point flex, 2.0 in. span
AS-401-3-SA2		3110	
AS-401-3-SA3		3763	
$\overline{X}$	-	3196	
S.D.		1035	
AS-401-3-FT1	1.68	5559	4 point flex, 3.5 in. span, 1.0 in. load
AS-401-3-FT2		4928	
AS-401-3-FT3		5617	
$\overline{X}$	-	5368	

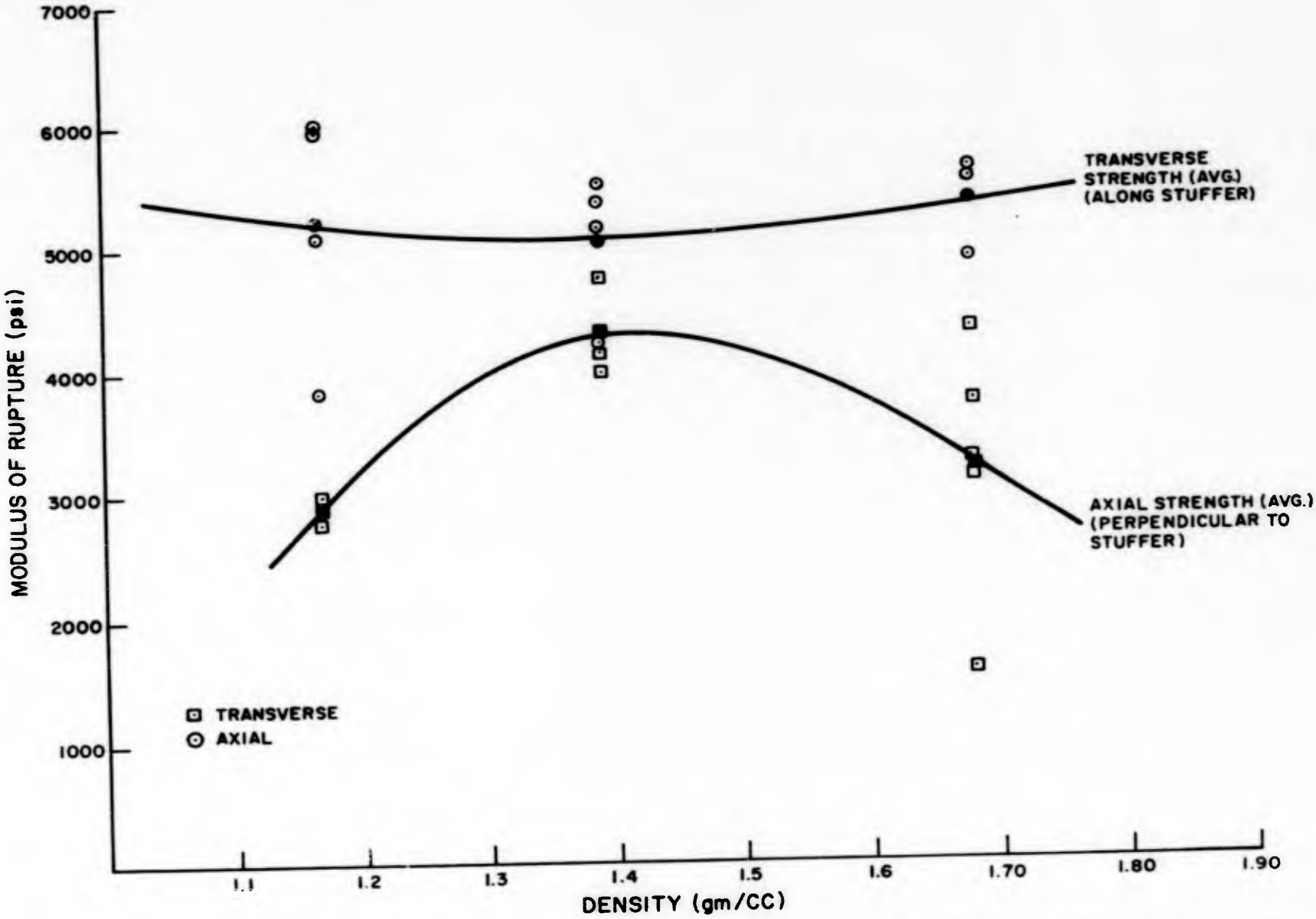

Figure 76. Strength Versus Stage of Densification: Ludox AS/Astroquartz 5-D Omniweave Composite

The specimens with a density of 1.17 did not break in the transverse direction. Yielding took place with an accompanying load drop. The specimen surface did not appear to have any cracks. Specimens tested in the axial direction did separate at failure and the fracture surface shows very little visible matrix material. There is little or no fiber movement apparent. Fiber ends are ragged and somewhat frayed. Figure 77 is a photograph of the transverse specimen after testing.

Specimens with a density of 1.39 all had fracture surfaces similar to that of the axial specimens of density 1.17. All specimens separated.

Specimens with a density of 1.68 show a great increase in brittle behavior. There is no fiber movement. Fiber ends are cleanly broken with no fraying. Infiltration seems very uniform (Figure 78). Axial specimens show perpendicular fiber splitting. The transverse silica fibers are visible in Figure 78 with a high optical reflectance.

The 5-D Omniweave material does have an obvious strength increase over the 4-D material matrix, at low to intermediate, 1.2-1.4 gm/cc composite density levels, verifying the "space-frame" model of Reference 2. At lower density levels, the material is rigid, but does not appear to be extremely brittle. The next step is to determine the effect of deionized Ludox AS on the mechanical behavior of the 5-D material. A property improvement similar to that experienced in the 4-D material should occur.

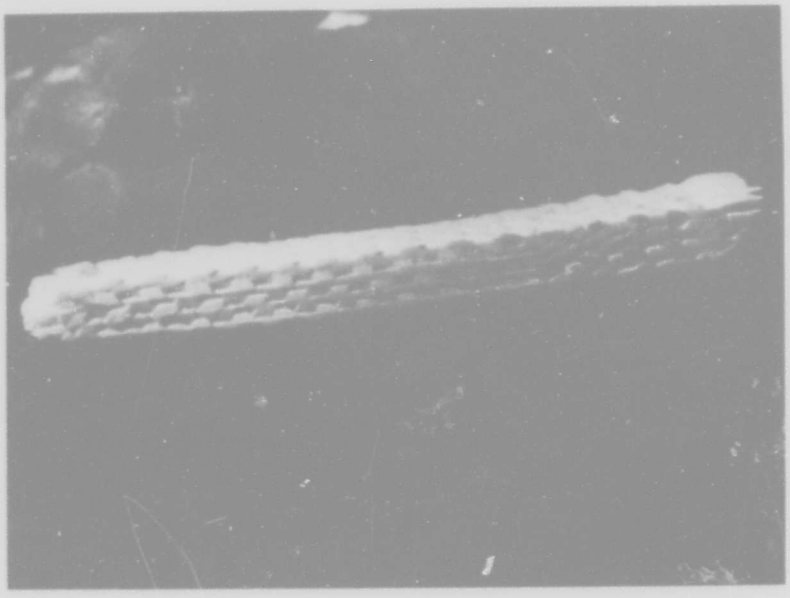

Figure 77. Transverse Flexure Bar of Standard AS Ludox 5-D After Testing (1.17 gm/cc)

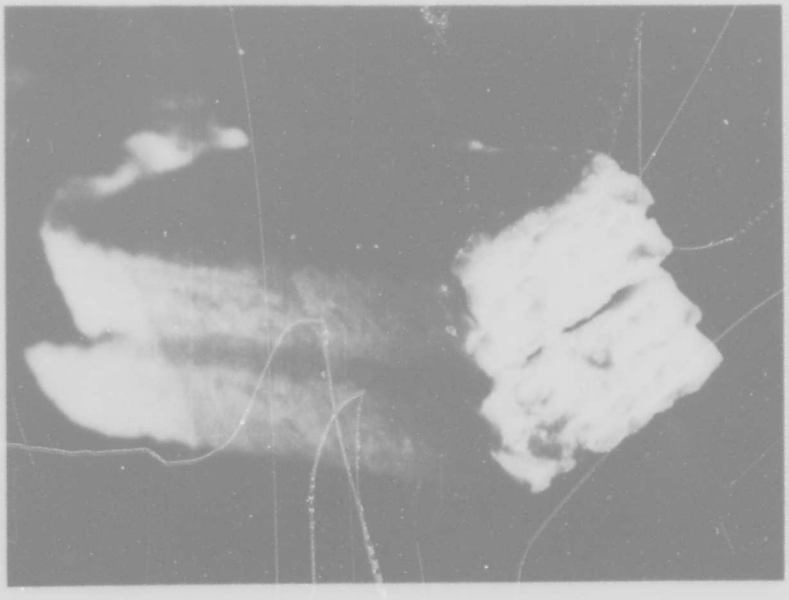

Figure 78. Fracture Surface of Standard AS Ludox 5-D Flexure Bar (1.48 gm/cc, Note Transverse, "Fifth Direction" Fibers in Fracture Surface)

3.2.4 MARKITE HYBRID CHARACTERIZATION

Flexure tests were performed on silanized Markite hybrids and standard SR-350 Markite hybrids. The physical characteristics of the individual flexure specimens are listed in Paragraph 2.4.3.3.

Due to the size of the specimens, three-point flexure was used to determine the ultimate flexural strength of these composites. The beam length was 1.25 inches for most specimens and 1.75 inches for specimens P2A and P2B. This was the same sample size and testing technique used for the Markite development work of References 1 and 2.

Specimen configuration was a rectangular bar which measured approximately 0.35 inch x 0.20 inch x 1.5 inch to 2.0 inches. Previously tested ADL-10 tensile specimens were used to provide the material for these flex tests.

Ultimate flexural strengths are tabulated in Table 33 for all specimens. These results are grouped according to parent tensile specimen and type of impregnation: silane or SR-350. An average is given for each group and a standard deviation is given where sufficient data exists to make the calculation meaningful. In addition, a grand average is given for all specimens undergoing silanization to be compared with a grand average for all specimens impregnated with SR-350.

The overall grand averages show that the silanized ADL-10 specimens are weaker than the standard SR-350 impregnated specimens. Referring back to Paragraph 2.4.3.3, the densities (R4) are lower in the silanized hybrids. The initial densities of the ADL-10 material used in the silanization process are lower than the material used for SR-350 impregnation. Strength of the Markite Hybrid has been shown to be partially dependent upon the density as shown in the previous work in References 1 and 2. It is possible in this Markite hybrid state of the material where the matrix is more brittle that the density difference is the cause of the strength difference. However, the parent ADL-10 material samples were selected symmetrically from the 1 percent silane group to avoid any bias in the starting strengths.

Insufficient data exists here to make a definitive conclusion. Specimens impregnated with SR-350 and having the highest final density plus the lowest quartz fiber volume fraction (U1 series) were the strongest. The strength of specimen D in this series was lower than the others by a significant amount. An examination of the fracture surface revealed a void on one fractured face. The presence of this void could possibly reduce the strength level significantly. Since specimen D was the only specimen containing both a physical anomaly and an anomalous strength, another average has been calculated in Table 33 and eliminates the anomalous specimen. The resultant range and average of 5240 psi is indicative of the highest strength levels achieved in the present effort while using good material.

TABLE 33. ULTIMATE FLEXURAL STRENGTH: MARKITE HYBRIDS

Specimen	Ultimate Flexural Strength (psi)	Notes
P1A	Specimen failed in test set-up	
P1B	Specimen failed in test set-up	
P1C	3771	Silanized
P1D	3897	
$\bar{X}$ (mean failure stress)	3834	
Q2A	3465	
Q2B	2573	Silanized
$\bar{X}$	4188	
P2A	3610	
P2B	3663	SR 350
P2C	4953	
P2D	4525	
$\bar{X}$	4188	
S.D.	660	
R1A	Specimen failed in test set-up	
R1B	4781	SR 350
R1C	4991	
R1D	3938	
$\bar{X}$	4570	
U1A	4828	SR 350
U1B	5559	
U1C	5333	
U1D	3564	Failure surface shows void
$\bar{X}$	4821, S.D. = 892	AVG W/Defect
$\bar{X}$	5240	AVG W/O Defect

Grand Average with silane:3427 psi
Grand Average with SR 350:4522 psi

Fracture surfaces of all material appear to be quite similar. Fracture takes place in a very brittle fashion. All specimens make a very clean break with a minimum of ragged edges. A few specimens broke into more than two pieces when the area adjacent to the break shattered into a few small pieces. A closer look at the fracture surface in Figure 79 shows that the matrix material infiltration is good and it appears as though the individual fibers have cleaved. The fracture surface in general has a glassy, glazed look.

The load - deformation curves for this material were all linear to failure. This is another characteristic of a brittle material.

Figure 16 of Paragraph 2.4.3, "Markite Hybrids Background", shows a curve of tensile strength vs. stages in ceramicizing. The expected trend at the 3rd reimpregnation (R3) is extrapolated to 5500 psi. Therefore at R4 the extrapolated value should be higher. In this effort all tests were made in the R4 condition, and the upper point of the range is found to be approximately 5500 psi. This indicates that quite possibly the expected value of strength after reimpregnation does not increase in a linear fashion but experiences a decrease in slope somewhere between R2 and R4. All the present data and the past data are plotted together in Figure 80. In addition the tensile strength of the original ADL-10 tensile specimens used for the material in this case is plotted here from the data given in Figure 17.

In conclusion, the flexure tests on Markite hybrids tested after the 4th pyrolysis and reimpregnation revealed a lower strength than that anticipated. The silanized Markite hybrids are weaker than SR-350 impregnated material. The failures were brittle in contrast to the fibrous fractures observed for both the pyrolyzed and reimpregnated stages of the Markite 319 series described in Reference 2.

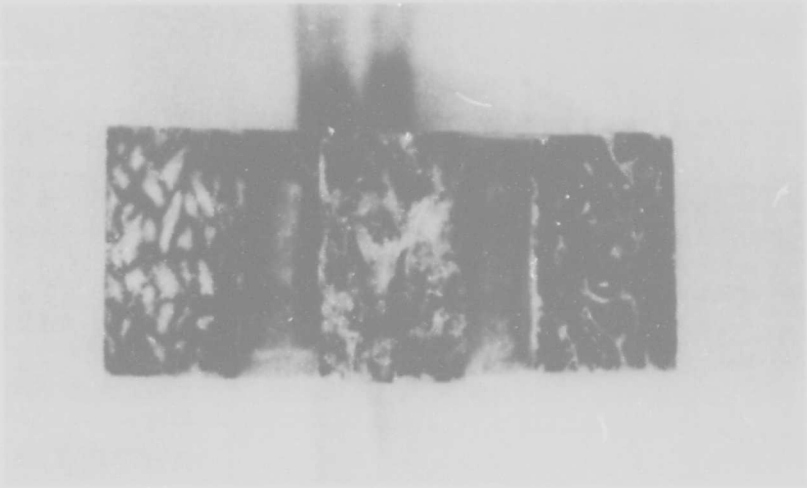

Figure 79. Three Fracture Surfaces of Markite Hybrid Materials. (Whiter Section at Left is Standard SR-350 Process; Middle Specimen "UID" has Void; Darker Section on Right Typical of Silane Final Impregnation)

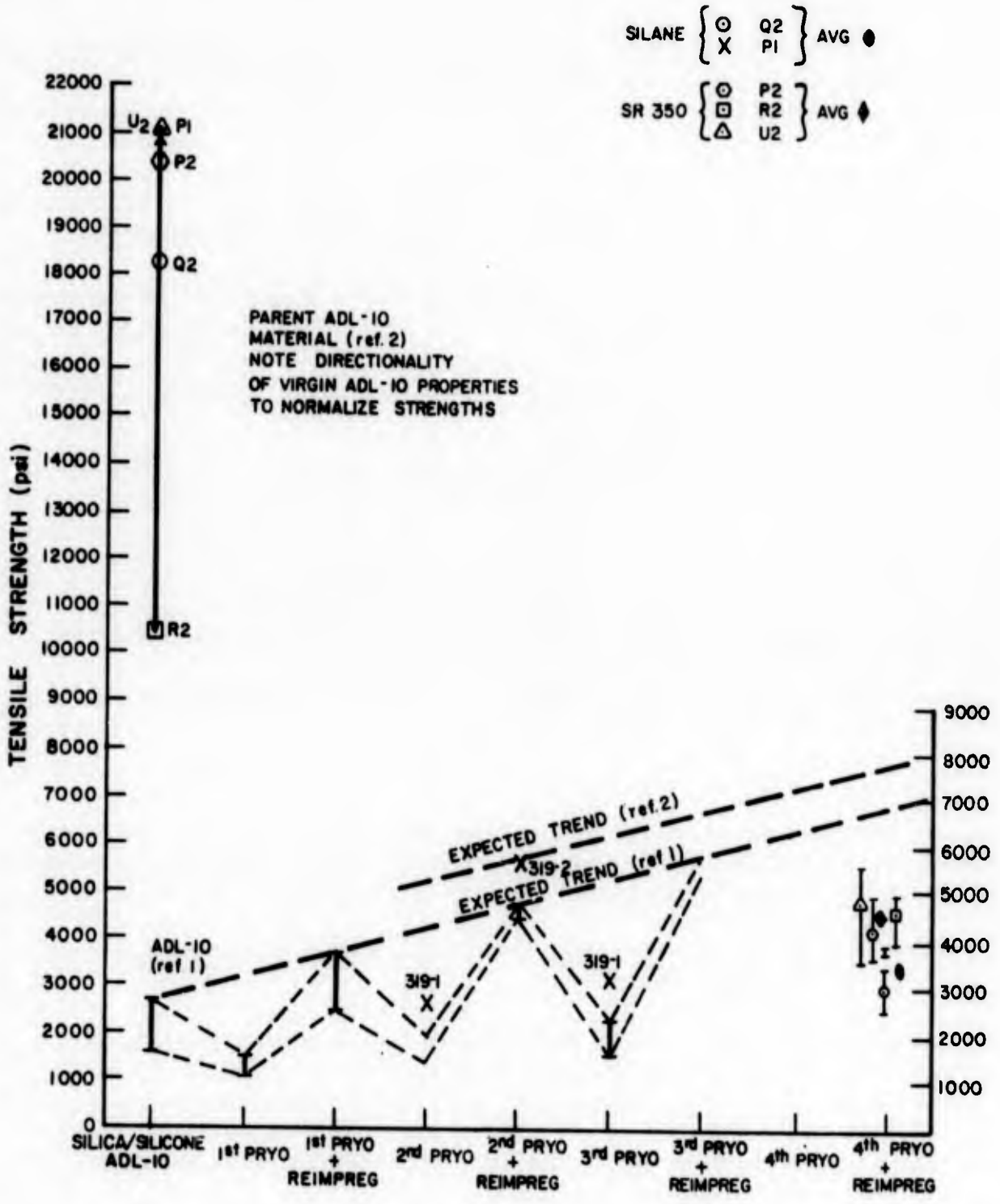

Figure 80. Tensile Strength Improvement with Processing Cycles: Two Markite Hybrid Processes

3.2.5 SILICA-BORIA MATRIX SYSTEMS

3.2.5.1 Mechanical Characterization of Silica-Boria/Astroquartz Omniweave Composites

Three silica-boria/Astroquartz specimens were tested in four-point flexure with span length of 4.0 inches and load length of 2.0 inches. The original intention of these specimen tests had been to test in tension, however the specimens were warped in the infiltration and firing process and were observed to be brittle, therefore the tests were performed in flexure. The formulation and processing of these specimens is described in Paragraph 2.4.4.1 and Table 16. The specimen size was approximately 0.30 inch x 0.60 inch x 4.25 inches in a rectangular closed weave configuration.

Modulus of rupture for each specimen is tabulated below in Table 34. Strengths are not very high, but are uniform.

TABLE 34. FLEXURE TEST RESULTS ON SILICA-BORIA/ASTROQUARTZ OMNIWEAVE COMPOSITES

Specimen	Modulus of Rupture (psi)	Comments
SB-400-1	465	-
SB-400-2	403	Failed under Load Pt.
SB-400-3	506	Failed under Load Pt.
$\bar{X}$	458	

Load deformation curves for this material are very erratic which may be caused by the initial warp or a condition of non-uniform deformation. Fracture surfaces show frayed fibers that are brittle and not able to move very much.

3.2.5.2 Mechanical Characterization of Silica-Boria-Alumina/Astroquartz Omniweave Composites

Three silica-boria-alumina/Astroquartz Omniweave fingers were tested in tension. The specimens were relatively straight, therefore, this was possible. These specimens are described in Paragraph 2.4.4.2 and Table 17. Specimen size was approximately 0.30 inch x 0.60 inch x 5.0 inches in a rectangular configuration. Textolite doublers were bonded to the ends of the ends of the specimens to distribute the load and prevent any fiber damage from the grips.

Tensile strengths are listed below in Table 35. Specimen No. 1 failed near the doubler, and the results are somewhat doubtful due to the possibility of stress concentration. Tensile strengths are extremely low and it appears the addition of alumina has degraded the performance of the material from the level of the silica-boria matrix version.

TABLE 35. TENSILE TEST RESULTS ON SILICA-BORIA-ALUMINA/ ASTROQUARTZ OMNIWEAVE COMPOSITES

Specimen	Tensile Strength (psi)	Comments
SBA-400-1	33.0	Failure near doubler
SBA-400-2	86.4	-
SBA-400-3	89.6	-
$\bar{X}$	69.7	-

Examination of the failure surfaces shows a very brittle fiber that is capable of no movement without breaking. The fibers which are protruding from the fracture surface are all broken farther down their length. The overall result is that ductility has decreased tremendously. Since the density is low (1.01), fiber movement is not restricted; however fibers fracture when moved and reduce overall strength drastically.

3.2.5.3 Mechanical Characterization of Boron Nitride Silica-Boria-Alumina Slip System

Four specimens were tested in 4 point flexure with a span length of 5 inches and a load length of 1.5 inches. Two fiber pretreatments were used with this system: a silicone resin pretreatment and specimens without the pretreatment. The processing and identification of these specimens is given in Paragraph 2.4.4.3 and Table 18. A listing of results follows in Table 36.

Some increase in composite strength has taken place, compared to the next best silica-boria composite; but the significant observation to be made is that the strain capability and ductility of these specimens was much increased; in fact they could have been tested as tensiles if this ductility was known before the flexure testing. Table 18 shows that the densities were in the range 1.11 to 1.14 gm/cc. The "BNQ" composites whose mechanical testing is described in the next section were produced with a yarn preimpregnation process when it was found that the thicker commercial slurries being used for the matrix could not be impregnated into 1 gm/cc Astroquartz Omniweaves similar

TABLE 36. FLEXURE TEST ON ALUMINA-SILICA-BORIA-BORON NITRIDE/ ASTROQUARTZ OMNIWEAVE COMPOSITES

Specimen	Modulus of Rupture (psi)	Type of Fiber Pretreatment
BNG-400-1	737	None
BNG-400-2	189	
$\bar{X}$	463	-
SRBNG-400-1	588	Silicone Resin
SRBNG-400-2	500	
	544	-

to those used here. A prepeg process and further work on the balance of the binder to BN ratio is clearly indicated for improvement of this system, which even in this first preliminary version showed the hoped-for fiber-matrix friction interaction properties.

3.2.6 GLASS-BONDED BORON NITRIDE/SILICA OMNIWEAVE COMPOSITES - "BNQ"

3.2.6.1 Mechanical Characterization of Post Weaving - Infiltrated BNQ Composites

Three tensile specimens from Omniweave strip no. 400 were infiltrated with Emulsion Types A, V & S as shown in Table 22. The finished parts were then tested in tension. Deformation was measured with an extensometer during the tension test. Results are presented below in Table 37 for the specimens infiltrated with the specific emulsion types.

TABLE 37. TENSILE TEST RESULTS ON POST WEAVING - INFILTRATED BNQ COMPOSITES

Specimen	Ultimate Tensile Strength (psi)	Elastic Modulus (psi)	Failure Strain %	Comments
BNQ/A-400-1	-	-	-	Crumbled & fell apart at doubler bond while inserting in grips.
BNQ/V-400-1	639	4674	4.44	Failed in grip
BNQ/S-400-1	568	7834	3.57	Failed in grip

The results for the S and V type infiltrated specimens appeared promising in terms of strain capability even for the low densification ratio of about 1.10 or 1.15 to 1.10. The specimen cross sections showed some uniform internal infiltration after a large filtration effect buildup on the outer surface, so that some of the boron nitride fiber-matrix lubrication effect has been achieved.

The A type specimens appear to be too brittle to be of value, therefore this series was eliminated from future investigations.

3.2.6.2 Characterization of BNQ/S406 Prepreg Omniweave Composites

Four tensile specimens preimpregnated with "S" type emulsion were fired at two different temperatures: 850°F and 1300°F (see Para. 2.4.6.2 and Table 24 for the specimen characterization). A definite difference is noted in the results of these tensile tests, both between firing temperatures and the previous post-weaving impregnated material. The tabulated data is given in Table 38 and load-strain curves are given in Figure 81.

TABLE 38. TENSILE TEST RESULTS ON BNQ/S406 PREPREG OMNIWEAVE COMPOSITES

Specimen	Firing Temp. (°F)	Ultimate Strength (psi)	Elastic Modulus (psi)	Poisson's Ratio	Failure Strain (%)	Comments
BNQ/S406-3	850	2492	44000	0.17	8.55	Strain by extensometer
BNQ/S406-4	850	2138	49000	0.33	6.89	...
$\bar{X}$	850	2550	46500	0.25	7.72	
BNQ/S406-1	1300	1890	34000	0.61	9.16	..
BNQ/S406-2	1300	2055	32000	0.56	10.7	Strain by crosshead motion
$\bar{X}$	1300	1973	33000	0.59	9.93	

The specimens which were fired at the lower (850°F) temperature appear to be the stronger material with a higher modulus and lower Poisson's Ratio.

Examination of the fractures reveals a very chalky white fracture surface in which the fibers experience a great deal of fraying on their ends. The specimen surfaces appear to show a good initial uniform deformation, since strain gages appear to remain intact even though there is significant deformation. The behavior of the material is particularly amenable to tensile testing since the fibers do line up easily to eliminate any bending with no damage.

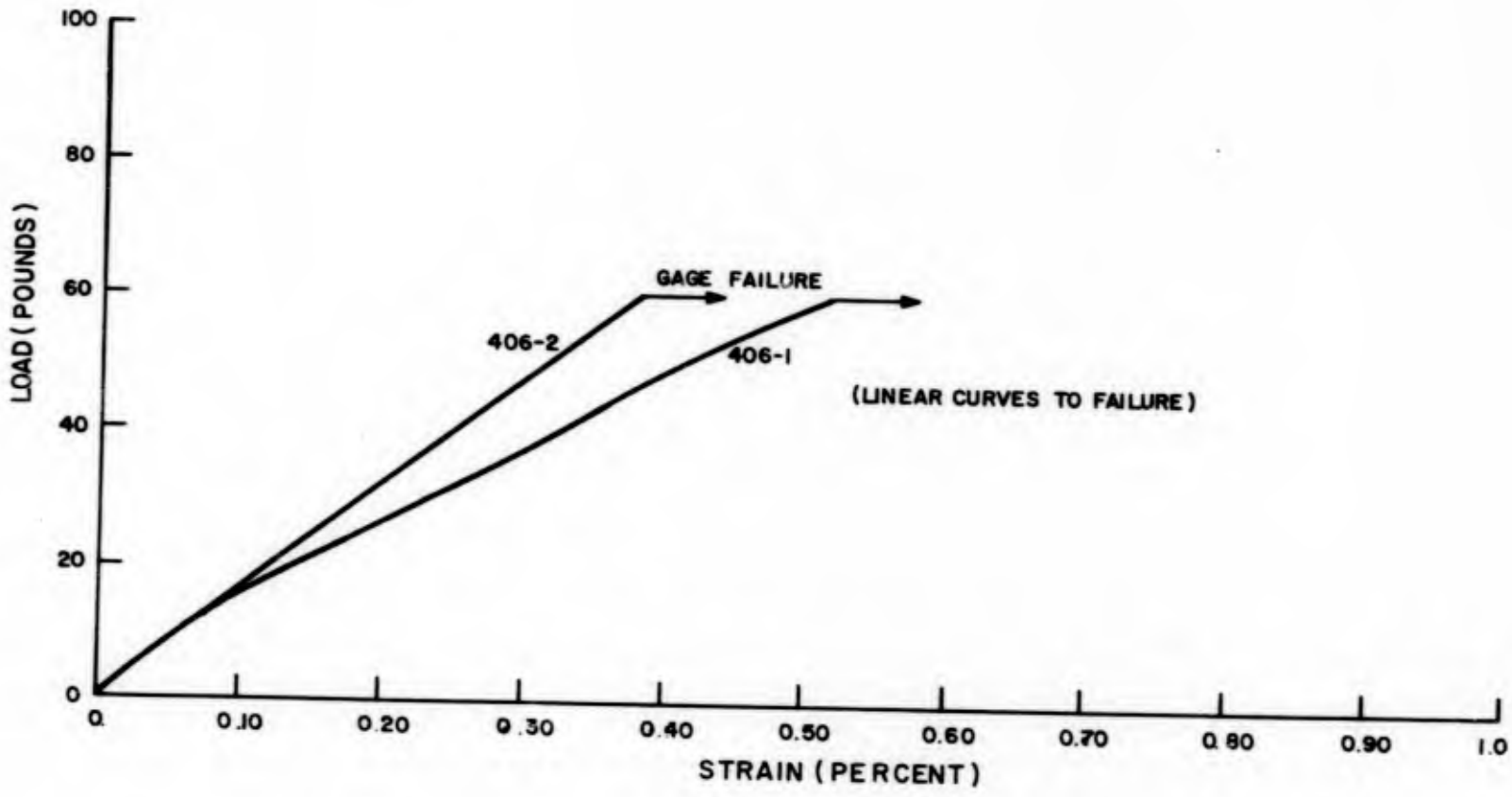

Figure 81. Load Versus Strain for BNQ/S406 Prepreg Omniweave Composites

The indications of this series of tests that the hoped for elastic and strain behavior could be achieved along with respectable tensile strengths encouraged further development of the BNQ prepreg technique which was modified for faster weaving of the type V matrix.

3.2.6.3 Characterization of BNQ/V-407 Prepreg Omniweave Composites

Eight segmented weave tensile specimens were prepared and tested from panel 407 Omniweave. The characteristics of the individual specimens are given in Table 25. The ends of the tensile specimens were impregnated with epoxy to allow densification and hardening for proper gripping action. Strain gages were mounted in the axial and transverse directions to measure initial behavior so that an elastic modulus could be determined (Fig. 82). The results are tabulated in Table 39.

TABLE 39. TENSILE TEST RESULTS ON BNQ/V-407 PREPREG OMNIWEAVE COMPOSITES

Segmented Specimen	Tensile Strength (psi)	Elastic Modulus (psi)	Poisson's Ratio	Ultimate Strain %	Comments
BNQ/V-407-1	4213	153,000	A	15.9	Ult. Strain by cross-head motion
BNQ/V-407-2	3952	95,000	B	14.6	Ult. Strain by cross-head motion
$\bar{X}$	4082	123,000		15.3	
BNQ/V-407-3	3589	-	-	-	After magnetic flyer impact at 2000 taps, see Para. 3.4.2.2
BNQ/V-407-4	1222	-	-	-	After magnetic flyer impact at 4000 taps.
BNQ/V-407-5	3362	75,000	0.25	6.82	Higher compaction and density, fired at 850°F.
BNQ/V-407-6	3288	10,000	B	19.6	
BNQ/V-407-7	625	75,700	0.35	C	Higher compaction and density, fired at 1200°F
BNQ/V-407-8	833	89,400	0.64	C	

A = Possible Gage Failure
B = Definite Gage Failure
C = Extensometer Slippage

Figure 82. BNQ/V-407 Prepreg Omniweave Composite Being Tested in Tension. Extensometer Attached to Measure-Deformation after Strain Gage Failure.

Process variations were introduced as individual sets of test results were received. Accordingly, average properties are taken across only these subsets of data, e.g., a mean failure stress of 4082 psi for the two specimens 407-1 and 407-2 with their mean fiber pitch angle of 32.5 degrees. As shown in Table 25, several processing parameters were varied. Stress-strain curves are given for specimens 1, 2, and 5 in Figures 83 and 84.

The noticeable conclusions from these tabulated mechanical properties are the degradation of strength with increasing impact load as shown in comparison os specimens 3 and 4 with the strength levels for 1 and 2. Specimen 3 shows a small degree of strength degradation at the 2000 tap level while specimen 4, which experienced an impact of 4000 taps has a strength level which drops dramatically. A noticeable difference is also seen in the failure modes of these two specimens: Specimen 4 experiences a large degree of fraying compared to specimen 3. The fractured specimen appears as though a spherical force pushed all the fibers out from the center of the specimen.

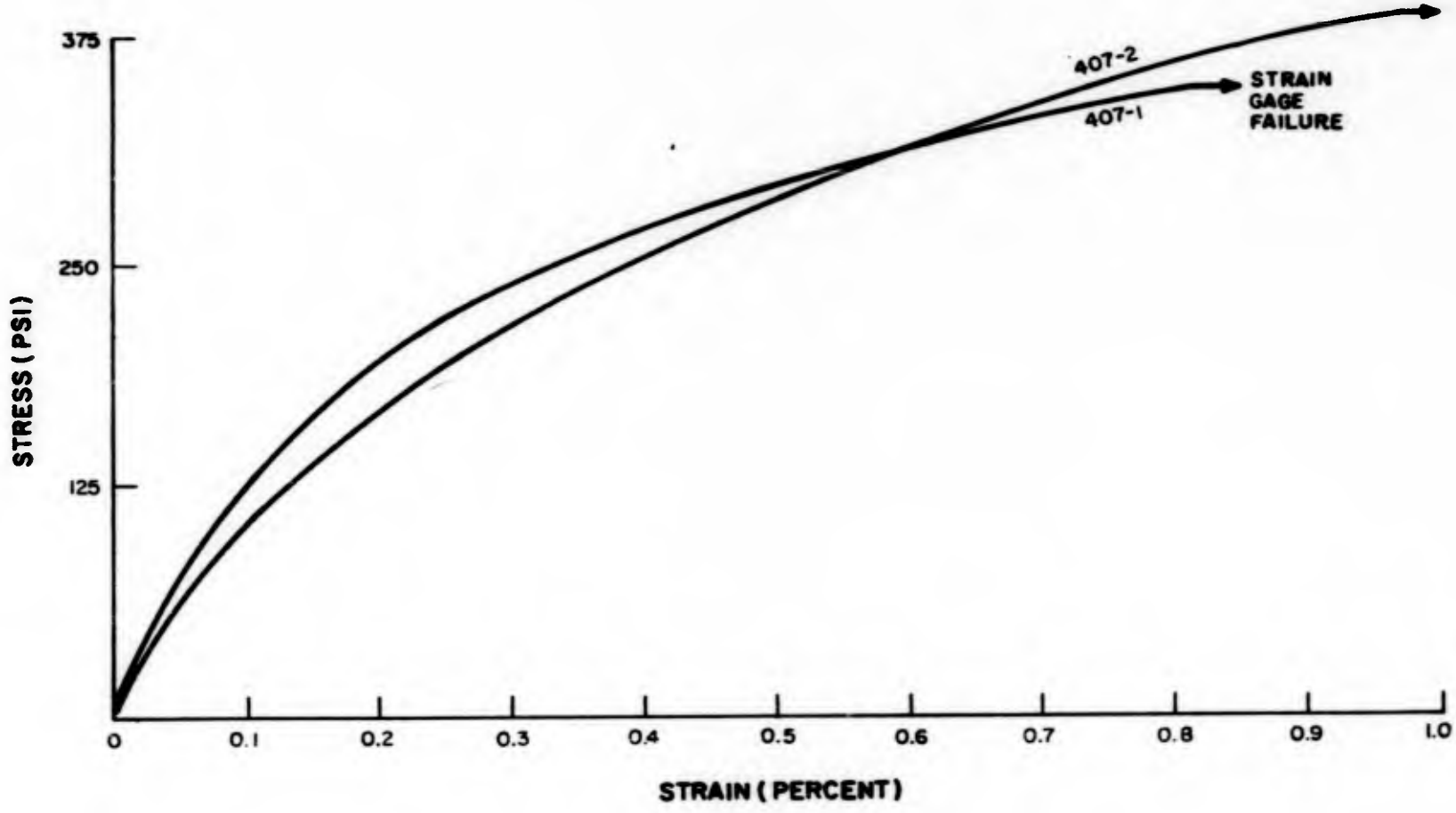

Figure 83. Stress-Strain for BNQ/V-407-1, 2

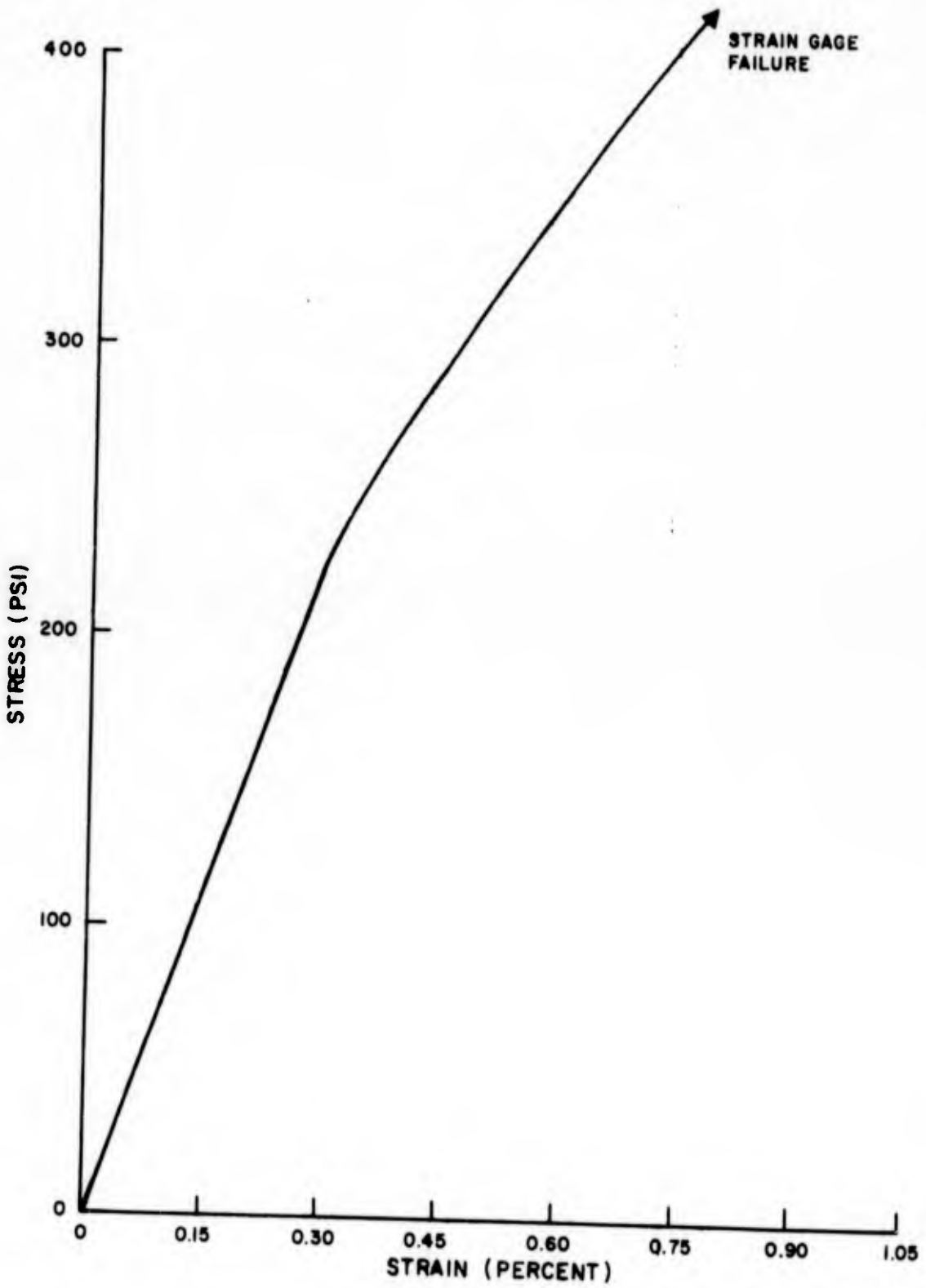

Figure 84. Stress-Strain for BNQ/V-407-5

Another conclusion as was evident in the "S" specimens was the effect of firing temperature on the strength of the composite. Specimens fired at 1200°F (7 & 8) had much lower strengths than the specimens which were fired at 850°F.

The surfaces of these specimens appear to be very unsuitable for the application of strain gages; even the clip-on extensometers slipped over the surface during a few of the tests. This was the reason for missing data points with some specimens. Portions of the upper portion of panel 407 (panel 407-9) were machined into directional tensile specimens as shown in Figure 46. All of this 407-9 panel was processed at the 850°F firing treatment which gave the highest strength in the closed-weave specimens. Textolite doublers were bonded on the specimen ends. The mechanical test results are tabulated in Table 40.

TABLE 40. TENSILE TEST RESULTS ON CUT-EDGE BNQ/V-407 PREPREG OMNIWEAVE COMPOSITES

Specimen	Direction	Ultimate Strength (psi)	Elastic Modulus (psi)	Failure Strain (%)	Poisson's Ratio	Comments
BNQ/V-407-9-1	Axial	351	30,000	3.95	0.33	Failure near doubler
BNQ/V-407-9-2	Axial	2888	222,000	A	0.26	
BNQ/V-407-9-1	Bias	3147	31,000	3.37	0.153	
BNQ/V-407-9-2	Bias	2584	22,000	A	0.260	
$\bar{X}$	Bias	2866	26,500	-	0.207	

A = extensometer slippage

From the strength data, there appears to be very little directional dependence in this composite. The only low value was obviously due to stress concentration at the doubler. Compared to the previous eight segmented weave axial specimens, these cut specimens in general have lower strengths attributable to lower strain tolerance as the cut fibers pull out of the matrix. The modulus results in the axial specimens vary considerably, probably due to a very inadequate surface for mounting strain gages. A total (100%) bond between gage and material cannot be insured, thus the results are variable. A stress-strain curve for these specimens is given in Figure 85.

Failure appears to occur by fraying of the fiber bundles and slippage to release the intertwining of the fibers. All fibers along the edges experience some degree of fraying.

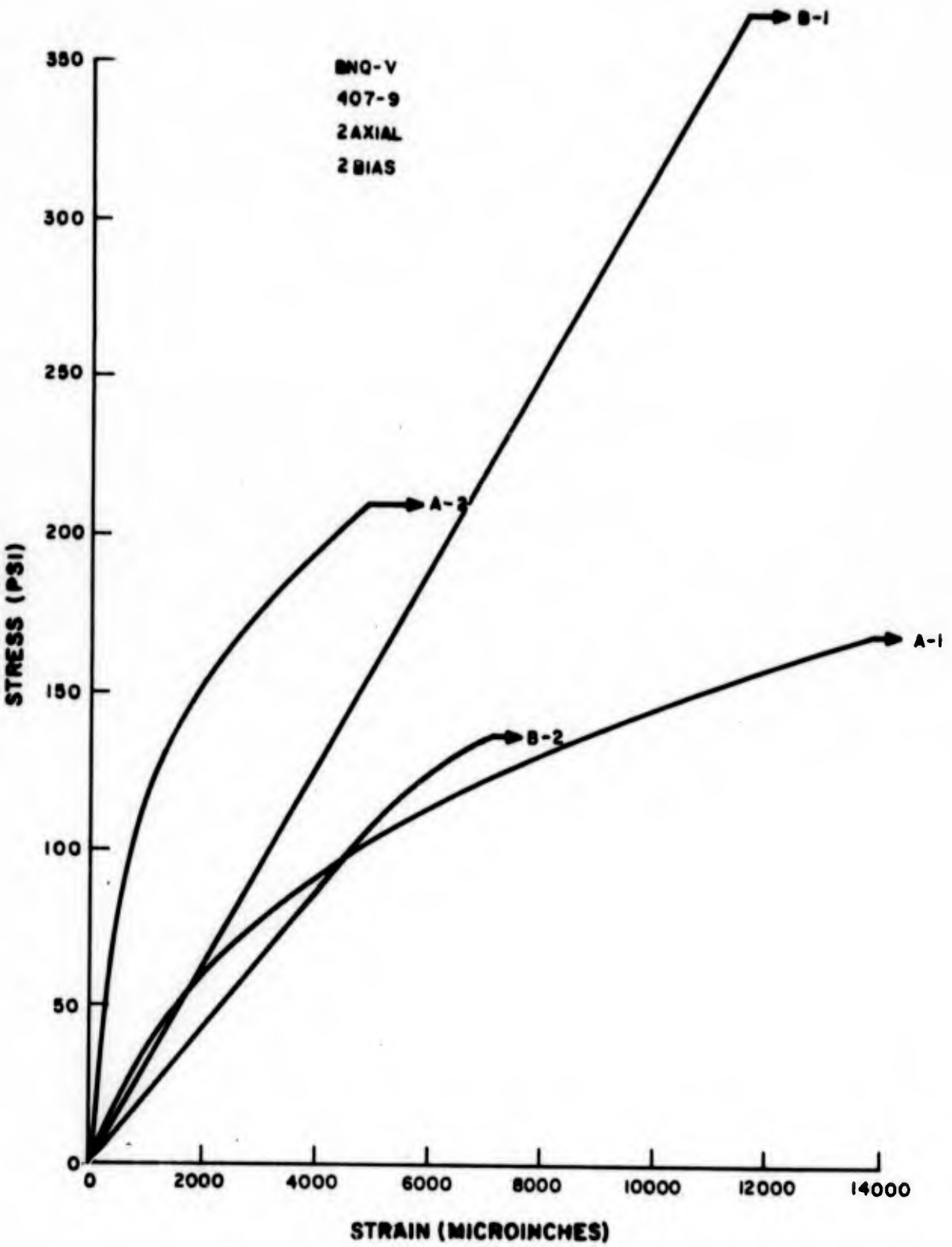

Figure 85. Stress-Strain for Cut Edge BNQ/V-407-9 Prepreg Omniweave Composite Specimens

3.2.6.4 Characterization of BNQ Bidirectional Laminates

Tensile tests were performed on 3 BNQ/S and 3 BNQ/V bidirectional composites to determine the elastic properties for analytic studies of the BNQ composite system capabilities. Strain gages were mounted on each specimen so that the axial and transverse strains could be determined. Strain gages could be mounted on the "S" type composite surface, however a surface treatment was necessary on the "V" type composite before gages could be mounted. The strain gages were monitored until specimen failure occurred. Figure 86 shows a typical gage mounting.

The resulting stress-strain curves (Fig. 87 and 88) show a two-stage linear stress-strain behavior for the "S" type bidirectional composite, while the "V" type composite experiences a one-stage linear behavior. Tabulated results are given in Table 41 for both types of BNQ bidirectional laminates.

The strengths of these laminates are very low and so are failure strains. The material can not be considered brittle, however, since it is flexible to the touch. These specimens were expressly prepared for the purpose of evaluating the fiber-matrix interaction (see Section 4 of this report) rather than for any specific structural application potential.

Failure shows a great deal of fiber fraying and delamination between individual lamina. The fibers have no flexibility for movement since they are not intertwined in the Omniweave mode but only layered on top of each other in a ± 45 degree arrangement.

Figure 86. Typical Strain Gage Mounting on BNQ Bidirectional Laminate Specimens

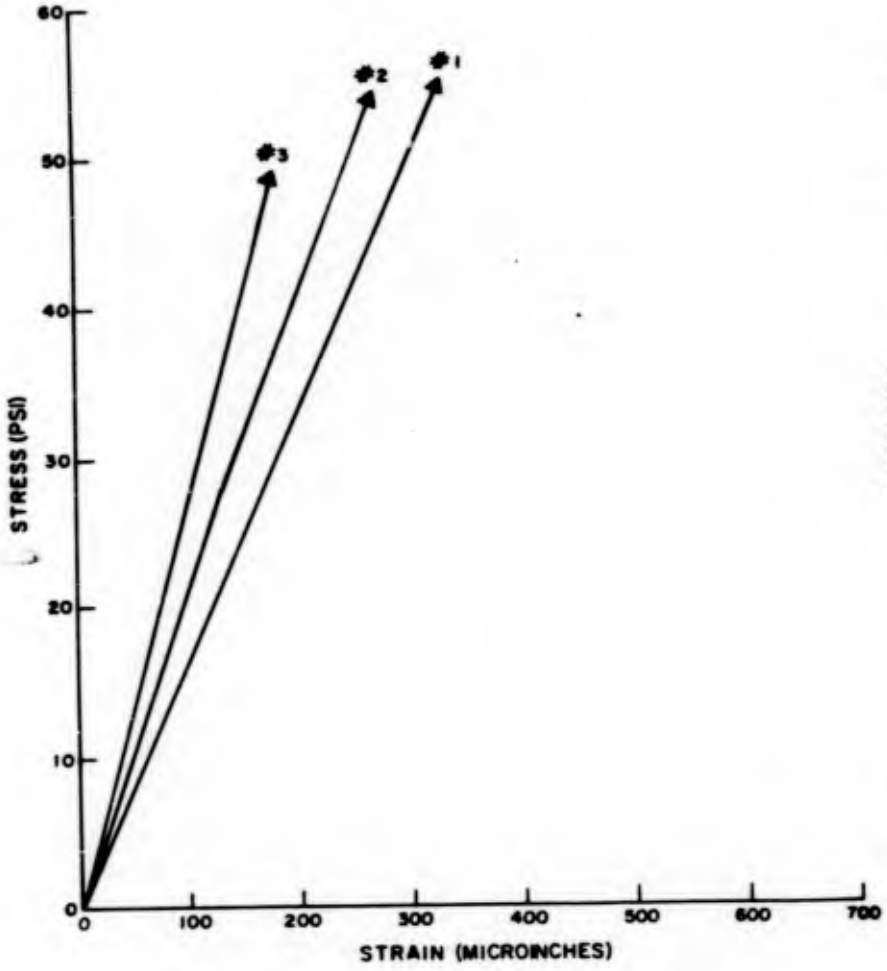

Figure 87. Stress-Strain for BNQ/S Bidirectional Laminates

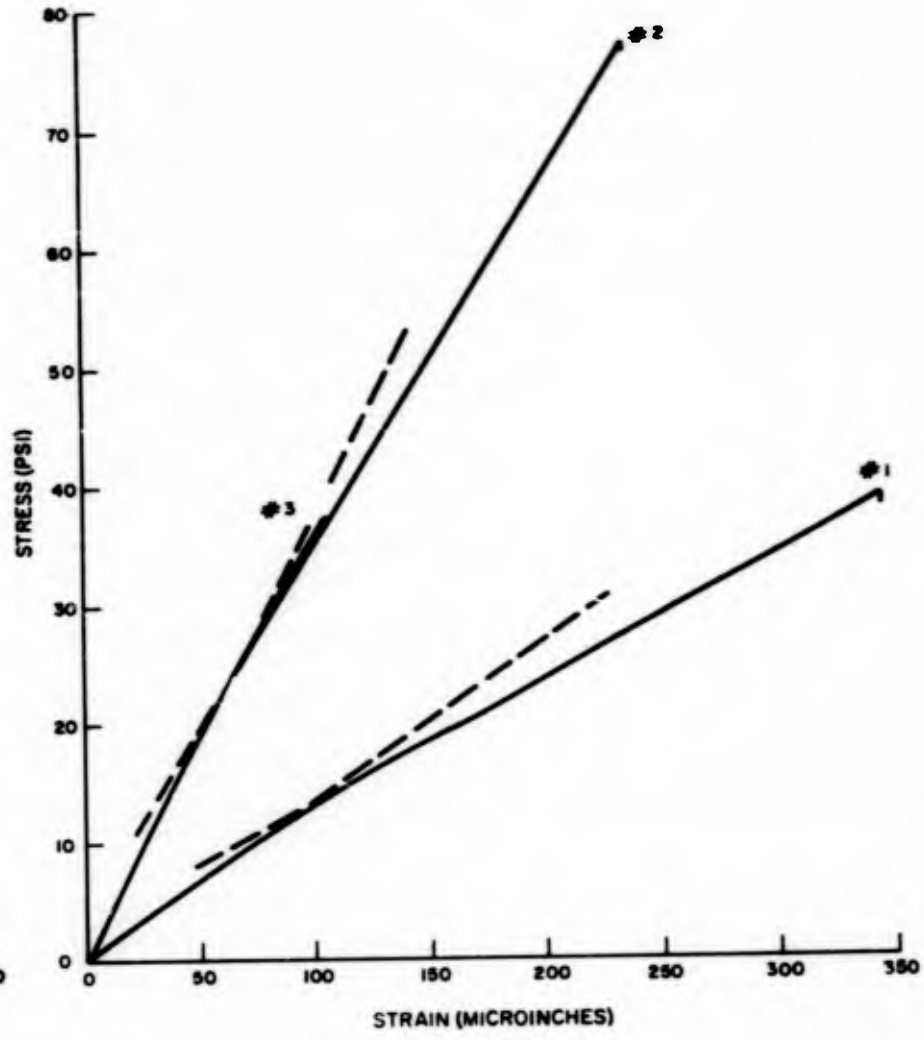

Figure 88. Stress-Strain for BNQ/V Bidirectional Laminates

TABLE 41. TENSILE TEST RESULTS FOR BNQ BIDIRECTIONAL LAMINATES

Specimen	Ultimate Strength (psi)	E_1 (psi)	E_2 (psi)	μ_1	μ_2	Failure Strain (%)
BNQ/V-1	29.3	131,000	96,000	0.44	0.42	0.034
-2	80.5	405,000	322,000	0.565	0.445	0.022
-3	37.7	402,000	343,000	*	*	0.010
$\bar{X}$	49.1	313,000	254,000	0.503	0.433	0.022
BNQ/S-1	57.3	178,000	-	0.287	-	0.045
BNQ/S-2	56.4	234,000	-	0.408	-	0.026
BNQ/S-3	50.1	274,000	-	0.555	-	0.018
$\bar{X}$	54.6	229,000	-	0.417	-	0.030

3.3 ULTRASONIC MEASUREMENTS

Ultrasonic measurements were made using longitudinal waves at a frequency of 0.73 MHz. A buffer-block technique was employed, as has been the case with all previous measurements for this series of programs. In this technique, an initial pulse transit time and attenuator reading are obtained for the signal transmitted through an aluminum buffer block. The test specimen is then inserted in series with this block, resulting in a change in transit time and attenuation of the signal. The change in transit time is the transit time through the specimen. The change in attenuation is due both to specimen attenuation and to changes in interface reflection losses. The velocity and density data are used to calculate reflection losses so that the attenuation in the specimen can be calculated.

Ultrasonic velocity and attenuation data are given in Table 42, in the same format used in References 1 and 2.

TABLE 42. ULTRASONIC VELOCITY AND ATTENUATION DATA; LONGITUDINAL WAVE, FREQUENCY = 0.73 ± 0.02 MHz

Specimen	Density (g/cm^3)	Thickness (cm)	Velocity (mm/ μ-sec)	Attenuation (dB/cm)	Remarks
ADL-10: SR-350 Resin/Silica Omniweave (2.00 in. diameter pucks)					
401-3	1.82	0.894	2.04	61	
401-4	1.90	0.899	2.19	23	
401-5	1.87	0.907	2.49	26	
402-1	1.81	0.904	1.86	53	
402-2	1.88	0.904	2.56	13	
403-1	1.59	1.067	2.24	50	
403-2	1.59	1.062	2.23	50	
403-3	1.55	1.059	1.43	57	
403-4	1.58	1.054	2.20	57	
403-5	1.58	1.049	2.23	52	
403-3B	1.60	0.907	2.07	40-60	(Specimen no. 3 with back-face ground.)
404-US1	1.62	0.782	2.27	55	
404-US2	1.62	1.062	1.96	43	
404-US3	1.60	1.062	1.74	44	
404-US4	1.66	0.782	2.05	48	
402-1 Position A	1.84	0.897	2.36	34	4 x 6-inch plates, each measured at two locations
Position B		0.902	2.30	44	
402-2 Position A	1.83	0.884	2.31	56	
Position B		0.869	2.22	51	
403-1 Position A	1.63	1.062	2.44	49	
Position B		1.072	2.37	35	
403-2 Position A	1.61	1.057	2.14	45	
Position B		1.057	2.25	32	
ADL-4D6: Ludox Colloidal Silica Omniweave (1.5 in. square plates)					
404-2-US1	1.56	1.015	2.00	46	
404-2-US2	1.56	1.016	1.94	50	
					After plate slap at RESD
404-2-US1	1.53	1.021	2.56	54	2000 Taps
404-2-US2	1.51	1.026	2.33	58	3000 Taps

3.4 SHOCK TESTING

3.4.1 HIGH LEVEL IMPACT TESTING TO DETERMINE THE FAILURE THRESHOLD OF ADL-10 HARDENED ANTENNA WINDOW MATERIAL

3.4.1.1 Introduction

This report describes the plate impact testing which was performed in the Effects Technology, Inc. (ETI) exploding foil laboratory in order to determine the failure threshold of ADL-10 hardened antenna window material. The testing was performed under General Electric Purchase Order Number 037-C91011. Thirteen specimens were supplied in the form of 5 cm diameter discs, nominally 1 cm thick. Ten of the specimens were used to determine damage thresholds for the as-molded and machined conditions. Two specimens were instrumented with carbon piezoresistive stress gages on the rear surface in order to determine the rear surface stress at the failure threshold. The 13th specimen was used as a back-up piece on the two stress gage tests in order to prevent spallation of the gages and to extend the recording time.

Exploding foil test techniques and calibration procedures are discussed in Paragraph 3.4.1.2. Descriptions of the as-received material properties and impact test conditions are given in Paragraph 3.4.1.3. Also included in Paragraph 3.4.1.3 is a brief discussion of some relevant aspects of stress wave theory and evaluation of the range of probable errors introduced into the stress and impulse calculations by use of the acoustic approximation.

Test results are given in Paragraph 3.4.1.4. The extent of damage was found to increase with delivered impulse. Large increases in specimen thickness were recorded for impulses on the order of 5 ktap for 1-cm thick specimens. Substantially lower impulses were required to produce equivalent damage in the machined specimens. In those cases where catastrophic failure occurred, the mode of failure was front surface spall. Measured back-face stresses for the threshold condition were 3.0 and 4.7 kbar.

Paragraph 3.4.1.5 contains a comparison of the exploding foil plate impact test results with the results obtained by General Electric using aluminum flyer plates driven by magnetic repulsion, a discussion of air cushion and release wave effects, and suggestions for further work in characterizing the ADL-10 materials.

3.4.1.2 Impact Testing Techniques

Plane stresses were generated at one face of the material specimens by high velocity impact of thin plastic flat-plate projectiles in air. These plates were accelerated by the explosions which accompanied high energy electrical discharges through thin aluminum foils (Ref. 17 and 18).

The basic circuit diagram of the exploding foil apparatus is shown in Figure 89. With a foil connected across the capacitor bank, the charging switch is closed, and the capacitor bank is charged to the desired voltage. Charging current is provided by a 20 kV power supply. The series circuit consisting of a 12 kJ capacitor bank, a spark gap, and the foil is completed by ionizing the air in the spark gap. Air ionization is initiated by applying a high voltage pulse to a pair of pointed electrodes located between the capacitor electrodes. The pulse is obtained from a high voltage trigger generator and coupled to the trigger electrodes through a step-up transformer.

Breakdown of the spark gap initiates discharge of the capacitor bank through the foil, and the resulting high amplitude current flowing through the foil causes the foil to explode. The foil is part of a carefully fabricated assembly. The details of foil assembly design and fabrication vary considerably and depend on the nature of the test, the impact velocity intended, and the diagnostic information desired.

A schematic of a typical foil assembly is shown in Figure 90. When the foil explodes, a pressure pulse is generated which is substantially plane. The pressure pulse causes a projectile plate to shear out of the Mylar sheet and accelerate with very little tilt. After a short free run (about 0.32 cm) the projectile plate impacts the test specimen. At this time the volume available to the foil vapor has increased to several hundred times the volume originally occupied by the foil, so the gaseous pressure pulse is reduced to a negligible value. Projectile plate velocities are varied by using different types of foil assemblies and by changing the voltage to which the capacitor bank is charged.

Plate impact tests were performed using 0.0356 cm thick Mylar as projectiles. The areal dimensions were 5.08 x 5.08 cm. Impact velocities were determined on separate tests performed under identical conditions. To measure projectile plate velocities, foil assemblies are fabricated which are identical to those used in shots on test specimens, except that the impact surfaces of the projectile plates are either aluminized or ruled with ink lines. The test specimen for a velocity calibration shot is a flat Plexiglas plate. Projectile plate velocities were measured with an image converter streak camera after the acceleration was complete, usually within two to three-tenths microsecond before impact.

The experimental geometry for projectile velocity measurements is shown in Figure 91. A grid on transparent photographic emulsion is glued to the impact side of the Plexiglas plate. The surface of the projectile plate is illuminated by backlight shining through the transparent grid, causing an image of the grid to be projected onto the mirrored surface of the projectile plate. In aligning the apparatus prior to firing a test shot, a projection lamp is used for backlighting and the image of the grid, reflected from the mirrored surface of the projectile plate, is focused on the streak camera slit and viewing screen. During the alignment procedure, magnification is adjusted to the desired value by positioning of the objective lens and streak camera. After alignment is completed, the projection lamp is replaced by an exploding foil backlight and a streak camera picture is taken with the projectile motionless in order to check the focus and magnification.

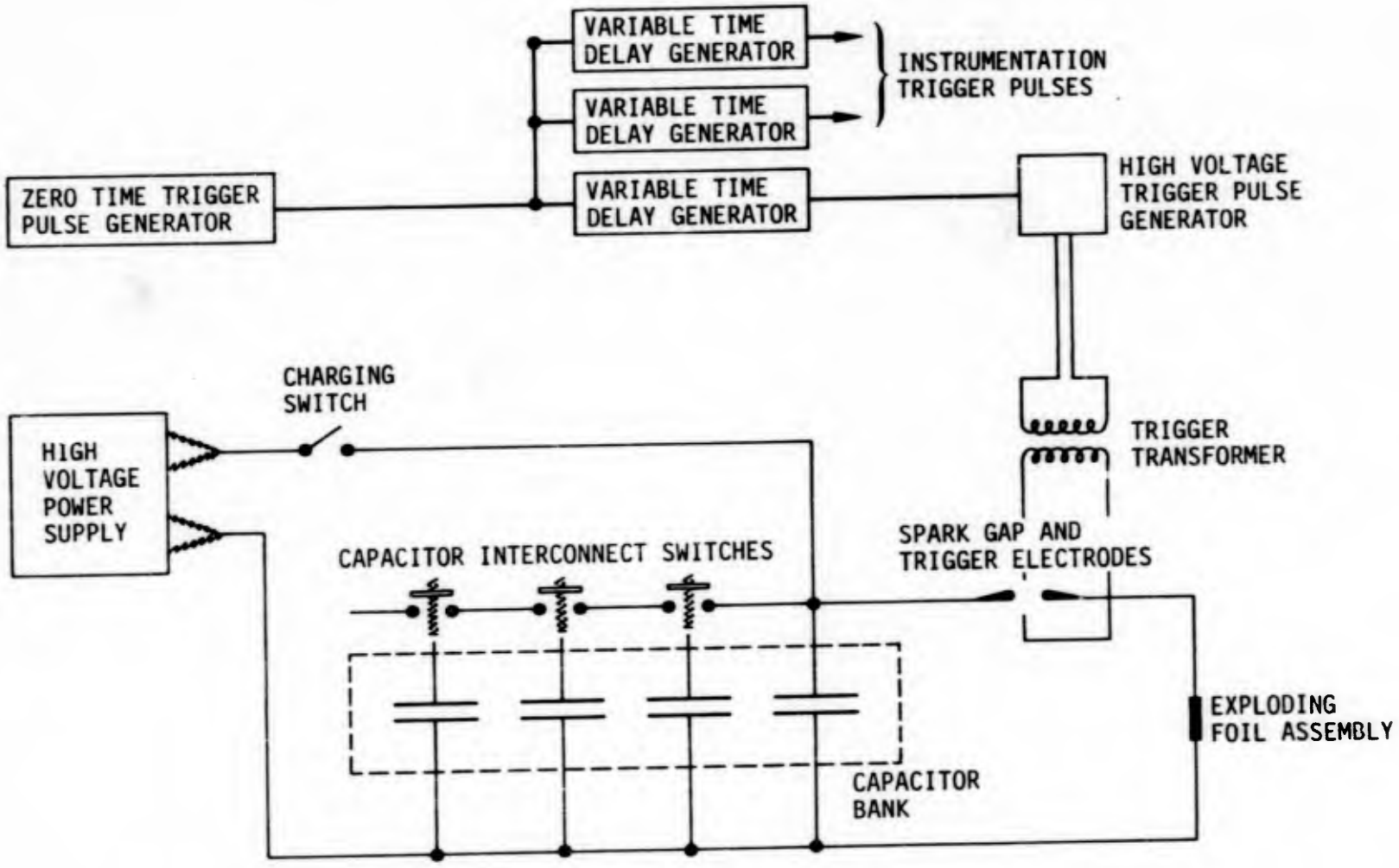

Figure 89. Circuit Diagram of Exploding Foil Apparatus

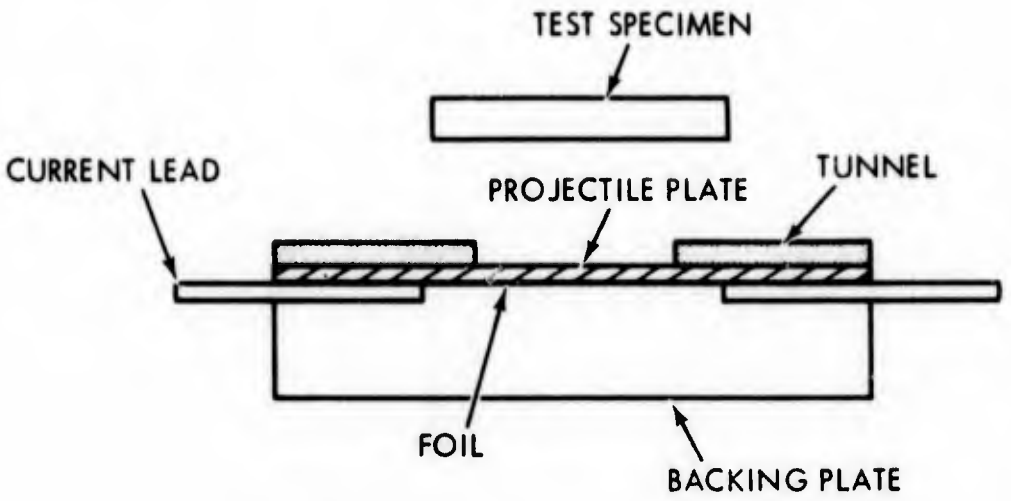

Figure 90. Typical Exploding Foil Assembly

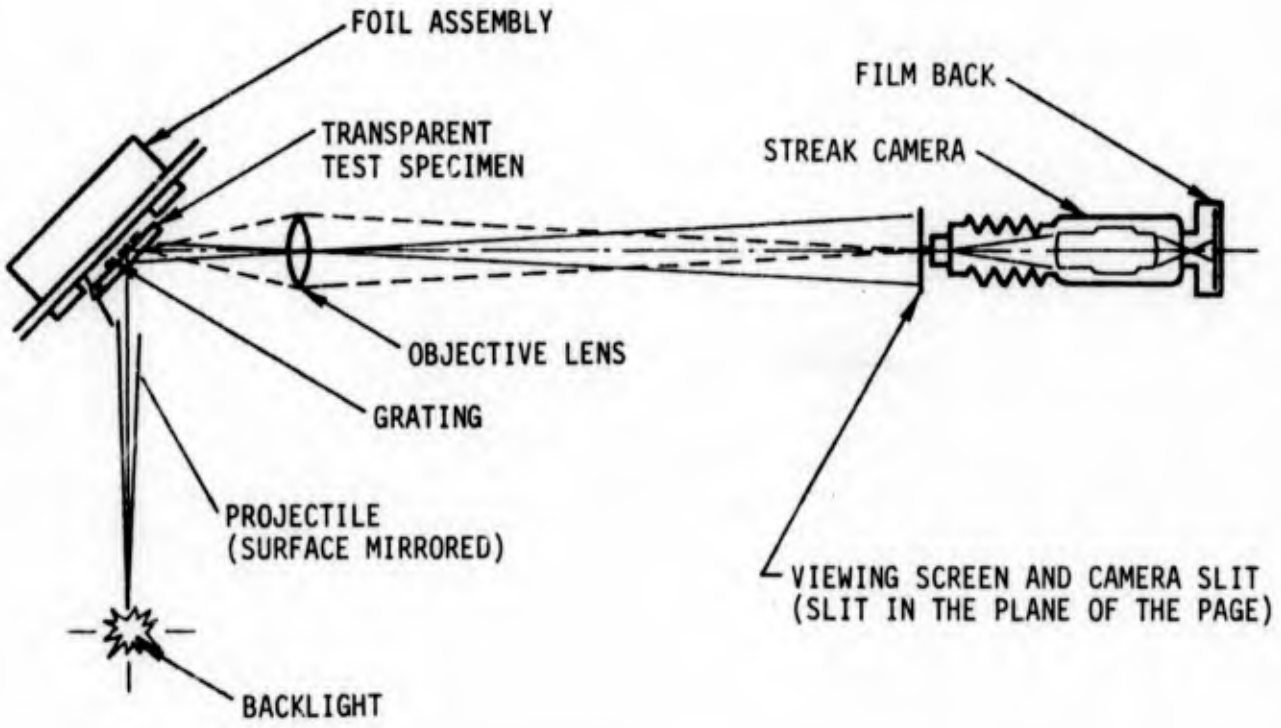

Figure 91. Experimental Geometry for Streak Camera Measurements of Projectile Velocity

After the optical alignment is satisfactory, the main capacitor bank and backlight capacitor bank are both charged. In firing a shot, trigger pulses are sent to both capacitor banks and the streak camera in a properly timed sequence. The timing sequence allows the backlight to come to maximum intensity just prior to the beginning of projectile motion. The camera is triggered and begins streaking at the same time.

When the projectile plate moves, the motion is projected onto the plane of the camera slit which views this component of the motion of an element of the projectile surface. The motion viewed by the camera slit is recorded on film where it appears as a displacement versus time history of the image of the grid. The projectile velocity is obtained by differentiation of the displacement versus time traces on the streak camera film record.

The technique described above gives a continuous measurement of projectile plate velocity and permits this measurement to be made in exactly the same manner as the free surface velocity measurements on test specimens. It is not possible, using this technique, to measure projectile velocity on the damage tests. However, calibration exercises are conducted frequently and spot checks are made during most series of tests. Velocities are found to be reproducible from shot to shot within 5 percent.

The quality of the data obtained from plate impact experiments can be impaired by nonsimultaneity of the projectile impact. Many experiments have been performed in order to assess the extent of nonsimultaneity which may occur under a wide variety of experimental conditions. The degree of nonsimultaneity may be expressed in terms of the elapsed time between the initiation and completion of contact over the entire flyer-target interface.

Simultaneity measurements are conducted in much the same manner as the velocity calibration measurements. In this case, however, the impact face of the Plexiglas target is mirrored, and the magnification in the streak camera optical system is reduced to permit viewing of the full width of the impact region. Initial projectile width is indicated by scribe lines in the mirrored surface which show up in the streak camera record. Projectile impact is indicated in the streak photograph by a sharp change in reflectivity of the mirror. The degree of nonsimultaneity can then be determined by measurement on the streak photograph of the elapsed time between initiation and completion of reflectivity change.

Nonsimultaneity may be present to varying degrees in any of several possible forms, depending upon the condition of the projectile plate at the time of impact. Three common causes of nonsimultaneity are nonparallelism of the projectile plate with respect to the plane surface of the target (tilt), gross bending of the projectile plate (bowing), and local variations in position-time history of the projectile (wrinkling). The harmful effects produced in each case vary considerably and depend upon the type of measurement

being made and the velocity of the projectile plate. Small deviations from simultaneity are not expected to be of great importance in damage tests since the component of particle velocity normal to the target free surface and other discontinuities will not be altered appreciably. However, the time from initial contact to complete contact between flyer and target should be no greater than the pulse width (back and forth wave transit time through the flyer). This is a reasonable maximum nonsimultaneity beyond which serious doubts arise as to the one-dimensionality of the experiment, and errors in measured damage threshold levels could be expected. This simultaneity criterion may be inadequate for shock and particle velocity measurements for equation-of-state and attenuation determinations.

3.4.1.3 Test Conditions and Shock Wave Considerations

Specimens from three plates of ADL-10 material were subjected to flyer plate impact testing. Densities and ultrasonic properties of the specimens were supplied by General Electric and are reproduced in Table 43. All specimens were 2 inches in diameter. The specimens were fixed to Plexiglas supports by a small quantity of epoxy applied to four points on the specimen circumference. The specimen boundary was, therefore, essentially free from lateral constraints. Lateral release waves are generated at the free boundaries of a material subjected to impulsive loading. These lateral release waves can interfere with the stress wave propagating in the material, resulting in nonrepresentative damage (Ref. 19). The specimens were made with fairly large diameter-to-thickness ratios in order to minimize effects of lateral release waves; however, no data is available for the ADL-10 materials with which to evaluate the effectiveness of the geometry.

Plate impact tests were performed using 2 inch x 2 inch x 0.014 inch Mylar flyers. Impact conditions for all tests are listed in Table 44. Flyer velocities were obtained from separate calibration tests and the flyer momentum (per unit area) was obtained from the expression

$$M = \rho_f h_f V \ , \qquad (1)$$

where $\rho_f = 1.39$ gm/cm^3 is the density of Mylar, $h_f = 0.0356$ cm is the flyer thickness and V is the impact velocity. For convenience, the momentum per unit area is expressed in kilotaps where 1 ktap = 10^3 gm/cm sec = 10^3 dyne sec/cm^2.

Impact stresses, pulse durations, and delivered impulses were calculated using the equation-of-state for Mylar (Ref. 20), the calibrated impact velocities and the acoustic impedances of the individual specimens. It must be emphasized that this procedure can lead to serious errors in the calculated values of impact stress and delivered impulse. Consideration of continuity requirements for stress and particle

TABLE 43. MATERIAL PROPERTIES

Specimen Identification	Specimen Thickness (cm)	Acoustic Velocity (cm/μ sec)	Density (gm/cm^3)	Acoustic Impedance (gm/cm$^2\mu$ sec)	Attenuation (dB/cm)	Comments
402-1	0.904	0.186	1.81	0.337	53	Velocity difficult to read accurately
402-2	0.904	0.256	1.88	0.481	13	
402-3	0.894	0.204	1.82	0.371	61	
402-4	0.899	0.219	1.90	0.416	23	
402-5	0.907	0.249	1.87	0.466	26	
403-1	1.067	0.224	1.59	0.356	50	
403-2	1.062	0.223	1.59	0.355	50	
403-3	1.059	0.143	1.55	0.222	57	Back face machined Velocity difficult to read accurately
403-4	1.054	0.220	1.58	0.348	57	
403-5	1.049	0.223	1.58	0.352	52	
404-1	0.785	0.227	1.62	0.368	55	Both faces machined
404-2	1.067	0.196	1.61	0.317	43	Front & rear faces pitted
404-4	0.785	0.205	1.65	0.338	48	Both faces machined

TABLE 44. 14-MIL MYLAR FLYER PLATE IMPACT TEST CONDITIONS

Test Number	Specimen Identification	Flyer Velocity (cm/μ sec)	Flyer Momentum (ktaps)	Impact Stress* (kbars)	Initial Pulse Duration* (μ sec)	Delivered Impulse* (ktaps)	Test Type
3529	403-1	0.082	4.05	15.4	0.232	3.58	Damage
3534	403-5	0.120	5.93	23.2	0.211	4.86	Damage
3554	403-2	0.145	7.17	28.7	0.199	5.70	Damage
3557	403-4	0.130	6.43	25.1	0.206	5.18	Damage
3559	403-3	0.145	7.17	21.0	0.216	4.55	Damage
3560	402-2	0.110	5.44	25.1	0.206	5.18	Damage
3561	402-1	0.145	7.17	27.8	0.201	5.57	Damage
3579	402-3	0.145	7.17	29.5	0.197	5.82	Stress Measurement
3608	402-5	0.145	7.17	33.8	0.189	6.39	Stress Measurement
3623	404-1	0.110	5.44	21.6	0.215	4.64	Damage
3627	404-2	0.130	6.43	23.7	0.210	4.96	Damage
3638	404-4	0.082	4.05	13.5	0.239	3.20	Damage

*Calculated values based on the material acoustic impedance

velocities at the impact interface are used to define the impact equations. Continuity of stress requires that

$$\rho_{of} U_{sf} \Delta U_{pf} = \rho_{om} U_{sm} \Delta U_{pm} \quad , \tag{2}$$

where U_s and U_p are the shock and particle velocities, respectively, and the subscripts f and m refer to the flyer and specimen material, respectively. The initial particle velocity in the flyer plate is the impact velocity V. The initial particle velocity in the specimen is zero. Upon impact, the particle velocity in the flyer is reduced to $U_p = U_{pm}$, the particle velocity in the specimen. Therefore, $\Delta U_{pf} = V - U_p$, $\Delta U_{pm} = U_p$ and

$$\rho_{of} U_{sf} (V - U_p) = \rho_{om} U_{sm} U_p \quad . \tag{3}$$

Since stress is equal to the product of impedance and particle velocity, the stress in the specimen is given by

$$\sigma = Z U_p \quad , \tag{4}$$

where $Z = \rho_{om} U_{sm}$ in the impedance of the specimen. This is the impact equation which was solved to obtain the impact stress given in Table 44.

For most materials, a linear relationship is known to exist between shock velocity and particle velocity, i.e.:

$$U_s = C_o + S U_p \tag{5}$$

where S is a dimensionless constant and C_o is the intercept of the U_s versus U_p curve at zero particle velocity. In the acoustic approximation, U_s is assumed to be equal to the zero pressure sound speed, so that

$$\sigma = Z_o U_p \text{ (acoustic approximation)} \tag{6}$$

where Z_o is the acoustic impedance (equal to the product of initial density and longitudinal sound speed). Thus, errors in calculated stresses listed in Table 44 can be attributed to the variation of shock velocity with particle velocity. Most materials for which the U_s versus U_p relationship is known, exhibit slopes in the range $o \leq S \leq 2$.

The magnitudes of the probable errors due to ignoring the variation in shock velocity can be investigated by generating a family of stress versus impact velocity curves

based on nominal values of density and sound speed, using S as a parameter. To generate the family of curves, shock velocities in the flyer and specimen are expressed in the form of Equation 5 and substituted for U_{sf} and U_{sm} in Equation 3. Equation 3 may then be written in the form

$$AU_p^2 + BU_p + C = 0 \tag{7}$$

where A, B and C are functions only of S and V for a given specimen material. The solution of this equation gives

$$U_p = U_p\ (S, V) \tag{8}$$

where the dependence on S is shown explicitly for use in the parameter study. Stress can then be calculated using Equation 4 which may be expressed in the form

$$\sigma = \sigma\ (S, V)\ . \tag{9}$$

Stress versus impact velocity curves for a typical ADL-10 specimen (ρ_o = 1.60 gm/cm^3, C_o = 0.22 cm/μsec) are shown in Figure 92 for several values of S in the range $o \leq S \leq 2$ and for $o \leq V$ 0.2 cm/μsec. Clearly, the calculated stresses can deviate significantly from the linear (S = o) case for stresses greater than a few kilobars, and rather large uncertainties must be assigned to the higher calculated impact stresses.

The uncertainties in impact stress also give rise to uncertainties in the calculated values of delivered impulse. Impulse is defined as

$$I = \int \sigma\, dt\ . \tag{10}$$

where t is time. For stress pulses generated by impact of a low impedance flyer plate the stress is constant for the duration of the pulse, τ, and the impulse may be written

$$I = \sigma\tau\ . \tag{11}$$

Thus, impulse is directly dependent upon stress and any error in the stress calculation will also show up in the impulse calculation. There is, however, an additional indirect dependence of the pulse width on the impact conditions which tends to reduce the error in calculated impulse.

Upon impact, a stress wave is generated in the flyer plate which propagates into the flyer material until it arrives at the rear surface of the flyer in a time

$$t_1 = h_f/U_{sf} \tag{12}$$

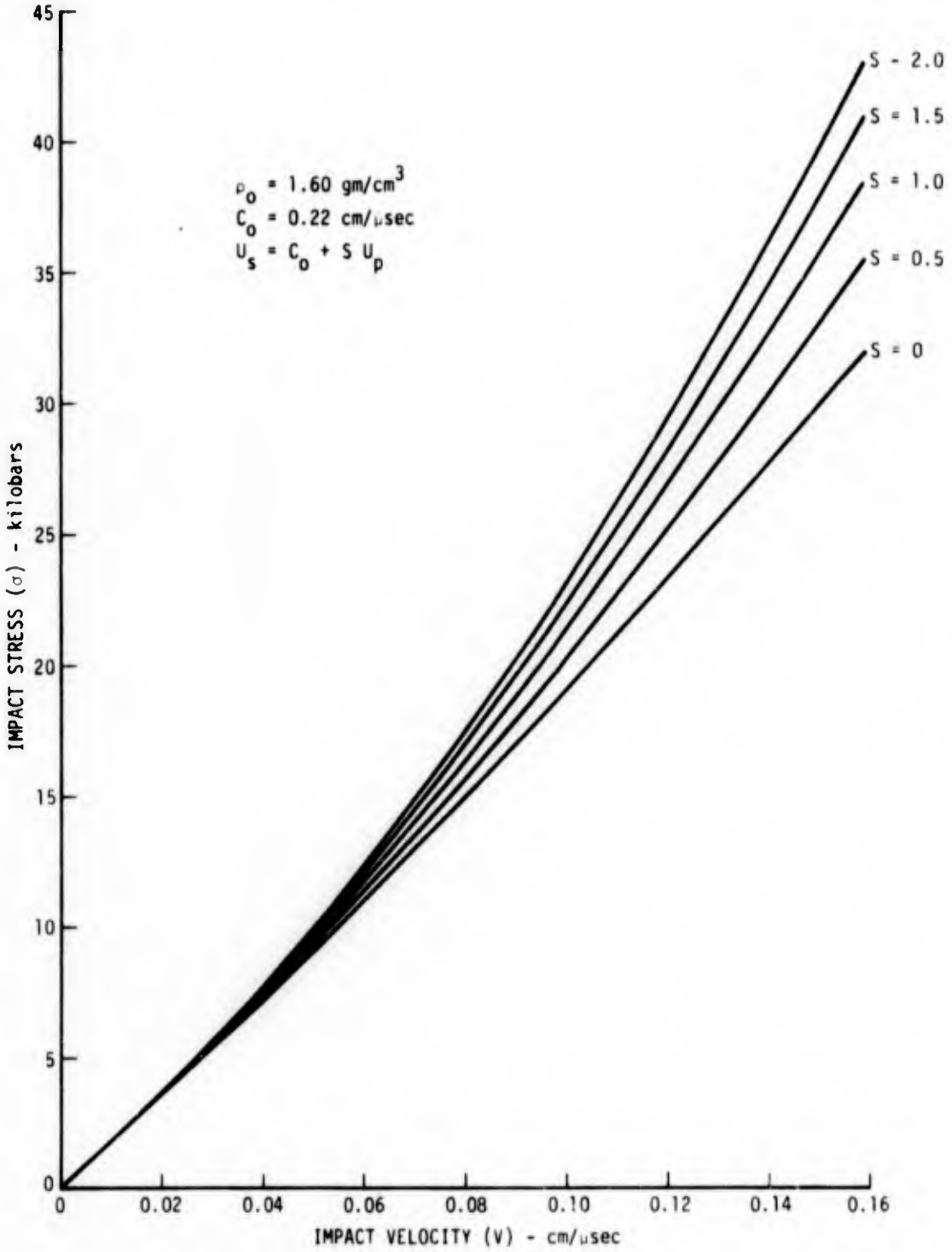

Figure 92. Impact Stress Versus Flyer Plate Impact Velocity for a Typical ADL-10 Material, Using Various Values for the Slope of the U_s Versus U_p Curve

where h_f is the thickness of the flyer. A release wave is then generated at the rear surface which propagates back through the compressed material toward the impact surface as a zero-stress condition. This release wave travels at a rate approximately equal to the shock speed in the material. However, the material is in the compressed state during this time, so the distance through which the release wave travels is reduced to

$$h'_f = \frac{\rho_{of}}{\rho_f} \quad h_f \tag{13}$$

where ρ_f is the material density in the compressed region. Conservation of mass requires that

$$\rho_{of} U_{sf} = \rho_f (U_{sf} - \Delta U_{pf}) \tag{14}$$

(where $\Delta U_{pf} = V - U_p$) so that

$$\frac{\rho_{of}}{\rho_f} = 1 - \frac{\Delta U_{pf}}{U_{sf}} \tag{15}$$

and

$$h'_f = \left(1 - \frac{\Delta U_{pf}}{U_{sf}}\right) h_f \quad . \tag{16}$$

The time required for the release wave to traverse the compressed flyer is, therefore

$$t_2 = \left(1 - \frac{\Delta U_{pf}}{U_{sf}}\right) \frac{h_f}{U_{sf}} \tag{17}$$

and the total pulse duration, $t_1 + t_2$ is equal to

$$\tau = \left(2 - \frac{\Delta U_{pf}}{U_{sf}}\right) \frac{h_f}{U_{sf}} \quad . \tag{18}$$

The particle velocity in the flyer increases with stress; therefore, τ will decrease with stress. The net effect is that impulse (the product of stress and pulse width) will vary less rapidly than stress with variations in impact velocity.

Since ΔU_{pf} and U_{sf} are functions only of V and U_p for a given flyer material, and U_p is a function of S and V, Equation 18 can be written in the form

$$\tau = \tau (S, V). \tag{19}$$

Combining Equation 19 with Equation 9, the expression for impulse (Equation 11) can be cast in the form

$$I = I(S, V) . \tag{20}$$

A family of I versus V curves is shown in Figure 93 for values $o \leq S \leq 2$ and $o \leq V \leq 0.2$ cm/μ sec. Although the fractional error in calculated values of impulse introduced by ignoring the variation of shock velocity with particle velocity is less than the corresponding error in calculated stress, it can be significant above 2 ktap.

The results of these two parameter studies point out the need for equation-of-state data for the ADL-10 materials. While the acoustic approximation simplifies the stress and impulse calculation and provides a quick method for evaluating materials in screening tests, the actual calculated values may be in error by 30 percent or more.

3.4.1.4 Test Results

A series of ten tests was performed to determine the damage resistance of as-molded and machined ADL-10. The results of these tests are given in Table 45. The primary mode of failure was found to be removal of material at the impact surface (front face spall). Thickness measurements were made before and after impact. A net increase in thickness was recorded for all impact levels below the threshold for front face spall. In Figure 94, thickness increase is plotted versus delivered impulse divided by initial thickness. Normalization to the initial thickness was selected as a means of minimizing scatter due to different amounts of stress wave attenuation in specimens of widely different initial thickness. The figure indicates a high probability of a large thickness increase above 5 ktap. Growth in thickness appeared to be largest for the 404 type specimens which had both surfaces machined. The as-molded 404 specimen also exhibited a large thickness increase. The thickness increase for the 402 material was moderate at fairly high impulse levels. The as-molded 403 type material exhibited a relatively slow rate of thickness increase with impulse up to fairly high levels, but failed catastrophically at 5.7 ktap. The rear surface of specimen 403-3 was machined, and this specimen showed a moderately large increase in thickness at an intermediate impulse level.

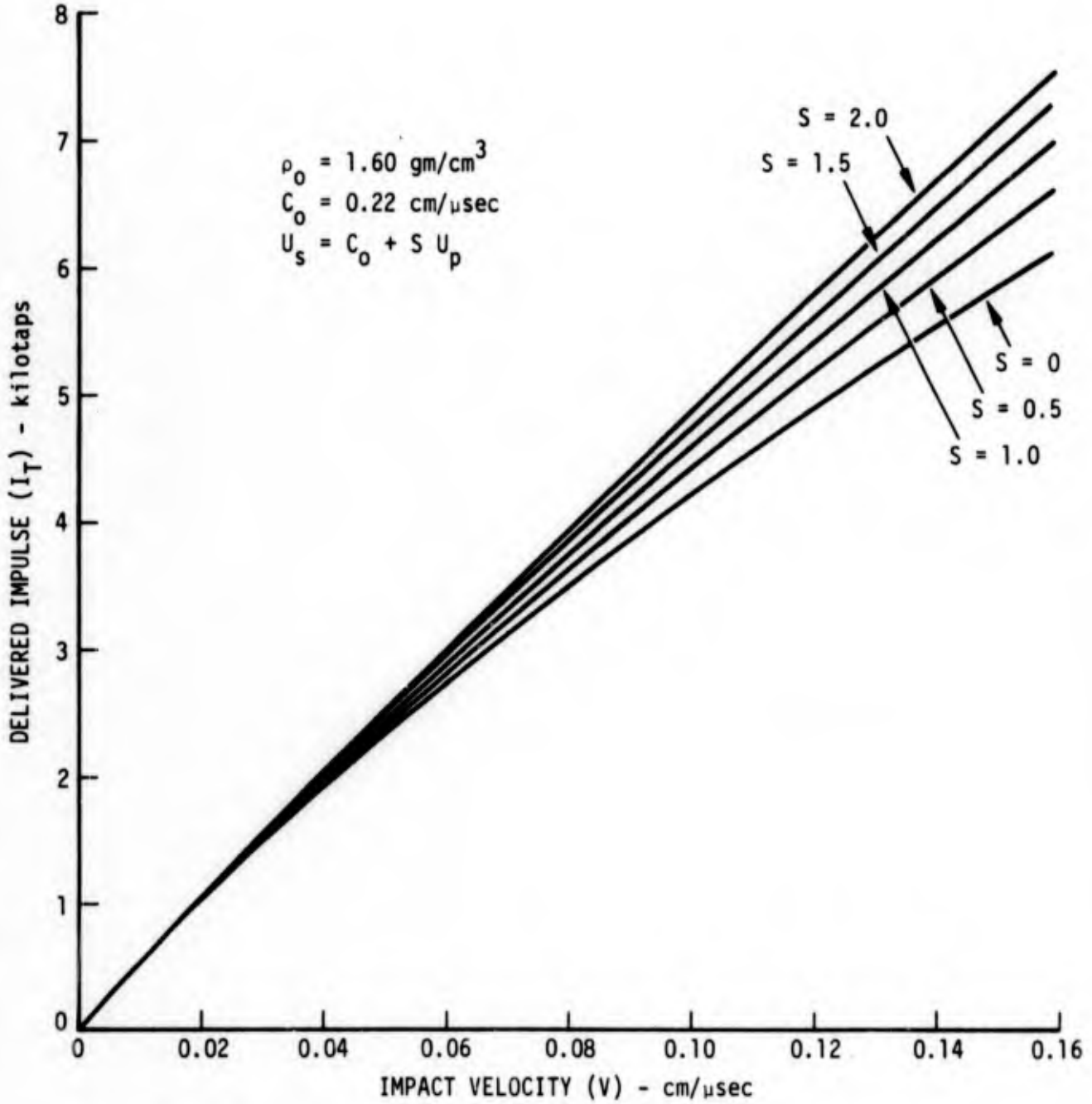

Figure 93. Delivered Impulse Versus Flyer Plate Impact Velocity for a Typical ADL-10 Material, Using Various Values for the Slope of the U_s Versus U_p Curve

TABLE 45. DAMAGE TEST RESULTS

Test Number	Specimen ID	Delivered Impulse † (ktaps)	Specimen Thickness		Thickness Increase (cm)	Comments
			Pre-Test (cm)	Post Test (cm)		
3561	402-1	5.57	0.904	0.945	0.041	Roughening of front face, slight roughening of back face.
3560	402-2	5.18	0.904	0.928	0.024	Very slight front face crushing, roughening of back face.
3554	403-2	5.70	1.062	—	SPALL	Severe front face crushing. Matrix material removed to a depth of ~ 0.8 cm, fibers removed to a depth of ~ 0.4 cm from front face.
3557	403-4	5.18	1.054	1.066	0.012	Slight front face crushing, slight back face spall.
3534	403-5	4.86	1.049	1.059	0.010	Slight front face crushing.
3559	403-3*	4.55	0.907	0.958	0.051	Gross lateral fracture. Slight roughening of front and rear faces.
3529	403-1	3.58	1.067	1.071	0.004	No visible damage.
3627	404-2	4.96	1.067	1.207	0.140	Partial spall of front face. No apparent back face damage.
3623	404-1**	4.64	0.785	—	SPALL	Severe front face crushing. Matrix almost completely crushed, fibers removed to a depth of ~ 0.2 cm from front face.
3638	404-4**	3.20	0.785	0.841	0.056	Matrix spall at rear face, slight matrix spall at front face.

† Calculated values based on the material acoustic impedance.

* Back face machined.

** Both faces machined.

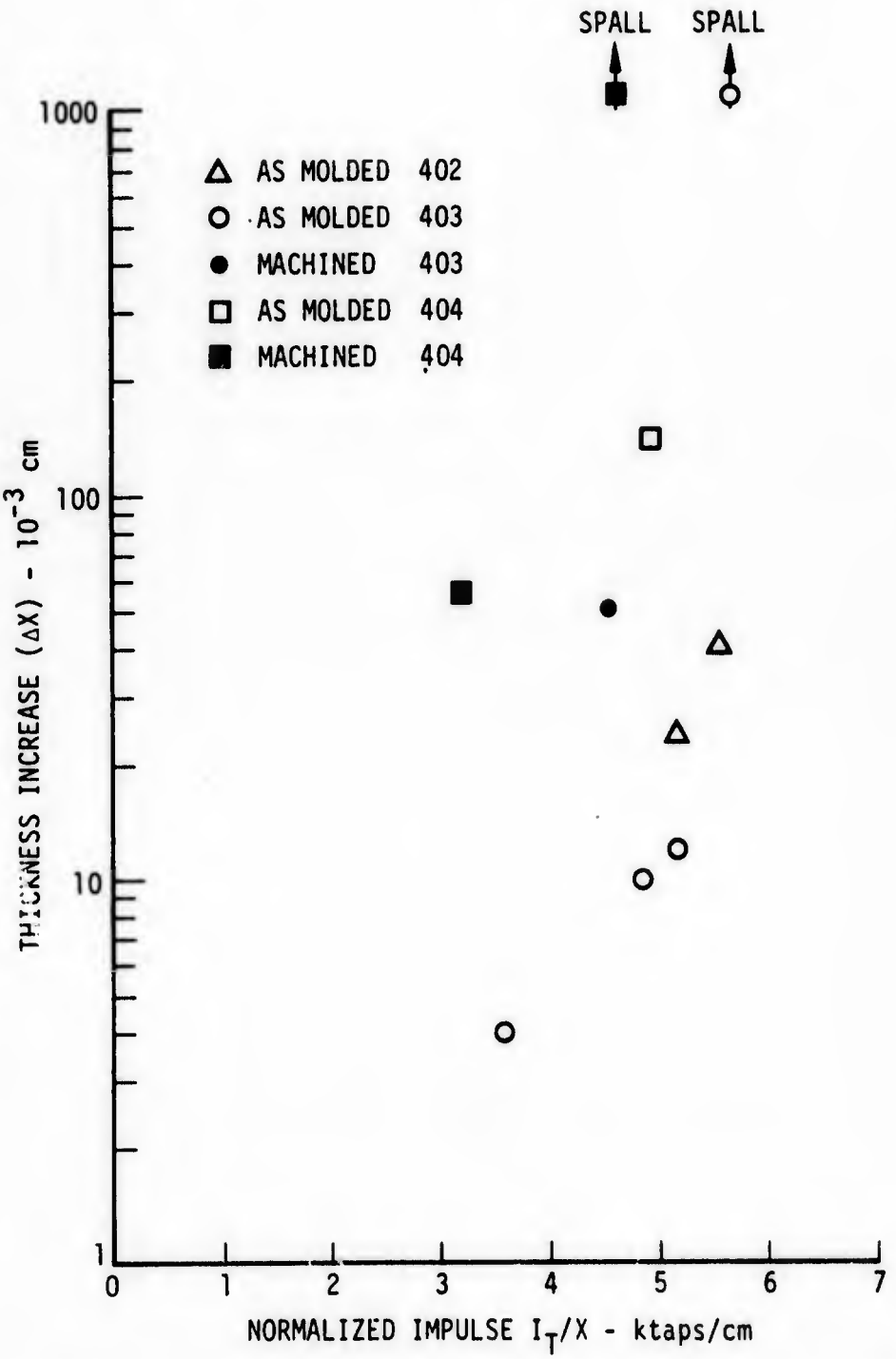

Figure 94. Increase in Thickness of Impacted ADL-10 Materials Versus Normalized Impulse Delivered to the Specimen

These results indicate that the catastrophic failure threshold levels I_{TH} for the materials are:

as-molded 402: $I_{TH} > 5.57$ ktap

as molded 403: $5.18 \text{ ktap} < I_{TH} \leq 5.70$ ktap

machined 403: $I_{TH} > 4.55$ ktap

as-molded 404: $I_{TH} > 4.96$ ktap

machined 404: $3.20 \text{ ktap} < I_{TH} \leq 4.64$ ktap .

However, these results are based on a very limited number of tests and should not be considered strictly valid unless they are confirmed by more extensive testing.

Two tests were performed in which material specimens were impacted at impulse levels near threshold, and the rear surface stress was measured with an in-material carbon piezoresistive gage (Ref. 21 and 22). In both tests, 402 type specimens were used, and another 402 specimen with similar impedance was used as a back-up piece to confine the gage and extend the reading time. The results of these two tests are listed in Table 46. Oscilloscope traces obtained on the two tests are reproduced in Figure 95. The measured peak stress transmitted through the first specimen was 3.09 kbar. The stress-time plot obtained by reduction of the carbon gage oscilloscope trace from this test is shown in Figure 96. The back-up piece was recovered and examined. No damage was observed and, considering the level of the transmitted stress, no appreciable alteration in impedance was anticipated. Therefore, the same back-up piece was used on the second stress measurement test. A large electrical noise signal was observed on the second test, which greatly reduced the reading accuracy. The recorded peak stress was 4.5 kbar with a probable error of 0.7 kbar.

TABLE 46. MEASUREMENT OF TRANSMITTED STRESS FOR THE DAMAGE THRESHOLD CONDITION IN ADL-10

Test Number	Specimen ID	Specimen Thickness (cm)	Impact Stress* (kbars)	Transmitted Stress** (kbars)	Specimen Thickness After Impact (cm)	Comments
3579	402-3	0.894	29.5	3.09 ± 0.15	0.872	Large electrical noise signal
3608	402-5	0.907	33.8	4.5 ± 0.7	0.897	

*Calculated values based on the material acoustic impedance

**Specimen No. 402-4 was used as a back-up block for Test No. 3579, recovered and used again on Shot No. 3608.

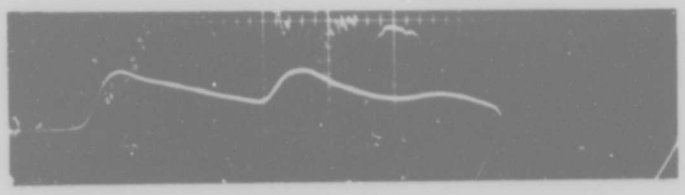

TEST NO. 3579 VERTICAL SCALE: 10 V/div
SPECIMEN 402-3 HORIZONTAL SCALE: 0.5 μsec/div

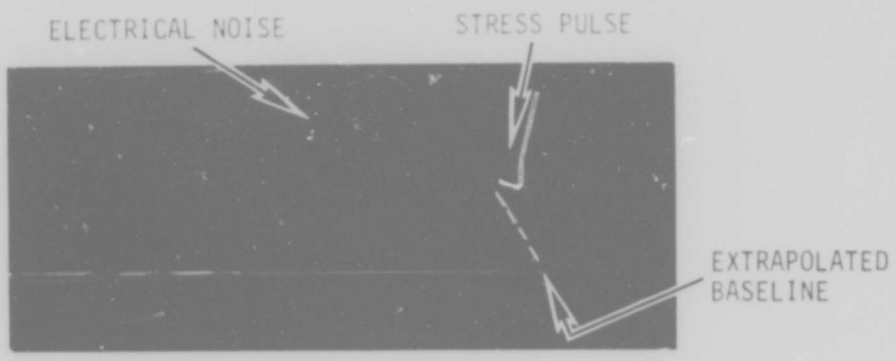

TEST NO. 3608 VERTICAL SCALE: 20 V/div
SPECIMEN 402-5 HORIZONTAL SCALE: 2 μsec/div

Figure 95. Oscilloscope Traces Obtained from Plate Impact Tests on ADL-10 Materials Using Carbon Stress Gages.

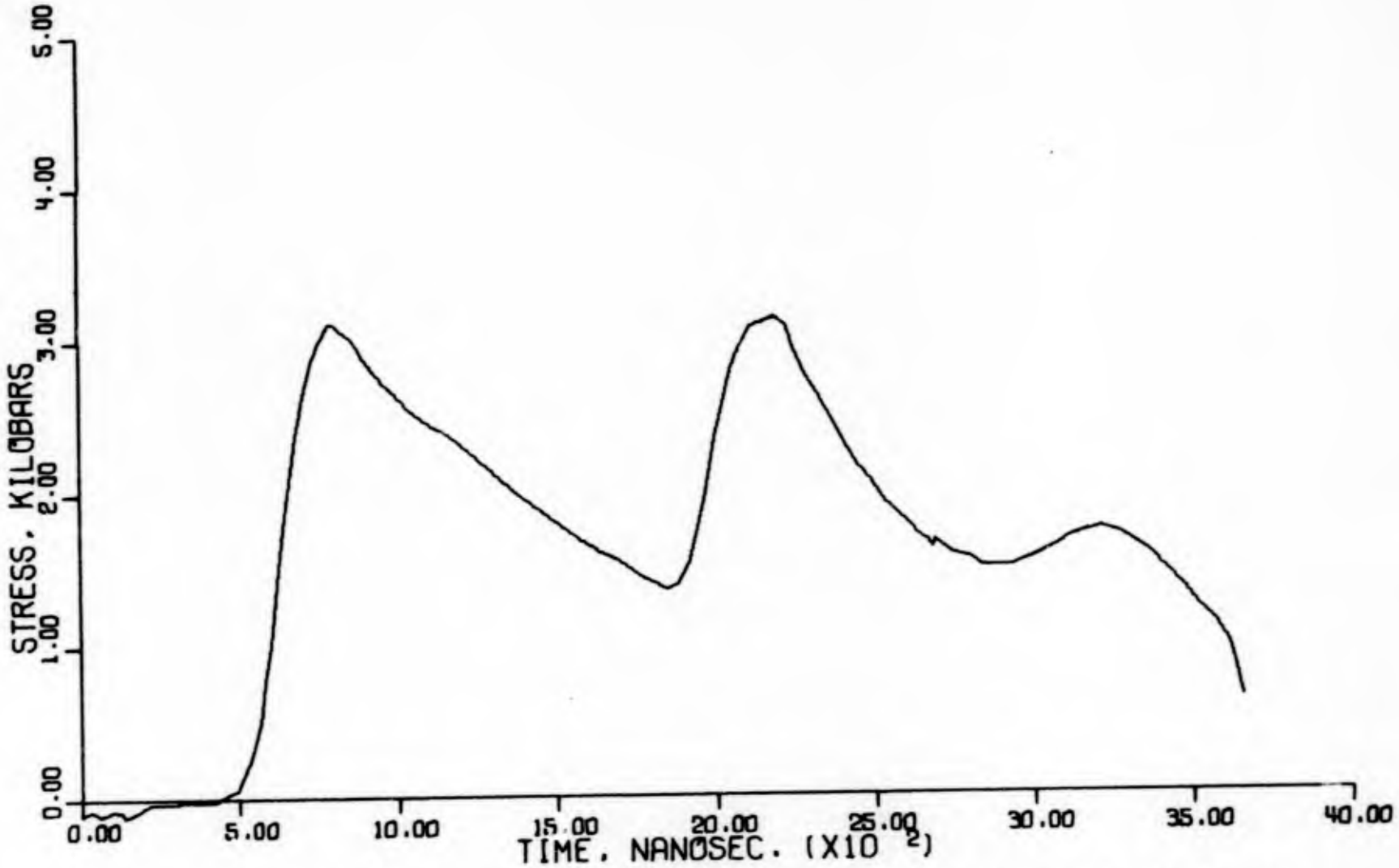

Figure 96. Stress versus Time at the Rear Surface of ADL-10 Impacted with a 14 mil Mylar Flyer Plate at 0.145 cm/μsec.

Impact stresses for the two tests were calculated, as discussed in Paragraph 3.4.1.3. Comparison of the transmitted stresses with impact stresses indicates a slightly larger amount of attenuation for specimen 402-3 than for 402-5; however, the transmitted stresses were on the order of 10 percent of the calculated impact stresses for both tests.

Specimen thicknesses were measured before and after testing, and the values obtained are included in Table 46. Net thickness decreases of 0.022 cm and 0.010 cm were observed due to compression of the material upon impact. The presence of the back-up block prevented propagation of the tensile wave back into the material; therefore, increase in thickness (as found in the damage tests) was prevented.

3.4.1.5 Discussion

Previous plate impact testing of ADL-10 materials was performed at General Electric Company (Ref. 2) using a magnetically accelerated aluminum flyer. Strikingly different failure modes are reported for the magnetic flyer tests as compared to the exploding foil tests discussed in this report. The damage observed on the magnetic flyer tests was primarily back-face delamination or spall; the damage observed on the exploding foil tests was primarily in the form of material removal at the front face.

Several fundamental differences between the two test methods are noted which complicate the attempt to compare the test results. The impedance of aluminum is considerably larger than the impedance of the ADL-10 materials, whereas the impedance of Mylar is slightly less than the impedance of the specimens. As a result, the impulsive load delivered by an aluminum flyer plate is characterized by a flat-topped stress pulse followed by a gradual decay to zero stress. By contrast, the Mylar impact is an essentially rectangular pulse. These differences are illustrated in the graphs of Figure 97, which were obtained using the SWAP-9 computer code to solve for the impact of a 12-mil aluminum flyer travelling at a velocity of 0.140 cm/μsec, and a 14-mil Mylar flyer travelling at 0.120 cm/μsec. The impedance of the target specimen was taken to be 0.35 gm/cm^2 μsec in both cases.

These impact conditions were selected for the calculation because the aluminum impact case is representative of an actual magnetic flyer plate test for which the reported impulse was approximately 4 ktap and the Mylar impact case is representative of an actual exploding foil flyer plate test which produced an impulse in the same range. Comparison of the two graphs shows that the peak stress in the aluminum flyer case is approximately twice the peak stress obtained with the Mylar flyer, and the duration of the peak is approximately half the duration of the pulse obtained in the Mylar impact. The long tail on the aluminum stress-time curve is attributed to ring-down of the stress in the flyer. It is possible that the higher impact stresses in the aluminum impact produce a larger amount of rear-face damage, compared to the damage produced by the lower stresses in the Mylar impact while the long compressive tail tends to surpress tensile wave damage at the front face.

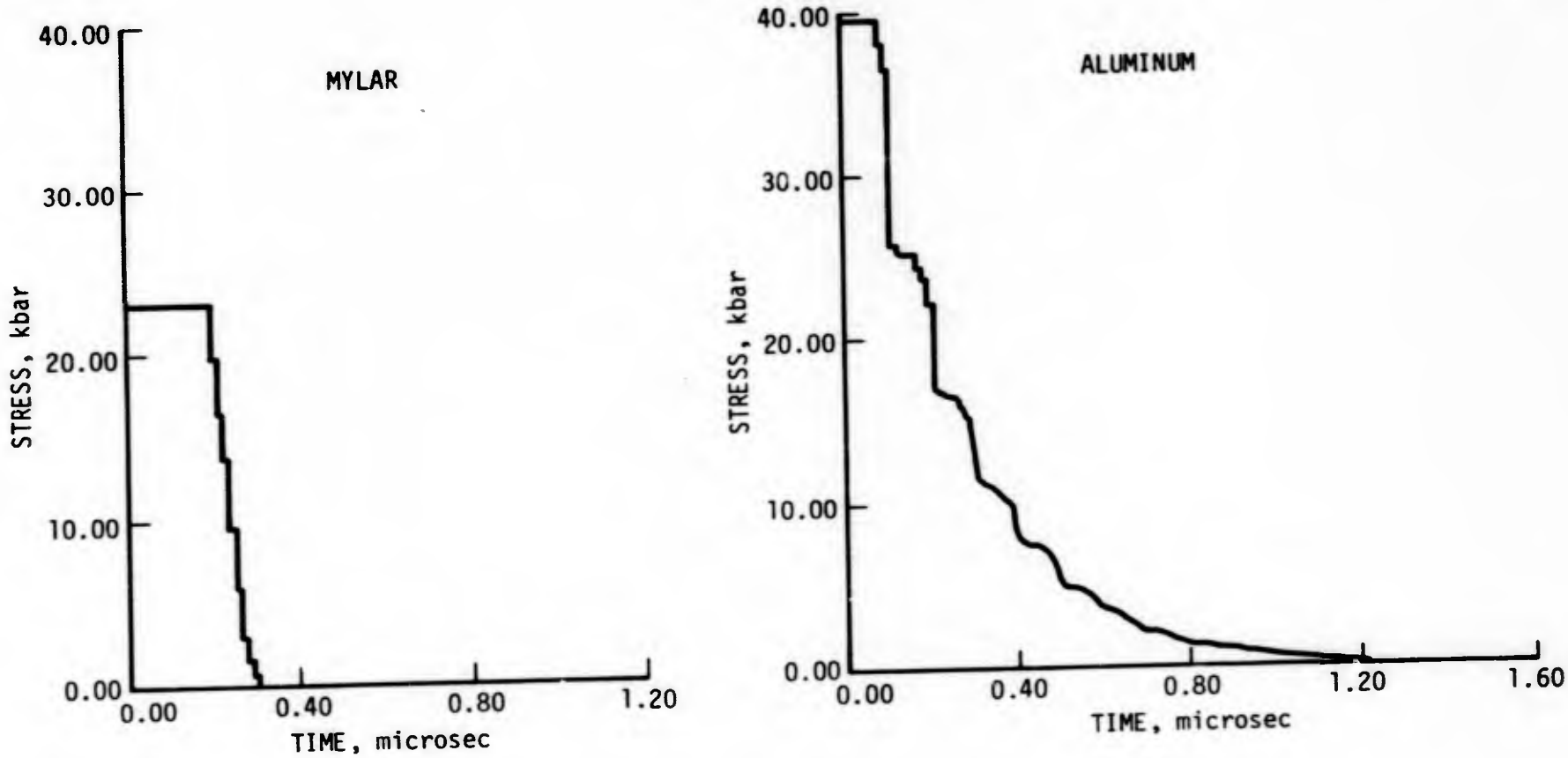

Figure 97. Stress-Time Computer Plots for Mylar and Aluminum Impacting Typical ADL-10 Materials

Further confusion arises in any attempt to compare the results solely on the basis of delivered impulse. The impulse delivered to the test specimen is equal to the area under the stress-time curve (c. f. Equation 10). In the case of the Mylar impact, this is closely approximated by the product of amplitude and duration of the peak stress. Although the same product is commonly used to define the delivered impulse in magnetic flyer tests, it clearly represents only the initial (or prompt) impulse delivered to the ADL-10 materials. In fact, the integral under the total stress-time curve is equal to the total flyer momentum (11.4 ktap) for the magnetic flyer case. Analysis of the aluminum impact case illustrated in Figure 97 shows that less than 40 percent of the impulse is contained in the prompt portion of the curve.

In addition to the late-time impulse due to the high impedance of the aluminum flyer relative to the impedance of the specimen material, the delivered impulse can continue to increase after impact due to continued repulsion of the flyer by the magnetic field.

Two potential sources of error in interpretation of the test results are common to the two test methods: air cushion effects and the effects of lateral release waves. When plate impact tests are performed under ambient conditions, the air between the flyer plate and specimen will be compressed as the flyer plate approaches the specimen. This will result in the generation of low-amplitude precursor waves propagating into the flyer plate and the specimen. The precursor wave traveling into the flyer can cause an appreciable slowing of the flyer before impact; the precursor wave traveling in the specimen can cause a reduction in the peak stress and, thereby, an alteration in the material response.

Lateral release waves caused by expansion of the free boundaries of the test specimen can result in damage characteristics which are not truly representative of the material damage response (Ref. 19). The effects of lateral release can be minimized by placing thick, high impedance blocks in contact with the lateral boundaries. This procedure can be used to essentially eliminate lateral strain at the specimen boundaries. Although lateral stresses may still be present near the edges, these are normally much less effective in altering the normal response of the material.

The purpose of this discussion has been to point out that a considerable amount of work remains before the results of the damage tests performed to date can be completely understood. The reasons for the difference in failure modes observed in magnetic flyer and exploding foil plate impact tests has not been resolved, and the magnitude of the effects of the air cushion and lateral release at the specimen boundaries are not known. In addition, as pointed out in Paragraph 3.4.1.3, accurate calculations of stress and impulse depend upon the generation of equation-of-state data for the materials.

3.4.2 MAGNETIC FLYER SHOCK TESTING ON INORGANIC HARDENED ANTENNA WINDOW MATERIALS

3.4.2.1 Facility, Description and Improvements

Four aluminum foil magnetic flyer plate tests were conducted at GE-RESD on candidate inorganic hardened antenna window materials. The facility consists of a 50 kilojoule, 50 kilovolt, low inductance, low resistance capacitor bank switch system that is used primarily for impulse testing of planar and curved targets using metallic flyers. Figure 98 shows the bank and flyer head, as recently installed with provision for capability enlargement. Figure 99 shows the associated capacitor charging equipment and oscilloscope and recording equipment for data reduction. The capacitor bank consists of twenty Maxwell capacitors (each with a nominal capacitance of 1.6 microfarad) coupled in parallel to a planar strip transmission line. The total stored energy is equivalent to 4000 taps on the nominal 2 inch x 2 inch samples tested for this program.

In the magnetic flyer technique for shock loading materials, the stored energy of the capacitor bank is rapidly discharged into a single turn loop consisting of two series connected halves. As illustrated in this schematic Figure 100, one-half of the loop consists of a massive load block of a fixed geometry. The second half is the flyer plate itself which was formed from an aluminum sheet 12 mils thick and shaped to the configuration of the first half loop. The thickness of the flyer controls the time duration and shape of the shock pressure pulse produced in the target material by impact of the flyer. The flyer is insulated from the load block by a thin layer of Mylar and the target material is placed a few millimeters from the flyer. The discharge of the capacitor bank into this single loop produces equal but opposite kiloampere currents flowing in close proximity to each other. The second half of the loop is then magnetically accelerated in microseconds to a relatively constant supersonic velocity (0.6 mm/μsec). Under these conditions, the impact of the flyer upon the target results in a rapid deposition of a large amount of momentum and energy within a thin surface layer of the target material (see Figure 101). Since this deposition occurs in a time which is short compared to a thermal conduction time, the material seeks to relieve itself of these local high densities through the formation and propagation of a shock wave. If the intensity of the shock wave is great enough, the material will spall and delaminate at the rear surface. As reported earlier, (Ref. 2) the 4000 tap capability of this facility was not sufficient to cause any appreciable damage to the target ADL-10 material tested during the previous program and the flyer impact measurements of this program on ADL-10 to determine its failure threshold were performed by the exploding foil plate impact method under subcontract at Effects Technology, Inc. A comparison of the differing impact failure mechanisms associated with the two test techniques has been given above in Paragraph 3.4.1.5.

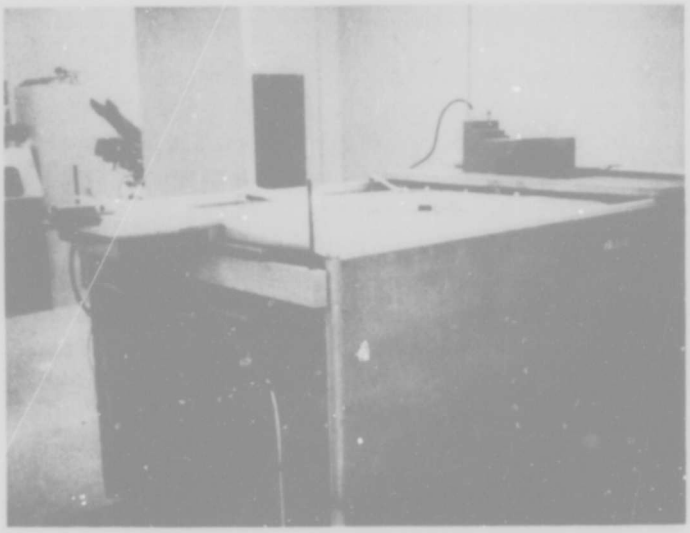

Figure 98. Enlarged Magnetic Flyer Facility, Flyer Head at Left. Note Instrumentation Outside Door.

Figure 99. Capacitor Charging, Oscilloscope and Recording Equipment for Data Reduction of Magnetic Flyer Tests.

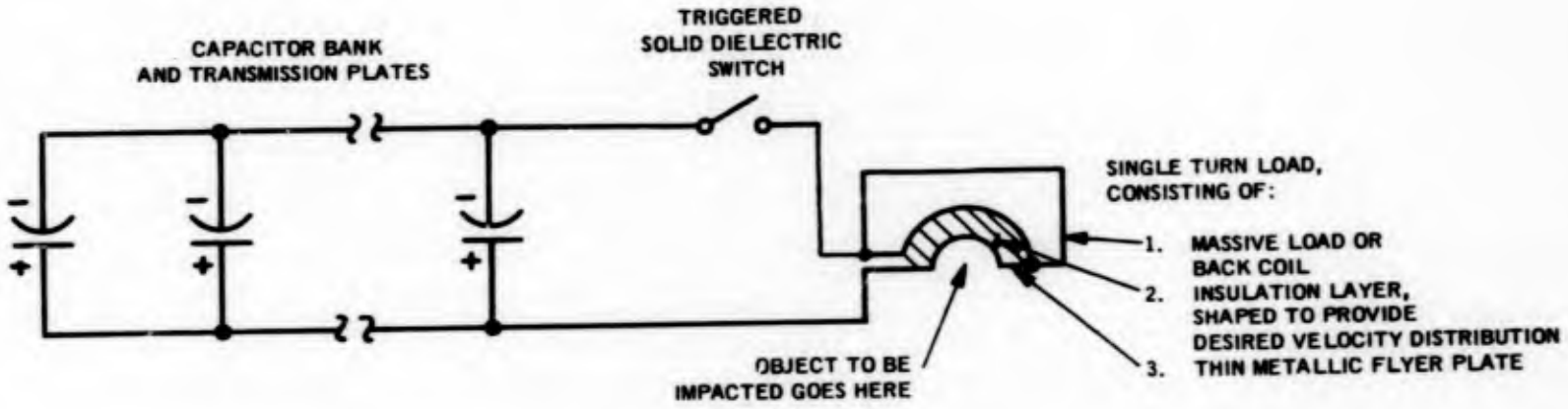

Figure 100. Schematic of Magnetically-Driven Flyer Plate System

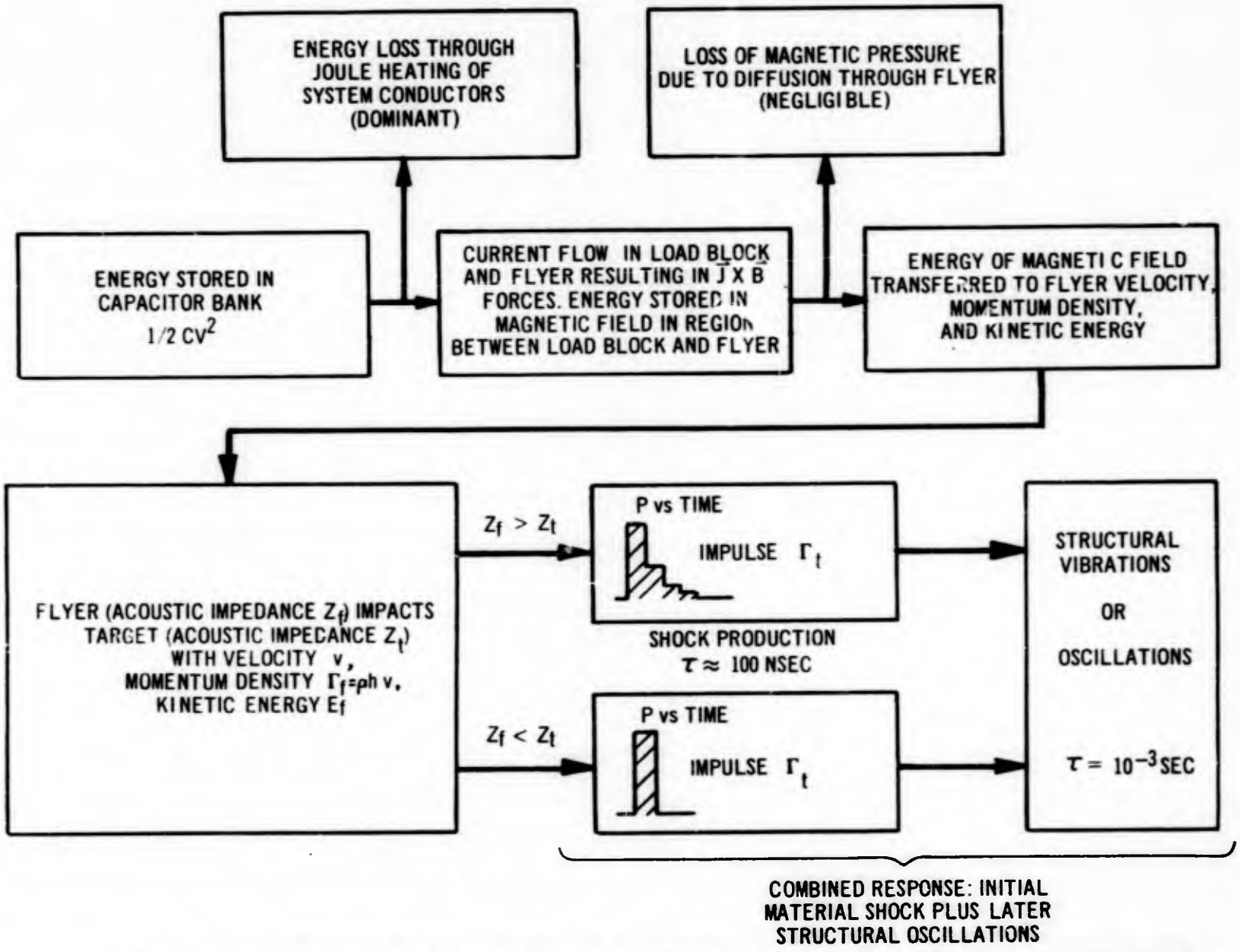

Figure 101. Physical Processes Involved in Magnetic Flyer Combined Response Impulse Testing

Concurrent with the current effort but independent of the program, the capacitor bank was re-designed such that twice the energy or about 7500 taps can be accomodated. The configuration of the bank was changed to accomodate twenty additional capacitors while at the same time protecting the electrical characteristics required for the fast response and higher current levels. The last remaining task is the procurement and physical installation of the twenty additional diagnostic tool in determining the failure threshold levels of the target materials at impact levels above the present 4000 taps limit.

3.4.2.2 Test Results

Four samples, two each of the Ludox colloidal silica and BNQ materials were tested by magnetic flyer aluminum plate impact at GE-RESD. Two tensile bar specimens of BNQ-V were impacted, the first at 2000 taps and the second at 4000 when no apparently serious damage was inflicted. The two specimens are shown in Figure 102 after test. The test data are given in Table 47.

Two 1-1/2 inch square samples of Type ASDI Ludox Colloidal Silica/Astroquartz 4-D Omniweave were impacted at 2000 and 3000 taps. This material was machined on both faces down to 0.40-inch thickness before test, as were the similar flexure bars prepared from plate 404-2 (detailed plate layout given in Fig. 61). The data in Table 47 show that no visible damage occurred with only slight increases in ultrasonic attenuation.

The immediate indication is for flyer plate testing at higher impulse levels for both this same 1-cm thickness of ASDI material and for larger thicknesses up to 1 inch, a common use thickness for similar materials. This testing should be done by both the shorter pulse time mylar exploding foil technique which will better detect the front face crushing mechanism and the longer pulse time aluminum flyer method which has the twin advantages of forcing the backface failure mechanism and its ready availability at GE-RESD for material optimization studies.

3.5 ELECTROMAGNETIC CHARACTERIZATION

3.5.1 METHOD OF RF MEASUREMENTS

The materials tested on this program were limited in physical size and in some cases difficult to machine. Due to this sample size restriction, a resonant cavity measurement technique was employed because of the small sample size and disc geometry requirements of this technique: a 1/2-inch diameter and nominal thickness of 1/16 inch.

A block diagram of the measurement apparatus is shown in Figure 103. An aluminum re-entrant cavity which resonates at approximately 250 mHz was used. RF energy from a signal source is coupled to the cavity by a small loop. Another small loop is used to sample the energy in the cavity. This sampled RF energy was crystal detected and measured with a DC microvoltmeter.

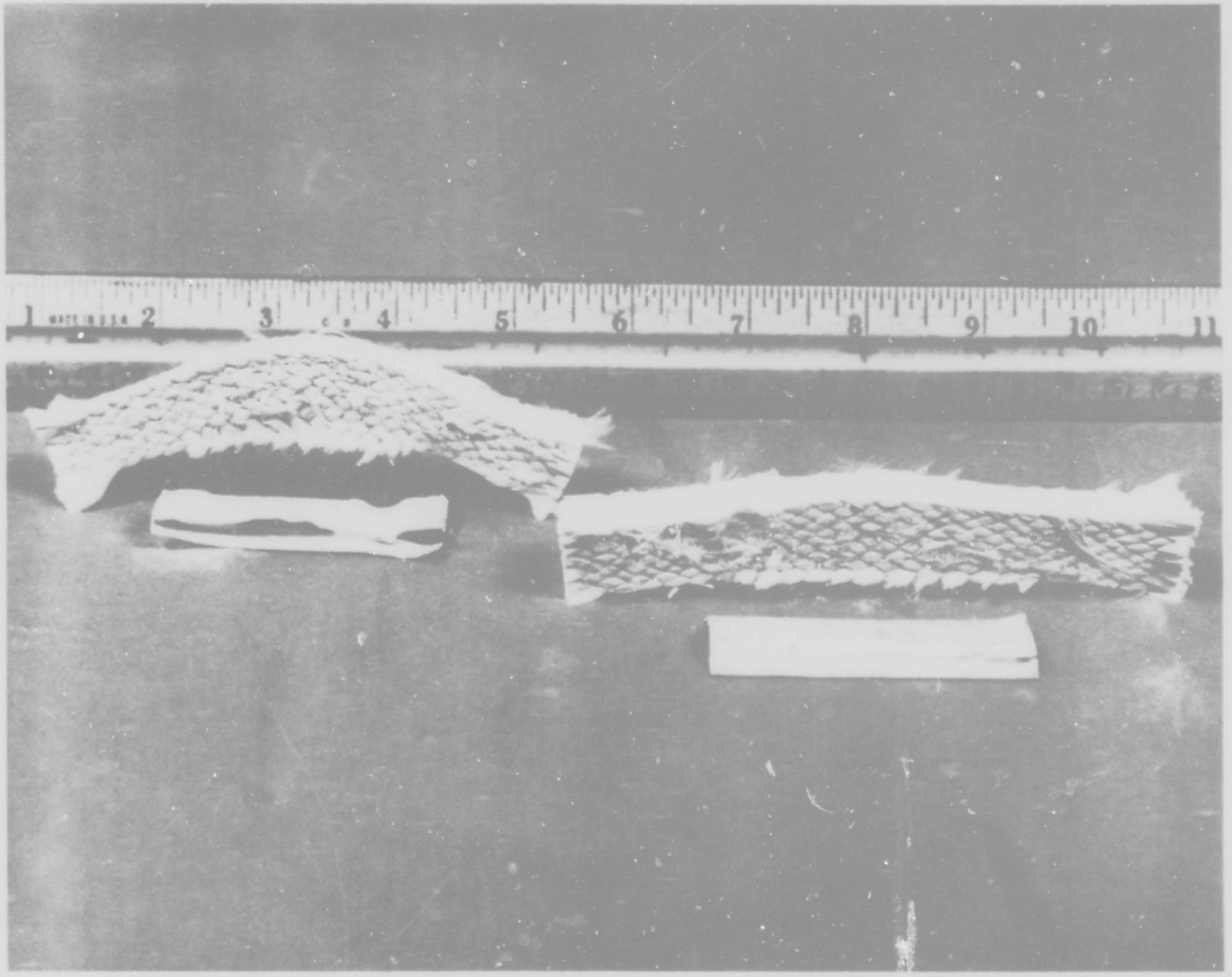

Figure 102. BNQ-V Tensile Bar Specimens After Aluminum Foil Magnetic Flyer Impact Tests at 2000 taps (Right) and 4000 taps (Left); Aluminum Foil Flyers Shown in Foreground

TABLE 47. ALUMINUM FOIL MAGNETIC FLYER PLATE TEST RESULTS

Specimen ID	Aluminum Flyer		Impulse (taps)	Remarks
	Velocity $\frac{(\text{mm})}{(\ \mu\text{sec}\ )}$	Thickness (mm)		
BNQ-V				
407-3	0.25	0.38	2000	tensile test bar; bent (Fig. 102), strength unaffected at 3800 psi.
407-4	0.52	0.38	4000	tensile test bar; bent, surface frayed (Fig. 102); strength dropped to 1200 psi.
ASDI-404-2				
US1/404-2	0.25	0.38	2000	No visible damage, US attenuation increased from 46 to 54 db/cm, thickness increased from 1.015 to 1.016 cm.
US2/404-2	0.37	0.38	3000	No visible damage, US attenuation increased from 50 to 58 db/cm, thickness increased from 1.021 to 1.026 cm.

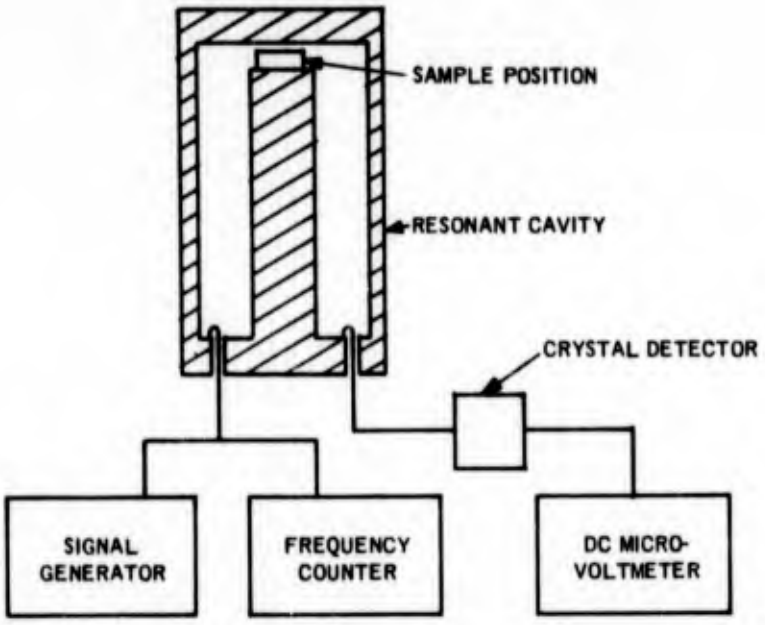

Figure 103. Cavity Measurement Technique

The measurement procedure is to first measure the resonant frequency and width of resonance of the empty cavity. Then these measurements are repeated with the sample in place in the gap between the end of the post and the top of the cavity. From this data, the complex dielectric constant, $\epsilon' - j\epsilon''$, of the sample can be calculated. The mathematical procedure for the data reduction is described in Reference 23.

3.5.2 CARBORUNDUM BN COATINGS

The pure coating materials as received from Carborundum Co. were made into 1/10-inch thick specimens for dielectric property determinations on the basic candidate matrix. Samples of Series A, S and V BN coatings which were fired at various suitable temperatures between 250°F and 1200°F were measured and the resulting data is shown in Table 48. It is clear that all three series materials have loss tangents less than the acceptable maximum goal for these programs of 0.01 when fired to a high temperature (1000 or 1200°F). The importance of the high temperature firing is shown dramatically with the two series V samples. When the series V is fired to 250°F, the loss tangent is almost 0.1 and when fired at 1200°F, the loss tangent reduces to as low as 0.0005.

TABLE 48. DIELECTRIC PROPERTIES OF CARBORUNDUM BN COATINGS AT APPROX. 250 MHz

Coating	ρ (gm/cc)	$\epsilon' - j\epsilon''$	Tan δ
Series V ($MgSiO_4$ flux) fired to 250°F	1.14	2.66 - j0.252	0.095
Series V fired to 1200°V	1.11	2.29 - j0.0013	0.0005
Series S Al_2O_3 flux fired to 650°F	1.13	2.66 - j0.040	0.015
Series S fired to 1200°F	1.30	2.81 - j0.014	0.005
Series A $AlPO_4$ flux) Fired to 1000°F	0.78	1.83 - j0.0014	0.0007

3.5.3 SILICA-SILICA OMNIWEAVE COMPOSITES

One sample of an HS type Ludox silica-silica Omniweave 4-D composite, with a density of 1.47 gm/cc was measured and the properties are given in Table 49. The loss tangent of the material was 0.011, slightly above the accepted maximum. A measurement was attempted for the denser 4-D HS material, (1.7 gm/cc) but was unsuccessful because of difficulty in cutting the specimen into a measurable sample geometry.

A sample of ammonium - stabilized Type AS Ludox silica omniweave, as received, was measured and was found to have a high loss tangent, 0.034. It was suspected that this was from the hygroscopic nature of this type of composite material (Ref. 4). This indeed was the reason. A sample was heated to 390°F for 16 hours and measured approximately 10 minutes after removal from the furnace. This resulted in a slight decrease in dielectric constant, Table 49, and a significant decrease in loss tangent from 0.034 to 0.009. After the sample was exposed to lab air for one hour it was remeasured and the loss tangent had increased from 0.009 to 0.027. This hygroscopic condition is unacceptable for antenna window materials but fortunately the condition can be corrected by chemically stabilizing the silica surface as described in Reference 4.

TABLE 49. DIELECTRIC PROPERTIES OF COMPOSITE AT APPROX. 250 MHz

Material	Density ρ (gm/cc)	$\epsilon' - j\epsilon''$	tan δ
HS Ludox/4-D Silica Omniweave as received Flexure Sample HS-381-6	1.42	2.63 0.028	0.011
AS Ludox/5-D Silica Onmiweave as received Panel 401-3 Flexure Sample σ FT2	1.7	3.32 0.113	0.034
Same as above after being heated to 390°F for 16 hrs. in air - and measured 10 min. after removal from furnace	..	2.81 0.025	0.009
Same sample measured 1 hr. after removal from oven	..	3.09 0.082	0.027
Silane-Derived Silica Matrix Broken Flexure Bar MTS-381-2	1.07 (local density)	1.97 0.009	0.0046
Markite Hybrids P1A flexure bar (silane)	1.93	2.99 0.019	0.0064
P2A flexure bar (SR-350)	1.97	3.54 0.014	0.0039
BNQ-Type V, 850°F firing as received	1.32	2.15 0.023	0.011
BNQ-same sample as above, heated to 390°F for 16 hrs. measured 10 minutes after removal from oven	-	2.06 0.010	0.005
(measurements 6 hours later with sample exposed to lab air showed no measureable change in dielectric properties)			
BNQ-V-9 from channel flow test fused surface material	1.35	2.73 0.045	0.017

3.5.4 SILANE-DERIVED SILICA/ASTROQUARTZ OMNIWEAVE

A specimen of Astroquartz Omniweave locally densified to 1.07 gm/cc by repeated impregnation and pyrolysis of methyl-trichlorosilane was tested in the cavity. Some difficulty was also experienced in preparing an ideal geometry 1/2-inch diameter, 1/16-inch thick disc from the broken flexure bar. The relatively high value of 0.0046 for such a low density increase above the 1.00 gm/cc 381 Omniweave beginning density indicates that this particular specimen processing would have resulted in a higher than acceptable loss tangent if the densification had proceeded to the intended 1.7 gm/cc minimum level. However, study of the silane pyrolysis method of producing a silica matrix was discontinued because of the difficulty in achieving this density increase.

3.5.5 MARKITE HYBRIDS

One sample each of the two Markite Hybrid materials was measured in the cavity and the data are also given in Table 49. The two 1/2-inch diameter, 1/16-inch thick cavity specimens were taken from flexure bars P1A and P2A after mechanical testing. The loss tangents for both the standard SR-350 and the newer silane-derived hybrid are both low at 0.0039 and 0.0064. This result shows the expected improvement over the Markite Hybrid results reported in Table 30 of Reference 2. The difference is the higher final pyrolysis temperature of 1800°F before final reimpregnation. Note that this low loss property was found despite the definite dark, charred internal appearance of the hybrid specimens observed after flexure testing.

3.5.6 GLASS-BONDED BORON NITRIDE FILLED QUARTZ OMNIWEAVE - BNQ

A sample of BNQ omniweave was measured in the as-received condition and the data is shown in Table 49. The loss tangent was slightly high, 0.011. To check for hygroscopicity, the sample was heated to 390°F for 12 hours and remeasured as for the silica-silica sample above. The loss tangent dropped from 0.011 to 0.005 showing some hygroscopicity. But unlike the silica-silica omniweave, the BNQ omniweave shows no immediate tendency to pick up water from the air. A measurement after 6 hours exposure to lab air showed no measurable change in the dielectric properties.

The BNQ-V channel flow sample* appeared to have three distinct layers. See Figure 105. The top of the sample was a thin white translucent layer which had been melted. The middle layer (also thin, ≈1/16-inch) was dark in color where some chemical change had occurred. The remainder of the sample appeared to be in the virgin state. The complex dielectric properties of each layer would obviously be different due to the

---

*See Paragraph 3.6 for description of ablation testing

difference in physical and chemical state of the material of each layer. It was not possible to cut samples from each layer for measurement because of the fragile nature of the sample. An attempt was made, however, to measure an effective average dielectric property for the three layers by cutting a thin sample for the cavity which included the top two layers and some of the virgin material. We were also unable to cut this sample because the material was too fragile. We did however make one measurement of the effective average by placing some of the crumbled sample material in the gap of the cavity, see data in Table 49.

Because of the possibilities of compounded internal reflection and scattering effects when using a cavity gap specimen of poor geometry, an erroneously high apparent loss tangent may be measured. Under these circumstances, the BNQ-V channel flow data are believed to be biased high.

A more valid dielectric test of ablation test samples is the wave guide transmission coefficient measurement (see Ref. 2) but there was not enough material for this test.

3.6 THERMAL CHARACTERIZATION

Thermal conductivity measurements were made on a sample of BNQ-V from the preimpregnated process Omniweave No. 407-9. The measurements were made on a Dynatech TC-1000 Comparator using a 2-1/2 inch square specimen as shown in the detailed sampling plan layout of Figure 62 (Para. 3.1.3) reference to which shows that a 2-1/2 inch long, 1-1/2 inch wide section was then taken from the 2-1/2 inch square for subsequent tunnel type ablation testing.

The results of thermal conductivity measurements are shown as Figure 104 compared to that for clear transparent fused silica (e.g. Corning 7940), a standard antenna window material, and the lowest ADL-10 value measured in previous work.

A single test was conducted at the G.E. Hyperthermal Arc Facility to evaluate a 4.0-inch long by 1.75-inch wide boron nitride quartz specimen (BNQ-V/407-9). The channel flow mode of testing was utilized, and the test conditions were: a heat flux of 1100 Btu/ft^2-sec, an enthalpy of 7000 Btu/lb, and an edge pressure of 2.4 atmospheres.

The post-test specimen is shown in Figure 105a, and a section view of the model is shown in Figure 105b. Measurements of the specimen's recession along the centerline showed that one inch from the edge had the largest recession of 0.172 inch. The in-depth thermocouple history for this specimen shown as Figure 106 illustrates that a severe temperature gradient existed through the first 100 mils of the material; while at the end of the run the backface thermocouple showed only a 30°F rise, indicating very low effective thermal conductivity.

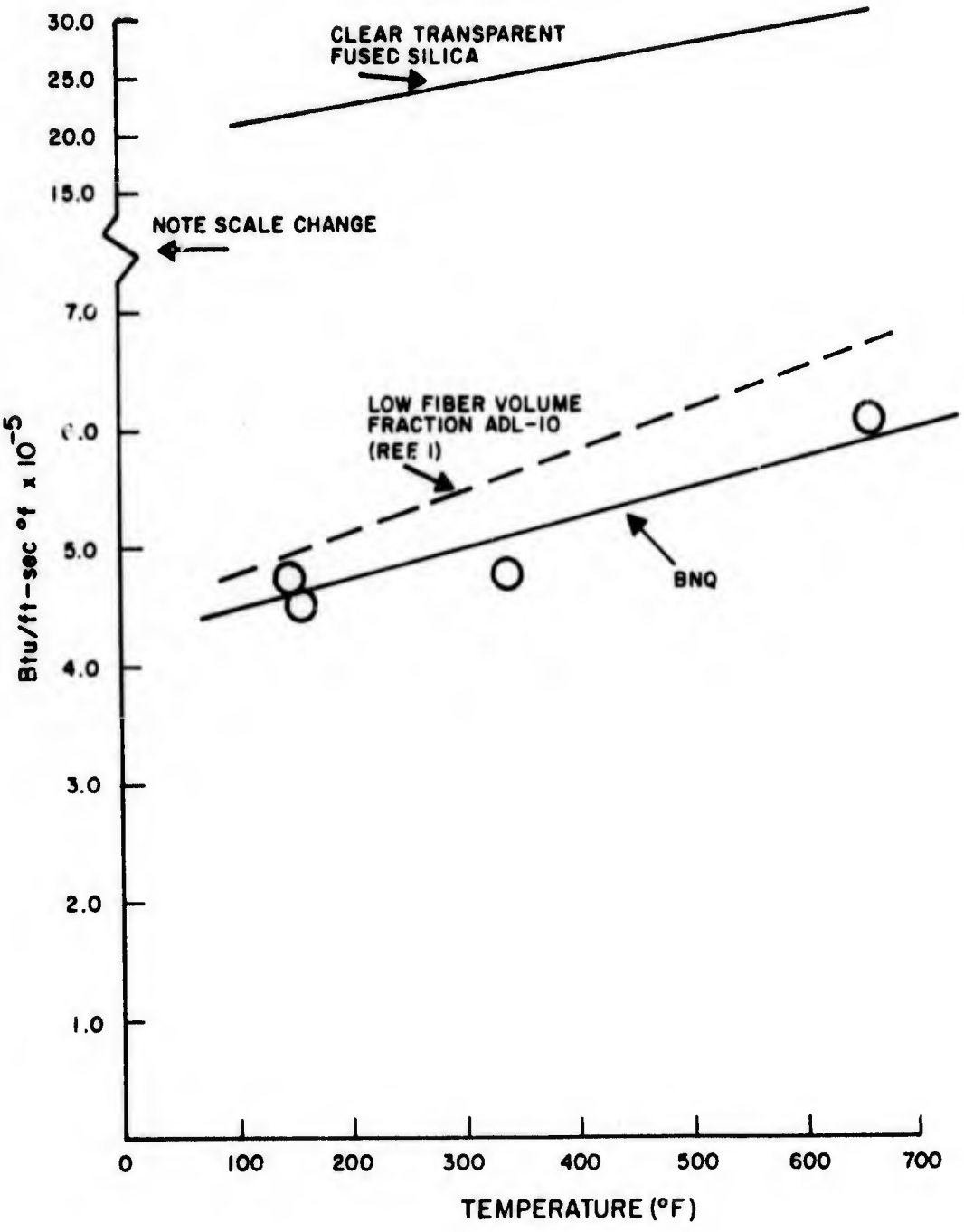

Figure 104. Thermal Conductivity of BNQ-V (1.21 gm/cc)

In evaluating the test data, an average value for Q* was computed to be used as a comparison against other materials. The value computed, 6005 Btu/lb, was found to be the same order of magnitude as the Q* values for phenolic refrasil and fused silica exposed to the same heating environment.

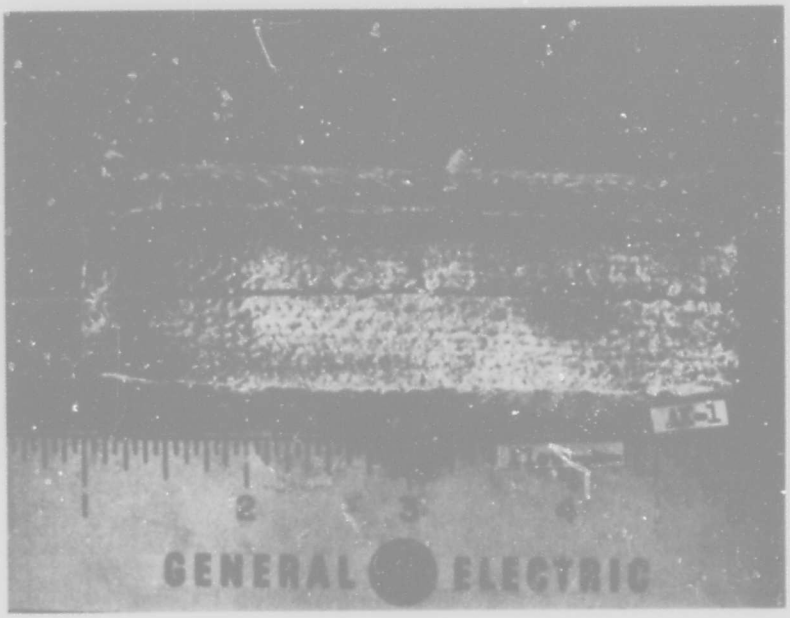

(a) view of face, showing ablation in channel (edges protected by holder, specimen already sectioned for side view.)

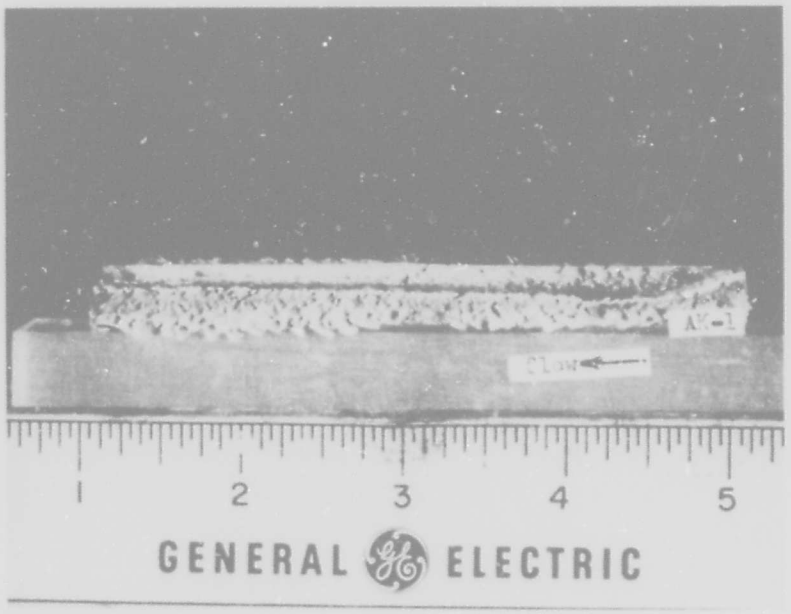

(b) side view of sectioned specimen

Figure 105. Post Test Views of BNQ-V/407-9 Channel Flow Specimen

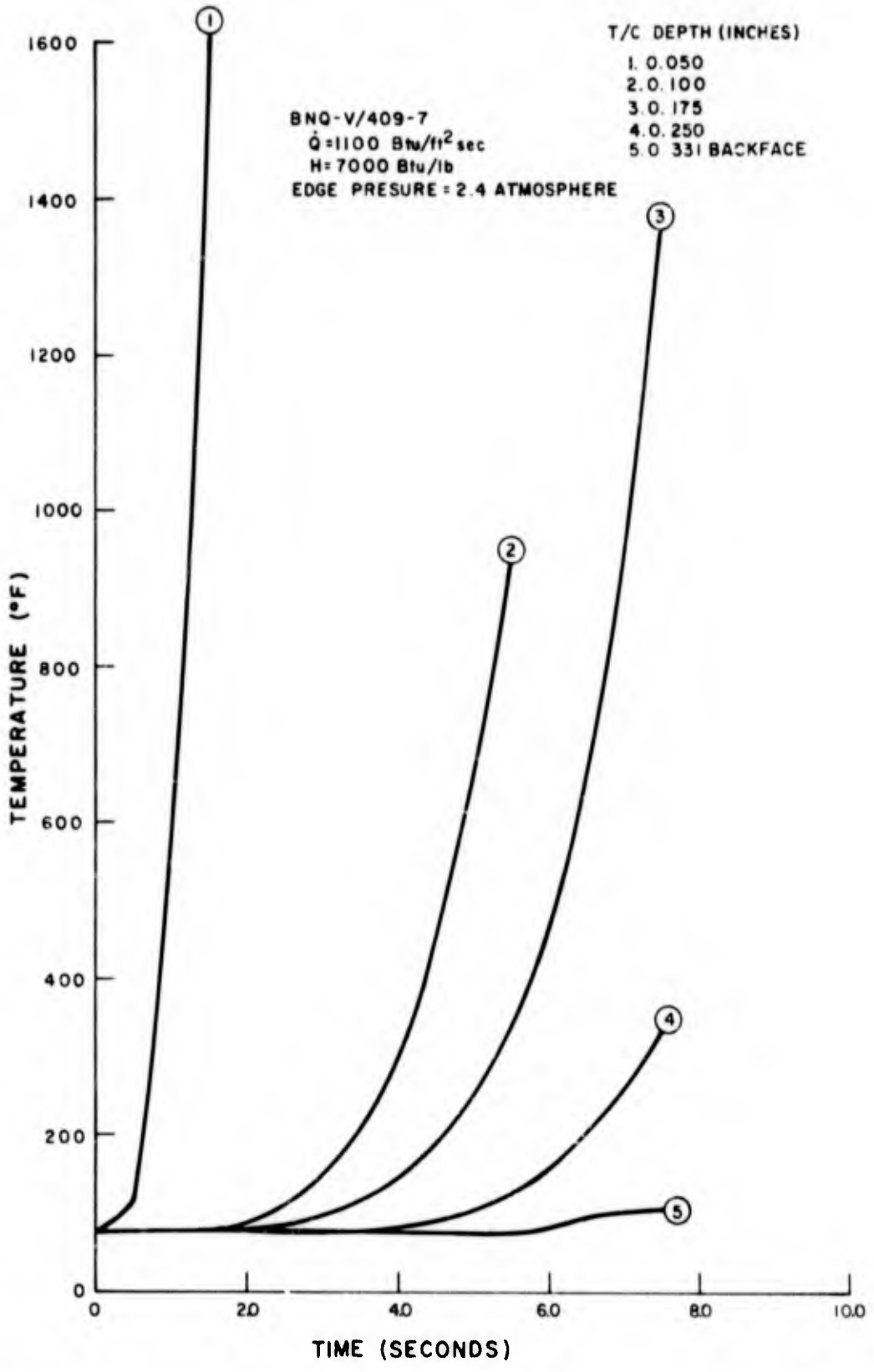

Figure 106. Channel Flow Ablation Test Thermocouple Histories, BNQ/V/409-7

SECTION 4.0

TABLE OF CONTENTS

4.0 OPTIMIZATION STUDY OF ADL-10 AND ANALYTICAL EXPLORATION OF OTHER OMNIWEAVE-SILICA MATERIALS

4.1 INTRODUCTION

The major aim of the study described in this report has been to provide an analytical assessment of Silica-Omniweave composite materials as a function of material geometry, applied loads, and matrix properties. The Materials Sciences Corporation has performed this study for the General Electric Company to determine the theoretical structural performance of Silica-Omniweave reinforcement in a silicone matrix; to determine the structural performance capability of the above composite material, designated ADL-10, for optimum weave configurations; to provide guidelines for experimentally manufacturing optimum weave configurations; to explore the performance capabilities of these types of materials employing other matrix materials.

A detailed description of the 4-D, Omniweave, class of materials is contained in Reference 2, along with the motivating rationale for examining this class of composite materials, and will not be repeated here. The reader unfamiliar with 4-D composite materials is referred to Reference 2, Section 4.

The present study is an extension of work described in Reference 2 and differs as follows:

a. Optimum fiber geometries have been investigated by assuming an initial 1 x 1 x 1 weave density of less than theoretical maximum density. The weave is then distorted such that the "lock-up" angle of the fiber is achieved, such that the resulting weave is at the theoretical maximum density for the given fiber angles.

b. Axial modulus and tensile strength of ADL-10 has been determined for fiber angles varying from 10 to 45 degrees, assuming total fiber volume fraction of 45 and 50 percent.

c. Strength of ADL-10 in a 1 x 1 x 1 weave geometry has been determined for various loading orientations and compared to the corresponding strength of a 3-D and a 5-D silica/silicone composite.

d. Strength capability of silica/silica composite (e.g., Markite) in a 1 x 1 x 1 4-D and 3-D weave, with voids between fibers has been determined for several loading conditions.

e. Strength estimates for a 4-D silica/boron nitride composite have been examined.

4.2 OPTIMIZATION STUDY OF ADL-10

Early weaves indicated that less than theoretical maximum fiber density was being achieved in the as-woven 4-D material when woven in a 1 x 1 x 1 configuration (i.e., with projected fiber angles of 45 degrees). Since maximum strength would be achieved only when the fiber density was at its maximum attainable value, the possible benefits of distorting the initial woven material such that the fiber angles achieved a "lock-up" configuration was investigated. When the fibers are in a lock-up position, the weave will have achieved the maximum attainable fiber density, for the given configuration, assuming that the fiber bundles can distort to achieve maximum packing.

A procedure has been developed for estimating the final geometry and density (and hence, the axial tensile strength) as a function of the initial geometry and density. The analysis computes the angle at which a material which is woven at less than maximum density will "lock-up" (that is, reach a geometry of maximum density) assuming that the plan form and through-the-thickness angles are equal to each other both in initial geometry and in the final geometry. These calculations assume that the fibers are straight except for bends at the edges of the fabric, and they also assume that the rovings are distorted into hexagonal cross-sections due to distortion pressures (see Ref. 2).

The analysis was used to compute predicted "lock-up" angles and associated axial tensile strengths as a function of as-woven density, ρ_o, assuming that the initial projected angles are 45 degrees; that is, the material is woven in a 1 x 1 x 1 configuration. Figure 107 shows the variation in "lock-up" angle as a function of initial, as-woven (unimpregnated) density, ρ_o.

In Reference 2, an analysis was developed for predicting the axial tensile strength of a 4-D material produced by the Omniweave process. Figure 70 of Reference 2, which has been extended to projected fiber angles of 45 degrees and is presented here as Figure 108, presents the predicted strength of ADL-10 as a function of fiber angle which results from that analysis. The results are valid for a symmetric configuration. Using the results of Figures 107 and 108 it is possible to predict the strengths of ADL-10 and composites in the "lock-up" configuration as a function of as-woven density. The results are shown in Figure 109.

The ratios of dimension changes required to accomplish the geometries defined in Figure 1 are presented in Figure 110. Here are shown the relative changes in length, c/c_o, and the relative change in lateral dimensions (widths and thickness), represented by a/a_o, that occur between the as-woven and "lock-up" configurations.

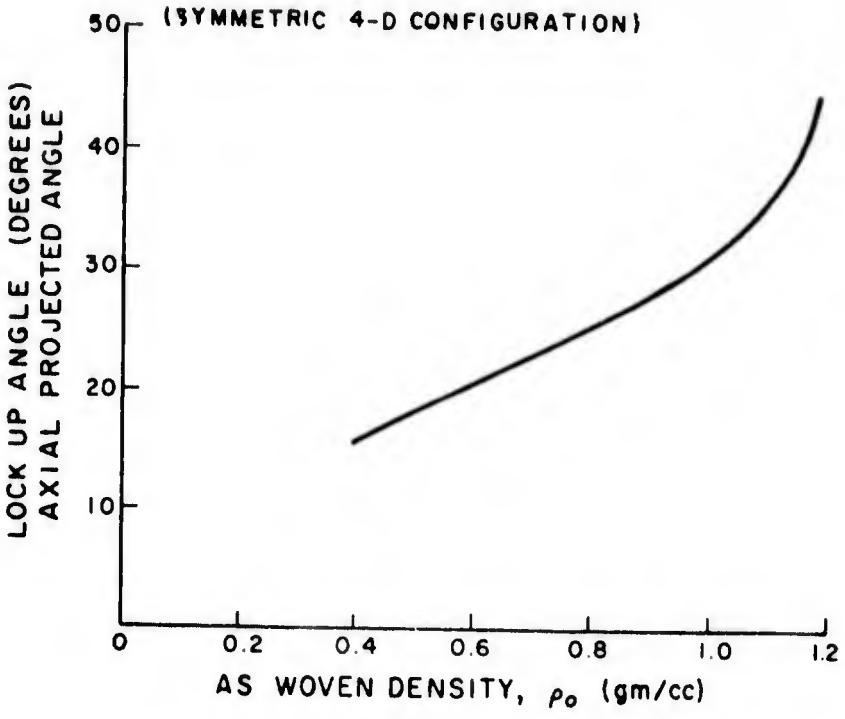

Figure 107. Lock-Up Angle as a Function of Initial Density

As an example, consider a scarf woven in a 1 x 1 x 1 geometry and having an as-woven density of 1.0/cc. Assume that the as-woven width, thickness and length (w_o, t_o, l_o) are 6 inches, 0.5 inch, and 8 inches, respectively. From Figure 110 we find that in the "lock-up" configuration the width and thickness will be 80 percent (0.8) of the as-woven values while the length will be 30 percent (0.3) greater. That is, the final width, thickness, and length in the "lock-up" configuration are $w_f = 0.8 \times 6 = 4.8$ inches, $t_f = 0.8 \times 0.5 = 0.4$ inches, and $l_f = 1.3 \times 8 = 10.4$ inches.

4.3 ADL-10 STRENGTH ANALYSES

Strength estimates of ADL-10 have been made using the MULTI computer program as described in Reference 2. Total fiber volume fractions of 45 and 50 percent were considered along with a symmetric 4-D configuration with projected fiber angles varying from 10 to 45 degrees. The fiber and matrix properties input to the MULTI program were the same as used previously for ADL-10; namely, a fiber modulus of 10.4×10^6 psi and a matrix modulus of 0.20×10^6 psi and Poisson's ratio values of 0.20 and 0.35 for the fiber and matrix, respectively. The matrix elastic modulus had been computed in Reference 2 from SR-350 flex modulus data under the assumption that five percent of the composite or ten percent of the matrix is void.

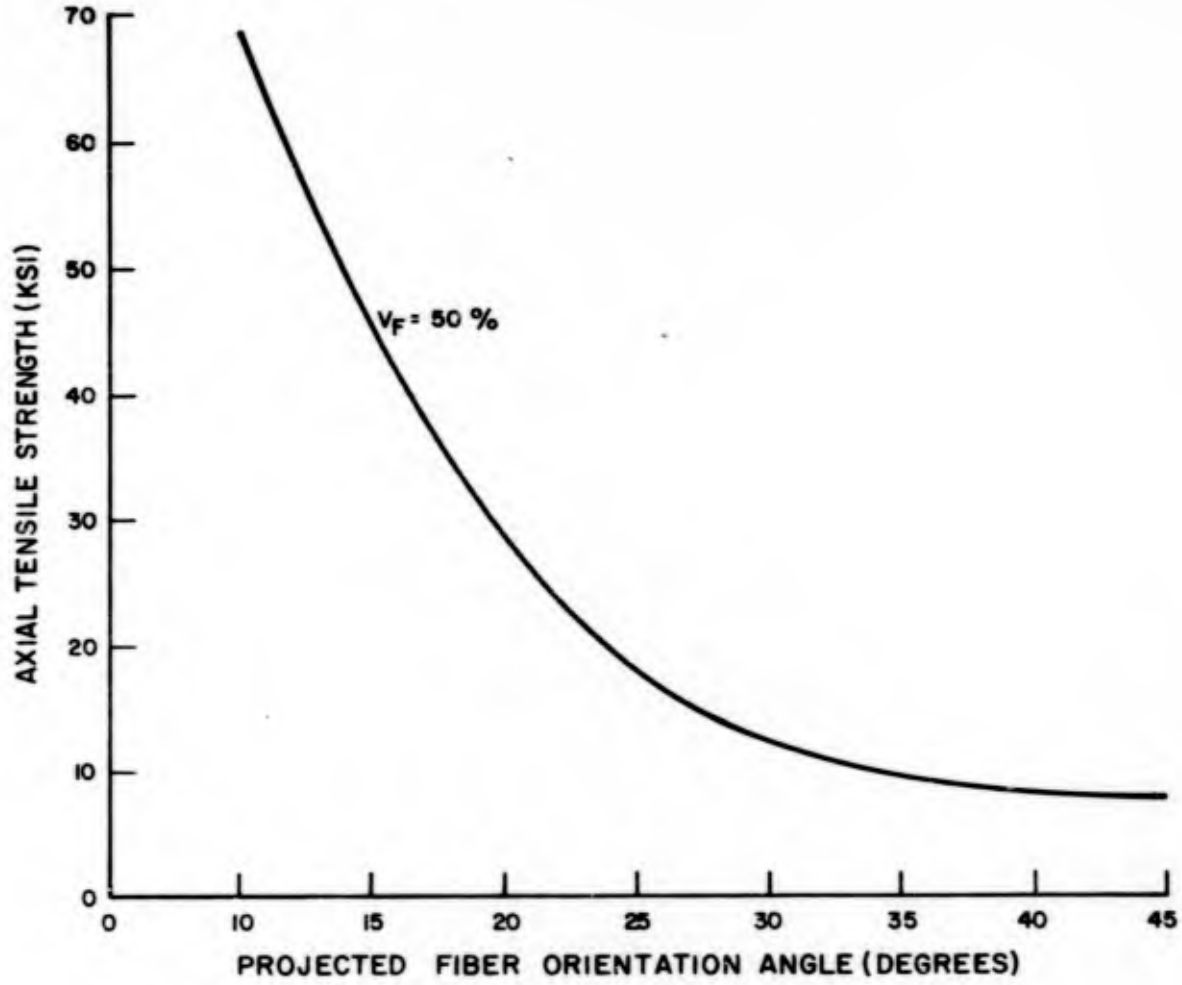

Figure 108. Axial Strength as a Function of Projected Fiber Angle for Axial Load and Symmetric 4-D Configurations

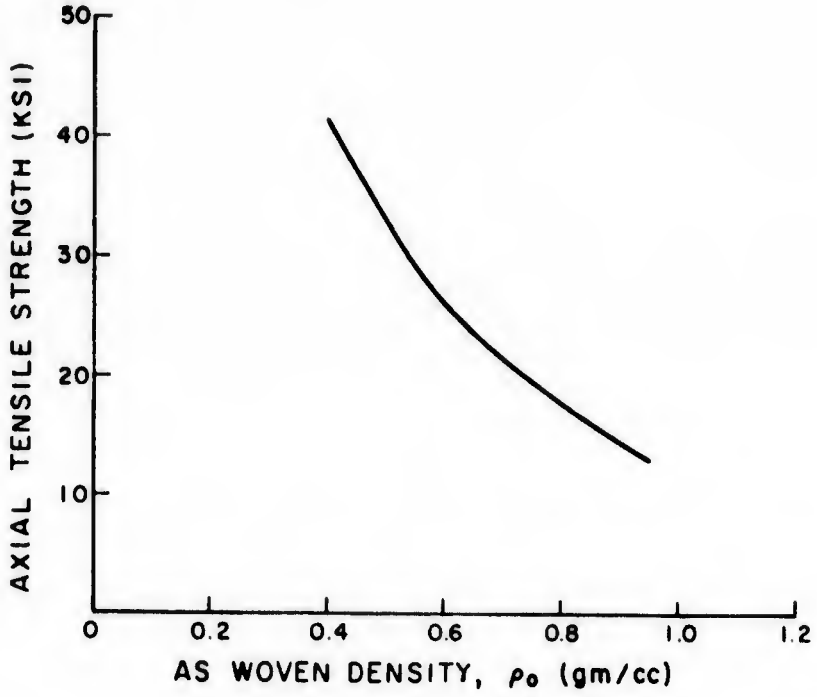

Figure 109. Predicted Axial Strength in Lock-Up Geometry as a Function of Initial Geometry

The theoretically predicted axial moduli as a function of fiber volume fraction and projected fiber angle are presented in Figure 111. It should be noted that the analysis employs admissible displacement fields and hence presents an upper bound for modulus prediction. Therefore, it may be expected that the predicted moduli may err on the high side.

The predicted axial tensile strength of ADL-10 for fiber volume fraction of 45 and 50 percent and various projected fiber angles are shown in Figures 112, 113, and 114. A maximum stress failure criteria has been used in these figures for various values of maximum allowable fiber tensile strength and shear strength, generating the family of curves shown in Figures 112, 113, and 114. Given the fiber tensile and shear strength, and the projected fiber angle, the axial tensile strength is determined by the lower strength indicated by the corresponding curves.

For example, consider $V_f = 0.50$, with a fiber tensile strength of 100 ksi and shear strength of 4.5 ksi, with a projected fiber angle of 20 degrees. From Figure 112, at $\theta = 20$ degrees we find that a shear strength of 4.5 ksi indicates that a shear failure of the fiber will occur at an applied axial stress of 28 ksi. Likewise for a fiber tensile strength of 100 ksi, Figure 112 indicates (at $\theta = 20$ degrees) that the fiber will fail in tension for an applied axial stress of 61.6 ksi. Clearly, the fiber would fail

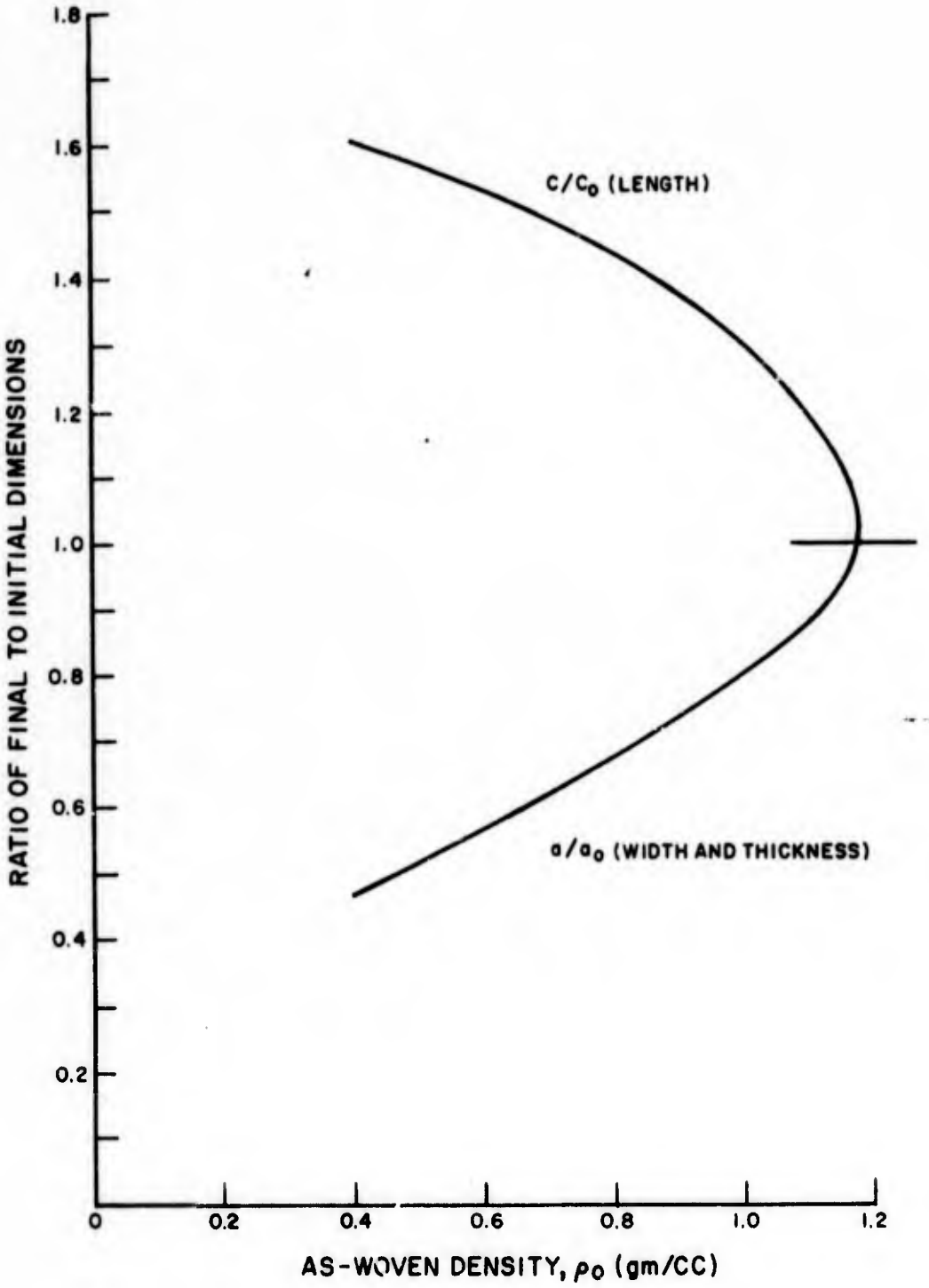

Figure 110. Relative Changes in Length and Width Between As-Woven and Lock-Up Configurations as a Function of As-Woven Density

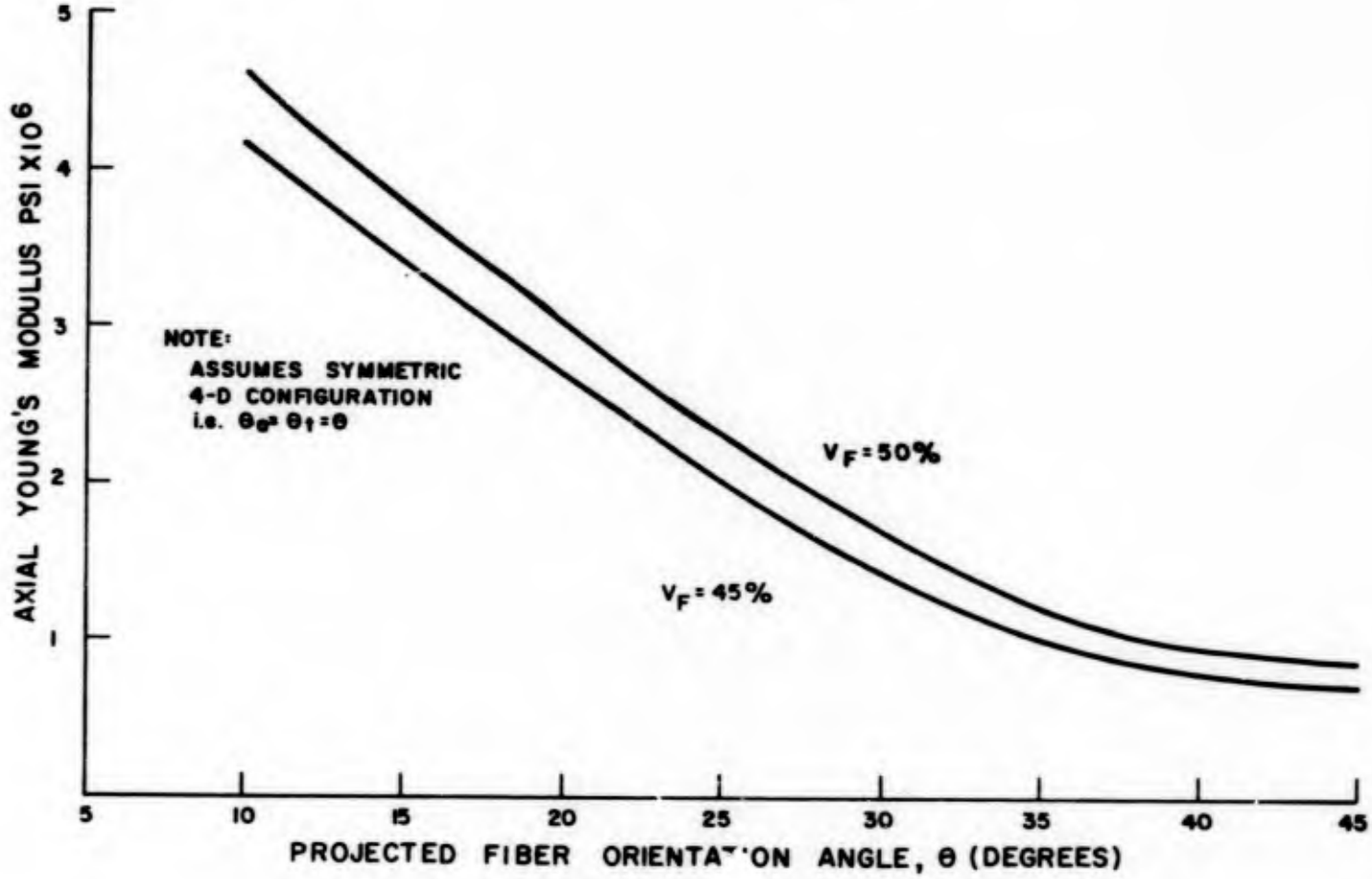

Figure 111. ADL-10 Axial Modulus as a Function of Projected Fiber Angle and Fiber Volume Fraction

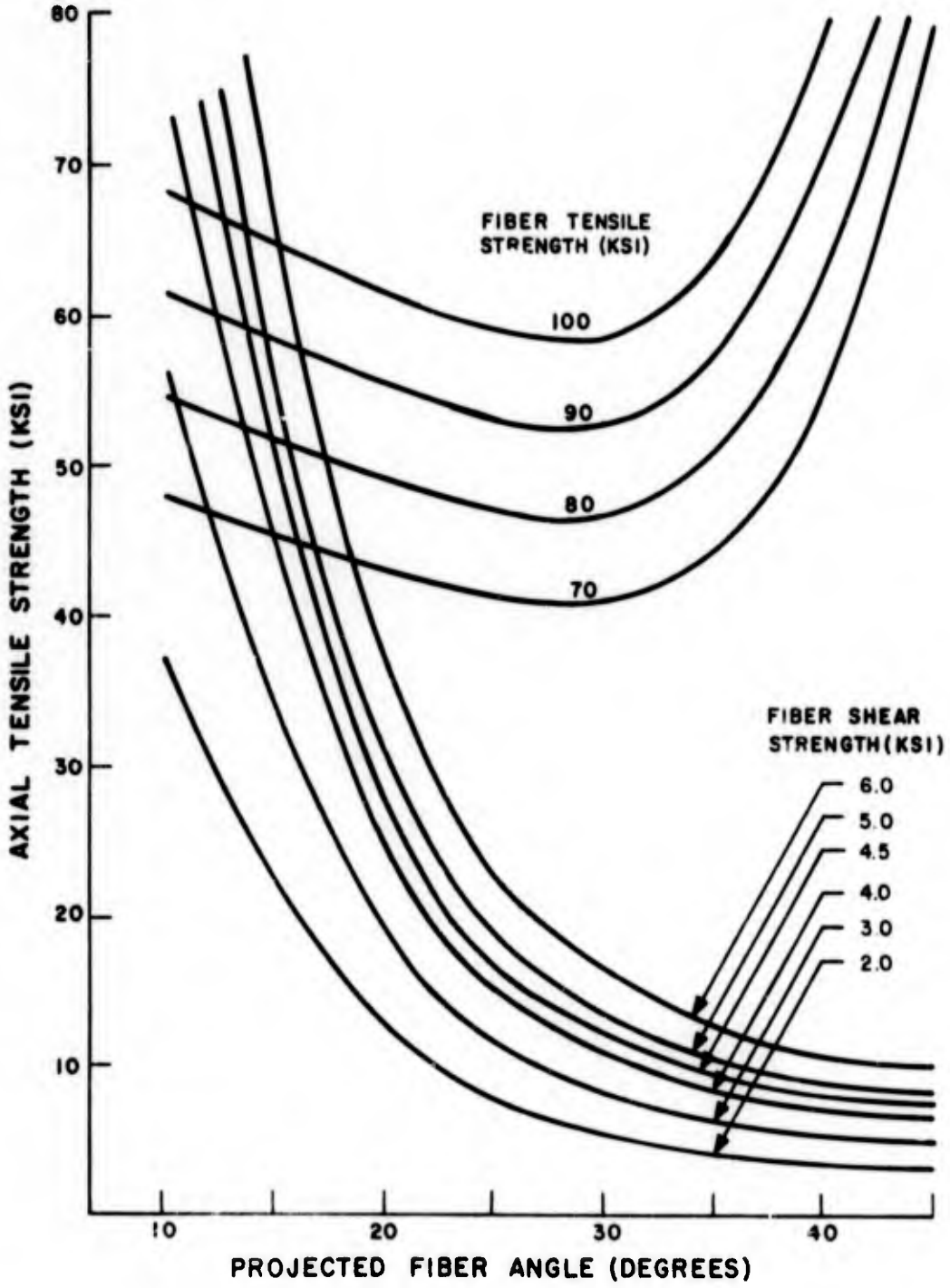

Figure 112. ADL-10 Axial Tensile Strength, Fiber Volume Fraction = 0.50

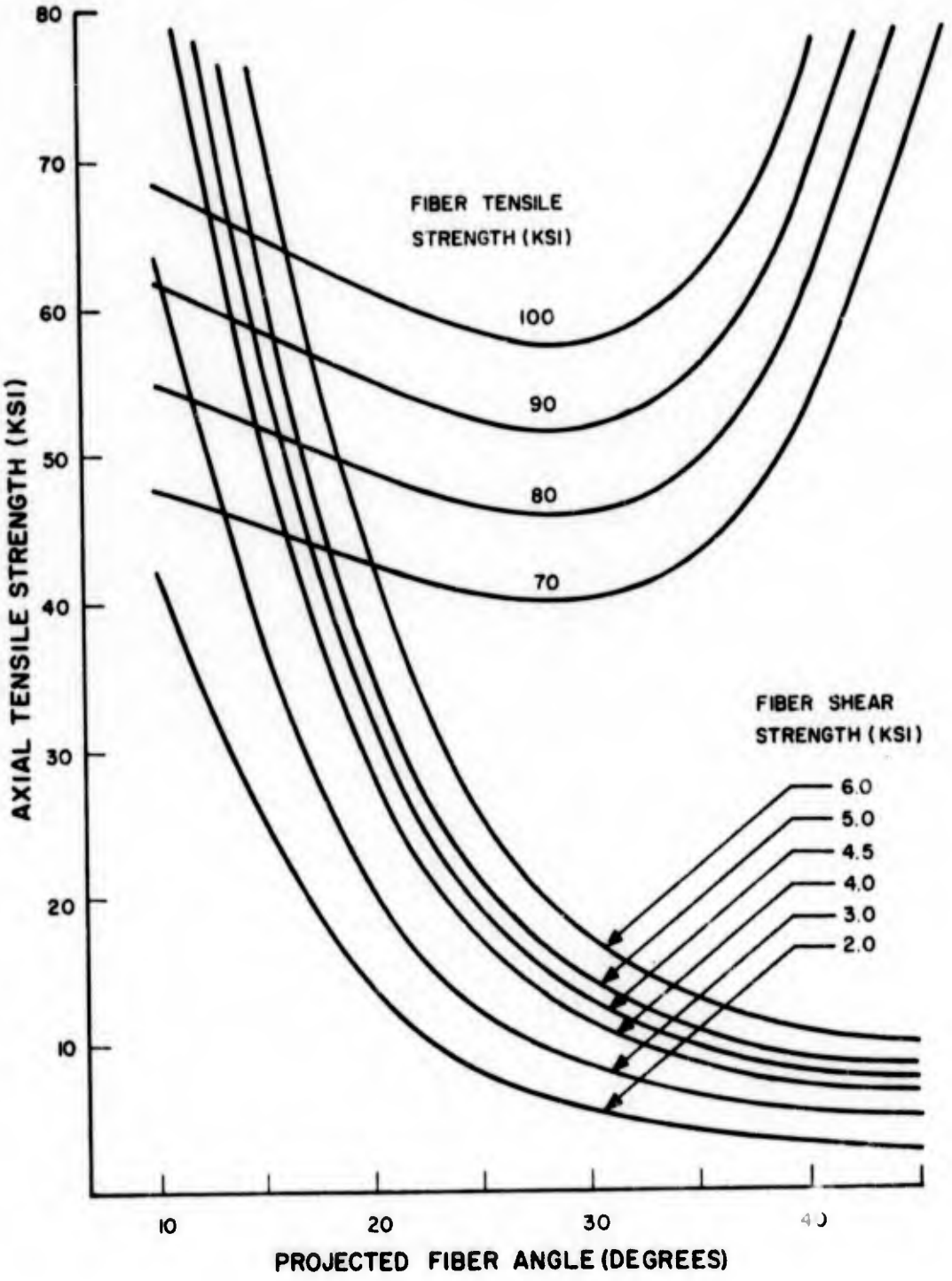

Figure 113. ADL-10 Axial Tensile Strength, Fiber Volume Fraction = 0.45

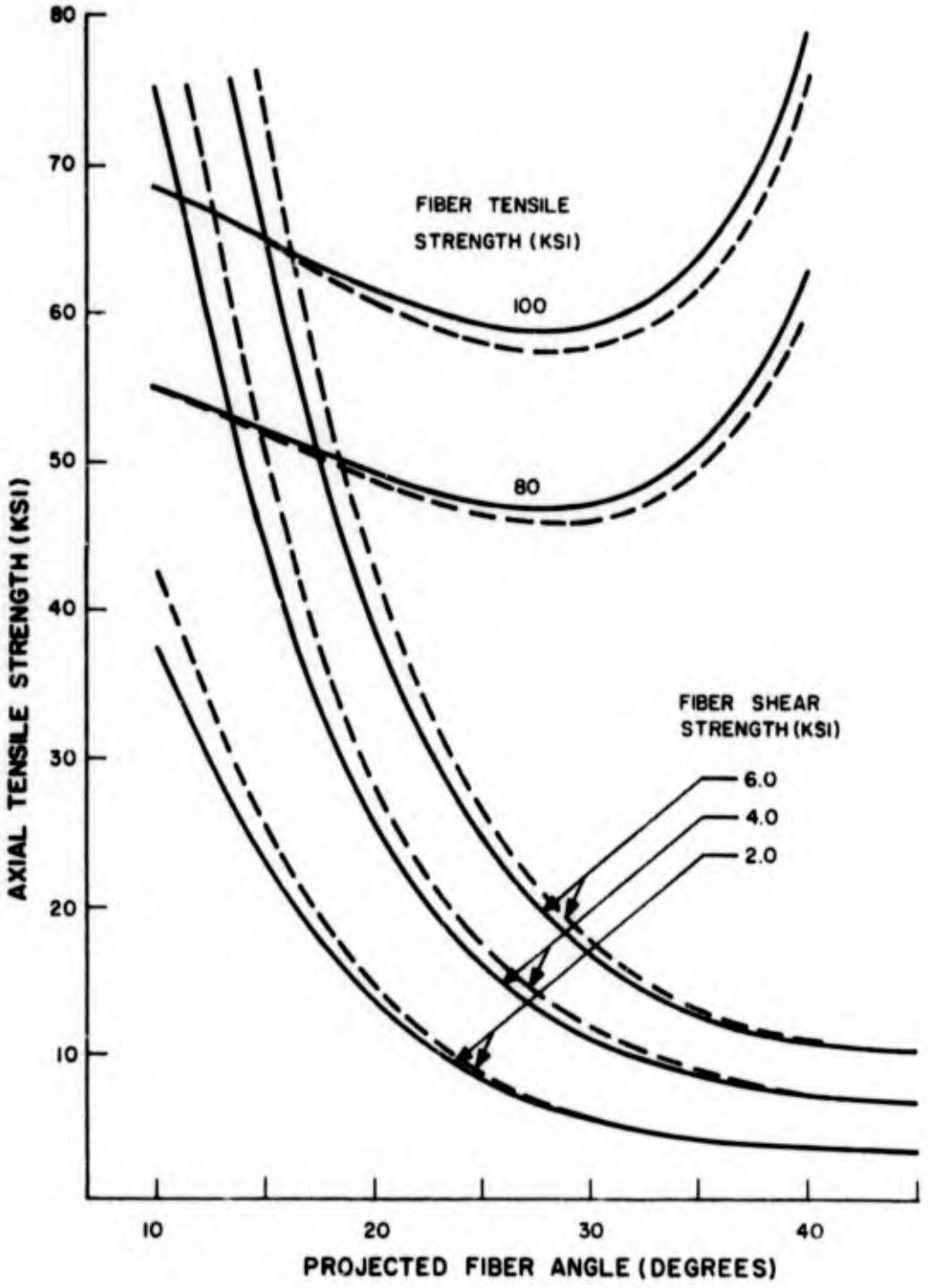

Figure 114. ADL-10 Axial Tensile Strength - Comparison Between Cases

in shear before a tensile stress of 61.6 ksi could be applied. Hence, shear governs, and the theoretical axial strength is 28 ksi. For the above case, if the projected fiber angle is lowered below about 12.5 degrees, tensile failure of the fiber will occur before shear failure, and tension governs. Clearly, for the majority of cases of interest for ADL-10, shear failure of the fiber governs the axial strength.

The comparison of strengths between $V_f = 0.45$ and $V_f = 0.50$ shown in Figure 114 indicates an interesting result of changing fiber volume fraction. Namely, axial strength due to fiber failure in tension decreases with decreasing volume fraction as expected. However, axial strength limited by shear failure of the fiber increases with decreasing volume fraction at low projected fiber angles. This result occurs due to a reduction in composite axial and shear modulus with decreasing volume fraction, which in turn results in lower shear stresses being applied to the fiber.

4.4 COMPARISON OF 3-D, 4-D, AND 5-D THEORETICAL STRENGTHS

The often stated attractiveness of multi-directional composites is the ability of these materials to handle loading in directions other than in the fiber direction and in shear. To examine the statement a little more closely and to determine the amounts of improvement which might be obtained with a 4-D or 5-D composite over the more conventional 3-D composite, an analysis of these materials was made using the MULTI program and various loading conditions.

For all three materials it was assumed that the total fiber volume fraction was 50 percent, with fiber and matrix properties being the same in all cases and equal to those used in the ADL-10 analyses. The 3-D material was assumed to be balanced in that one-third of the total number of fibers were placed in each of the three fiber directions. The 4-D material was also assumed balanced with one-fourth of the fibers in each direction, and the fibers were assumed to be in a 1 x 1 x 1 weave yielding a projected fiber angle of 45 degrees. For the 5-D material, one-fifth of the fibers were placed in each of the five fiber directions, resulting in 80 percent of the fibers being in diagonal directions and 20 percent being in one of the three edge directions. The 5-D material was additionally assumed to have a 1 x 1 x 1 configuration, which resulted in projected fiber angles of 45 degrees.

The results are summarized in Table 50. The fiber strengths were assumed to be 100 ksi in tension and 4.5 ksi in shear. In all cases, fiber shear strength governed failure, thus the choice of fiber shear strength would modify all results in Table 50 proportionally. The inherent axial strength of the 3-D materials is apparent in Table 50.

Note that for face diagonal loading and body diagonal loading relative to the unit cell, the 3-D strength drops to 30 and 37 percent of the axial strength, respectively. This clearly illustrates a very significant strength reduction for off axis loading of 3-D. For 4-D material the axial load case is the weakest loading direction with face diagonal

TABLE 50. COMPARISON OF 3-D, 4-D, AND 5-D SILICA/SILICONE UNDER VARIOUS LOADING CONDITIONS

Strength Assumptions: Fiber UTS = 100 ksi
Fiber Shear Strength = 4.5 ksi

Material Loading	3-D	4-D	5-D
Axial Tension	20,880	7,715	7,560
Face Diag. Load	6,080	10,350	10,635
Body Diag. Load	7,715	17,940	15,050
Face Shear	3,040	11,960	8,440
Diag. Shear	3,635	16,915	9,830

NOTE: For transverse loading the 3-D and 4-D strengths are the same as for axial loading, but for 5-D loaded in the direction of the fifth fiber, results show a 65 percent increase in strength to 12,480 psi.

and body diagonal (loading along one fiber) resulting in 34 and 132 percent increases in strength over the axial strength. The 5-D shows an increase in strength of 41 and 100 percent of the axial load capability for face diagonal and body diagonal loading, respectively, and a 65 percent increase in strength for transverse loading in the fifth fiber direction (see Table 50).

The obvious conclusion from the tensile load cases is that there is considerable strength variation in all cases with the least variation occurring in 5-D and the most in 3-D material. Note, however, that when the axial strength of 4-D material is sufficient for a given application, the off-axis strength will be greater. A 3-D component which may be adequate for axial loads, on the other hand, may be design critical for any off-axis loading.

Consider next the strengths due to applied shear stresses indicated by the analyses. The advantage of 4-D material over 3-D is obvious when one considers that the 4-D material will exhibit roughly four times the strength in shear of corresponding 3-D material. The shear strength of 4-D material is in fact roughly equal to the tensile strength.

Comparison of predicted strengths with measured values indicates in general that the ADL-10 is capable of achieving its theoretical strength (Ref. 2). Loading in a face diagonal direction of panels 331-1 and 331-2 yielded tensile strengths of 7500 psi and 18,000 psi, with molding pressure changing from 150 psi to 1,000 psi, respectively,

and a fiber pitch angle of 40 degrees. These values agree well with a predicted 10,350 psi strength for this loading, even though the predicted strength is for a fiber pitch angle of 45 degrees. Had a fiber pitch angle of 40 degrees been used, the predicted strength would have been only slightly higher.

Panels 402 and 403 were loaded in an axial direction, giving tensile strength of 4300 psi and 3500 psi for molding pressures of 910 psi and 20 psi, respectively, which does not compare well with a predicted strength of 7700 psi. However, panel 402, which received the higher molding pressure was treated initially along with panel 403 in Reference 2. The fiber volume fraction of panel 402 was 74 percent which is above the theoretical maximum, indicating that the weave was damaged during distortion. This damage could explain the low measured strengths.

4.5 ANALYSIS OF SILICA/SILICA MATERIAL

An approximate analysis of "Markite" was performed in Reference 2 to assess anticipated strength levels. That analysis has been extended to assess the capabilities of 3-D and 4-D silica/silica material under axial and off-axis loading.

The analysis assumes that the effects of fiber orientation and phase volume fraction can be assessed on the basis of the assumption that the matrix formed predominately along the fiber bundles, leaving voids in the interstices between these fiber pencils. The MULTI computer code cannot adequately handle a problem of this type since for the given properties, the analysis model represents simply a nearly isotropic material with voids, and does not account for bending of the fiber bundles. Consequently, a frame element was analyzed (as in Ref. 2) to estimate the structural capability of these materials.

The basic frame element is shown in Figure 115. The body diagonals of the rectangular parallelepiped represent the fibers in a basic Omniweave material. If we consider a vertical plane containing the diagonals we find that the fibers contained in this plane form a parallelogram such as DOGO'. It is assumed that the matrix material concentrated at the fiber intersections, such as D, O, G, O', etc. produces rigid joints.

Under these assumptions, a space frame resists an applied load P by both axial and bending stresses in the diagonal members. The addition of horizontal fibers along the face diagonals AF, BE, CH and DG or along the face edges HD, HG or HE will reduce the bending stresses in the diagonal members and improves material strength. The expressions for axial stress, f_a, and bending stress, f_b, in the diagonal frame members have been obtained in Reference 5.

The ultimate stress that a frame can carry is determined by setting $f_a + f_b = f_u$, where f_u is the fiber tensile strength. This equation defines, the ultimate load on on a single frame which yields the failure strength of the material, p_u.

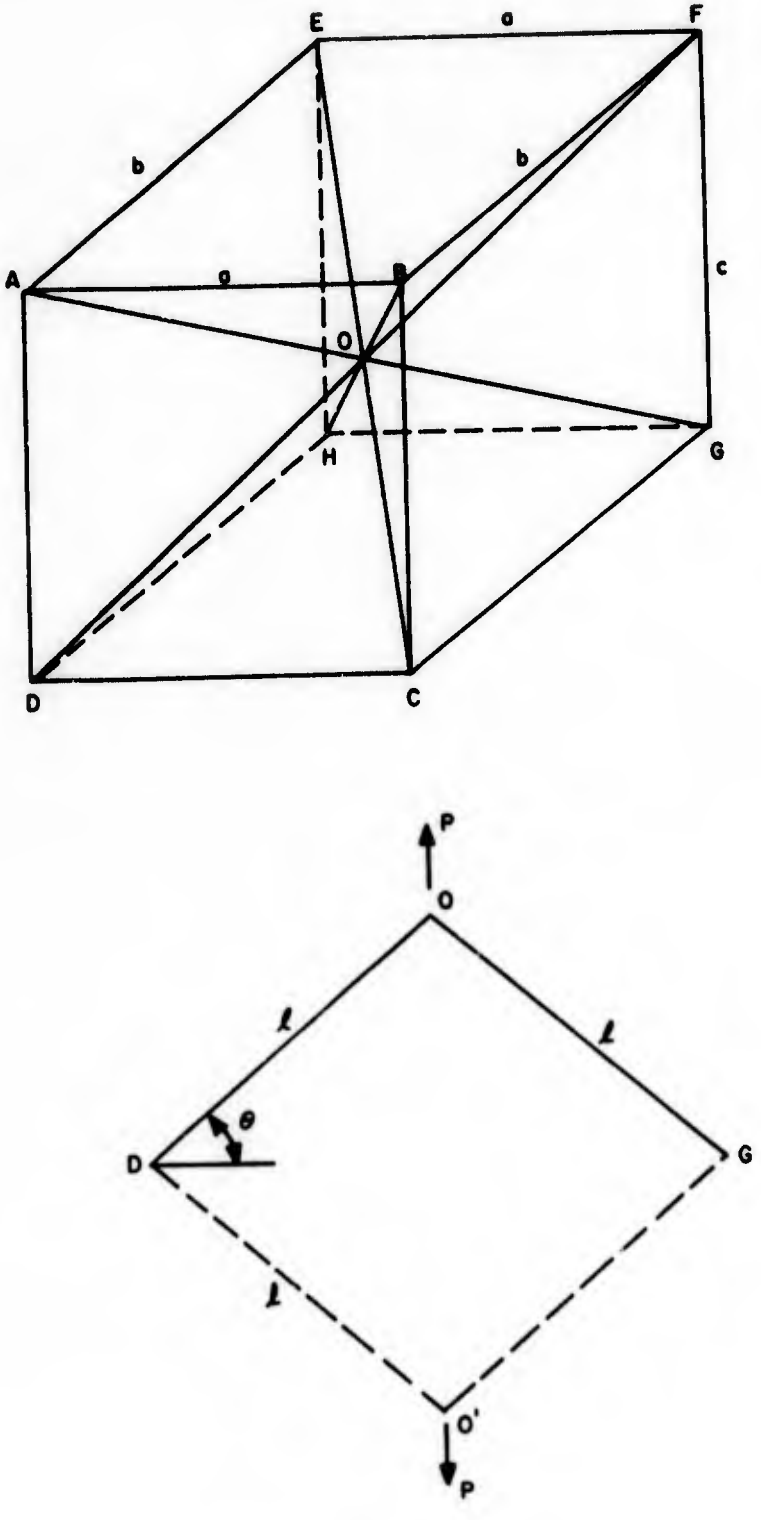

Figure 115. Frame Model

In Reference 2, the axial strength of silica/silica material was computed assuming an ℓ/d of 5.0. In the present work the ℓ/d corresponding to fiber volume fractions ranging from 0.20 to 0.70 for both 3-D and 4-D fiber configurations have been used. Figure 116 gives the relations between ℓ/d and fiber volume fraction for symmetric 3-D and 4-D unit cells. It should be noted that although this analysis results in a quite high estimate of strength in bending and tension, the results do not appear to be unreasonable. In addition, it is reasonable to expect that the effective ℓ/d value for the 4-D material will be larger than the theoretical value for the 4-D unit cell, resulting in a reduction in 4-D axial strength under the axial strength of the corresponding 3-D silica/silica material.

Examining Figures 117 through 120 the superiority of 4-D material over 3-D material becomes apparent for non-axial loading. The 3-D material's off axis tensile strength decreases by about 30 percent for face diagonal loading and increases over the axial strength for body diagonal loading. Consequently, one must conclude that the 4-D weave material will exhibit significantly improved structural performance capabilities over 3-D material when used in structures which will be subjected to loading states which are not directed along the three orthogonal fiber directions.

4.6 ANALYSIS OF BORON NITRIDE/QUARTZ COMPOSITES

Developing an analytical model for Boron Nitride Matrix Material presents an interesting challenge. Boron Nitride can be described as resembling talcum powder in that it can be easily broken up into a powdery material. Thus, the material model must exhibit very low extensional and shear resistance, while being able to exhibit a high hydrostatic deformation resistance. A mathematical model of the matrix material can be achieved with the MULTI computer program by supplying low extensional and shear moduli, while specifying Poisson's ratio at values very close to one half. Since the bulk modulus of the material is a function of $1/(1-2\nu)$, proper choice of Poisson's ratio can yield the desired values for bulk modulus.

An additional complication must be considered, however, for the materials manufactured under the present program. That is, all of the Boron Nitride/Quartz materials fabricated possessed in the neighborhood of 50 percent porosity, along with very low fiber volume fractions (roughly 15 to 20 percent). The results of the above means that one must visualize a composite with low fiber volume fraction, with the remaining material being partly a powdery type matrix and a considerable amount of free space. For a material of this type one can easily postulate the effect of different load intensities on a specimen, as discussed below.

Laminates (±45 degrees) of Boron Nitride/Quartz were fabricated and tested in an effort to determine some experimental values for matrix shear modulus. The fiber

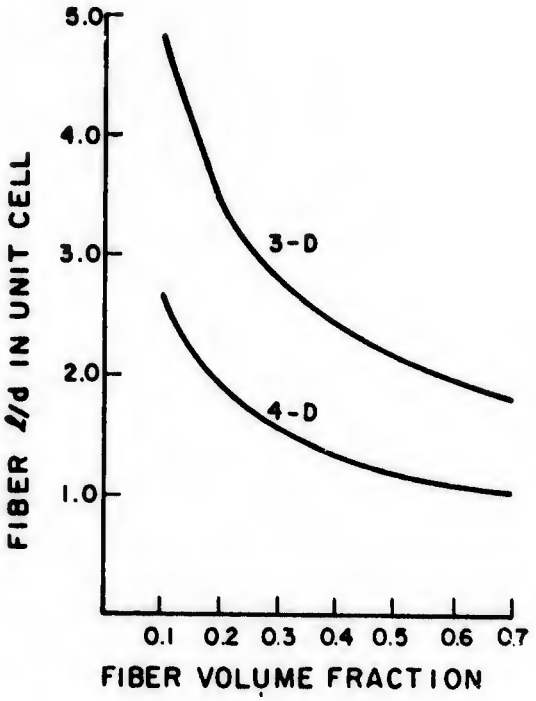

Figure 116. Relation Between Fiber Volume Fraction and ℓ/d for 3-D and 4-D

volume fractions and void contents were roughly the same as the Omniweave specimens of the same material. The results indicated that the matrix failed at very low stress levels (30 to 80 psi) and correspondingly low strain levels (roughly 250 micro-inches/inch. Matrix failure of these specimens initiated total specimen failure since the ±45 degree laminate geometry is not a stable weave configuration.

Consider next an omniweave composite of Boron Nitride/Quartz. On initial loading one might expect an elastic modulus representative of the matrix/fiber system. However, at very low applied stress levels one would expect the matrix to fail and begin redistributing itself in the void regions of the material, which would give rise to a slight drop in composite modulus. Since the fiber volume fraction is very low, continued loading would simply continue distorting the material, changing fiber angles and forcing matrix into more void regions until one of two things occur. First, if the matrix content is low enough or the void content high enough, distortion can take place until the fibers reach their maximum packing positions and fiber lock-up occurs. If fiber lock-up occurs, additional loading will indicate a significant increase in extensional modulus and failure will be governed by a fiber netting analysis. The second possible occurrence is that the matrix material will distort until all of the

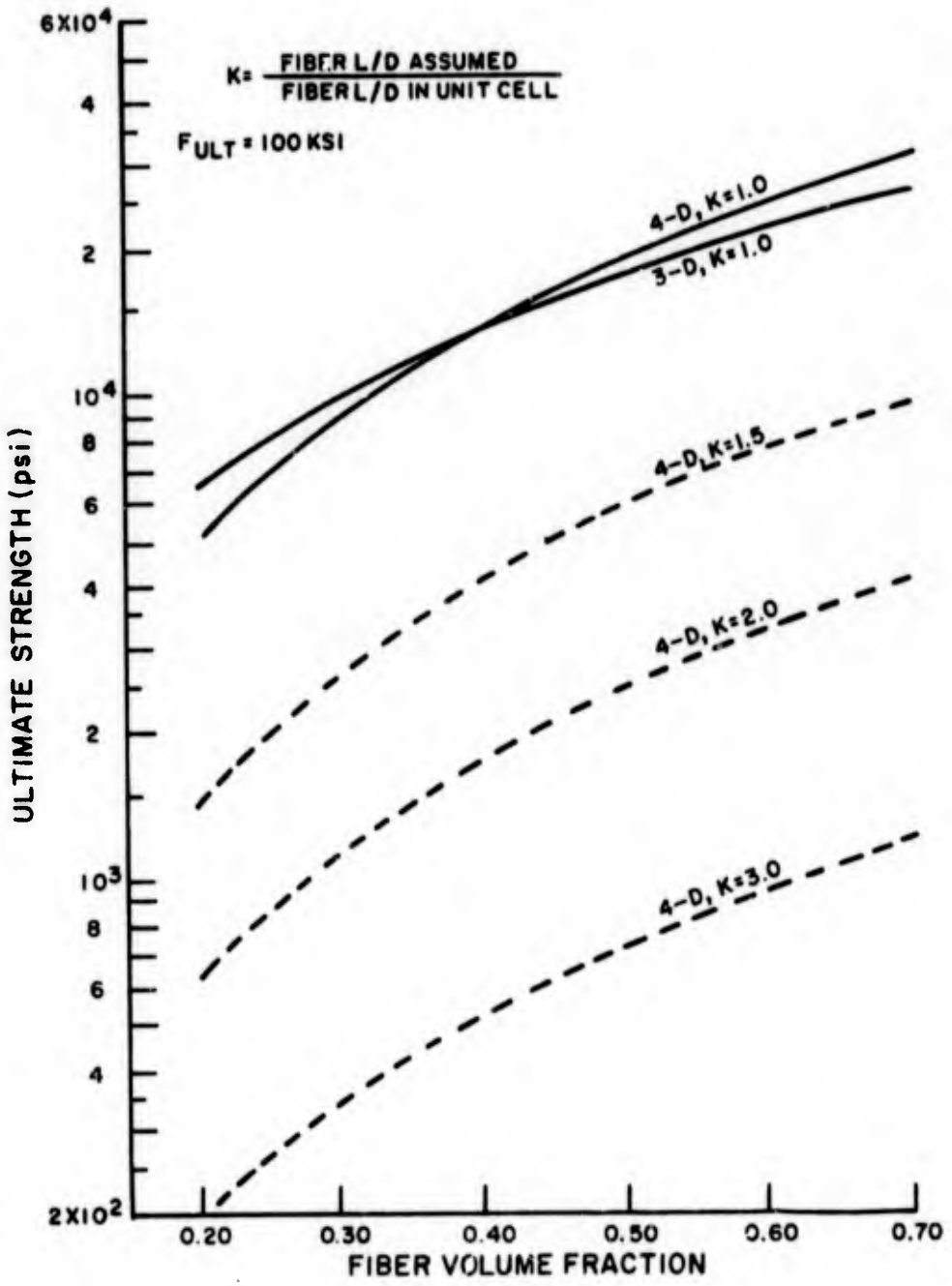

Figure 117. 3-D and 4-D Silica/Silica
Strength for Axial Loading

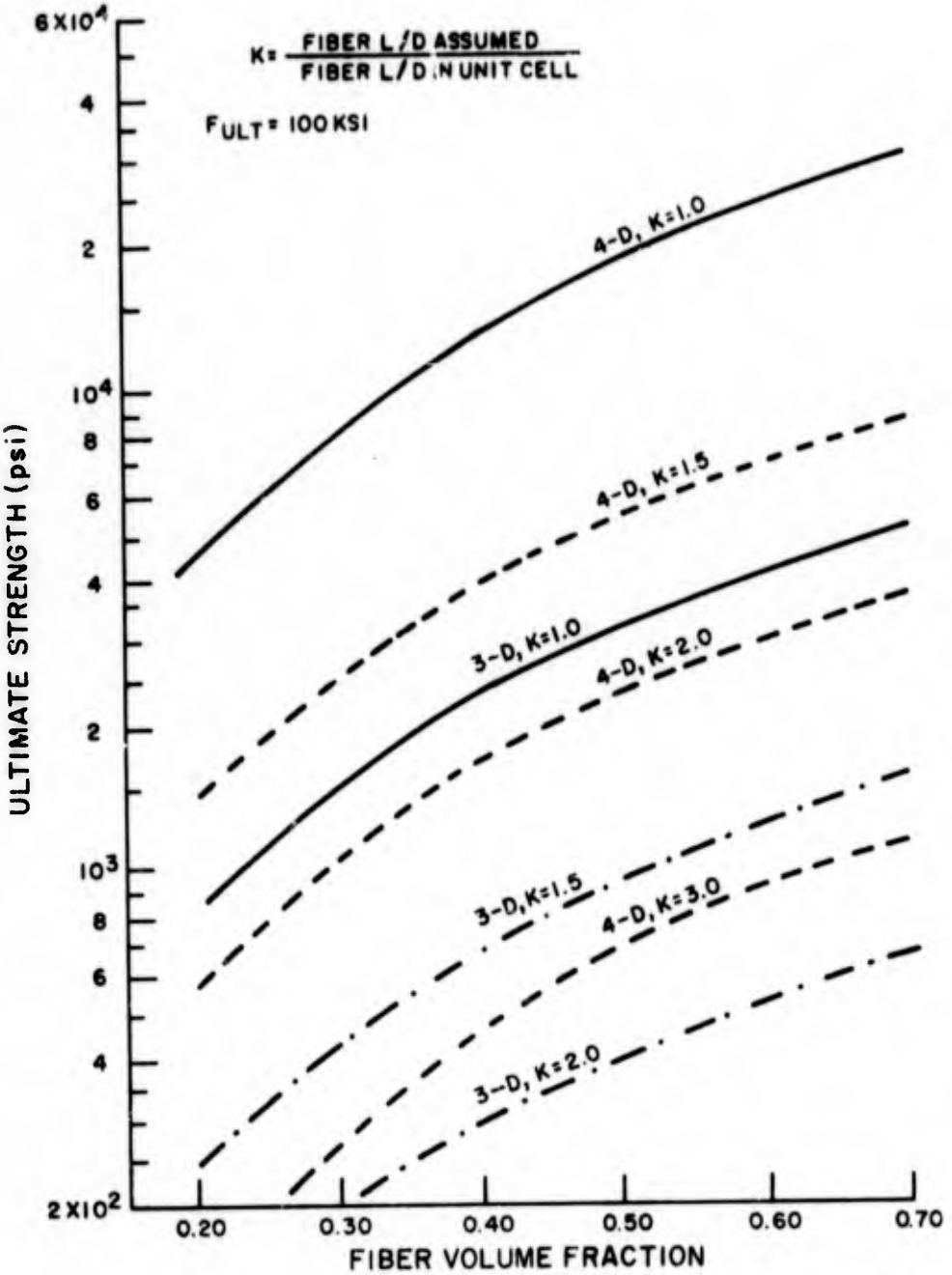

Figure 118. 3-D and 4-D Silica/Silica Strength for Face Diagonal Loading

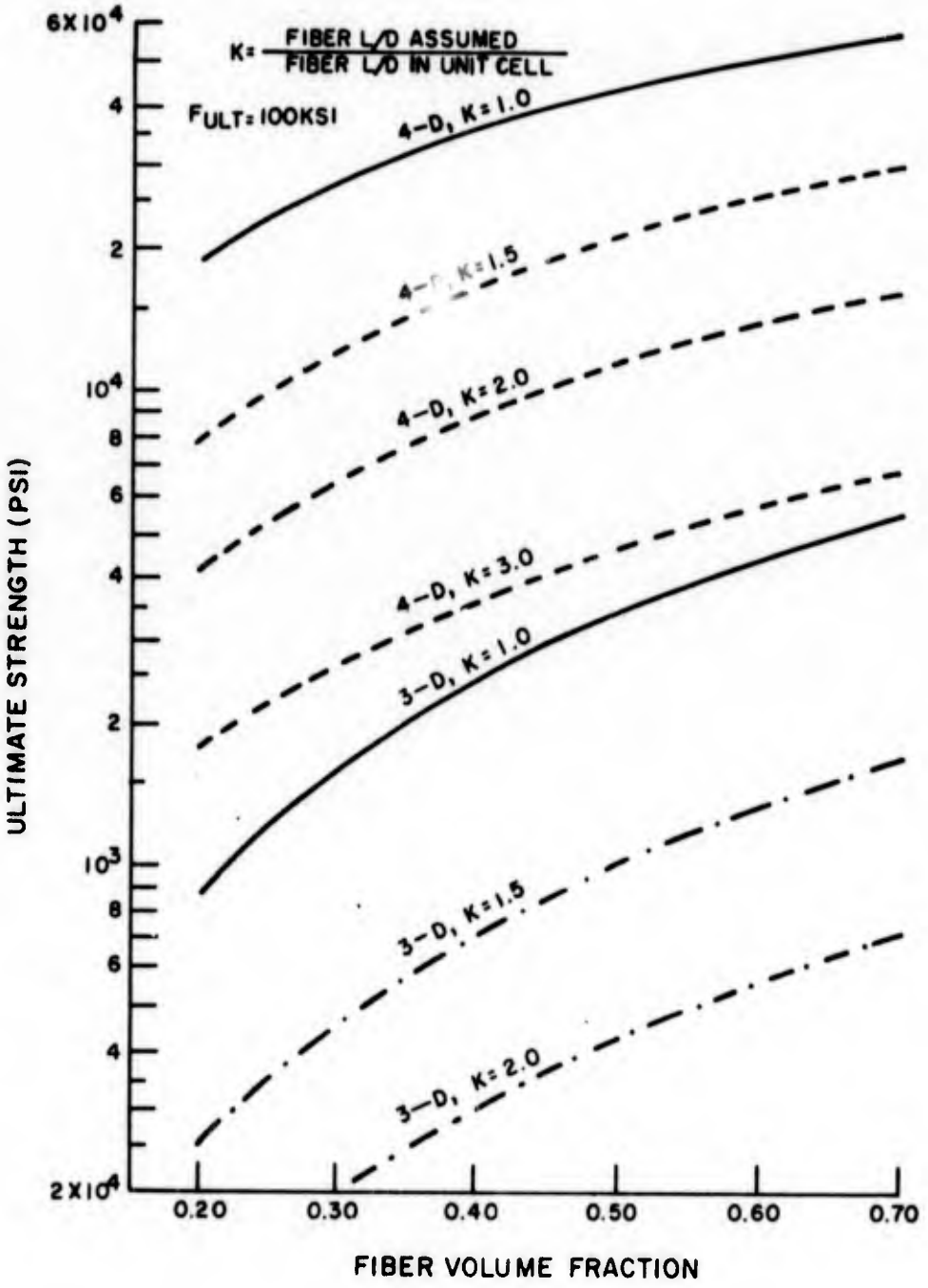

Figure 119. 3-D and 4-D Silica/Silica Strength for Body Diagonal Loading

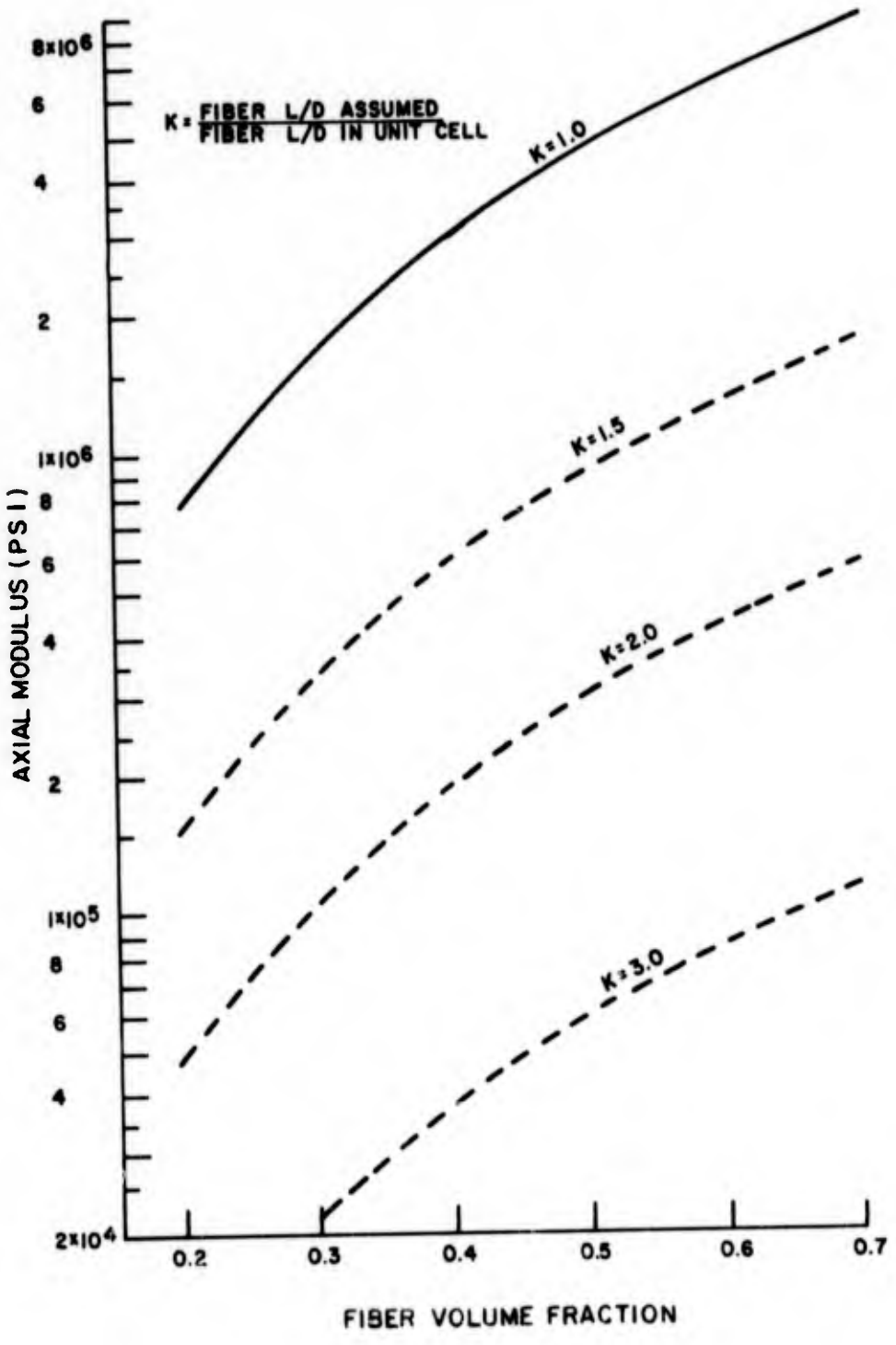

Figure 120. Predicted Axial Modulus of 4-D Silica/Silica Material

void material is filled with matrix. At that point, the matrix will continue to compress under increasing load but the bulk modulus of the packed matrix will resist further deformation. At this point, the fiber geometry will be at some orientation other than the "lock-up" orientation. For this case, continued loading will yield an elastic modulus of a material with some new fiber angle and volume fraction, and little or no void content in the matrix. Failure would then be governed by the final configuration and the fiber shear and extensional stresses which result.

To sum this model of failure, one would anticipate a stress-strain curve consisting of essentially three portions as shown in Figure 121. Namely, a small initial curve due to the initial material, a second section representing matrix and fiber angle changes, and a third section representative of a stress-strain behavior of either a "locked up" fiber configuration, or the behavior of a composite with new fiber angles and little or no void content.

The experimental data supports the above failure hypothesis as illustrated by the following example. Consider Specimens BNQ-V407-1 and 2, the stress-strain data obtained for these specimens is shown in Figure 122, along with the reported ultimate stress and strain. Note that the strain gages failed long before specimen failure (1 percent versus 15 percent strain). One can clearly define an initial region and second region of the stress-strain curves, with the transition occurring at very low stress levels. To estimate whether or not a third, or stiffening, portion of the stress-strain curve occurred, one can estimate the modulus of the second section, and thus estimate the failure stress at failure strain assuming linear behavior. Doing so one would estimate failure stress levels of 3380 psi and 3720 psi for specimens 1 and 2, respectively. Since the reported failure stress levels of 4213 psi and 3952 psi for specimens 1 and 2 are above the linear estimates, some hardening, or stiffening of the specimens must have occurred prior to failure, indicating the probable occurrence of either fiber "lock-up" or matrix/void compaction, resulting in a new stable fiber/matrix configuration.

Consider also the stress-strain data for Specimen BNQ-V-407-B-1, which is linear from 0 psi to 350 psi. This specimen indicates that an initial stiffness may have not been present. Extrapolating this stress-strain curve to the reported failure strain of 3.37 percent, one would predict a failure stress of 1040 psi, which, if any decrease in modulus occurred should over predict the failure strength. However, the failure stress was 3147 psi, which again indicates some increase in tangent modulus occurring prior to failure.

The MULTI computer program can do little towards predicting the behavior of the Boron Nitride/Quartz composites produced during this program. The presence of high void content means that large fiber angle changes will take place, requiring a large deformation analysis.

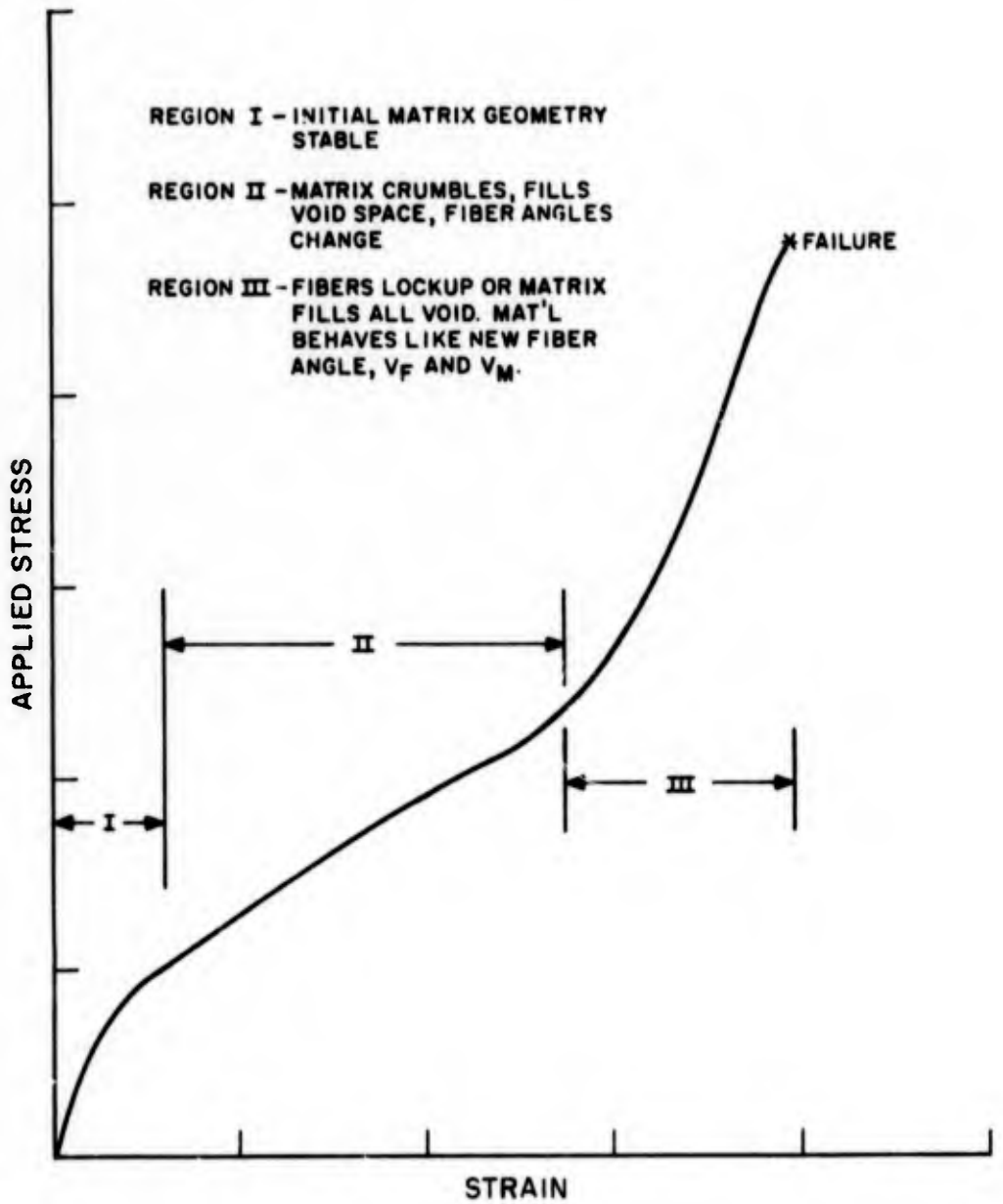

Figure 121. Postulated Stress/Strain Behavior of Boron/Nitride-Quartz Omniweave

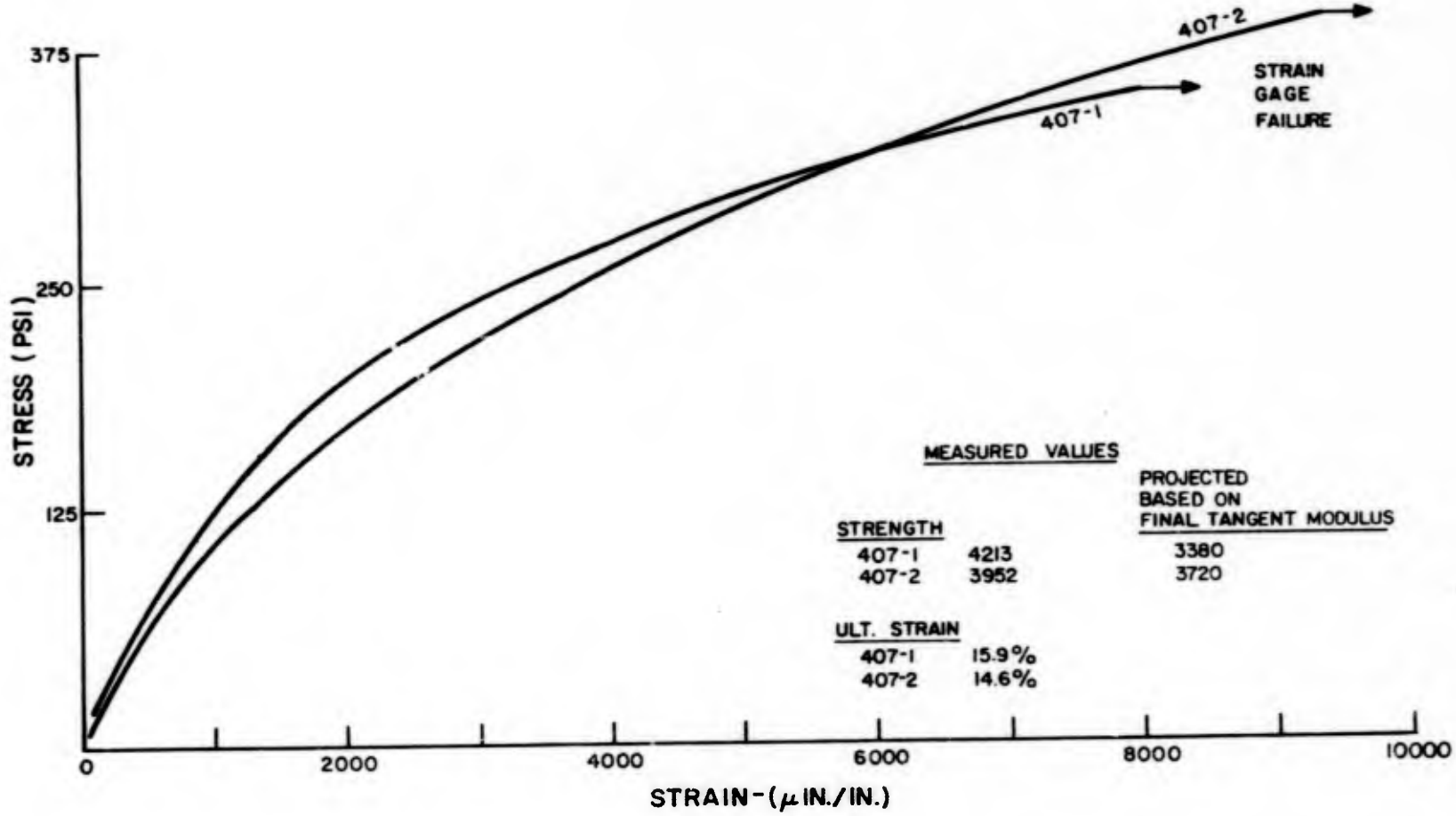

Figure 122. Stress/Strain Data for Specimens BNQ-V-407-1&2

One can however, determine the fiber configuration at either fiber "lock-up" or when the matrix compacts such that no further fiber angle changes are possible, given the initial fiber angles, volume fraction, and matrix content. Based on the final configuration and using the previously discussed techniques for considering weave distortion, one can then estimate the strain which the unit cell experienced in deforming from the initial configuration to the "lock-up" configuration, or to any other configuration as a function of either final projected fiber angle or final void content.

Several of the test specimen configurations produced during the program have been analyzed to determine the possible fiber distortions which may have taken place during loading, namely, the geometry of Specimens BNQ-V-407-1,2 and of Specimens BNQ-S-406-1 through 4 were studied. The initial projected fiber angles, assuming that the weave had equal angular projections on the planes parallel to the weaving direction, and the initial fiber and matrix volume fractions were used to determine the resultant fiber, matrix, and combined volume fractions for weave distortions. The results are plotted in Figures 123 and 124.

The figures represent two sets of initial conditions as shown. Starting at the initial weave geometry, loading will elongate the unit cell, resulting in lower projected fiber angles and a smaller unit cell volume. Since the initial volume of fiber and matrix in each unit cell must remain constant, the fiber and matrix volume fractions must increase with decreasing projected fiber angles. The limits on deformation are, of course, that the total volume fraction of fiber plus matrix cannot exceed unity, and the fiber volume fraction cannot exceed the theoretical maximum for the given weave geometry. Whichever of these two conditions is met first will determine the limiting decrease in projected fiber angle. One minus the sum of the matrix and fiber volume fraction represents the void content, and this quantity is also indicated in the figures.

If one postulates that the matrix can compact to zero void content, then the limiting fiber angles are 22 and 26.5 degrees. However, it is reasonable to expect that the final configurations will have a fairly large void content since the matrix cannot freely disperse throughout the specimen during loading. One would expect that regions of matrix may become entrapped during loading and hence regions of the fibers will not be free to rotate and failure would initiate at those sites.

The projected fiber angles versus void content is easily obtained from Figures 123 and 124. Given the initial fiber configurations and the angles during loading one can define the elongation of the unit cell, $C-C_i$, and hence can define the strain imposed on the unit cell during deformation from the initial configuration to any given projected fiber angle (or void content). Since the strains induced during geometry change will be large compared to mechanical strains within the fiber, the strain to failure of the specimen can be approximated as the weave distortion strain.

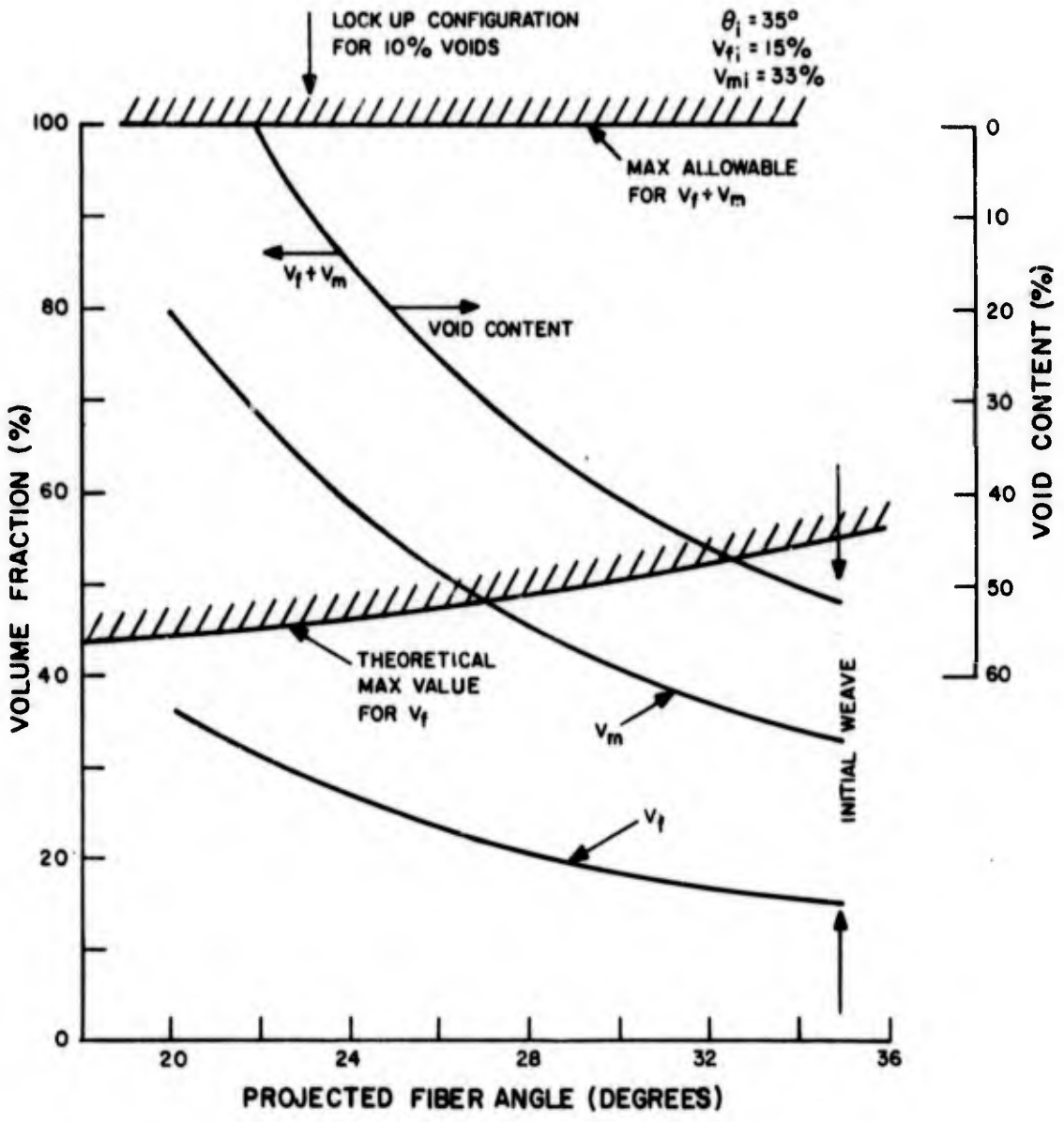

Figure 123. Fiber/Matrix Volume Fractions Versus Void Content for Specimens: BNQ-V407-1, BNQ-V407-2

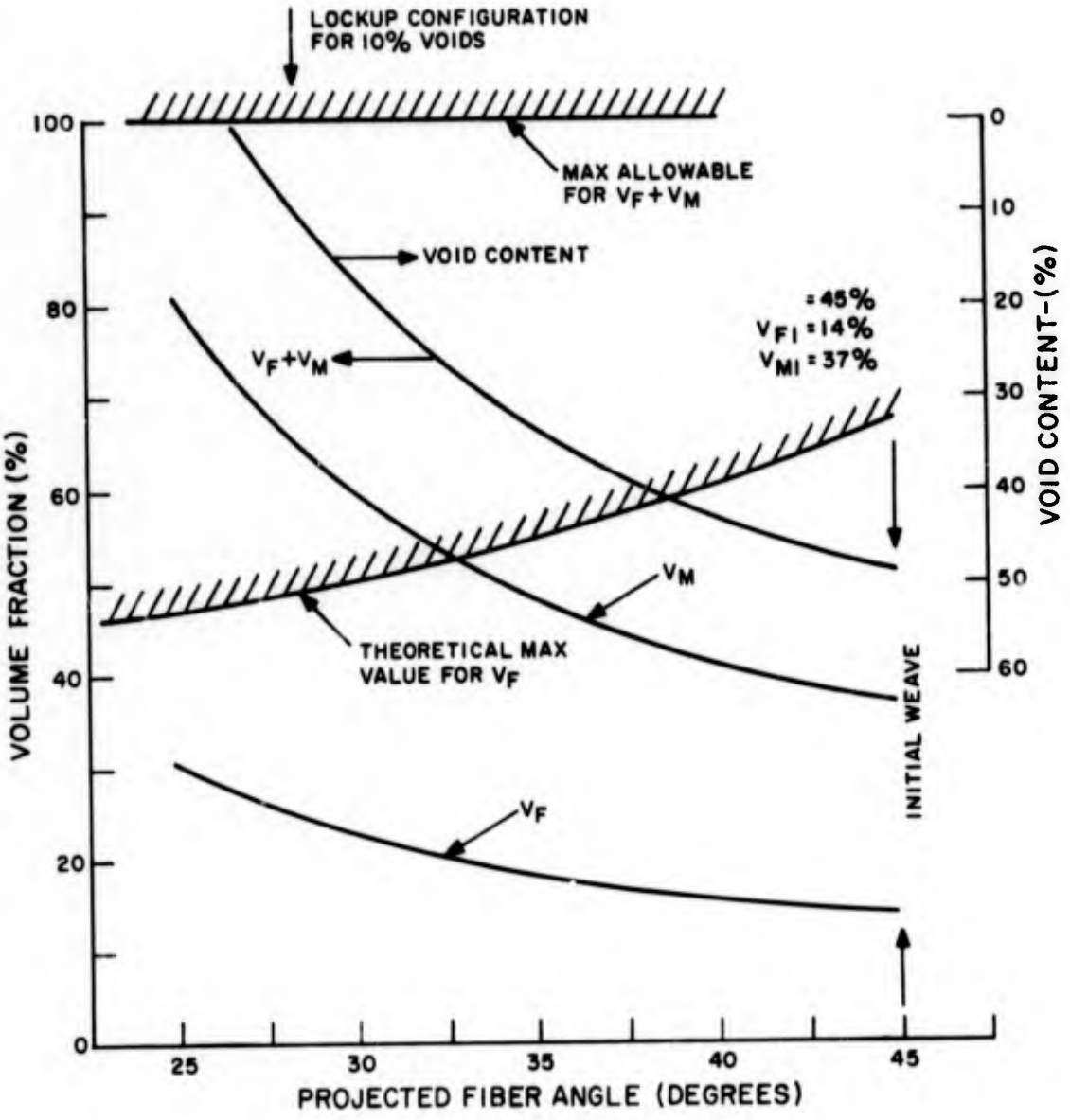

Figure 124. Fiber/Matrix Volume Fractions Versus Void Content for Specimens: BNQ-S406-1,2, BNQ-S406-3,4

Figure 125 presents the weave distortion strain as a function of void content for the specimen configurations considered. Also included in Figure 125 are the strains to failure measured on several specimens. Since the void content or projected fiber angle just prior to fracture was not determined, the data could be plotted anywhere along the abcissa. The important message is the fact that the predicted strains are indeed good estimates of the experimentally measured values, indicating that the previous discussion on the failure process must possess some credibility and justifies further investigation.

Figures 126 and 127 present curves corresponding to those of Figures 123 through 125, but for an initial weave volume fraction in the neighborhood of 45 percent. Thus, these figures predict the behavior of future Boron Nitride/Quartz omniweave for improved weave density, assuming the initial void contents are reduced to 20 - 30 percent. Note in Figure 127 that the fiber "lock-up" angle restricts the amount of void reduction possible, and indicates that a unit cell distortion strain of approximately 14 percent would be obtainable for the conditions considered.

4.7 CONCLUSIONS AND RECOMMENDATIONS

The results of the analytical study show good correlation with the experimental results, hence, the analytical studies can be of use for optimization of processing and weaving variables. The study of ADL-10 has shown the dependence of axial strength on the transverse shear capability of the fiber for the practical range of weaving angles. In addition, it has been shown for the silica/silicone materials that the 4-D weave geometry with 45-degree projected fiber angles, will exhibit lower axial strength but will possess significantly higher off axis load and shear load carrying capability than a corresponding 3-D weave.

For the silica/silica materials the study has demonstrated the strength dependence on the effective fiber length resisting load. For this class of materials, treating the geometry as a three-dimensional truss, one again finds that the 4-D geometry will have lower axial strength but significantly increased off axis and shear load carrying capability over an equivalent 3-D material. The full potential of this class of materials will be realized for a matrix system which provides rigid joints between the fibers, yet does not aid in propagating a crack through the material, such that failure cannot proceed in a "weakest link" mode. The smooth failure surfaces exhibited by some of the specimens tested indicate that the matrix material is causing the composite to behave more like a continum with voids than a fibrous composite.

The Boron Nitride/Quartz composite materials appear to possess a complex failure process which warrants further study. The very high strains to failure obtained in tests of these materials indicates that the material should have excellent plate-slap and thermal strain capability. The behavior of these materials could not be fully studied in this program, but the high strengths and strains to failure indicate a need

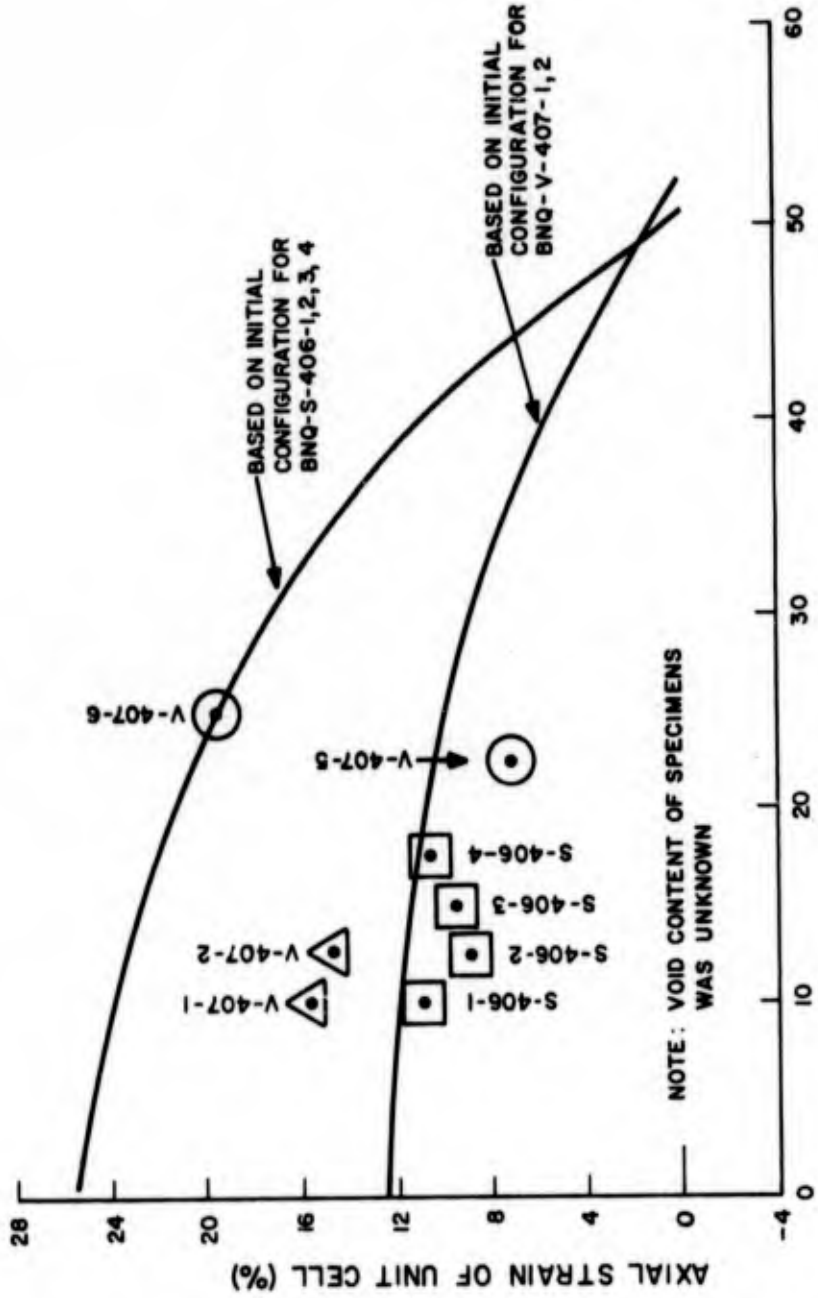

Figure 125. Axial Strain Induced in Unit Cell if Initial Specimen Geometries are Distorted During Loading to Given Void Contents

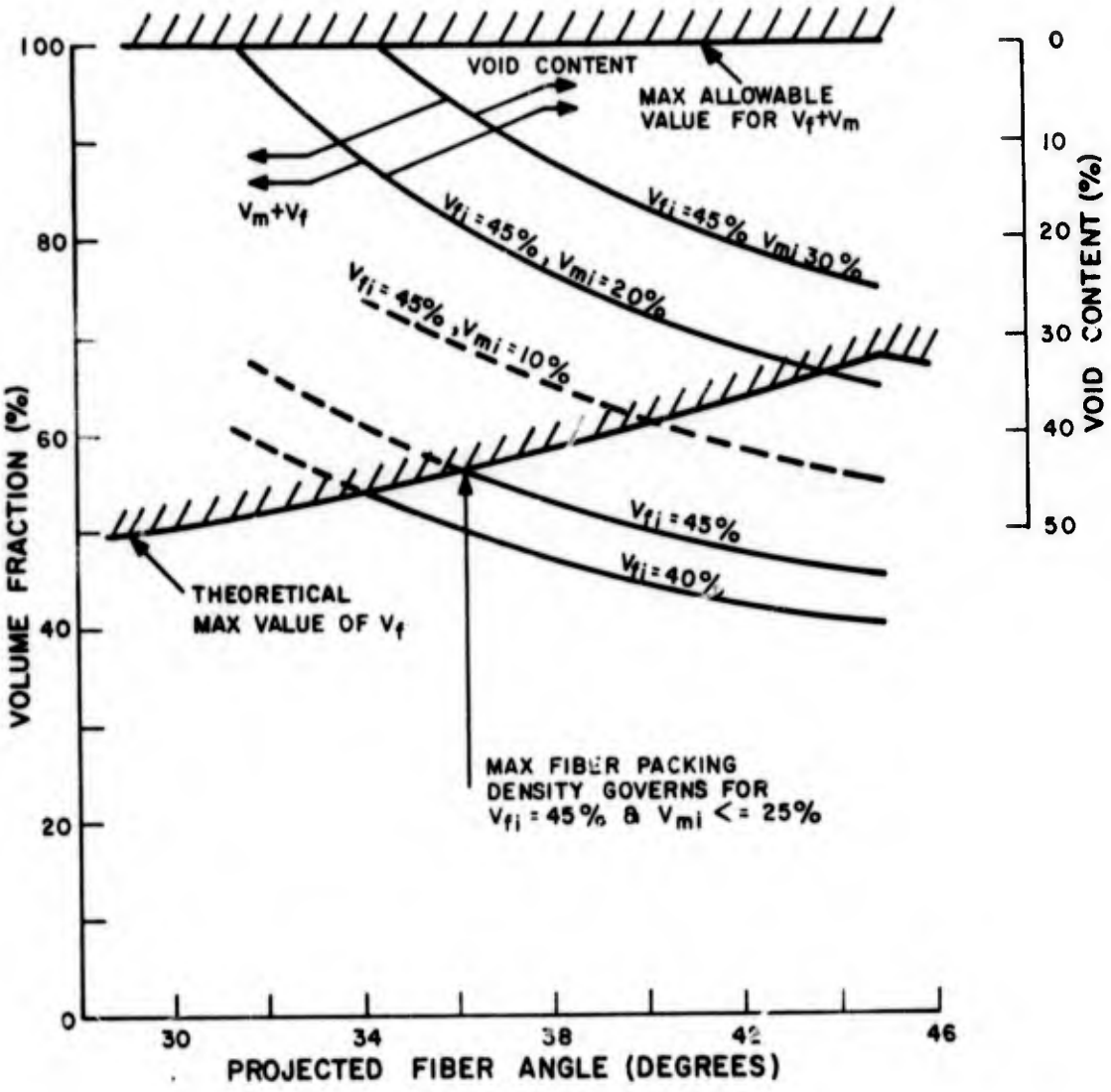

Figure 126. Possible Fiber/Matrix Volume Fractions During Loading for Future Weaves with Increased V_{fi}

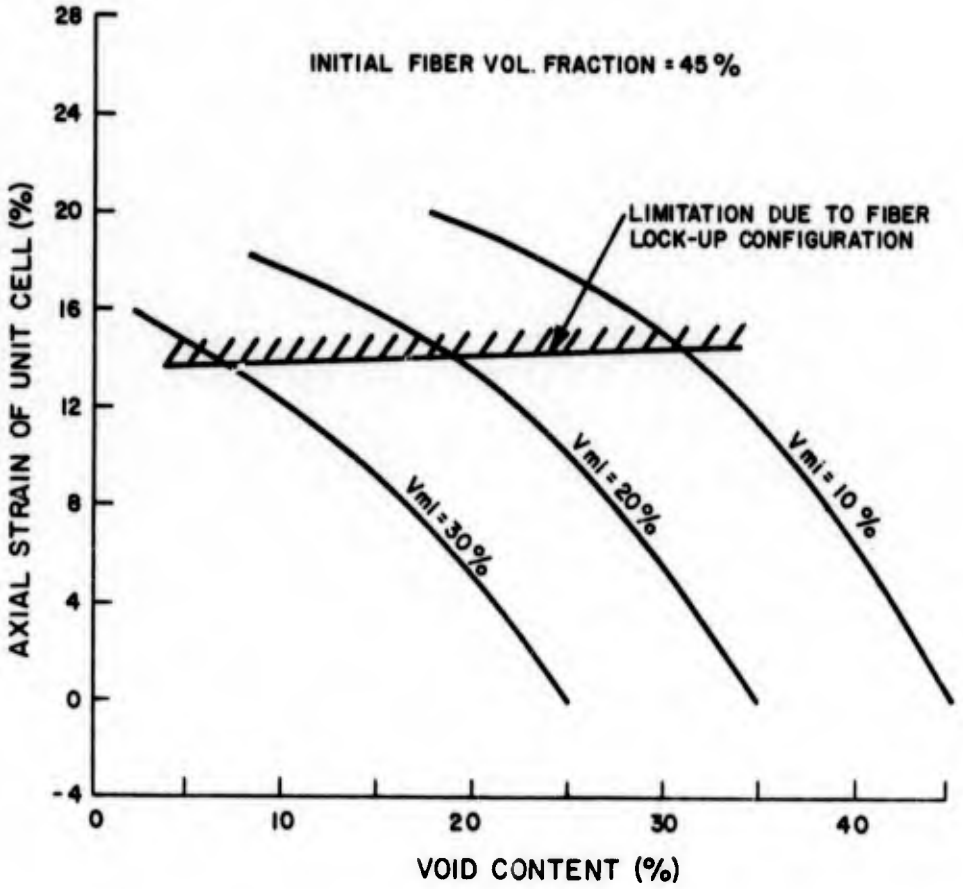

Figure 127. Axial Strain Induced in Unit Cell for Possible Improved Initial Weave Density

to further develop and understand these materials. The excellent agreement between the predicted range of strain to failure and the measured values indicates that the assumption of large weave distortions occurring during loading is correct, and can lay the foundation for development of an analytical model for predicting the stress at failure, given the initial specimen configuration.

The Boron Nitride/Quartz material warrants further analytical and experimental development. The large strains to failure for the material offers several benefits. For dynamic (impulse) loads, the material will provide extremely fast attenuation of the stress waves. Not only does the 4-D weave configuration offer excellent off-axis load carrying capability, but the ability of the fibers to distort under loads implies that for off-axis loading the unit cells will distort in an unsymmetrical fashion, orienting the fibers as much as possible in the direction of the applied loading, thus, providing even greater load carrying capability in the off-axis directions over configurations with fixed fiber positions.

SECTION 5.0

TABLE OF CONTENTS

5.0 CONCLUSIONS AND RECOMMENDATIONS

The critical performance properties of materials developed on these programs are summarized and compared to state of the art and competitive hardened antenna window materials in Table 5-1, for reference in review of these conclusions and recommendations.

5.1 CONCLUSIONS

1. Exploding foil impact tests have established the failure threshold of a representative range of ADL-10 samples in an as-molded 1-centimeter thickness at approximately 5000 taps with measured rear surface stresses of 3.0 to 4.7 kbar. The effect of machining the as-molded faces is to lower this threshold to a value between 3200 and 4600 taps, depending on the composite density and fiber volume fraction.

The failure mechanism is front face spall in this shorter impulse testing which better simulates the relevant weapons effects, as compared to the backface spall result observed earlier in aluminum flyer magnetic repulsion testing.

2. It was found that ADL-10 material produced in this program according to the optimized process described in References 2 and 3 failed to reproduce the strength levels demonstrated in that work unless the silane fiber-matrix coupling agent was employed. ADL-10 composite without coupler had a tensile strength range of 3,000 - 6,000 psi, while the silane-coupled material had a strength in excess of 10,000 psi.

The effect of machining 0.050 inch (equivalent to 1 fiber bundle) from both faces of 1/2-inch thick tensile bars cut from molded ADL-10 plate material was to reduce its strength to 3/8 of the as-molded value for silane-coupled material, and to 2/3 for non-coupled material. This clearly indicates the wisdom of employing the material in the as-molded state.

3. The Ludox aqueous colloidal silica composite densification process has been applied to Astroquartz Omniweave multidirectional reinforcement fabric with excellent success, achieving flexure strengths of 20,000 - 30,000 psi, matching those reported for three-directional reinforced silica-silica composites based on the same process. One-centimeter thick specimens withstood magnetic flyer plate impacts at 2000 and 3000 taps with no visible damage and only slight ultrasonic attenuation increase.

4. A new inorganic hardened antenna window material class based on densification of high purity fused silica Omniweave with glass phase - bonded boron nitride has been developed and designated "BNQ" - for "boron nitride/quartz". Development optimization studies with Carborundum Series S, V and A BN coatings point to a magnesium silicate glass-bonded BN matrix. With solution of the principal composite fabrication difficulty by a roving prepreg process, axial tensile strengths of 4000 psi and an extraordinarily high strain capability of approximately 7-8 percent were measured for early

TABLE 51. ANTENNA WINDOW MATEIALS FOR R/V & ABM APPLICATIONS
(all properties at room temperature unless noted)

	Transparent Fused Silica (E. G. Corning 7940)	Slip Cast Fused Silica (E. G. Corning 7941)	Silica Omniweave/SR 350 Resin (ADL-10)	3-D Silica/Colloidal Silica (AS3DX)	Silica Omniweave/Colloidal Silica (ADL-4D6)	Silica Omniweave/Glass Bonded BN (BNQ)
Tensile Strength (psi)	6,800	5,400 - 9,000	10,000 - 20,000	5,000 min. (flexural)	20,000 - 30,000 (short beam flexural)	4,000
Tensile Modulus (10^6psi)	10.5	8.4	1 - 2	4	3.2 (flexural)	0.1
Failure Strain (%)			1 - 2%	1 - 2%	1 - 2% +	2% + (7-8% for 1.3 gm/cc)
Hardening Threshold (taps) (thickness)	500 - 1,500	500 - 1,500	5,000 (3/8" thickness)	4,000 - 5/8" 6,000 - 1"	3,000 + (3/8")	4,000 (1/2")
Dielectric Constant	3.8	3.3	3 - 3.3	2.9	2.8 - 3.1	2
Loss Tangent (Heating Limit)	0.0016 - 22	0.0002 -	0.002 - 0.005 (100 BTU/ft^2-sec, 2800°F surface temp.)	0.008 -	≤ 0.01 -	0.005 -
Thermal Conductivity (150°F) (10^{-5} Btu/ft-sec-F°)	22	15	10	8.8		4.5
Q-Star (Btu/lb)		11,000		4,200 - 6,000		6,000
Density (gm/cc)	2.2	1.9 - 2.1	1.8	1.7	1.7	1.3 (prototype) 1.8 (goal)
Relative Cost	Low	Lowest	Low-Moderate	Highest	Highest	Moderate-High

Developmental Material

developmental BNQ composites of only 15-23 percent silica fiber volume fraction. Magnetic flyer testing of 1/2-inch thick tensile bars showed no loss of tensile strength (4000 psi) after 2000 taps impulse and a reduction to the order of 800 psi for 4000 taps. The RF/dielectric properties are excellent and appear insensitive to atmospheric moisture pickup. The thermal conductivity is low, comparing to low density ADL-10, about 1/4 that of transparent fused quartz at 150°F. High shear environment ablation testing shows a Q-star equivalent to that of phenolic refrasil and fused silica.

5. The "space-frame" model for a low density ductile silica-silica composite which was proposed in Reference 2 has been verified. A 5-D Astroquartz Omniweave was specifically designed and woven for this purpose and the Ludox AS densification process was used to densify sections of weave to 1.17, 1.39 and 1.68 gm/cc densities. Flexure testing shows a complex dependence of strength and modulus on densification and direction (perpendicular or parallel to the 5th direction) and a high degree of ductility. This ductile ceramic material concept constitutes a new design option to balance directional strength, elastic and thermal transport properties against density, particularly in a high temperature oxidative or corrosive atmosphere where graphite or metallic materials are limited for extended operation.

6. An extensive analysis has been performed comparing the structural potential of 3, 4 and 5-directional composites. The ADL-10 analysis of Reference 2 has been extended to include large fiber pitch angles and a sensitivity analysis has been performed via the MULTI program to show the limiting effects of varied fiber - matrix shear strength and fiber tensile strength.

The off-axis capability of these three reinforcement constructions is compared - including a thorough analysis of the system silica/silica. It is shown that the 4-D construction is uniformly superior for off-axis stresses and in the important case of the ceramic silica/silica system, for the desired high fiber volume fractions of 50 percent or greater, the 4-D axial strength is predicted to be comparable to or greater than a similar 3-D composite.

This unanticipated result has been confirmed by the experimental measurements on panel 404-2 deionized Ludox AS/Astroquartz 4-D Omniweave.

7. A body of comparative data has been assembled on competitive methods for densification of high density and purity silica reinforcement, normalized to nominally 1 gm/cc Astroquartz 4-D Omniweave.

- The process for silica matrix densification by pyrolysis of Methyltrichlorosilane proved too low in yield, attaining a limiting maximum of only 1.13 gm/cc, with an apparently unacceptably high (for this density) loss tangent of 0.005.

- Markite Hybrid process studies showed disappointingly low strength even in the "R4" state of repeated pyrolysis and reimpregnation. The densification percent yield of this process was shown to be either 84 or 25 percent, depending on interpretation of the compounded molding/impregnation process, as compared to an unambiguous 70 percent for the Ludox aqueous silica process in which the composite is cast, without any compression of the densified Omniweave.

- The silica-boria systems, on which valuable experience had been gained during GE-RESD's REI low density reusable external insulation studies for NASA's Space Shuttle Program, were found at the stage of development carried out, to be relatively impractical for penetration into and densification of high density silica reinforcements. A silica-boria-alumina/BN slip was formulated and, although the by now familiar difficulty of achieving more than a 15 - 20 percent densification was encountered, it showed the hypothesized high ductility behavior expected of the BN infiltrated matrix.

- The two CVD processes, for SiO_2 and BN, were both also found to be of limited value for infiltration of high starting density silica reinforcement. The silica CVD process based on ethylorthosilicate should however be suitable for the necessary surface sealing of water vapor-permeable silica-silica composites.

5.2 RECOMMENDATIONS

1. The composite hardened antenna window system Ludox AS/Astroquartz 4-D Omniweave ("ADL-4D6") should be further developed and optimized for structural strength, elastic and shock resistance properties.

   a. Development should include study of the effects of fiber and colloidal silica matrix treatments, optimizing the fiber volume fraction, bulk density and porosity relationships.

   b. Characterization should include:

      (1) pure uniaxial tensile testing, compression and shear, with flexure testing as a screening test.

      (2) flyer plate testing with both mylar and aluminum flyers (to evaluate pulse width effects), at thicknesses of 0.4 inch (1 cm), 5/8 inch and 1 inch and determination of the equation of state of the optimized material.

      (3) ablation testing in a range of environments including the high heat flux, enthalpy and shear case, supported by high temperature thermal conductivity data.

The purpose and effect of this first recommendation would be to enable a timely and valid assessment of the capability of the generic composite system: aqueous colloidal silica-derived matrix/silica multidirectional fibrous reinforcement, in the 4-D configuration, providing a design option to the state-of-the-art 3-D material, AS3DX.

2. Development of the composite hardened antenna window system: glass-bonded boron nitride/Astroquartz 4-D Omniweave ("BNQ") should be continued. The sequence of development should be:

a. investigation of alternate BN/glass refractory mixtures, the alternate use of pre-and-post-weaving impregnation techniques and the influence of firing temperatures, with the goal of achieving 50 percent nominal fiber volume fraction BNQ composites.

b. tensile and impact testing on the partially optimized BNQ's with the goal of achieving minimum strengths of 5000 psi, strain capability above 5 percent, a modulus of greater than 10^5 psi and a damage threshold above 5,000 taps.

c. RF dielectric and/or ablation testing at levels including but not limited to high heat flux, enthalpy and shear, supported by basic thermal conductivity data to high temperatures with a goal of demonstrating compatibility with current heat shield systems such as silica/phenolic.

3. A coordinated analysis and basic experimental effort is recommended to determine the cause of the anomalous failure of apparently highly characterized multidirectionally reinforced composites to consistently achieve their theoretical structural capability. The experience of these programs in improving the strength of ADL-10 to its theoretical value and the experimental data on possible variations of the material would guide work on a silica-phenolic Omniweave composite. The study would be primarily restricted to composite systems using high purity silica reinforcements and organic matrices such as phenolic resin and SR-350 silicone resin. The methods employed would include:

a. application of the baseline analytical methods and results typified by the analysis Sections (4) of this report and Reference 2.

b. fundamental study of the fiber-matrix interaction using both phenolic and SR-350 resins in experiments with single fibers and unidirectional composites.

c. an experimental sensitivity study of the SR-350 and phenolic resin matrix systems. This would include shear modulus and failure stress measurements on samplings of commercial material with aging and storage effects as parameters.

The two-fold goal of this recommended work would be to determine if otherwise highly sophisticated hardened ablative materials studied in the recent past at significant government expense have failed to show the anticipated overall performance levels because of failures in the basic fiber matrix interaction and to seek near term solutions to the important silica-phenolic multidirectionally reinforced composite instances where this has occurred.

If this goal were achieved, the effect would be to recoup effort expended on these high performance materials systems. The ABM Systems/Reduction of Vulnerability Program would thereby be provided with a wider range of design options at a high cost effectiveness due to redemption of past DOD efforts which are presently considered inconclusive or unsuccessful.

6.0 REFERENCES

1. BRAZEL, J. (Editor), "Hardened Antenna Window Materials - Final Report", AMMRC CR-70-15, General Electric Co./RESD, September, 1970.

2. BRAZEL, J. (Editor), "Advanced Hardened Antenna Window Materials Study", AMMRC CTR 72-1 (AD #741-384), General Electric Co./RESD, February 1972.

3. BRAZEL, J. and L. MARKOWITZ, "Development and Characterization of Silicone-Silica Composite Hardened Antenna Window Materials Based on Omniweave Multidirectional Reinforcement", General Electric Co./RESD, in Proceedings of the Eleventh Symposium on Electromagnetic Windows, Georgia Institute of Technology, August, 1972.

4. PLACE, T.M. and D. W. BRIDGES, "Fused Quartz-Reinforced Silica Composites for Radomes", Aeronutronic Division/Philco-Ford Corporation, in "Proceedings of the Tenth Symposium on Electromagnetic Windows:, Georgia Institute of Technology, July, 1970.

5. TANZILLI, R.A., "Development of An External Ceramic Insulation for the Space Shuttle Orbiter", NASA CR-112038, April 1972.

6. TANZILLI, R.A., "Development of An External Ceramic Insulation for the Space Shuttle Orbiter, Part 2 - Optimization, March 1973.

7. ENGLERT, W.J., and F. A. HUMMEL, "The System B_2O_3-SiO_2-P_2O_5" J. Glass Technol. 39, 126T (1955).

8. ROCKETT, T.J. and W. R. FOSTER, "Phase Relations in the System Boron Oxide-Silica," J. Am. Ceram. Soc., 48, (2) 75-80 (1965).

9. NAS 1-10533 - Mod #10, "Development of an External Insulation for the Space Shuttle Orbiter."

10. GIELISSE, P. J. and W. R. FOSTER, "Quarterly Report #931-8", The Ohio State University Research Foundation, p.6, Oct. (1961)

11. ROOTARE, H. M. and A. C. NYCE, "Use of Porosimetry in the Measurement of Pore Size Distribution in Porous Materials", Int. J. Powder Met., 7 (1), 3-11, (1971).

12. GEBHARDT, J., "Proceedings of the 10th Conference on Carbon", pp 53-54 (1971, D. Bauer et al., ibid 57-61).

13. POWELL, C. F., J. H. OXLEY and J. M. BLOCKER, Jr., "Vapor Deposition", J. Wiley and Sons, New York, N.Y., pp 391-397.

14. BRAUN C. A. and A. W. LAUBENGAYER, J. Am. "Chem. Soc. 77", pp 3699-3700 (1955)

15. GEBHARDT, J. SAMPE, "Proceedings of the 4th Technical Conference," Palo Alto, Calif.

16. CORBORUNDUM CO., TECHNICAL CERAMICS DIVISION, "Bulletin No. A-2005-B".

17. GRAHAM, M. E., R. E. WENGLER and D. V. KELLER, "Shock Wave Measurements in Exploding Foil Testing", ISA Transactions, 9, 133-140, 1970.

18. KELLER, D. V. and R. E. WENGLER, "Exploding Foil Technology and Vulnerability Assessment (U)", Radiation Effects Meeting Proceedings, Air Force Weapons Laboratory, WLX 70-306, pp. 105-160, 3-4 December 1969 (SRD).

19. JONES, O. E. and A. L. STEVENS, "Effects of Radial Release Waves in Plate Impact Experiments", Bulletin of the American Physical Society II, 15, 1606, December 1970.

20. DAVIES, F. W. and J. R. PENNING, JR., "Hugoniot Equation of State of Mylar", Preprint of Report No. D2-125304-1, The Boeing Company, 1967.

21. NAUMANN, W. J., "Carbon Stress Gage Development", Effects Technology, Inc. Contract Report CR 72-103, DNA 3027F, April 1973.

22. NAUMANN, W. J., "Carbon Stress Gage Handbook", Effects Technology Inc. Contract Report CR 72-101, 20 October 1972.

23. DECECCO, A., J. HANSON and L. MCCOOG, "Dielectric Properties of Selected Materials as a Function of Temperature at UHF Frequencies", GE-RESD PIR(U)-8155-1933, 19 December 1967.